# PHARMACOLOGICAL IMPROVEMENT OF ONCOLYTIC VIROTHERAPY

Mohammed Selman

Thesis submitted to the

Faculty of Graduate and Postdoctoral Studies

in partial fulfillment of the requirements

for the Doctorate of Philosophy in Biochemistry

Department of Biochemistry, Microbiology & Immunology

Faculty of Medicine

University of Ottawa

## Abstract

Oncolytic viruses (OV) are an emerging class of anticancer bio-therapeutics that induce antitumor immunity through selective replication in cancer cells. However, the efficacy of OVs as single agents remains limited. We postulate that resistance to oncolytic virotherapy results in part from the failure of tumor cells to be sufficiently infected. In this study, we provide evidence that in the context of sarcoma, a highly heterogeneous malignancy, the infection of tumors by different oncolytic viruses varies greatly. Similarly, for a given oncolytic virus, productive infection of tumors across patient samples varies by many orders of magnitude. To overcome this issue, we hypothesize that the infection of resistant tumors can be achieved through the use of selected small molecules. Here, we have identified two novel drug classes with the ability to improve the efficacy of OV therapy: fumaric and maleic acid esters (FMAEs) and vanadium compounds. FMAEs are enhancing infection of cancer cells by several oncolytic viruses in cancer cell lines and human tumor biopsies. The ability of FMAEs to enhance viral spread is due to their ability to inhibit type I IFN production and response, which is associated with their ability to block nuclear translocation of transcription factor NF-κB. Vanadium-based phosphatase inhibitors enhance OV infection of RNA viruses *in vitro* and *ex vivo*, in resistant cancer cell lines. Mechanistically, this involves subverting the antiviral type I IFN response towards a death-inducing and proinflammatory type II IFN response, leading to improved OV spread, increased bystander killing of cancer cells, and enhanced anti-tumor immune-stimulation. Both FMAEs and vanadium compounds improve therapeutic outcomes of OV treatment in syngeneic tumor models, leading to durable responses, even in models otherwise refractory to OV and drug alone. Overall, we showcased novel avenues for the development of improved immunotherapy strategies.

## Acknowledgements

This thesis would not have been possible without the aid and support of several people. First, I would like to thank my supervisor Dr. Jean-Simon Diallo for his guidance, motivation and continuous support during the duration of my PhD. Furthermore, I would like to thank to my thesis committee members, Dr. Mary-Ellen Harper, Dr. Tommy Alain and Dr. Douglas Gray for their helpful advice throughout the course of the program. I would also like to thank the many collaborators for their work and valuable input: Dr. Debbie C. Crans, Dr. Brian A. Keller, Dr. Larissa Pikor, Dr. Fabrice Le Boeuf, Dr. John C. Bell and Dr. Carolina Ilkow. A special thanks to Dr. Fanny Tzelepis for teaching me new skills and all her effort and help with the many immunological experiments, and Andrew Chen for all his help managing the numerous *in vivo* experiments. Sincere thanks for all the hard work from honors students that I had the privilege to supervise and work with: Chris Rousso, Paula Ou and Anabel Bergeron. Finally, thanks to family, friends and all current and former lab members of the Diallo lab for their ongoing support.

## Table of Contents

## List of Abbreviations

| | |
|---|---|
| 7-AAD | 7-Aminoactinomycin D |
| ANOVA | Analysis of variance |
| Bax | BCL2 Associated X |
| BMOV | Bismaltolato oxovanadium |
| BSO | Buthionine sulfoximine |
| CDK | Cyclin-dependent kinase |
| CTCL | Cutaneous T-cell lymphoma |
| CTLA-4 | Cytotoxic T-lymphocyte-associated protein-4 |
| DEF | Diethyl fumarate |
| DEM | Diethyl maleate |
| DMEM | Dulbecco's Modified Eagle's Medium |
| DMF | Dimethyl fumarate |
| DMM | Dimethyl maleate |
| DNA | Deoxyribonucleic acid |
| ECM | Extracellular matrix |
| eIF2a | eukaryotic initiation factor 2 alpha |
| FA | Fumaric acid |
| FAE | Fumaric acid esters |
| FDA | U S Food and Drug Administration |
| FMAE | Fumaric and maleic acid esters |
| G | Glycoprotein |
| GAF | IFN-γ-regulated DNA-binding factor |
| GAS | IFN-γ activation sequence |
| GCL | Glutamate Cysteine Ligase |
| GM-CSF | Granulocyte-macrophage colony-stimulating factor |
| GO | Gene Ontology |
| GSH | Glutathione |
| HDAC | Histone deacetylase inhibitor |
| HEPS | 4-(2-hydroxyethyl)-1-piperazineethanesulfonic acid |
| HR | Higher responders |
| HSV-1 | Herpes simplex virus 1 |
| IAP | Inhibitors of apoptosis proteins |
| IFIT1 | Interferon-induced protein with tetratricopeptide repeats 1 |
| IFITM1 | Interferon-induced transmembrane protein 1 |
| IFN | Interferon |
| IFNGR1 | IFN-γ receptor 1 |
| IKK | IκB kinase |
| IRF | IFN-regulatory factor |

| | |
|---|---|
| IRSE | Interferon-stimulated response element |
| ISGF3 | Interferon-stimulated gene factor 3 |
| IT | Intratumoral |
| IV | Intravenous |
| IVIS | *in vivo* imaging system |
| JAK | Janus kinase |
| JC | John Cunningham |
| JX-594 | Pexastimogene devacirepvec |
| KEAP1 | Kelch-like ECH-associated protein 1 |
| LPS | Lipopolysaccharides |
| LR | Lower responders |
| M | Matrix |
| MG1 | Marabex |
| MMF | Monomethyl fumarate |
| MOI | Multiplicity of infection |
| MS | Multiple sclerosis |
| mTOR | mammalian target of rapamycin |
| MV | Measles |
| MxA | Myxoma resistance protein A |
| N | Nucleoprotein |
| NF-κB | Nuclear factor kappa-light-chain-enhancer of activated B cells |
| NK | Natural killer |
| NRF2 | Nuclear factor (erythroid-derived 2)-like 2 |
| OHSN-REB | Ottawa Health Science Network Research Ethics Board |
| OV | Oncolytic Virus |
| P | Phosphoprotein |
| PBS | Phosphate-buffered saline |
| PD-L1 | Programmed death-ligand 1 |
| PD1 | Programmed cell death protein 1 |
| PDA | Pancreatic ductal adenocarcinomas |
| PFU | Plaque forming units |
| PI3K | Phosphoinositide 3-kinase |
| PKR | Protein kinase R |
| PML | Progressive multifocal leukoencephalopathy |
| PRR | Pattern recognition receptors |
| PTP | Protein tyrosine phosphatases |
| PTP1B | Protein-tyrosine phosphatase 1B |
| qPCR | Quantitative polymerase chain reaction |
| RECIST | Response Evaluation Criteria In Solid Tumors |
| RIG-1 | Retinoic Acid Inducible Gene 1 |

| | |
|---|---|
| RIPK3 | Receptor Interacting Protein Kinase 3 |
| RNA | Ribonucleic acid |
| ROS | Reactive oxygen species |
| RPMI | Roswell Park Memorial Institute |
| SC | Sub-cutaneous |
| Smac | Second mitochondrial activator of caspase |
| SMC | Smac mimetic compounds |
| STAT1 | Signal transducer and activator of transcription 1 |
| STAT2 | Signal transducer and activator of transcription 2 |
| T-Vec | Talimogene laherparepvec |
| TBK1 | TANK-binding kinase 1 |
| TFNα | Tumor necrosis factor alpha |
| TGF-β | Transforming growth factor-β |
| TK | Thymidine kinase |
| TLR | Toll-like receptors |
| VOx | Vvanadium(V) oxytriethoxyde |
| VS | Vanadium(IV) oxide sulphate |
| VSV | Vesicular stomatitis virus |
| VVdd | double-deleted vaccinia virus |
| wt | wild-type |

## List of Figures

# Chapter 1 - General Introduction

## Cancer

Cancer is not simply defined as the abnormal growth of cells, but is in fact an intricate and dynamic disease driven by mutation, epigenetic reprogramming, and crosstalk with its microenvironment. The development of cancer is shepherded by well described hallmarks of cancer biology such as sustained proliferative signaling, evasion of growth suppressors, resistance to cell death and reprogramming of energy metabolism *(1)*. These factors result in, for instance, replicative immortality, induction of angiogenesis, and the ability to evade immune detection *(1)*. Today, multiple strategies are used for the treatment of cancer, from standard surgery to cytotoxic treatment such as radiation and chemotherapy. In addition, there has been a rise in the field of immunotherapy which promotes the body's immune system to specifically target the cancer such as checkpoint inhibitors targeting immunosuppressive signalling pathways on T-cells or cancer cells *(2)*. Despite tremendous advancement in cancer treatment technologies, cancer is still the leading cause of death in Canada; with an average of 565 Canadians diagnosed with cancer every day of which 221 Canadians succumb to it. According to estimates, 1 out of 4 Canadians is expected to die from cancer *(3, 4)* .

## Oncolytic virotherapy

Oncolytic virotherapy has emerged as a viable alternative to conventional cancer therapies, such as radiation and chemotherapy that often lack in efficacy and cause severe

side effects. Oncolytic virotherapy refers to treatments using replicating viruses that preferentially infect and kill cancer cells without harming normal cells.

Some early clinical observations of cancer patients with tumor regression or remission were associated with patients' viral infections, for instance, influenza infection was linked to the remission of leukemia as documented in 1904 *(5, 6)*. This was followed by a report in 1922 where vaccinia virus was shown to inhibit the growth of several mouse and rat tumors *(7)*. This led to the first patient trials using natural viruses to treat cancer in the 1950s, which showed some anti-tumor effect but unacceptable toxicities *(5)*. Since the advent of molecular engineering, a broad spectrum of DNA and RNA viruses have been selected or engineered to improve viral oncolysis and have been tested clinically for their anticancer properties, including adenovirus, measles virus, parvovirus, reovirus, vesicular stomatitis virus, seneca valley virus, and coxsackievirus *(8)*. Despite the diversity of the viruses tested, only two OVs have been approved for clinical use. First, in 2005, Oncorine, a type-5 adenovirus with a partial deletion in the E1B gene was approved in China for the treatment of head and neck cancer *(9)*. In 2015, the U.S. Food and Drug Administration (FDA) approved the first OV in North America for the treatment of melanoma, talimogene laherparepvec (T-Vec) an engineered herpes simplex virus *(10)*.

**Mechanism of action of oncolytic viruses**

The mechanisms of action of OV therapy are multi-modal and targets several pathways. These can be mediated by the virus' natural ability or through transgene expression. Altogether, this results in a combination of direct lysis of tumor cells, anti-angiogenic effects, and the induction of an antitumor immune response *(11)*. Lysis of cancer cells occurs following selective viral replication in the tumor. The spread of viral infection within malignant tissue results in the continuous amplification of the parental virus, until it is stopped by an antiviral immune response or a lack of susceptible cancer cells. Oncolytic viruses can be classified into two groups - viruses with a natural tropism for cancer cells or viruses that are genetically modified to selectively replicate in cancer cells *(8)*. For example, the removal of the viral thymidine kinase (TK) from the herpes or vaccinia viruses attenuates those viruses in normal tissues due to a paucity of endogenous nucleotides available for efficient viral replication. In contrast, tumors functionally complement this gene deletion in support of their own replicative needs and thus support viral replication *(12, 13)*. Viral proteins that support the attachment of the virus to host cells can also be modified to target the virus to specific receptors overexpressed in malignant tumors *(14, 15)*. Furthermore, replacing endogenous viral promoters with tissue-specific promoters for viral genes that are crucial for successful replication can improve selectivity of OVs *(16, 17)*.

Owing to multiple factors, including low expression of major histocompatibility complex (MHC) antigens as well as cytokine secretion profiles that antagonize local immune responses, tumors and their microenvironments are inherently immunosuppressive *(18)*. Infection of tumor cells by OVs induces release of several antiviral and pro-inflammatory cytokines, leading to a localized inflammatory response

*(8, 11)*. This is followed by an infiltration of various innate and adaptive immune cells into the tumor in addition to the activation of resident lymphocytes. MHC I proteins, recognized by the cytotoxic T lymphocytes (CTLs) infiltrated within the tumor, display the viral- and cancer-associated antigens on the cell surface, resulting in a systemic antitumor (and antiviral) immune response *(11, 19)*. The generation of systemic adaptive antitumor immunity is thought to be critical and result in long-term protection against tumor recurrence *(20, 21)*.

**Oncolytic virus platforms**

Most of the oncolytic viruses currently in development exhibit a relatively broad spectrum of antitumor activity *in vitro*, typically against both epithelial and hematological malignancies*(8)*. Naturally occurring viruses have different entry routes, life cycles, structures, and tropisms manifesting in distinctive clinical symptoms. Therefore, OVs derived from these viruses can also be expected to be more efficient against specific malignancies. OVs can also be engineered to target specific cell-surface receptors or nuclear transcription factors to target specific malignancies *(8)*. Evaluating and comparing the potency of various OV platforms is therefore a reasonable first step toward identifying the best candidate for clinical translation of OVs for the treatment of specific malignancies. For example, in human pancreatic ductal adenocarcinomas (PDA), oncolytic activity of VSV, adenoviruses, sendai virus, and respiratory syncytial virus were compared. *In vitro*, oncolytic VSV showed greater oncolytic activity compared to the other viruses, with the conclusion being that VSV may be a promising oncolytic agent against PDA *(22)*, but further clinical evaluation is still to come.

**Oncolytic herpesvirus**

Herpesviruses are dsDNA viruses with a broad spectrum of hosts. Their genomes range in size from about 125 to 240 kbp, and encode approximately 70 to 165 genes *(23)*. Herpesviruses infection is pervasive among humans, in particular infection with herpes simplex virus 1 and 2 (HSV-1 and HSV-2), varicella zoster virus, Epstein–Barr virus, or the cytomegalovirus *(24)*. HSV infection can undergo lytic or latent presentation. During lytic infection, HSV-1 genes are expressed that regulate viral DNA synthesis and create an environment favorable for protein synthesis, contribute to encapsulation of viral DNA, and promote viral envelopment *(25)*. Globally, an estimated two-thirds of the population under 50 is infected with HSV-1, however the majority of people with HSV-1 infection are unaware they are infected *(26)*. Interestingly, recent progress has been made exploiting the unique features of herpes viruses as an oncolytic virus platform. Particularly, HSV-1 has several advantage over other OVs, including its broad spectrum of infectivity of cancer cells; how it can be genetically manipulated to express multiple transgenes; numerous antiviral drugs (such as acyclovir) provide a safety mechanism against unfavorable replication of the virus; and HSV-1 does not integrate with the host genome even during latency *(25, 27)*.

T-Vec (Talimogene laherparepvec) is a genetically engineered herpes virus with deletions in the γ34.5 and α47 genes leading to cancer-specific replication and attenuation of its pathogenicity. To further promote the antitumor response, the human granulocyte-macrophage colony-stimulating factor (GM-CSF) gene was inserted in the oncolytic herpesvirus *(28)*. Based on the results of a recent phase III clinical trial with patients featuring metastatic melanoma lesions in the skin and lymph nodes, the U.S. FDA

approved T-Vec for the treatment of metastatic melanoma. The phase III clinical trial indicated that median overall survival and durable response rate was significantly higher in the T-Vec arm compared with the GM-CSF arm. The most common adverse events with T-Vec were fatigue, chills, and pyrexia, and, furthermore, no fatal treatment-related adverse events were documented *(29)*. Based on the observation that intratumoral injection of T-Vec induced systemic antitumor immunity, a phase 1b clinical trial testing the impact of T-Vec on cytotoxic T-cell infiltration and therapeutic efficacy of the anti-PD-1 antibody pembrolizumab was carried out. The data suggested that T-Vec can improve the efficacy of checkpoint inhibitor (anti-PD-1) therapy by changing the tumor microenvironment *(30)*.

**Oncolytic poxviruses**

Poxviruses are dsDNA viruses with a large linear genome encoding 150 to 300 genes. Its life cycle takes place within the cytoplasm of the infected cell *(31)*. Poxviruses are known to have a wide host range, with the Entomopoxvirinae subfamily infecting insects and the Chordopoxvirinae subfamily infecting vertebrates. Poxvirus infections commonly lead to the formation of lesions, skin nodules, or disseminated rash, however poxviruses vary in virulence. The variola virus, the causative agent of smallpox, is human-specific and highly virulent only to humans, while closely related cowpox viruses naturally infect a broad range of animals and only cause relatively mild disease in humans *(32)*.

The Vaccinia virus, raccoon poxvirus, yaba-like disease virus, and the myxoma virus have been investigated for their oncolytic potential as these viruses undergo productive lytic replication in most human cancer cells. Oncolytic poxviruses are attractive platforms for cancer therapy because of the following characteristics: safety in humans, ease of production, stability of virus (can be stored as dry powder for prolonged periods of time without significant loss of infectivity), and easy genetic manipulation for the expression of various anticancer transgenes as well as the replication cycle in the cytoplasm eliminating any risk of integration *(25, 33)*.

JX-594 (pexastimogene devacirepvec, Pexa-Vec) is one of several vaccina strain tested in clinical trials *(34)*. To render viral replication selective to cancer cells, it was genetically engineered to contain a mutation in the TK gene through insertion of the human GM-CSF gene, which upon expression in infected cancer cells promotes the antitumor immune response *(35, 36)*. Phase I and II clinical trials reaffirmed the safety profile of the treatment. However, in a phase IIb clinical trial comprised of patients with advanced stage hepatocellular carcinoma, JX-594 did not improve overall survival *(33, 37, 38)*. Nevertheless, JX-594 in combination with various chemotherapy agents or checkpoint inhibitors is currently under clinical evaluation (NCT01636284, NCT02562755, NCT02977156, NCT03071094).

**Oncolytic reovirus**

Reoviruses are non-enveloped, dsRNA viruses with a genome composed of 10 to 12 segments encoding 10 to 14 genes. Human infection with reoviruses commonly occurs causing mild infections limited to the gastrointestinal or respiratory tract *(31)*. Reoviruses are known to replicate preferentially in cells with the activated Ras pathway, which modulates cell growth, differentiation, and survival *(39)*. This results in their inherent ability to selectively replicate in cancer cells given that approximately 30% of human tumors have an activating mutation of the Ras pathway *(39, 40)*. The dsRNA-activated protein kinase (PKR) binds to dsRNA and activates downstream signals halting protein synthesis and viral replication. PKR is inactivated in Ras-transformed cells, promoting viral infection of dsRNA viruses, such as reoviruses *(41)*. In contrast to other OV platforms, introducing mutation or introducing transgenes in reoviruses is not easily accomplished *(25)*.

Numerous clinical trials have been carried out using reovirus. In a phase I trial in patients with advanced solid tumors, common treatment-related adverse events included nausea, vomiting and fevers, and transient flu-like symptoms *(42)*. However, reovirus did not cause any dose-limiting toxicity (with doses up to 10E10 PFU per injection). In one phase II trial evaluating single-agent reovirus in metastatic melanomas, there was a failure to meet previously defined efficacy criteria. Recently, a number of Phase II clinical trial evaluating reovirus combinations with chemotherapy agents also failed to meet previously defined efficacy criteria. Phase II and III clinical trials are presently underway testing reovirus combinations with various checkpoint inhibitors *(43)*.

**Oncolytic rhabdoviruses**

Rhabdoviruses are negative ssRNA viruses with a broad host range, including plants, insects, fish, mammals, and reptiles. The vesicular stomatitis virus (VSV), a member of the Vesiculovirus genus, is an arthropod-borne virus that primarily affects rodents, cattle, swine, and horses, and causes a relatively localized and non-fatal illness. Human infection is rare and usually asymptomatic. The VSV genome is constituted of 5 genes encoded by a negative sense, ssRNA genome, found in all rhabdoviruses in the order of 3′-N-P-M-G-L-5′ *(31, 44)*.

Viral RNA forms a helical nucleocapsid complex with the nucleoprotein (N). The nucleocapsid also encompasses the phosphoprotein (P), some of which is bound to the viral RNA-dependent RNA polymerase, the large (L) protein. The nucleocapsid complex and the viral polymerase complex (P and L proteins) form the ribonucleoprotein. The ribonucleoprotein is enveloped in a lipid bilayer, acquired from the host cell membrane during the budding process. The matrix protein (M) and the glycoprotein (G) are membrane-associated proteins. The M protein associates with the nucleocapsid and the lipid bilayer, maintaining the compact structure of the virion. The G protein is an integral membrane protein, which controls viral entry, mediated both by cell attachment via the LDL receptor and membrane fusion *(31, 45, 46)*.

VSV is highly sensitive to the effects of the antiviral cytokines known as type I interferons (IFN); however, the wild-type virus is quite capable of shutting off IFN

production through the actions of its M protein, which blocks host mRNA export from the nucleus *(47)*. In order to make VSV sensitive to an IFN-mediated antiviral response, a variant was engineered with a complete deletion of methionine at amino acid position 51 (Δ51). While normal cells have robust antiviral mechanisms, most cancer cells have mutations that lead to a defective IFN-mediated antiviral response, resulting in cancer-specific replication of VSVΔ51 *(48, 49)*.

Maraba virus, a member of the Vesiculovirus genus, was identified from *in vitro* screening of a panel of rhabdoviruses on cancer cells as the most potent rhabdovirus strain *(50)*. To increase specificity towards cancer cells, mutations of the G (Q242R) and M (L123W) proteins were introduced to the Maraba virus to further attenuate it in normal cells. This engineered virus, designated as MG1, had a 100-fold greater maximum tolerable dose than wild-type Maraba in a murine model, and resulted in durable cures when administered in syngeneic and xenograft murine tumor models *(50)*.

Beyond its oncolytic activity, the MG1 virus can effectively reduce metastatic disease following cancer surgery by boosting natural killer (NK) cell activity *(51)*. MG1 and VSV can also be engineered to encode tumor-associated antigen and be utilized as a boosting vector in a heterologous prime-boost vaccination regimen *(52–55)*. This rhabdovirus-based oncolytic vaccination regimen generates an efficient antigen-specific T-cell immune response, extending median survival and leading to complete remission in murine melanoma tumor models *(52)*. The prime-boost vaccination regimen is under clinical evaluation with favorable safety profiles reported thus far (NCT02285816). Furthermore, oncolytic VSV expressing IFNβ is under clinical evaluation for the

treatment of various solid tumors, multiple myeloma and acute myeloid leukemia (NCT02923466, NCT03017820).

**Type I and type II interferon pathways**

IFNs are cytokines that can block viral infection, inhibit cell proliferation, and modulate innate and adaptive immune responses. The IFN family includes three main classes of cytokines: type I IFN (IFNα, IFNβ, and IFNω), type II IFN (IFNγ), and type III IFN (IFNλ1, IFNλ2, and IFNλ3). IFNβ is produced by most cell types, while IFNα is primarily generated by haematopoietic cells. IFNγ is predominantly produced by NK and NK T-cells for the modulation of the innate immune response, and by cytotoxic T-cells once antigen-specific immunity is initiated *(56–58)*.

Type I IFNs bind a common cell-surface receptor composed of two subunits of IFNα receptor 1 and 2 (IFNAR1, IFNAR2) while IFNγ binds a distinct cell-surface receptor also composed of two subunits, namely IFNγ receptor 1 and 2 (IFNGR1, IFNGR2). These receptors interact with members of the janus-activated kinase (JAK) family: tyrosine kinase 2 (TYK2) and JAK1 for the IFNAR, and JAK1 and JAK2 for the IFNGR. Activation of the receptors by IFN binding is followed by its autophosphorylation and activation of the associated JAK, leading to differential activation of STAT1 and STAT2 (signal transducer and activator of transcription) transcription factors by tyrosine phosphorylation. Phosphorylation of STATs leads to their dimerization and nuclear translocation to activate transcription of IFN-stimulated

genes (ISGs). Some of these genes are regulated by both type I and type II IFNs, whereas others are selectively regulated by one or the other. Type I IFNs induce the formation of the ISG factor 3 (ISGF3) complex composed of a STAT1-STAT2 dimer and IRF9 that binds specific elements known as IFN-stimulated response elements (ISREs); while type II IFN primarily leads to the formation of STAT1-STAT1 dimers that bind IFNγ-activated-sequence (GAS) elements *(56)*.

Type I IFN leads to the induction of hundreds of ISGs, many of which exert antiviral functions by directly targeting pathways and functions required during the virus life cycle *(59)*. For example, oligoadenylate synthetase (OAS) and latent endoribonuclease (RNaseL) results in the detection and subsequent degradation of viral RNAs. Upon binding to dsRNA, protein kinase R (PKR) limits viral translation by phosphorylating the initiation factor eIF-2. PKR is an important component of IFN-induced resistance to VSV *(60, 61)*. Mx proteins (such as MXA) are dynamin-like GTPases and are effective against a broad range of RNA viruses, including VSV *(62)*. MXA was shown to specifically inhibit VSV mRNA synthesis by affecting elongation of the viral RNA chain. Interferon inducible transmembrane (IFITM) proteins inhibit early steps in the life cycles of various viruses, by blocking entry or viral particle trafficking, overexpression of IFITM1 inhibits replication of VSV *(60)*.

Upon viral infection, production of type I IFN arises in response to the stimulation of pattern recognition receptors (PRRs); such as RNA helicases like retinoic acid-inducible gene I (RIG-I) that binds to cytosolic viral RNA; or by the activation various Toll-like receptors (TLRs) which can recognizes dsRNA (TLR3), ssRNA(TLR7/8), unmethylated CpG DNA (TLR9). This converges with the activation of IFN-regulatory

factor (IRF) family of transcription factors that induce the transcription of genes encoding type-I IFNs. PRR stimulation leads to activation of TANK-binding kinase 1 (TBK1) that is responsible for the phosphorylation of IRF3 and IRF7 on specific serine residues, resulting in their homodimerization or heterodimerization. These dimers then translocate to the nucleus and activate the transcription of type-I IFN genes *(63)*.

**The NF-κB pathway**

In addition to IFR3 and IRF7, the transcription of type-I IFNs also requires the coordinated binding of nuclear factor-κB (NF-κB) transcription factor *(64)*. The resulting complex is more stable and effective at bringing about transcription of IFNβ than the individual components bound independently to the IFN promoter *(65)*. Recent studies have indicated that NF-κB is mostly required during the early phase after virus infection, which substantially impacts the host response to viral infection *(66)*. Beyond IFN production, NF-κB plays an important role in regulating the response to pathogens, promoting inflammation and the regulation of cell proliferation and survival *(67)*. Active NF-κB transcription factors form dimeric combinations of Rel proteins, p50, p52, RelA (p65), RelB, and c-Rel. Both p50 and p52 are derived from large precursors, p105 and p100. With most cell types, the predominant form of NF-κB is the p50:p65 heterodimer. In unstimulated cells, NF-κB dimers are retained in the cytoplasm in an inactive state by the binding of a family of inhibitors of IκB kinase (IKK) including IκBα, IκBβ, and IκBε.

The interaction with IκBs masks the nuclear localization sequence in the NF-κB complex, sequestering the factor within the cytoplasmic compartment *(68)*.

Viruses, lipopolysaccharides, cytokines, mitogens, growth factors, and stress-inducing agents promote NF-κB translocation to the nucleus and DNA binding. Upon stimulus, degradation of IκB proteins is initiated through phosphorylation by the IKK complex, which consists of two catalytically active kinases, IKKα and IKKβ, and the regulatory subunit, IKKγ (NEMO). Phosphorylated IκB is targeted for ubiquitination and proteasomal degradation, which consequently releases the bound NF-κB dimer, resulting in its translocation to the nucleus *(69)*.

In fact, many viruses have evolved distinct strategies to control the activity of NF-κB transcription factors *(67)*. Furthermore, pharmacological inhibition of NF-κB activity is able to facilitate viral infection *(70)*.

**Defects in type I IFN signaling in cancer**

IFN also plays an important role in immunosurveillance for malignant cells *(71)*. Loss of type I IFN signaling from cancer cells, stromal cells, or immune cells promotes an immunosuppressive environment, resulting in tumor development *(71)*. For instance, patients with breast cancer, melanoma, or gastrointestinal cancer were shown to have reduced type I IFN signaling in T-cells and B-cells, leading to downstream functional defects in T-cell activation *(72)*. Loss of type I IFN signaling has also been found to lead to metastatic dissemination. IRF7-driven type-I IFN responses produced by primary

mammary tumors was lost in bone metastatic cells. Restoration of IRF7 signaling and type I IFN production in highly metastatic murine tumor cells suppressed their ability to form metastases in bone. Similar patterns were found in patients, where elevated expression of IRF7-regulated genes in primary tumors was found to be associated with prolonged bone metastasis–free survival *(73)*.

Cancer cells are known to have defective antiviral immune responses, resulting in robust infection by OVs *(74)*. For instance, defects in type- I IFN production and responses are thought to be chief in cancer cells *(48, 75)*. Downregulation of the IFNAR was associated with resistance to IFN therapy in bladder cancer; however its suppression was demonstrated to facilitate VSV replication and oncolysis in bladder cancers *(76)*. The response to type I IFN is unfavorable to tumor formation, inducing an antiproliferative, antiangiogenic, antiviral, and proapoptotic environment *(71, 77, 78)*.

However, a subset of tumors retains the capacity to mount strong antiviral defenses, rendering OV therapy ineffective. Resistance to oncolytic VSV in pancreatic ductal adenocarcinoma and mesothelioma was associated with the ability of cell lines to produce and respond to type I IFN *(79, 80)*. Likewise, tumor responses to type I IFN secreted by tumor-associated lymphocytes is sufficient to maintain a functional antiviral defense, causing resistance to OV infection *(81)*. In sarcoma cell lines, resistance to oncolytic measles was associated with high basal expression of IFN-stimulated genes, such as RIG-1 and IFIT1 *(82)*. Similarly, expression levels of the IFN-stimulated gene MxA correlates with acquired and innate resistance to oncolytic adenovirus *(83, 84)*.

**Resistance to OV**

Resistance to cancer therapeutics is a major barrier to the efficient treatment of cancer patients. Treatment-resistant cancer cells can exist prior to treatment or evolve as a result of cancer therapy. Resistance to conventional cancer therapy, such as chemotherapy or radiotherapy, occurs through various mechanisms, including genetic and epigenetic changes in the cancer cell or the tumor microenvironment *(85)*.

In the context of OV, pre-clinical and clinical trials have showcased the heterogeneity in therapeutic responses to OV treatment *(81, 84, 86–89)*. Numerous studies have described the diverse mechanisms underlying resistance to OVs, where poor infection of tumors is an important obstacle to the resistance in OV therapy. Barriers to viral infection can be present constitutively, halting infection before it occurs whereas others are triggered by OVs infection *(89)*.

Solid tumors consist of a complex microenvironment composed of normal cells (including fibroblasts, tumor vasculature, macrophages, and various forms of immune cells) and structural components (such as the ECM). The components constituting the tumor microenvironment can be important physical barriers that prevent the efficient infection of a tumor.

The ECM can block the cell-to-cell spread of viruses, which has been observed in numerous OV platforms, including oncolytic adenovirus *(90)*, herpesvirus *(91)*, and the Semliki Forest virus *(89)*. To circumvent this physical barrier, tumor injection with ECM-degrading enzymes, such as trypsin, collagenase, or dispase, can enhance OV infection *(92)*. Studies have also shown that encoding the ECM protease, matrix metalloprotease 9 (MMP9) within the oncolytic vaccinia or herpes virus improves viral spread within the tumor *(93, 94)*.

The presence and recruitment of certain immune cells is an important factor in the resistance to OV therapy. For instance, the presence of tumor-associated myeloid-derived suppressor cells (MDSC) was identified as a key mediator of resistance to oncolytic vaccinia virus *(95)*. Oncolytic herpesvirus was shown to trigger the recruitment of CD163+ phagocytic cells, thereby limiting viral infection *(96)*. Depletion of $CD163^{+}$ macrophages resulted in increased infection within a glioblastoma tumor model *(96)*. Furthermore, tumor-associated macrophages were demonstrated to induce a protective antiviral state in ovarian and breast tumors, leading to resistance to oncolytic VSV *(81)*.

**Breaking resistance to OV: Viral sensitizers**

The identification of pharmacological agents that can functionally enhance OVs to improve therapeutic benefit has been an area of intense investigation and has been recognized as critical to maximize the therapeutic impact of OVs in the clinic. In

particular, multiple groups have identified pharmacological compounds that facilitate viral infection in cells *(97)*. The word Viral Sensitizer (VSe) has been previously coined to describe this group of agents *(98)*. Several VSes have been shown to improve OV activity by facilitating viral infection of cancer cells but not in normal cells *(97, 99, 100)*.

As previously discussed, dysfunctional IFN pathways are common in cancer cells, however a subset of malignancies retain functional IFN pathways, leading to resistance to OV infection. Hence, while the specific targets of many of these VSe drugs are unknown, studies have shown that they effectively disable cellular antiviral defenses via different mechanisms, often targeting type I IFN production or signaling *(97)*.

Many enzymes that are involved in epigenetic modulation are responsible for the regulation of both cellular and viral genes at the transcriptional level, in particular histone deacetylases (HDACs) that condense the chromatin structure by deacetylating histones *(101)*. Notably, HDACs were shown to be required for the induction of several ISGs *(102)*. Various HDAC inhibitors, including valproic acid, trichostatin A, suberoylanilide hydroxamic acid (SAHA), and MS-275 have been suggested to suppress type I IFN signaling, facilitating infection of various OVs, including HSV *(103, 104)*, vaccinia *(105)*, VSV *(106)*, and the Semliki Forest viruses *(106)*.

The mammalian target of rapamycin (mTOR) is a master regulator of cellular translation, including translation of viral proteins. Furthermore, mTOR was also shown to specifically control the translation of IFNs *(107)*. Consequently, rapamycin, an mTOR

inhibitor, has shown to improve OV activity on several platforms, including oncolytic VSV*(108)*, HSV*(109)*, and adenovirus*(110)*. Rapamycin was able to suppress IFN production during VSV infection, increasing infection and efficacy of oncolytic VSV in glioma tumor models *(108)*.

Sunitinib, an FDA-approved drug, is a RTK inhibitor used for treatment of metastatic renal cell carcinoma and gastrointestinal stromal tumors. Interestingly, sunitinib has shown to impair the activity of PKR and RNaseL, two ISGs *(111)*. Its combination with VSV sunitinib decreased phosphorylation of the PKR substrate, eIF2-α, increasing viral infection in cancer cells *(112)*.

Direct inhibition of the JAK/STAT pathway has also been tested using various JAK inhibitors, including ruxolitinib that is clinically applicable to the treatment of myelofibrosis *(113)*. For instance, ruxolitinib was able to break the resistance to oncolytic VSV in several cancer cell lines *(79, 114, 115)*.

Triptolide, a natural compound derived from a traditional Chinese medicinal plant with anti-inflammatory properties, was reported to inhibit the innate antiviral response by blocking type I IFN signaling downstream of the activation of IRF3 *(116)*. Consequently, triptolide enhanced infection and oncolysis of VSV in resistant cancer cells, leading to delayed tumor growth and prolonged survival of tumor-bearing mice *(116)*. Recent literature has identified triptolide as an inhibitor of RNA polymerase II-mediated

transcription via covalent binding to the XPB protein *(117)*; however the direct target leading to IFN suppression is unknown.

Several promising VSe candidates were also identified upon screening a diverse chemical compound library for the ability to enhance replication and spread of VSVΔ51 in a resistant mouse breast cancer cell line *(98)*. One class of compounds identified were microtubule-destabilizing agents clinically employed for the treatment of numerous diseases, including as chemotherapeutics for cancer. Microtubule destabilizing agents, such as colchicine, increased the spread of VSVΔ51 by suppressing the mRNA translation of type I IFN *(118)*.

VSe1 (3,4-dichloro-5-phenyl-2,5-dihydrofuran-2-one) was the top hit of the aforementioned high-throughput screen and increases infection of VSVΔ51 by over 1000-fold in resistant cancer cells, resulting in increased virus-mediated cytotoxicity, and delayed tumor progression in murine tumor models *(98)*. Furthermore, structure–activity relationship studies of VSe1 seeking to identify the relationship between the chemical structure and its biological activity enabled the design of VSe1 analogues that enhance OVs and gene therapy vectors. Lead compounds could increase VSVΔ51 infection up to 2000-fold *in vitro* in resistant tumor cells while retaining selectivity for cancer cells over normal tissues *ex vivo* and *in vivo (119)*.

Several VSes have been identified, and while most studies enhanced OV infection *in vitro* and *in vivo*, few studies demonstrate a combination treatment that leads to a delay

in tumor growth, improvement in overall survival or complete tumor regression. A number of the identified VSes have never been tested or are not clinically approved for human use, which impairs clinical translation.

In addition to VSes, several studies have described drugs that potentiate the cytotoxic capacities of OVs. For instance small molecule inhibitor of IRE1α enhances oncolytic rhabdovirus-mediated cytotoxicity through the modulation of endoplasmic reticulum stress response pathways *(120)*. Furthermore, Smac mimetic compounds (SMC), which sensitize cells to apoptosis by inhibiting the activity of inhibitor of apoptosis proteins (IAP), can mediate bystander killing of cancer cells through the cytokines (IFNβ, IFNα, TNFα) induced during OV infection *(121)*. More recently, SMC were also found to promote CD8+ T-cell antitumor responses by targeting tumor-associated macrophages, when combined with VSVΔ51*(122)*.

**Fumaric acid esters**

Fumaric acid esters (FAEs) have been first been approved for the oral treatment of psoriasis in 1994 in Germany. More recently, in 2013, the U.S. FDA approved dimethyl fumarate (DMF), an FAE, for treatment for multiple sclerosis (MS). Several systematic reviews showed that the use of FAEs in the management of psoriasis or MS is an efficient and safe treatment option, especially for patients unresponsive to other agents *(123–126)*. DMF is an α,β-unsaturated carboxylic acid ester that is highly electrophilic and rapidly reacts with nucleophiles via a Michael addition reaction. Upon oral

administration, DMF is believed to be rapidly metabolized by intestinal esterases to its bioactive metabolite, monomethyl fumarate *(127)*.

Clinical and preclinical studies suggest that DMF has both anti-inflammatory and cytoprotective properties. However, the exact mechanism of action by which DMF is able manage MS is not fully understood. DMF has been shown to: (i) inhibit the NF-κB pathway; (ii) activate the antioxidant transcription factor nuclear factor (erythroid-derived 2)-like 2 (NRF2); and (iii) at higher concentrations, induce oxidative stress *(128, 129)*.

NRF2 regulates the gene expression of cytoprotective proteins, regulating the antioxidant response. The NRF2 transcription factor is retained in the cytoplasm by the kelch-like ECH-associated protein 1 (KEAP1), the functional inhibitor of NRF2 activation *(130, 131)*. Upon oxidative stress or the presence of electrophiles, these molecules can bind KEAP1 cysteine residues resulting in an allosteric conformational change that destabilizes the interaction of KEAP1 with NRF2. This allows NRF2 to accumulate and translocate to the nucleus to regulate cytoprotective gene expression *(132)*. FAEs, like DMF, are highly electrophilic agents, and can covalently link to thiol groups (cysteine residues) on macromolecules, including KEAP1, and hence subsequently activate NRF2 *(133)*. It was long hypothesized that the activation of NRF2 was an essential step for efficient treatment of MS. However, recent reports show evidence that the anti-inflammatory activity of DMF in the therapy of MS patients occurs through alternative pathways, independent of NRF2 *(134, 135)*.

Glutathione (GSH), a tripeptide formed by glutamic acid, cysteine, and glycine, maintains the intracellular redox balance by scavenging ROS with the aid of GSH

peroxidase. GSH also functions in the detoxification of xenobiotics and some endogenous compounds *(136)*. In contrast to the antioxidant effect of DMF via NRF2, at high concentrations, DMF was shown to deplete cellular levels of GSH as it can react spontaneously with thiols in GSH via a Michael-type reaction, resulting in increased cellular ROS and the onset of cellular apoptosis *(137)*.

In addition to KEAP1, DMF can also covalently bind to thiol groups on the NF-κB transactivator subunit p65, in particular cysteine 38, which is essential for blocking its nuclear translocation and transcriptional activity *(138)*. Upon stimulation of NF-κB by TFNα or lipopolysaccharides (LPS), DMF was shown to suppress NF-κB activity, resulting in suppression of inflammatory cytokine production, altered maturation and function of antigen-presenting cells, and immune deviation of T helper cells (Th) from the Th1 and Th17 profile to a Th2 phenotype *(139)*.

**DMF as cancer treatment**

Beyond the treatment of MS and psoriasis, DMF has also shown promise in the treatment of several diseases, including Parkinson's disease, asthma, inflammatory bowel disease, osteoarthritis, chronic pancreatitis, retinal ischemia, and various malignancies *(129, 140)*. In particular, DMF has been shown to exhibit anticancer properties owing to its capacity to inhibit the NF-κB pathway as well as promoting oxidative stress by inducing cellular ROS *(141)*.

Activation of the NF-κB pathway contributes to cancer progression and aggressiveness, and hence can be exploited to eliminate tumors *(142)*. For instance, in cutaneous T-cell lymphoma (CTCL), which is resistant to cell death based on constitutive NF-κB activation, DMF was shown to induce cell death in primary patient-derived CTCL and cell lines, dependent on its activity on the NF-κB pathway. *In vivo*, DMF delayed CTCL tumor growth and prevented the establishment of metastases *(143)*. Similarly, DMF was also shown to suppress NF-κB activity in multiple breast cancer cell lines, halting cell proliferation and delaying tumor growth *(138)*.

Interestingly, DMF was also demonstrated to sensitize tumors to chemotherapy *(144, 145)*. Resistance to chemotherapy and radiotherapy is mediated through several genes regulated by the NF-κB pathway and its inhibition sensitizes tumors to cell death by chemotherapeutic agents and radiation *(146, 147)*.

In various gastrointestinal cancers, DMF was shown to induce apoptosis via oxidative stress *(148, 149)* or necroptosis by depleting cellular GSH and subsequently activating MAPKs *(141)*. In an orthotopic and subcutaneous CT26 colon tumor model, daily administration of DMF impaired tumor growth *(149)*.

DMF has also been extensively tested preclinically in the treatment of melanomas. DMF impairs melanoma growth and metastasis in syngeneic and xenograft mouse tumor models *(150)*. DMF was shown to inhibit melanoma proliferation and induce apoptosis by the downregulation of bcl-2 and induction of p53 and PARP-1 cleavage *(151)*. Furthermore, evidence has suggested that DMF inhibits melanoma cell

invasion and metastasis by suppressing the expression and activities of various MMPs *(152)*.

**Vanadium**

Vanadium is a transition metal ubiquitously distributed in soil, water, and air *(153)*. Transition metals have the capacity to adopt multiple oxidation states, where vanadium in particular exists in four common oxidation states: +5, +4, +3, and +2. Under physiological conditions, in humans, vanadium is present in two stable oxidation states: +4 or +5 in the form of vanadyl cations ($VO2^{+}$) or as vanadate ions ($H2VO4^{-}$), respectively *(154)*. Vanadate is a structural analog to a phosphate anion with a similar size, charge, and structure *(155)*. By mimicking phosphate, vanadate can interact with various physiological substrates as a substitute to phosphate. In particular, vanadate has a high affinity for the active site of tyrosine protein phosphatases (PTPs), resulting in reversible and competitive inhibition of a broad range of PTPs *(154, 156)*. Several studies have also shown the effect of vanadium compounds on the activity of other enzymes involving phosphate reactions, including ATPases, alkaline phosphatase, ribonucleases, phosphodiesterases, phosphoglucomutase, and glucose-6-phosphatase *(154, 156, 157)*.

Pharmacologically, vanadium compounds are of interest because of their antidiabetic effects attributed to its ability to inhibit protein-tyrosine phosphatase 1B (PTP1B), which results in the hyperactivation of the insulin receptor. Several preclinical studies and clinical trials of vanadium compounds for the treatment of diabetes have been

carried out *(158)*. Clinical trial results were disappointing in terms of efficacy; however, they revealed that vanadium compounds are reasonably tolerated in humans *(155, 156, 158)*.

Vanadium compounds administered orally enter the bloodstream via absorption from the gastrointestinal tract. Once in the bloodstream, vanadium compounds can bind to various metabolites, such as lactate and citrate, and proteins like transferrin, immunoglobulin, and serum albumin*(155)*. Vanadium present in the +5 oxidation state enters cells through phosphate channels while vanadium present in the +4 oxidation state enters cells via passive diffusion. In the case of transferrin-binding vanadyl cations, vanadium can also enter the cell via endocytosis. Once in the cell, vanadate is rapidly reduced by cellular antioxidants (such as NADPH, glutathione, ascorbate, catechols) to vanadyl ions. Unabsorbed vanadium exits the body through feces whereas absorbed vanadium is cleared in the urine. A small proportion accumulates for longer periods of time in tissues with a high appetite for phosphate, such as the bone *(155, 156)*.

Vanadium compounds have been reported to exert a broad range of immunomodulatory activities *(159)*. In T-cells, pervanadate alone was shown activate T-cells marked by its induction of CD69 and CD25, both markers of T-cell activation. This effect was attributed to increased intracellular influx of calcium and greater production of interleukin 2 *(160)*. Furthermore, the transcription factor, NFAT, a key regulator of T-cell development, was shown to be activated by vanadium and depended on ROS generation *(161)*.

**Vanadium compounds are promising anticancer agents**

The anticancer properties of vanadium compounds have been extensively investigated and were associated with several biochemical mechanisms *(162)*, including the disruption of cellular metabolism through the generation of ROS and depletion of glutathione, the alterations of cellular organelles, such as lysosomes, mitochondria, spindle proteins, such as actin and tubulin, overall leading to their antiproliferative effects or cell death *(157)*.

Evidence also suggests that vanadium compounds may also prevent metastatic progression. For instance, the spread of highly metastatic Lewis lung carcinoma (A11 cells) was suppressed by orthovanadate treatment *(163)*. While using the highly aggressive CT26 murine colon tumor model, an oxidovanadium (IV) complex was demonstrated to prevent metastatic dissemination of colon cancer cells to the liver *(164)*.

The process known as epithelial-to-mesenchymal transition (EMT), which results in epithelial cells losing their cell polarity and reduced cell-cell adhesion and increase in cell motility to assume a mesenchymal cell phenotype, is also an important mediator in tumor progression and metastasis *(165)*. Recently, vanadium compounds were reported to halt TGF-β-mediated EMT associated with a decrease in stem cell markers and mitochondrial potential *(166)*.

Preclinically, vanadium compounds were shown to have promising potential as anticancer therapeutics. Furthermore, anticancer properties of vanadium compounds were also shown to exhibit chemopreventive effects *(167)*. Early reports show that in 1-

methyl-1-nitrosurea-induced mammary carcinogenesis in rats, daily administration of vanadyl sulfate resulted in a decrease in cancer incidence and delayed the latency period of tumor appearance *(168)*. Similar results were elicited with daily administration of ammonium metavanadate *(169)*. The chemopreventive effects by vanadium compounds were associated with the modulation of the antioxidant response and that of drug metabolizing enzymes, for instance by increasing the levels of several detoxifying hepatic enzymes (glutathione-S-transferase and UDP-glucuronyl transferase) and the cytochrome P450 *(169)*. Reports also suggested that supplementation in vanadium reduced genomic instability by diminishing the single-strand breaks in the DNA of mammary cells *(170, 171)*.

**Sarcoma: a rare cancer in need of new therapies**

Sarcomas are malignancies originating from mesenchymal tissues composed of cells that would normally mature into bone, cartilage, muscle, fat, fibrous tissues and vascular tissues *(172)*. They are generally classified into either bone sarcomas or soft tissue sarcomas. Osteosarcoma is the most common bone sarcoma, and occurs predominantly in children and young adults. Both osteosarcoma and soft tissue sarcomas are highly metastatic, and most of the patients present metastasis upon diagnosis, hence worsening the prognosis of the disease *(173–175)*. Progress in cancer therapy has resulted in improved overall survival of cancer patients for most malignancies. However, in advanced stages, sarcoma patients, particularly patients with osteosarcoma, still face unacceptably high morbidity and mortality rates *(174, 176)*. Recent studies have shown that several OV platforms can infect and kill sarcoma cells *in vitro (177–180)*, and

preclinically in animal models, resulting in delayed tumor progression *(177–179, 181, 182).* Currently, a number of clinical trials investigating the treatment of sarcomas with OV are in progress *(183)*.

**Rationale and aim I**

Although studies suggest that OVs may be a promising therapeutic avenue for sarcoma, recent studies have focused on the descriptions of novel or improved versions of various OV platforms. However, studies comparing different oncolytic virotherapy platforms in the highly heterogeneous sarcoma are notable by their absence *(88, 184, 185).* This limits our ability to evaluate which OV may be the most promising to move forward with in sarcoma clinical trials. We considered that such a study could further help characterize the prevalence of resistance to OVs in sarcoma generally. Thus in Chapter 2, our goal was to evaluate a panel of clinically relevant oncolytic viruses in parallel in the context of sarcoma. In particular, we designed the study to evaluate the heterogenity of OV infection by evaluating it directly in a meaningful number of human sarcoma tumors obtained by surgery. The most promising OV based on our *in vitro* results, Maraba MG-1, was then tested in an immunocompetent murine sarcoma model.

**Rationale and hypothesis II**

The identification of pharmacological agents that can functionally enhance OVs to improve therapeutic benefit has been an area of intense investigation and recognized as critical to maximize the therapeutic impact of OVs in the clinic *(8)*.

***Identification of novel "immunosuppressive" VSes and evaluation of their in vivo safety and efficacy.*** Strategies aiming to suppress antiviral immune responses, specifically with immunosupressants such as cyclophosphamide, rapamycin, and histone deacetylase inhibitors, have shown promise *in vitro* but variable effects in animal models, in addition to undesirable adverse effects in humans *(108, 186–188)*. FAEs, such as DMF, are a class of compounds with known anti-inflammatory and neuroprotective effects *(126, 189, 190)*. Clinical studies on the long-term use of DMF have not revealed any severe long-term adverse effects *(123, 191, 192)*. Given this and the documented positive effect of diverse immunosuppressants in combination with OVs, we hypothesize that DMF and other FAEs could enhance viral infection of several OVs, leading to increased therapeutic benefit. In Chapter 3, we therefore set out to evaluate the combination of DMF in combination with VSVΔ51 *in vitro* and *in vivo* and to identify the molecular mechanisms underlying the effect of FAEs on OV therapy.

***Identification of novel "immunomodulating" VSes and evaluation of their in vivo safety and efficacy.*** While numerous immunosuppressive drugs have been shown to facilitate viral infection using various OVs leading to delayed tumor progression, complete durable cures of tumors are infrequently reported using this approach. In contrast, combination with immune checkpoint blockade appears to lead to consistent improvements in durable complete responses in animal models and clinical trials *(30, 193–196)*. This could suggest that drugs capable of potentiating the immune responses to viral infection may also promote stronger antitumor immune responses, thereby leading to increased efficacy of OV therapy.

PTPs play an important role in the function of immune cells in addition to the direct regulation of cytokine signaling *(197, 198)*. Interestingly, numerous studies have shown that PTP-deficient mice have hyperactive immune states *(198, 199)*. We speculate that small molecule inhibitors of PTPs could modulate immune responses to viral infection and enhance the therapeutic benefit of OV treatment. To this end, in Chapter 4 we tested vanadium compounds that function as phosphatase inhibitors *(156)*. Vanadium compounds were screened for their ability to modulate VSVΔ51 infection in 786-0 cells, a human renal carcinoma cell line, which is highly resistant to infection with oncolytic VSV. Compounds were tested for tissue-specific enhancement of VSVΔ51 *ex vivo* and further evaluated for their *in vivo* efficacy. The molecular mechanisms underlying the effect of vanadium compounds on OV therapy was also thoroughly studied.

## Chapter 2 - Oncolytic Maraba virus MG1 as a treatment for Sarcoma

Fabrice Le Boeuf[1], Mohammed Selman[1,3], Hwan Hee Son[1,4], Anabel Bergeron[1,4], Andrew Chen[1], Jovian Tsang[1], Derek Butterwick[2], Rozanne Arulanandam[1], Nicole E. Forbes[1], Fanny Tzelepis[1], John C. Bell[1,3], Joel Werier[2,3], Hesham Abdelbary[2]*, Jean-Simon Diallo[1,3]*

[1] Centre for Innovative Cancer Research, Ottawa Hospital Research Institute, Ottawa, Ontario, Canada. [2] The Ottawa Hospital, Department of Surgery Orthopeadics, Ontario, Canada. [3] Faculty of Medicine, University of Ottawa, Ontario, Canada. [4] Faculty of Science, University of Ottawa, Ontario, Canada. * Equal contribution

Accepted May 2017; Published in International Journal of Cancer

Contribution: Conception and design: FLB; MS; JW; HA; JSD. Human Tissue Collection/Process: JW; JT; DB; HA. Animal work: MS; AB, AC; HHS. Analysis/data interpretation: FLB; MS; HHS; HA; JSD. Writing, review: FLB; FT; MS; NEF; RA; JCB; HA; JSD. Supervision: HA; JSD.

**Abstract**

The poor prognosis of patients with advanced bone and soft-tissue sarcoma has not changed in the past several decades, highlighting the necessity for new therapeutic approaches. Immunotherapies, including oncolytic viral (OV) therapy, have shown great promise in a number of clinical trials for a variety of tumor types. However, the effective application of OV in treating sarcoma still remains to be demonstrated. Although few pre-clinical studies using distinct OVs have been performed and demonstrated therapeutic benefit in sarcoma models, a side-by-side comparison of clinically relevant OV platforms has not been performed. Four clinically relevant OV platforms (Reovirus, Vaccinia virus, Herpes-simplex virus and Rhabdovirus) were screened for their ability to infect and kill human and canine sarcoma cell lines *in vitro*, and human sarcoma specimens *ex vivo*. *In vivo* treatment efficacy was tested in a murine model. The rhabdovirus MG1 demonstrated the highest potency *in vitro*. *Ex vivo*, MG-1 productively infected more than 80% of human sarcoma tissues tested,, and treatment *in vivo* led to a significant increase in long-lasting cures in sarcoma-bearing mice. Importantly, MG1 treatment induced the generation of memory immune response that provided protection against a subsequent tumor challenge. This study opens the door for the use of MG-1-based oncolytic immunotherapy strategies as treatment for sarcoma or as a component of a combined therapy.

## Introduction

Sarcomas are a rare and heterogeneous group of aggressive malignant solid tumors that, unlike carcinomas originating from epithelium, arise from a variety of mesenchymal tissues, such as muscle, connective tissue, and bone. Sarcomas require a multimodal therapeutic approach that consists of multi-agent chemotherapy, surgical resection and radiation. According to the National Cancer Institute, the overall 5-year survival rate for sarcoma patients is 50%, which drops to <20% for cases involving distant metastatic spread. As such, new treatment options for recurrent/metastatic sarcoma are direly needed.

Immunotherapy could provide an alternative to chemotherapy yet there has been little focus on sarcoma in this field. This is likely due to sarcoma's heterogeneous nature and the relatively smaller number of patients it affects compared to carcinomas. However, immune checkpoint inhibitors, which have revolutionized the immunotherapy field and that have been very successful to date in melanoma (e.g. anti-CTLA4, anti-PD-1), have so far failed as monotherapies for sarcoma*(200)*.

Oncolytic viruses (OVs) constitute another form of an immunotherapy platform that has showed promising results in a broad range of cancers. OVs are engineered to take advantage of several hallmarks of cancer in order to preferentially replicate in tumor cells. Cancer-selective infection by OVs leads to cancer cell lysis and the parallel production of inflammatory cytokines, leading to innate and adaptive immune responses against both virus and tumor*(8)*. OV treatment can lead to profound anti-tumor immune responses and cures in at least a subset of patients*(36, 201)*.

Amgen's oncolytic HSV-1 was recently the first OV to be approved by the US food and drug administration (FDA) for treatment of melanoma . Following in these footsteps, a variety of OVs are being tested clinically, including and not limited to vaccinia virus, reovirus, vesicular stomatitis virus (VSV), and the closely related maraba MG1 (Marabex$^{TM}$).

Contrasting sharply with carcinoma, only few pre-clinical studies have evaluated the efficacy of OV therapies in sarcoma models. Nonetheless, several OVs have been reported to effectively infect and kill human sarcoma cells *in vitro(177–180).* When tested in animal models, OV treatment delayed sarcoma progression *(177–179, 181, 182)* and a high frequency of complete response was observed in at least some studies*(182)* .

While these studies suggest that OVs may be a promising therapeutic avenue for sarcoma, there have been to date no head-to-head comparisons between different clinically relevant OVs in the context of sarcoma. This limits our ability to evaluate which OV(s) may be the most promising to move forward in sarcoma clinical trials. Also, most studies have exclusively employed xenograft models *(177, 178),* which do not recapitulate the important role of the immune system, for better or for worse*(202)* , in the response to OV therapy. In this study, we set out to evaluate the potential of a subset of promising oncolytic viruses in parallel in the context of sarcoma cell lines and human sarcoma explants obtained following surgery. The most promising OV based on those results was subsequently tested in an immunocompetent animal sarcoma model.

## Materials and Methods

**Cells.** Human bone osteosarcoma (U2OS; 143B), human Ewing's sarcoma (RD-ES), canine osteosarcoma (D17), human synovial sarcoma (SW982), mouse sarcoma (S180), and African Green Monkey kidney (Vero) cells were from ATCC.

**Viruses.** The vaccinia virus (VV) Western Reserve strain was from Dr. McCart (Mount Sinai Hospital, Toronto, Canada)*(203)*. $WyTK^-/eGFP^+$ (VVdd) is a Wyeth VV vaccine-derived oncolytic with disruption of thymidine kinase (*TK*) and vaccinia growth factor genes, with a green fluorescent protein (GFP) transgene expressed under a synthetic early-late promoter pSE/L in *TK* locus. VSVD51-GFP (VSVD51), has been described previously*(48)*. eGFP-tagged of Maraba, MG1- eGFP (MG1), was previously described*(50)*. HSV-1 N212 expressing GFP (HSV)*(204)* was a gift from Dr. Karen Mossman (McMaster University, McMaster, Canada). Type 3 dearing reovirus (Reolysin) was a gift from Dr. Patrick Lee (Beatrice Hunter Cancer Research Institute, Halifax, Canada).

***In vitro* cytotoxicity screen.** Sarcoma cell lines (RDES; D17; SW982 and 143B) were plated in 96-well plates to a confluency of 90%. These cells were infected at log dilutions with various oncolytic virus candidates (VSVD51; MG1; HSV-1; VVdd; Reovirus (Reo)), as indicated. At 48 hours post- infection, the monolayers were washed, fixed, and stained with 1% crystal violet solution. Stained monolayers were subsequently solubilized in 1% sodium dodecyl sulfate. Absorbance was read at 595 nm to score for viable cells.

**Sarcoma animal model.** *Virus replication in vivo:* S180 ($1x10^6$) tumors were established subcutaneously in 6-week-old female Balb/C mice (*N*=10 per group). Palpable tumors formed within 11 days after seeding. MG1 was administered intra-tumoraly or intravenously ($1x10^8$pfu/mouse). *Efficacy studies:* S180 tumors were treated with 3 doses of MG1 given intra-tumorally ($1x10^8$pfu/mouse) at days 8, 10 and 13, post-tumor implantation. Tumors were measured every 2–4 days using an electronic caliper. Tumor volume was calculated as $(L_1)^2x(L_2)/2$.

**Immunohistochemistry.** Formalin-fixed S180 tumors harvested from mice treated with MG1 or with PBS were paraffin embedded and cut into 5mm sections. Sections were deparafinized with 3% H2O2 in tris buffered saline (TBS) 10 min, rinsed in TBS 5 min, blocked with universal blocking agent Background Sniper (Biocare Medical; Brampton, ON, Canada) 20 min, incubated with primary antibody rabbit anti-VSV serum (12-24 hours 4°C) in 5% normal goat serum (NGS) blocking reagent (Cell signaling Technology). Secondary antibody goat anti-rabbit IgG (Jackson ImmunoResearch Laboratory) was used in 5% NGS 1h and developed for 5 min with 3,3-Diaminobenzidine (DAB) chromatogen kit (Biocare Medical, Concord, CA). Uninfected S180 tumor tissue was used as a negative control. Slides were counterstained in hematoxylin for 1min and mounted on cover slips with permount.

***Ex vivo* infection.** Primary cancer and normal tissue specimens were obtained from consenting patients who underwent tumor resection. Samples processing has been described previously *(205)* .

**Fluorescence microscopy.**To detect GFP production from recombinant MG1, human samples of tumor or normal tissue infected *ex vivo* as described above were observed under Axiovert S100 Fluorescence microscope 24hpi (Carl Zeiss Ltd, Toronto, ON).

**Animal Care.** All animals were handled in strict accordance with good animal practice as defined by the relevant national and local animal welfare bodies, and approved by appropriate committee in collaboration with the Office of Animal Ethics and Compliance (University of Ottawa, Animal Care Committee, OGHRI-58 protocol, Dr. Jean-Simon Diallo).

**Consent for use of Human Specimens.** The institutional review board of Ottawa Hospital Research Institute approved all studies involving human tissue specimens (OHREB#2003109-01H). Declaration of Helsinki protocols were followed and patients gave their written, informed consent.

**Statistical Analysis.** Students T-test was used to assess the statistical significance of differences observed between treatment groups *in vitro* and *in vivo*. Survival studies:

Gehan-Breslow-Wilcoxon test was used to determine the statistical significance of the therapeutic effect of MG-1 compared to control. P- values $<0.05$ were considered significant.

## Results

*Oncolytic Rhabdoviruses are Effective Against Sarcoma Cell Lines in vitro.*

As a first assessment of the potential of OV candidates as treatment for sarcoma, we compared head to head five promising OV platforms for their capacity to kill sarcoma cells *in vitro*. Herpes Simplex Virus-1 (HSVN212-eGFP; *HSV*), Reovirus (Reolysin; *Reo*), Vaccinia virus (VVdd-eGFP; *VVdd*) and two Rhabdoviruses, Vesicular Stomatitis Virus (VSVD51-GFP; *VSVD51*) and Maraba virus (MG1-eGFP; *MG1*), were tested in four different sarcoma cell lines. Human osteosarcoma (143B), canine osteosarcoma (D17), human Ewing's sarcoma (RD-ES) and human synovial sarcoma (SW982) were infected in vitro with different multiplicity of infection (MOI) of each OV. EC50 (effective concentration 50%) values were then determined at 48 hours post-infection (Figure 2.1). While cell lines showed variable sensitivities to OVs, both rhabdoviruses (MG1 and VSVD51) consistently demonstrated a high potency in their ability to kill sarcoma cells. However, MG1 was slightly more effective than VSVD51 for the majority of cell lines tested (Figure 2.1a, c-e), as it required a lower multiplicity of infection (MOI) to induce more than 50% cell death. These findings are consistent with the previous report evaluating rhabdoviruses in a panel of adenocarcinoma cell lines*(50)* . Although it required a higher MOI to induce sufficient cell death than for MG1, VVdd also demonstrated potent killing ability in several sarcoma cell lines. Reovirus and HSV were only effective in RDES Ewing's sarcoma cells. Indeed, this cell line was highly sensitive to all OVs tested. In contrast, SW982 synovial sarcoma cells were the most resistant cell line to OV infection

(Figure 2.1d). D17 and 143B osteosarcoma cell lines exhibited an intermediate sensitivity to OVs (Figure 2.1e), but were mostly refractory to both HSV and Reo. These data suggests that rhabdovirus-based OV platforms are more efficient at inducing virus-mediated cell death *in vitro* in a diverse set of sarcoma cell lines.

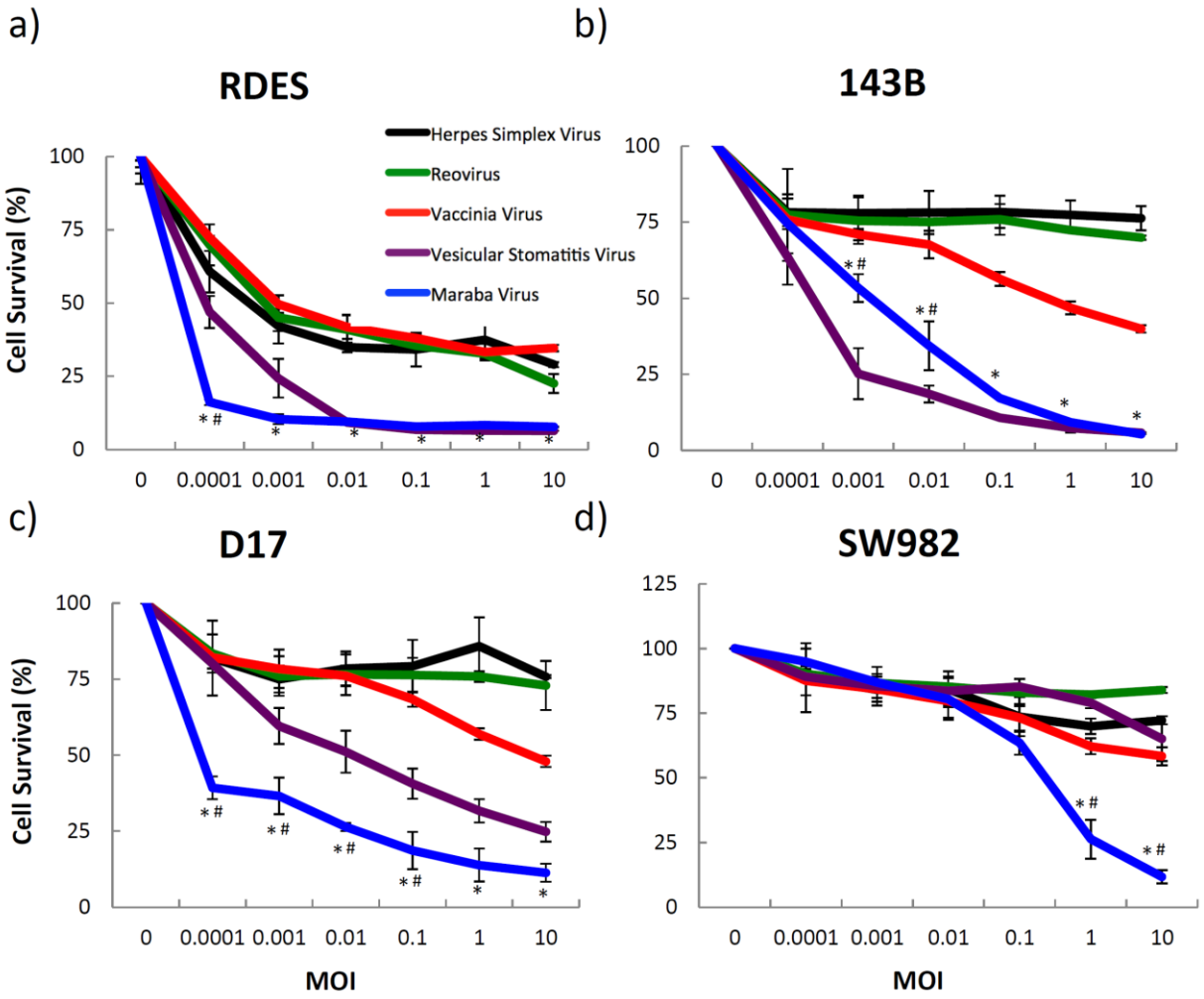


e)

| | HSV | REO | VV | VSV | MG1 |
|---|---|---|---|---|---|
| 143B Human OSA | >10 | >10 | 0.5 | 0.0005 | 0.005 |
| D17 Canine OSA | >10 | >10 | 5 | 0.01 | <0.0001 |
| RD-ES Human Ewing's Sacoma | 0.0005 | 0.0008 | 0.001 | 0.0001 | <0.0001 |
| SW982 human synovial sarcoma | >10 | >10 | 10 | >10 | 0.3 |

**Figure 2.1. Cytopathic effect of oncolytic viruses in sarcoma cells lines *in vitro*.** Sarcoma cells a) RDES, b) 143B, c) D17 and d) SW982 were plated in 96-well plates to a confluency of 90%. 24 hours later, cells were infected at log dilutions with VSVD51 (Vesicular Stomatitis Virus); MG1 (Maraba Virus); HSVN212-eGFP (Herpes Simplex Virus); VVdd (Vaccinia Virus); and Reolysin (Reovirus), as indicated. 48 hours post-infection, viable cells were assessed. Viability of cells was then plotted for each cell type relative to uninfected control. *: Statistical difference between Maraba virus and Vaccinia virus treatments. #: Statistical difference between Maraba virus and Vesicular Stomatitis virus treatments. (T-test *p-values* $< 0.05$). e) Table showing the MOI (multiplicity of infection) inducing 50% death (EC50) in 143B, RDES, D17 and SW982 cells.

*Human sarcoma specimens are susceptible to MG1 infection ex vivo.*

We next tested the ability of two of the most effective OV platforms *in vitro*, MG1 and VVdd, to productively infect human sarcoma specimens *ex vivo*. For many OV platforms, productive infection as defined by an infection that leads to release of infectious viral progeny, is considered important for the efficacy of OVs *in vivo*, particularly in the context of OVs encoding transgenes whose expression is directly linked to viral replication (e.g. rhabdoviruses) *(98, 206, 207)* . Therefore, measurement of virus replication *ex vivo* is a great alternative to assessing virus-mediated cancer cell killing since virus-induced cytotoxicity is difficult to accurately measure in live patient's specimens*(206)* . Human specimens freshly collected following surgery were processed and analyzed according to our previously published method*(205)* . Tissues that presented low viability assessed using alamar blue prior to processing were excluded from the analysis. A total of 21 specimens representing distinct sarcoma subtypes were subsequently cored and infected *ex vivo* with MG1 (Supplemental Figure 2) and 29 for VVdd (Supplemental Figure 3). Figure 2.2a shows the distribution of the sarcoma subtypes for MG-1-infected cores: osteosarcoma (OST, 29%), undifferentiated pleomorphic sarcoma (UPS, 24%), chondrosarcoma (CDS, 14%), leiomyosarcoma (LMS, 10%), rhabdomyosarcoma (RMS, 4%) and other types of sarcoma (O, 19%). Viral production was determined by plaque assay and expressed as a fold-change over input. We detected MG1 virus in 95% of the specimens tested (20 of the 21). Importantly, 86% of the samples (18 of the 21) showed productive viral replication (Figure 2.2b; virus levels exceeding that of virus input). In contrast, productive infection with VVdd was much less frequent and therefore eight additional specimens (3 UPS, 4 O and 1 RMS) were infected only with VVdd. In total, only 58%

of specimens infected with VVdd (17 of the 29) had detectable VVdd by plaque assay. Furthermore, only 24% (7 out of 29) showed evidence of productive infection that, on average, was several orders of magnitude lower than that observed for MG1 (Supplemental Figure 1). As MG1 expresses eGFP, eGFP expression was used as an additional measurement of tumor-specific OV infection in MG1- infected sarcoma or normal tissue specimens, originating from patients with diverse sarcoma etiologies. Regardless of sarcoma type, eGFP expressed from the MG1 virus was abundantly detected by fluorescent microscopy in sarcoma tissue, which corroborates and confirms our findings that MG1 productively infects sarcoma specimens (Figure 2.2c). As expected, we did not detect GFP expression in normal tissues, indicating virus replication is restricted to cancer cells. Collectively, these results suggest that MG1 is more effective than VVdd in its capacity to productively replicate in human sarcoma tissues *ex vivo*.

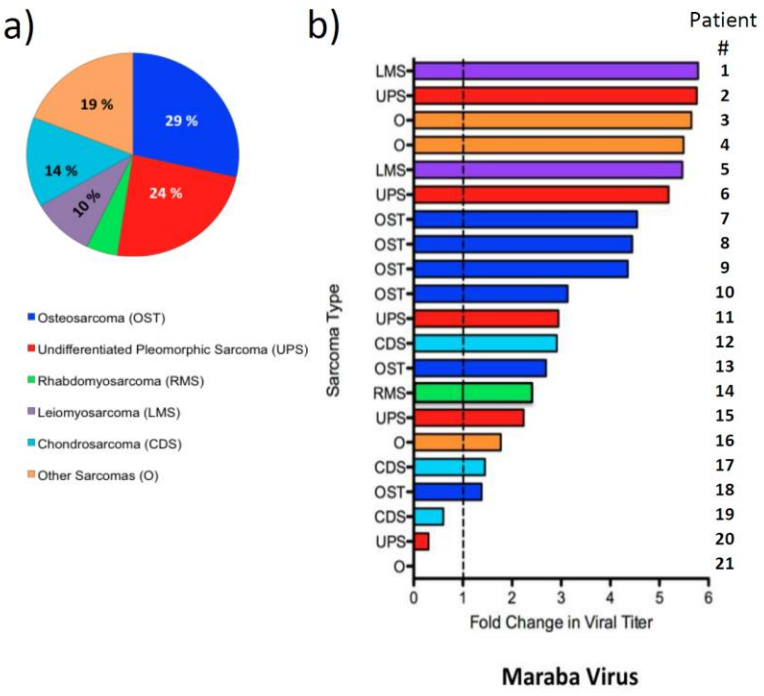
a)
b)
Patient #
19 %
29 %
14 %
10 %
24 %
Osteosarcoma (OST)
Undifferentiated Pleomorphic Sarcoma (UPS)
Rhabdomyosarcoma (RMS)
Leiomyosarcoma (LMS)
Chondrosarcoma (CDS)
Other Sarcomas (O)
Sarcoma Type
LMS 1
UPS 2
O 3
O 4
LMS 5
UPS 6
OST 7
OST 8
OST 9
OST 10
UPS 11
CDS 12
OST 13
RMS 14
UPS 15
O 16
CDS 17
OST 18
CDS 19
UPS 20
O 21
0 1 2 3 4 5 6
Fold Change in Viral Titer
Maraba Virus

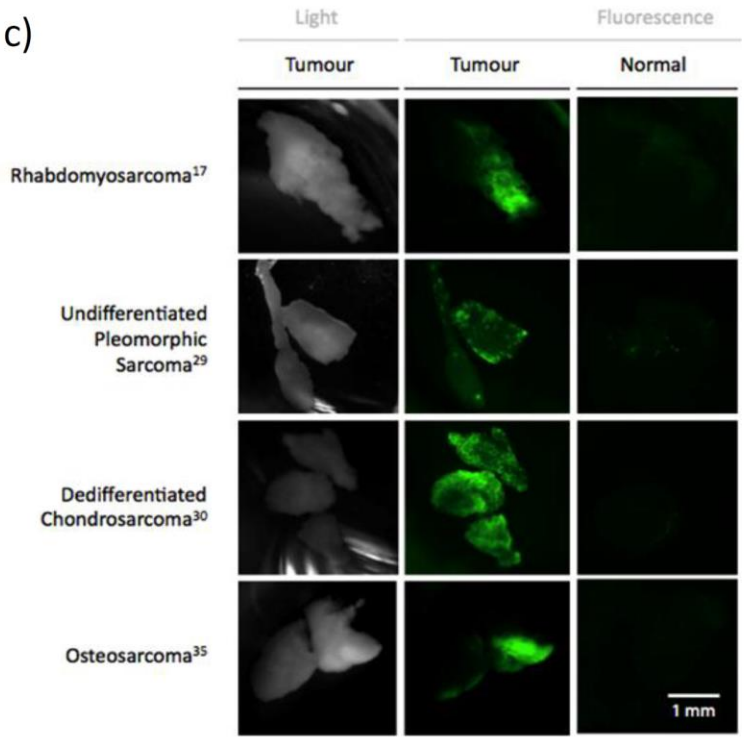
c)
Light
Fluorescence
Tumour
Tumour
Normal
Rhabdomyosarcoma[17]
Undifferentiated Pleomorphic Sarcoma[29]
Dedifferentiated Chondrosarcoma[30]
Osteosarcoma[35]
1 mm

**Figure 2.2. Productive infection of human sarcoma explants by MG1 and VV.** a) Various human sarcoma subtypes including Osteosarcoma (OST), Undifferentiated Pleomorphic Sarcoma (UPS), Rhabdomyosarcoma (RMS), Leiomyosarcoma (LMS), Chondrosarcoma (CDS) and other (O) sarcoma explants were process for *ex vivo* infection with MG1-eGFP. In percentage b) 24 hours after infection with MG1-eGFP, explants were homogenized and titered. Fold changes in viral titer compared to input virus have been plotted for each patients numerated from 1 to 21. c) Green fluorescent pictures were taken 24 hours after infection using MG1-eGFP of sarcoma tumor and normal human tissue.

*MG1 is an efficient therapeutic treatment in vivo.*

Our *in vitro* and *ex vivo* data led us to select MG1 for further *in vivo* evaluation as treatment for sarcoma. Given the potential contribution of the immune response in eliciting the anti-tumor effects of OV therapy, we tested MG1 on murine S180 metastatic sarcoma cells implanted subcutaneously in immune-competent Balb/C mice. We first tested whether MG1 could kill S180 cells in vitro (Supplemental Figure 4). Indeed we found that similarly to most human and canine cell lines, S180 cells were highly susceptible to MG1 killing (EC50 <0.0001). We subsequently tested whether MG1 could productively infect S180 tumors *in vivo* after intra- tumoral (i.t.) or intra-venous (i.v.) injection, as well as *ex vivo* in tumors collected from tumor-bearing mice (Figure 2.3). Similar to human specimens, e*x vivo* infection of tumor cores induced productive viral infection as depicted by plaque assay (Figure 2.3a) and eGFP expression (Figure 2.3b). We observed that i.v. injection of MG1 did not lead to a productive viral replication in the tumor (Figure 2.3a). However, we were able to detect virus infection after i.t. injection by both plaque assay of homogenized tumor and immunohistochemistry (Figures 2.3a and c)**.** Therefore, i.t. delivery of the virus was chosen to assess the effectiveness of MG1 to treat Balb/C mice bearing S180 sub-cutaneous sarcoma tumors. A schematic representation of the treatment regimen is showed in Figure 2.3d. Even though spontaneous remissions were observed in 40% of tumor- bearing mice injected with PBS (6/15), MG1 treatment slowed tumor progression (Figure 2.3e) and significantly increased the number of cured mice (80%, 11/15; *P-value=0.0276*; Figure 2.3f). To further investigate whether cured mice could reject new S180 tumors following S180 re- challenge, S180 tumor cells were re-implanted (day 90) on the opposite flank of cured mice from both PBS and MG1

treated groups (PBS=6; MG1=11; Figure 2.3d). While 100% of spontaneously cured mice from the PBS group developed tumors a week later, only 27% (3/11) of MG1-cured mice re-challenged with S180 cells developed tumors (Figure 2.3g) and these were smaller in size as compared to those from the PBS group (Figure 2.3h). However, similar percentage tumor take rate was observed in PBS and MG1-cured mice after challenge with syngeneic 4T1 breast cancer cells compared to naïve PBS group (Figure 2.3i). Altogether, these results suggest that MG1 delivered i.t. effectively replicates in S180 murine sarcoma tumors implanted in immunocompetent hosts, leading to eradication of 80% of tumors and protection from S180- specific re-challenge in all cured mice.

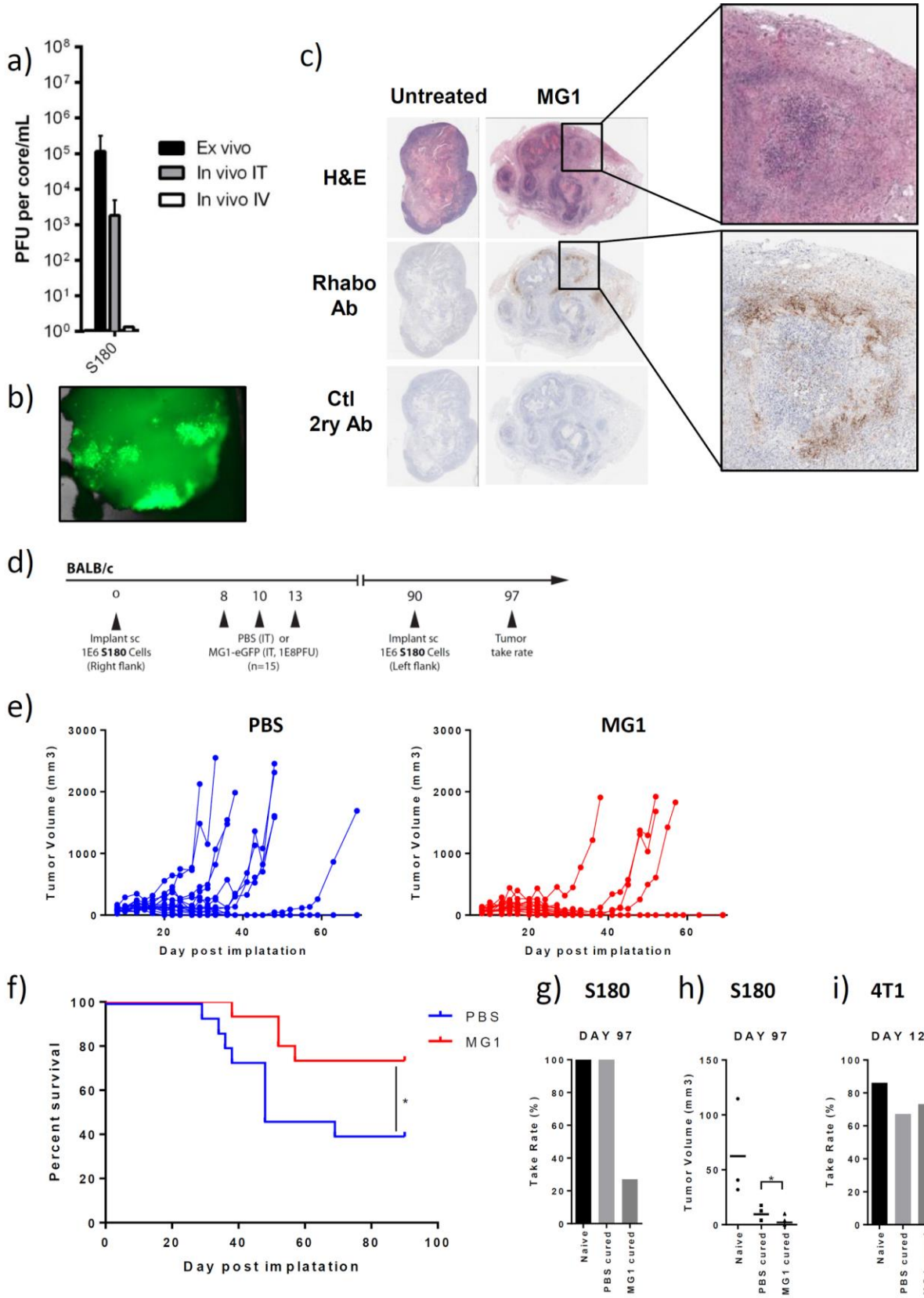
a)
PFU per core/mL
Ex vivo
In vivo IT
In vivo IV
S180
b)
c)
Untreated
MG1
H&E
Rhabo Ab
Ctl 2ry Ab
d)
BALB/c
0
8
10
13
90
97
Implant sc 1E6 S180 Cells (Right flank)
PBS (IT) or MG1-eGFP (IT, 1E8PFU) (n=15)
Implant sc 1E6 S180 Cells (Left flank)
Tumor take rate
e)
PBS
MG1
Tumor Volume (mm3)
Day post implatation
f)
Percent survival
PBS
MG1
Day post implatation
g) S180
DAY 97
Take Rate (%)
Naive
PBS cured
MG1 cured
h) S180
DAY 97
Tumor Volume (mm3)
i) 4T1
DAY 126
Take Rate (%)

**Figure 2.3. Maraba virus MG1 infects and replicates in murine sarcoma S180 tumors, leading to persistent anti-tumor effects.**

a) Murine S180 sarcoma cells were implanted sub-cutaneously in Balb/c mice ($2x10^6$cells). When tumors reached at least 5x5mm size, mice were injected with $10^8$ pfu MG1 by i.t. or i.v. route. 48 hours later, mice were sacrificed, tumors harvested, and homogenized for MG1 titration. In parallel, naïve mice were sacrificed and tumors harvested for *ex vivo* infection with MG1. 24 hours later, tumors were homogenized for MG1 titration. b) Fluorescent picture from *ex vivo* sample 24 hours after infection. c) S180 sarcoma tumor immunohistochemistry. Tumors were implanted as in a) and paraffin sections were prepared for rhabdovirus immuno-staining in untreated or MG1 treated mice. Secondary antibody staining (Ctl 2ry Ab) and Haematoxilin & Eosin stain (H&E) were used as controls Right panel shows the higher magnification of Rhabovirus immuno-staining from MG1 tumor treated mouse highlighting infected portion of the tissue as well as corresponding H&E stain. d) Schematic representation of S180 sarcoma implantation and treatment schedule. S180 were established subcutaneously in immunocompetent in Balb/c mice. All mice had palpable tumors by day 8. On day 8, 10 and 13, animals were injected i.t. with PBS or MG1 ($1x10^8$ pfu/dose). e) Plot graph representing tumor growth for each mouse corresponding to the PBS and MG1 treated groups (N=15). f) Kaplan- Meier plot outlining the time to S180 tumor endpoint (1600 $mm^3$) from experiment described in d-e). *$p$=0.0437 Log Rank test comparing MG1 to PBS. g) Cured mice from e-f) were re- challenged with S180 ($1x10^6$ cells) at day 90 and percentage take rate was plotted for day 97 (one week post re-challenge). h) Tumor size was measured at day 97 and plotted. *$p$=0.0209 two tailed t-test. i) 4T1 re-challenge percentage tumor takes rate at day 126, 10 days after tumor implantation. No significant differences were observed measured by unpaired t-test ($p$> 0.05).

## Discussion

Sarcoma currently requires a multimodal treatment approach, relying primarily upon surgical resection, with adjuvant chemotherapy and/or radiation therapy *(208)*. This aggressive approach is quite taxing for patients. Our study suggests that the oncolytic rhabdovirus MG1 has potential for the treatment of sarcoma. Among several other clinically relevant candidate OVs, MG1 was the most potent OV based on *in vitro* cell killing across a panel of four sarcoma cell lines. Close behind MG1 was VSVΔ51, another oncolytic rhabdovirus, followed by the vaccinia- based OV candidate, VVdd. However, from a heterogeneous panel of human sarcoma tissue processed *ex vivo*, we observed that MG1 outperformed VVdd in the ability to infect and replicate in tumor tissue. Overall, we found that the difference between Vaccinia and MG-1 observed in in vitro cytotoxicity assays was in line with the tissue explant viral growth data, wherein MG-1 grew more effectively than Vaccinia. However, we acknowledge there may be a number of normal cells (e.g. immune cells, endothelial cells, and cancer associated fibroblasts) that could further influence the capacity of viruses to infect tissue explants.

Lastly, using the immunocompetent murine subcutaneous S180 sarcoma model, we showed that MG1 treatment led to significantly more durable cures compared to control. Upon subsequent re-challenge with the same tumor cells, mice previously treated with MG1 were more readily protected from tumor re-growth. One caveat is that S180 tumors had a high frequency of spontaneous regression, which has

been reported by other groups *(209)*. Also given OV treatment for sarcomas would likely be assessed in the context of tumor resection, it will be interesting to pursue subsequent studies characterizing the effect of MG1 administered perioperatively following tumor resection or amputation in animal models. However, there is a general paucity in murine sarcoma models, which makes these studies challenging. Given we have shown that MG1 is effective in D17 canine sarcoma cells, a canine study would be of particular interest given the naturally high prevalence of osteosarcoma in dogs*(209)* and the similarity of clinical of disease progression and treatment in the veterinary setting.

Finally, while it seems less effective than MG1 and VSVD51, VVdd was also capable of killing sarcoma cell lines *in vitro*, and was able to infect a small proportion of *ex vivo* human sarcoma samples. However, it is unclear whether the same level of infection with VVdd is required to elicit an anti-tumor effect as compared to MG1. Our group has shown in clinical trials that intravenous injection of the vaccinia virus JX-594 ($3.10e7 pfu.Kg^{-1}$) led to replication of the virus in one patient with leiomyosarcoma, resulting in >16 weeks disease control by RECIST criteria*(201)*. Hence, this platform may merit more investigation for sarcoma treatment. Overall, our study open doors to use viral immunotherapeutic based platform to treat sarcoma. Notably, Maraba virus MG1 is clearly a promising candidate, which warrants further evaluation either alone or in a prime-boost strategy.

# Chapter 3 - Dimethyl Fumarate Potentiates Oncolytic Virotherapy through NF-kB inhibition

Mohammed Selman[1,2], Paula Ou[1,3], Christopher Rousso[1,3], Anabel Bergeron[1,3], Ramya Krishnan[1,2], Larissa Pikor[1], Andrew Chen[1], Brian A. Keller[1,2], Carolina Ilkow[1,2], John C. Bell[1,2], Jean-Simon Diallo[1,2]

[1]Centre for Innovative Cancer Research, Ottawa Hospital Research Institute, Ottawa, Ontario, Canada. [2]Department of Biochemistry, Microbiology and Immunology, University of Ottawa, Ontario, Canada. [3]Faculty of Science, University of Ottawa, Ontario, Canada

Accepted November 2017; Published Science Translational Medicine.

Contribution: MS, PO, CR, AB, RK, LP conducted in vitro experiments. MS, AC performed mouse experiments. MS, BAK processed patient tumor biopsies. BAK, CI isolated human-derived cell lines. MS, JSD participated in the conception and design of the study. MS, JSD wrote the manuscript with editorial contributions from LP, RK, BAK. JSD, JCB supervised the study.

From *M. Selman, P. Ou, C. Rousso, A. Bergeron, R. Krishnan, L. Pikor, A. Chen, B. A. Keller, C. Ilkow, J. C. Bell, J.-S. Diallo, Dimethyl fumarate potentiates oncolytic virotherapy through NF-kB inhibition. Sci. Transl. Med. 10, eaao1613 (2018).* Reprinted with permission from AAAS.

**Abstract**

Resistance to oncolytic virotherapy renders this treatment ineffective, and it is frequently associated with failure of tumor cells to get infected. Dimethyl fumarate (DMF), a common treatment for psoriasis and multiple sclerosis, has been also shown to have anticancer properties. In the present study, we show that DMF and various fumaric and maleic acid esters (FMAEs) enhance viral infection of several oncolytic viruses (OV) in cancer cell lines as well as in human tumor biopsies, improving therapeutic outcomes in resistant syngeneic and xenograft tumor models. This results in durable responses, even in models otherwise refractory to OV and drug monotherapies. The ability of DMF to enhance viral spread is due to its ability to inhibit type I IFN production and response, which is associated with its ability to block nuclear translocation of transcription factor NF-kB. This study demonstrates that unorthodox application of approved FDA drugs and biological agents can lead to improved anti-cancer therapeutic outcomes.

## Introduction

Deregulated metabolism and defective innate immune response are common characteristics of transformed cells*(74)*. This makes it possible to genetically engineer or select oncolytic viruses (OVs), which specifically infect and kill tumor cells without harming normal tissues. OVs can be generated from various viral backbones using diverse genetic approaches, and provide capacity for expressing therapeutic or imaging transgenes. Some of the early OV candidates have finally made their way to the clinic with the approval of talimogene laherparepvec (or T-Vec) based on herpes simplex virus 1 (HSV-1) for treatment of advanced melanoma *(29)*.

Pre-clinical and clinical trials have showcased the heterogeneity in the therapeutic response to OV treatment, in which a subset of patient tumors is refractory to infection with OVs *(8, 81, 84, 88)*. The identification of pharmacological agents that can functionally enhance OVs to improve therapeutic benefit has been an area of intense investigation and has been recognized as critical to maximize the therapeutic impact of OVs in the clinic *(8)*. Combination strategies with checkpoint blockade have shown promise recently *(30, 210, 211)* but do not address the frequent resistance of tumors to viral infection. To this end, strategies aiming to suppress antiviral immune responses, for example using immunosupressants such as cyclophosphamide, rapamycin, and histone deacetylase inhibitors, have shown promise in vitro but variable effects in animal models *(108, 186–188)*. Combinations of OVs with cyclophosphamide in particular are under clinical evaluation, with favorable safety profiles reported thus far (NCT01598129).

Fumaric acid esters (FAE) are a class of compounds with known anti-inflammatory and neuroprotective effects *(126, 189, 190)*. The mechanisms involved have yet to be fully elucidated but are thought to be mediated through the activation of the antioxidative transcription factor nuclear factor (erythroid-derived 2)-like 2 (NRF2) pathway*(189)*, the inhibition of NF-κB *(212)*, as well as functional depletion of glutathione (GSH)*(213, 214)*. FAEs (marketed as Fumaderm, Psorinovo) were first approved as a treatment for psoriasis in Germany. Recently, dimethyl fumarate (DMF), an FAE marketed as Tecfidera, was approved by the U.S. Food and Drug Administration (FDA) and the European Medicines Agency for the treatment of relapsing forms of multiple sclerosis and relapsing-remitting multiple sclerosis *(191)*. Clinical studies on the long-term use of DMF have not revealed any severe long-term adverse effects *(191, 192, 215)*. Recent reports suggest that DMF has anticancer potential, shown to suppress tumor growth and metastasis *(141, 144, 149–151, 216)* in addition to sensitizing tumors to chemotherapy*(144, 145)*. Furthermore, DMF is currently under clinical evaluation for the treatment of chronic lymphocytic leukemia and cutaneous T cell lymphoma (NCT02546440, NCT02784834). Given this and the documented positive effect of diverse immunosuppressants in combination with OVs, we set out to explore the possibility of using DMF in combination with oncolytic virotherapy in vitro and in vivo.

## Results

*Dimethyl fumarate enhances tumor-specific viral spread and oncolysis in vitro*

Little is known about the effect of DMF on viral infection. We first examined the impact of DMF (structure displayed in Figure 3.1A) on the growth of oncolytic vesicular stomatitis virus (VSVΔ51). Notably, VSV and closely related Maraba are currently undergoing clinical evaluation but face resistance to infection in approximately a third of cancers *(48, 88)*. 786-0 renal carcinoma cells are highly refractory to VSVΔ51 infection, however, a 4 hour pretreatment with DMF at doses between 50 and 200 μM increased VSVΔ51 virus growth at a low multiplicity of infection (MOI) by more than 100-fold (Figure 3.1B). Virus-encoded GFP expression was also greatly enhanced, as visualized by microscopy (Figure 3.1C). This effect was observed with pretreatment times up to 24 hours before infection, and after infection up to 8 hours (Supplemental Figure 1A). More broadly, DMF robustly enhanced infection in a panel of human and murine cancer cell lines (sarcoma, osteosarcoma, breast, colon, melanoma, ovarian) with a wide range of sensitivity to VSVΔ51 (Figure 3.1D). DMF also improved viral output of Sindbis virus and oncolytic herpes virus (HSV-1 mutant N212) after treatment in 786-0 cells (Figure 3.1, E and F). Furthermore, we also tested the effect of DMF on adenoviruses, which in addition to oncolytic virotherapy have been extensively used as gene therapy vectors *(217)*. Pretreatment of human lung adenocarcinoma A549 cells with DMF increased luciferase transgene expression of non-replicating adenovirus, E1A-deleted Ad5, over the course of 7 days by up to 20-fold (Figure 3.1G).

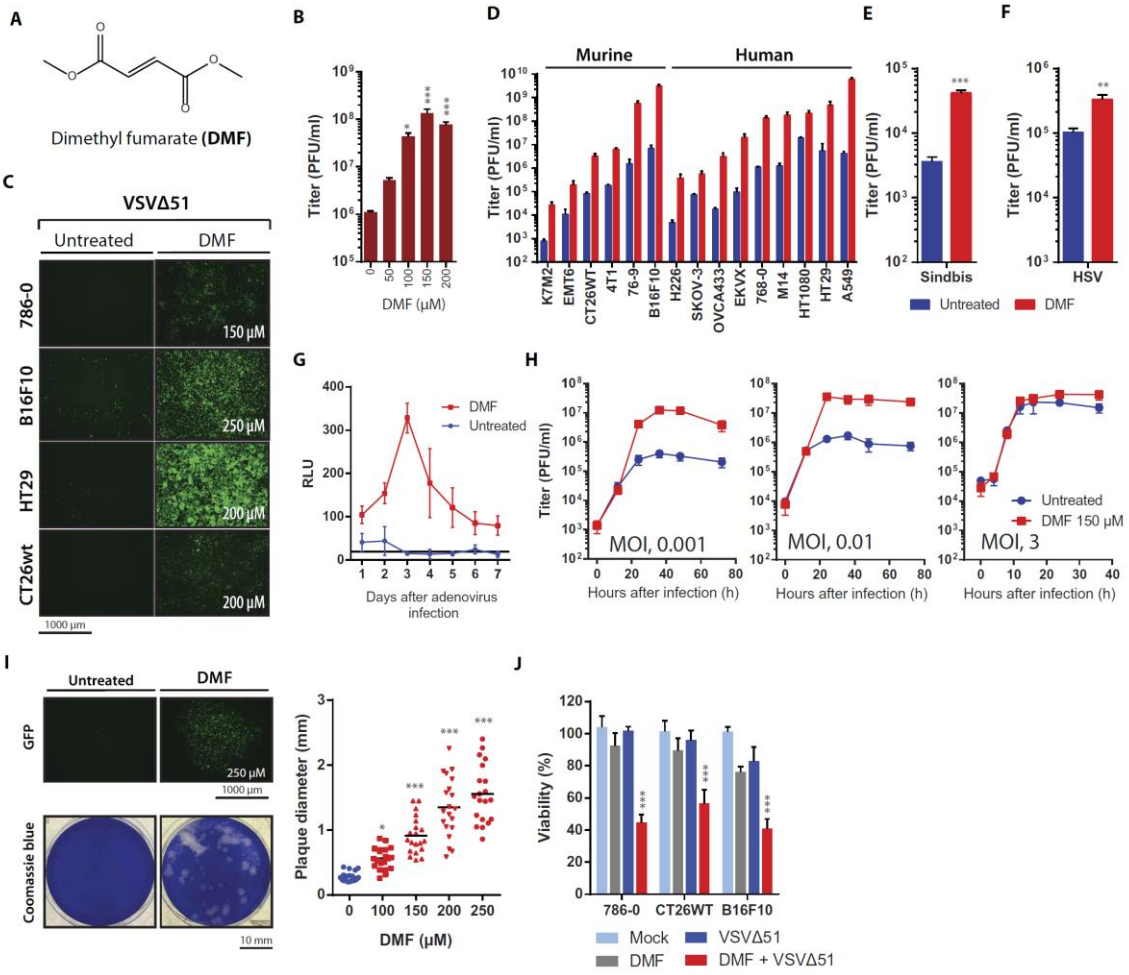
A
Dimethyl fumarate (DMF)
B
Titer (PFU/ml)
DMF (μM)
C
VSVΔ51
Untreated
DMF
786-0
B16F10
HT29
CT26wt
150 μM
250 μM
200 μM
200 μM
1000 μm
D
Murine
Human
K7M2
EMT6
CT26WT
4T1
76-9
B16F10
H226
SKOV-3
OVCA433
EKVX
768-0
M14
HT1080
HT29
A549
E
Sindbis
F
HSV
Untreated
DMF
G
RLU
DMF
Untreated
Days after adenovirus infection
H
Titer (PFU/ml)
MOI, 0.001
MOI, 0.01
MOI, 3
Hours after infection (h)
Untreated
DMF 150 μM
I
Untreated
DMF
GFP
250 μM
1000 μm
Coomassie blue
10 mm
Plaque diameter (mm)
DMF (μM)
J
Viability (%)
786-0
CT26WT
B16F10
Mock
DMF
VSVΔ51
DMF + VSVΔ51

**Figure 3.1**. **Dimethyl fumarate promotes viral infection.** (**A**) Structure of dimethyl fumarate. (**B**) VSVΔ51 resistant human renal cancer cell lines 786-0 were pretreated with DMF or left untreated for 4 hours and subsequently infected with VSVΔ51 (MOI: 0.01). Corresponding viral titers were determined 48 hours after infection from supernatants (n=3; mean +/- SD, one-way ANOVA; * $p<0.05$, *** $p<0.001$, as compared to the untreated condition). (**C,D**) Various human and murine cell lines were pretreated with DMF (150-250 μM) or left untreated for 4 hours and subsequently infected with VSVΔ51 (MOI: 0.01). 24 hours after infection, fluorescent images were taken of the infected cancer cells as shown in panel **C**. Corresponding viral titers were determined 48 hours after infection from supernatants, as shown in **D** (n=3-4; mean +/- SD, 2-tailed t-test; $p<0.05$ as compared to the untreated counterpart for each cell line). (**E,F**) 786-0 cells were pretreated with DMF (150 μM) or left untreated for 4 hours and subsequently infected with (**E**) Sindbis (MOI:10) or (**F**) HSV-1 (MOI: 0.01). Corresponding viral titers in supernatants were determined 48 hours after infection. (n=3; mean +/- SD, 2-tailed t-test; ** $p<0.01$, *** $p<0.001$ as compared to the untreated counterpart). (**G**) Human A549 cells were pretreated as in (**B**) and infected with an adenovirus expressing firefly luciferase (Ad5) at an MOI of 1. Luciferase activity was measured over the course of 7 days. Results are represented as relative light units (RLU), and background is indicated by a black line (n=3; mean +/- SD; $p<0.05$ by two-way ANOVA from day 2 to 5). (**H**) Multi-step (MOI: 0.001 and 0.01) and single-step (MOI: 3) growth curves. 786-0 cells were pretreated with DMF and infected with VSVΔ51 at MOI 0.001, 0.01, or 3; supernatants were titered by plaque assay (n=3; mean +/- SD). (**I**) 786-0 cells were pretreated with DMF for 4 hours and infected with VSVΔ51 (MOI: 0.0001). An agarose overlay was added after 1 hour of infection. Fluorescence microscopy of a representative plaque 48 hours after infection. The complete dose range is presented in Supplemental Figure 1B. Corresponding images of coomassie blue stain of the full wells and the graph of average plaque diameters illustrate the enhancement of the plaque diameters in presence of DMF (n=20; horizontal lines indicate means; one-way ANOVA; * $p<0.05$, *** $p<0.001$, as compared to the mock-treated counterpart). (**J**) 786-0, CT26WT, and B16F10 cell lines were pretreated and infected as in (**B**). Cell viability was assayed 48 hours after infection. Results were normalized to the average of the values obtained for the corresponding uninfected, untreated cells (n=8; mean +/- SD; ***$p<0.001$ by one-way ANOVA; as compared to VSVΔ51 condition).

Single and multi-step growth curves performed in 786-0 cells revealed that DMF enhanced the viral output of VSVΔ51 when using a low MOI, but not when using a high MOI (Figure 3.1H), indicating DMF inhibits mechanisms that impinge on viral spread rather than virus output per infected cell. To further explore the effect of DMF on virus spreading, 786-0 cell monolayers were infected with VSVΔ51 and overlaid with agarose to generate defined plaques of virus replication foci. DMF substantially increased the average plaque diameter of VSVΔ51 on fluorescent imaging and Coomassie Blue staining of infected cell monolayers (Figure 3.1I and Supplemental Figure 1B). To further assess the oncolytic effect of VSVΔ51 in the presence of DMF, we pretreated cancer cells with DMF before infection with VSVΔ51 at a low MOI, and cell viability was assessed with the metabolic dye alamarBlue, 48 hours after infection. Combined treatment with DMF and VSVΔ51 resulted in a decrease in cell viability in human 786-0 as well murine CT26WT and B16F10 cells (Figure 3.1J).

We further assessed the ability of DMF to enhance VSVΔ51 infection ex vivo in mouse-derived tissues. Tumor cores from mice subcutaneously implanted with CT26WT murine colon cancer cells or B16F10 murine melanoma cells, as well as cores from normal lung, muscle, and spleen were collected and subsequently infected with VSVΔ51-GFP in the presence or absence of 150 μM DMF. DMF robustly increased the growth of the virus in CT26WT and B16F10 cores by 31-fold and 13-fold, respectively, but did not increase virus growth in normal tissue cores (Figure 3.2A). Furthermore, DMF increased VSVΔ51 infection by > 10-fold ex vivo in primary human melanoma, lung, prostate, and

ovarian tumor samples, as observed by plaque assay and microscopy (Figure 3.2, B and C), as well as in various melanoma and ovarian patient-derived cancer cell lines (Figure 3.2D). Similar to the murine normal tissue cores, DMF did not promote virus growth in human normal lung and muscle tissues from various patients (Figure 3.2E).

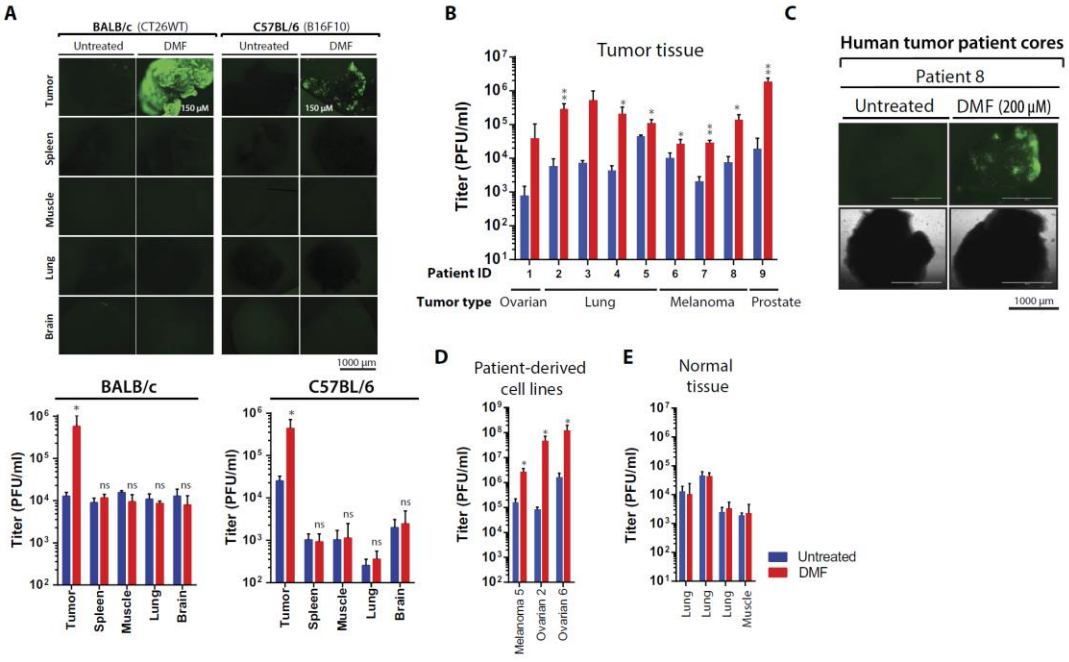
A
BALB/c (CT26WT)
C57BL/6 (B16F10)
Untreated
DMF
Tumor
Spleen
Muscle
Lung
Brain
150 µM
1000 µm
B
Tumor tissue
Titer (PFU/ml)
Patient ID
Tumor type
Ovarian
Lung
Melanoma
Prostate
C
Human tumor patient cores
Patient 8
Untreated
DMF (200 µM)
1000 µm
BALB/c
C57BL/6
Titer (PFU/ml)
Tumor
Spleen
Muscle
Lung
Brain
ns
D
Patient-derived cell lines
Melanoma 5
Ovarian 2
Ovarian 6
E
Normal tissue
Lung
Muscle
Untreated
DMF

**Figure 3.2**. **Dimethyl fumarate enhances infection ex vivo and in human clinical samples.** (**A**) CT26WT and B16F10 tumors were grown subcutaneously in BALB/c and C57BL/6 mice, respectively, and excised. BALB/c and C57BL/6 mouse spleens, muscles, lungs, and brain tissue were also collected and cored. Tumor and normal tissue cores were pretreated with 150 μM of DMF for 4 hours and subsequently infected with $1x10^4$ PFU of oncolytic VSVΔ51 expressing GFP. 24 hours after infection, fluorescent images were acquired for the tumor or normal tissue cores. Representative images from each triplicate set are shown in the upper panel. Viral titers from supernatant were determined 48 hours after infection and are shown in the lower panel (n=3-4; mean +/- SD; 2-tailed t-test; ns, not significant; * $p<0.05$, as compared to the untreated counterpart). (**B**) Indicated human tumor tissues were treated with DMF for 4 hours and subsequently infected with $1x10^4$ PFU of VSVΔ51 expressing GFP. Viral titers were determined 48 hours after infection (n=3-4; mean +/- SD; 2-tailed t-test; * $p<0.05$, ** $p<0.01$ as compared to the untreated counterpart). (**C**) Representative fluorescent and brightfield images are shown for patient 8. (**D**) Patient-derived cell lines were treated with DMF for 4 hours and subsequently infected with an MOI of 0.01 of oncolytic VSVΔ51 expressing GFP. Corresponding viral titers were determined 48 hours after infection (n=3; mean +/- SD; 2-tailed t-test; * $p<0.05$, as compared to the untreated counterpart). (**E**) Human normal tissue was treated as in **B** (n=3-4; mean +/- SD; 2-tailed t-test).

In addition to DMF, various fumaric and maleic acid esters (FMAEs) exhibit antiinflammatory and immunomodulatory properties *(218)*. We therefore tested whether other FAEs and their cis- and trans-isoforms (maleic acid esters) (Figure 3.3, A and B) have a similar impact to DMF on viral infection of cancer cells. Indeed, the cell-permeable FAE diethyl fumarate (DEF), and maleic acid esters dimethyl maleate (DMM) and diethyl maleate (DEM) robustly enhanced VSVΔ51infection, spread, and oncolysis in 786-0 and CT26WT cells in vitro (Figure 3.3C, Supplemental Figure 2 and S3). Enhanced infection was also observed with FMAEs in CT26WT tumor cores infected ex vivo (Figure 3.3D). DMF is rapidly hydrolyzed to monomethyl fumarate (MMF) by esterases in vivo, and subsequently to fumaric acid (FA) (as displayed in Figure 3.3B)*(219)*. Indeed, MMF is thought to be the active metabolite of DMF in the treatment of multiple sclerosis*(219)*. In 786-0 cells, MMF also enhanced infection of VSVΔ51 to a similar extent as DMF, albeit at higher effective doses. Fumaric acid (FA), in contrast with the cell-permeable esters MMF and DMF, had no impact on viral growth (Figure 3.3C, Supplemental Figure 2). Taken together, our data indicate that DMF and other cell-permeable FMAEs can dramatically enhance the spread of OVs in both mouse and human cell lines and cancer tissue explants.

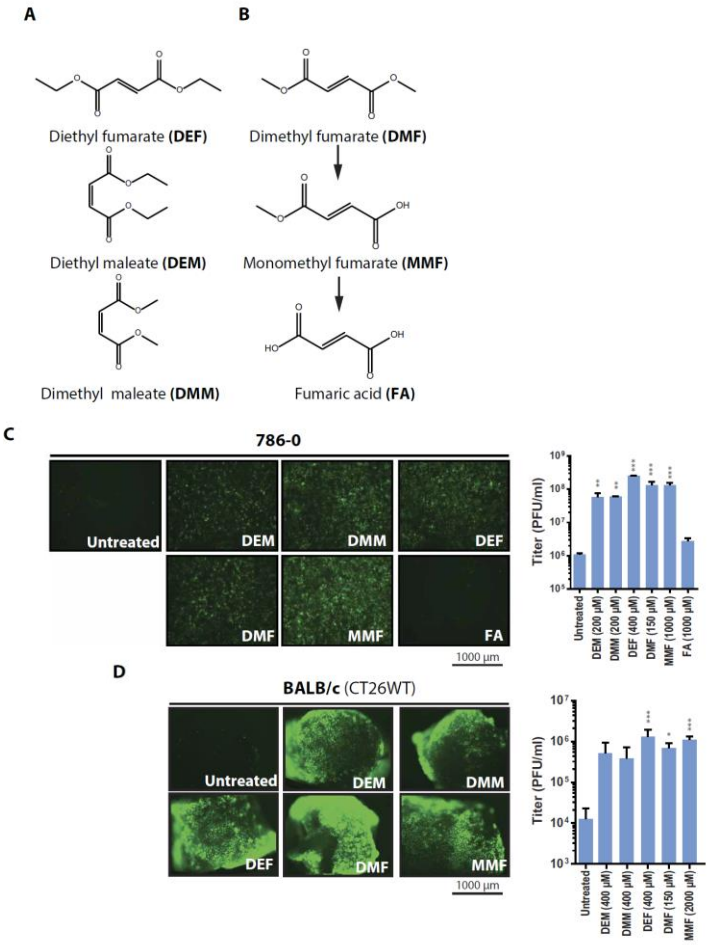
A
B
Diethyl fumarate (DEF)
Dimethyl fumarate (DMF)
Diethyl maleate (DEM)
Monomethyl fumarate (MMF)
Dimethyl maleate (DMM)
Fumaric acid (FA)
C
786-0
Untreated
DEM
DMM
DEF
DMF
MMF
FA
1000 µm
Titer (PFU/ml)
Untreated
DEM (200 µM)
DMM (200 µM)
DEF (400 µM)
DMF (150 µM)
MMF (1000 µM)
FA (1000 µM)
D
BALB/c (CT26WT)
Untreated
DEM
DMM
DEF
DMF
MMF
1000 µm
Titer (PFU/ml)
Untreated
DEM (400 µM)
DMM (400 µM)
DEF (400 µM)
DMF (150 µM)
MMF (2000 µM)

**Figure 3.3. Fumaric and maleic acid esters promote infection by VSVΔ51.** (**A**) Structures of fumaric acid esters (DEF) and maleic acid esters (DEM, DMM) are presented. (**B**) Metabolism of DMF. DMF is hydrolyzed into monomethyl fumarate (MMF), which in turn is metabolized into fumaric acid (FA). FA subsequently enters the TCA cycle. (**C**) 786-0 cells or (**D**) CT26WT ex vivo tumor cores were pretreated with various FMAEs and analogues for 4 hours, and subsequently infected with oncolytic VSVΔ51 expressing GFP at (**C**) an MOI of 0.01 or (**D**) $1x10^4$ PFU. 24 hours after infection, we obtained fluorescent images of the infected 786-0 cells or CT26WT tumor cores. Corresponding viral titers were determined from supernatants 48 hours after infection (n=3; mean +/- SD; one-way ANOVA; * $p<0.05$, ** $p<0.01$, *** $p<0.001$, as compared to the untreated counterpart).

*Dimethyl fumarate improves therapeutic efficacy of oncolytic rhabdoviruses*

Because DMF is a clinically approved drug and it broadly and robustly enhanced the growth and activity of VSVΔ51 in vitro in both human and mouse tumor explants, and did so preferentially in tumors opposed to normal tissues, we next evaluated the potential therapeutic benefit of combining DMF with oncolytic VSVΔ51 in vivo. To this end, we used both syngeneic and xenograft mouse tumor models, in which VSVΔ51 is ineffective as a monotherapy *(119, 220–222)*. Mouse CT26WT and B16F10 and human colon cancer HT29 cells were grown subcutaneously in Balb/c, C57BL/6, or nude mice, respectively. Mice were injected intratumorally with DMF for 4 hours, and subsequently infected with VSVΔ51 expressing luciferase. With the exception of the B16F10 model, DMF enhanced virus-associated luciferase gene expression specifically in tumors 24 hours after the first injection of virus, as assessed using an in vivo imaging system (IVIS) (Figure 3.4, A and B). In all three models, the combination therapy considerably delayed tumor progression (Figure 3.4C, table S1) and significantly prolonged survival compared with either monotherapy (combination therapy compared to VSVΔ51 alone; CT26WT: p=0.0008; B16F10: p=0.0039; HT29: p=0.0003) (Figure 3.4D). The combination therapy produced complete remission in approximately 20% of the mice in both the CT26WT and B16F10 models. The cured CT26WT-bearing mice that had received the combination regimen subsequently became immune to re-challenge with the same cancer cells (Figure 3.4E). However, when cured CT26WT-bearing mice were challenged with a foreign tumor (murine 4T1 breast cancer), cured CT26WT mice grew 4T1 tumors at a similar rate as the naive mice (Figure 3.4F). Altogether, these results indicate the effective generation of a specific and long-lasting anti-tumor immunity.

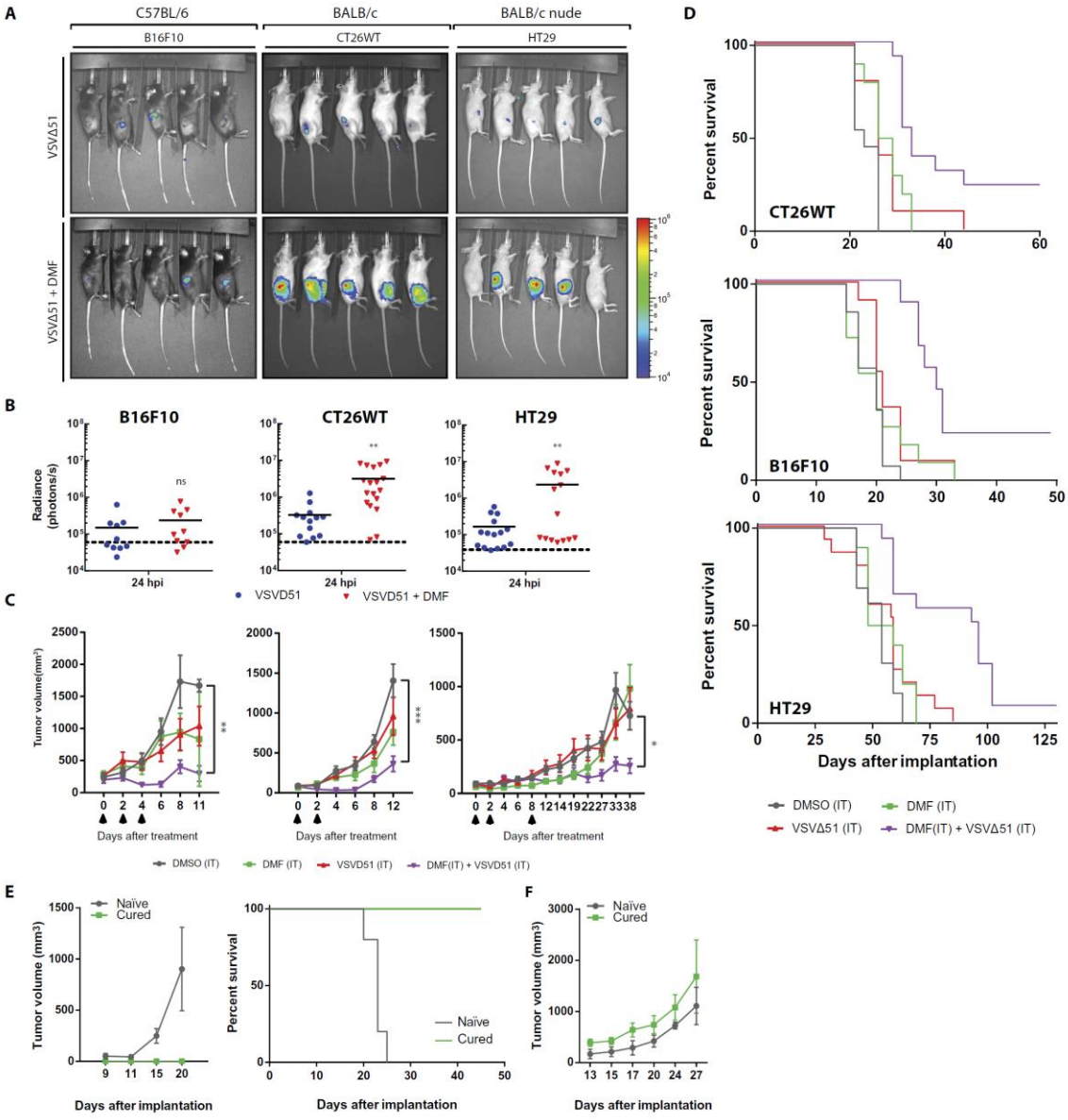
A
C57BL/6
BALB/c
BALB/c nude
B16F10
CT26WT
HT29
VSVΔ51
VSVΔ51 + DMF
B
B16F10
CT26WT
HT29
Radiance (photons/s)
ns
**
24 hpi
VSVD51
VSVD51 + DMF
C
Tumor volume(mm³)
Days after treatment
DMSO (IT)
DMF (IT)
VSVD51 (IT)
DMF(IT) + VSVD51 (IT)
D
Percent survival
CT26WT
B16F10
HT29
Days after implantation
DMSO (IT)
DMF (IT)
VSVΔ51 (IT)
DMF(IT) + VSVΔ51 (IT)
E
Naïve
Cured
Tumor volume (mm³)
Percent survival
Days after implantation
F
Naïve
Cured
Tumor volume (mm³)
Days after implantation

**Figure 3.4**. **Dimethyl fumarate enhances VSVΔ51 therapeutic efficacy in syngeneic and xenograft tumor models. (A-D)** CT26WT, B16F10, and HT29 tumor-bearing mice were treated intratumorally with the vehicle (DMSO) or 50 (B16F10) or 200 (CT26WT and HT29) mg/kg of DMF for 4 hours, and subsequently injected with $1x10^8$ PFU of oncolytic VSVΔ51 expressing firefly luciferase or the vehicle (PBS), intratumorally. The treatment was administered twice or three times, as indicated by arrows in panel **C**. 24 hours after infection, viral replication was monitored. (**A**) Representative bioluminescence images of mice. (**B**) Quantification of luminescence in photons/sec (n=10-18; horizontal lines indicate means; ns, not significant; **p < 0.01 by 2-tailed t-test, as compared to VSVΔ51 infected condition; dashed lines represent average background intensity). (**C**) Tumor volume (n=9-15; data shown as mean ± SEM; SD values are indicated in table S1; *p < 0.05, ** p<0.01, ***p<0.001 by two-way ANOVA; comparing DMF+VSVΔ51 to DMSO alone). (**D**) Survival was monitored over time. Log-rank (Mantel-Cox) test indicates that the combined treatment significantly prolonged survival over VSVΔ51 alone (CT26WT: n=10-13, p=0.0008; B16F10: n=9-14, p=0.0039; HT29: n=10-15, p=0.0003). (**E**) Tumor volume and survival were monitored after re-implantation of CT26WT in cured and naïve mice from **D** (n=3-5, mean +/- SD). (**F**) Tumor volume was monitored after implantation of 4T1 cells in CT26WT-cured and naïve mice (n=3, mean +/- SD).

*Fumaric and maleic acid esters inhibit the antiviral response*

To gain further insight into the possible mechanism mediating the enhancement of OVs by DMF and other FMAEs, microarray gene expression analysis was performed on 786-0 cells 24 hours after infection with VSVΔ51 in the presence or absence of DMF, DEM, DEF, or DMM. DMF-treated cells had a similar gene expression profile to cells treated with the other FMAEs tested (Supplemental Figure 4A). Upon infection with VSVΔ51, multiple antiviral genes were up-regulated as expected; however, DMF led to the inhibition of many of these (*IFITIM1*, *MX2*, *GBP4*, *IFI27*, *IFNA*, *CXCL10*), and upregulated various genes, including a number of redox response genes (*CYP4F11, CDK5RAP2, ANXA10 HMOX1, OSGIN1, TXNRD1, AKR1B10, AKR1B15, AKR1C1, AKR1C2*) (Figure 3.5A and B). GOterm analysis revealed that FMAE treatment of infected 786-0 cells inhibited the response to virus as well as type I IFN signaling (Figure 3.5C, Supplemental Figure 4B ). Consistent with repression of the type I IFN response, DMF decreased activation (phosphorylation) of both STAT1 and STAT2, 24 hours after infection (Figure 3.5D). Additionally, the expression of the antiviral protein IFITM1 was potently repressed by DMF, whereas the VSV viral proteins were increased (Figure 3.5E). Furthermore, DMF enhanced infection of VSVΔ51, but it had no impact on infection of 786-0 cells by wild-type VSV (wtVSV) (Figure 3.5E). Unlike VSVΔ51, wtVSV robustly inhibits Type I IFN production*(48),* and therefore we would expect the effect of DMF to be redundant in the context of wtVSV if a Type I IFN response is indeed involved in eliciting the pro-viral effects of DMF.

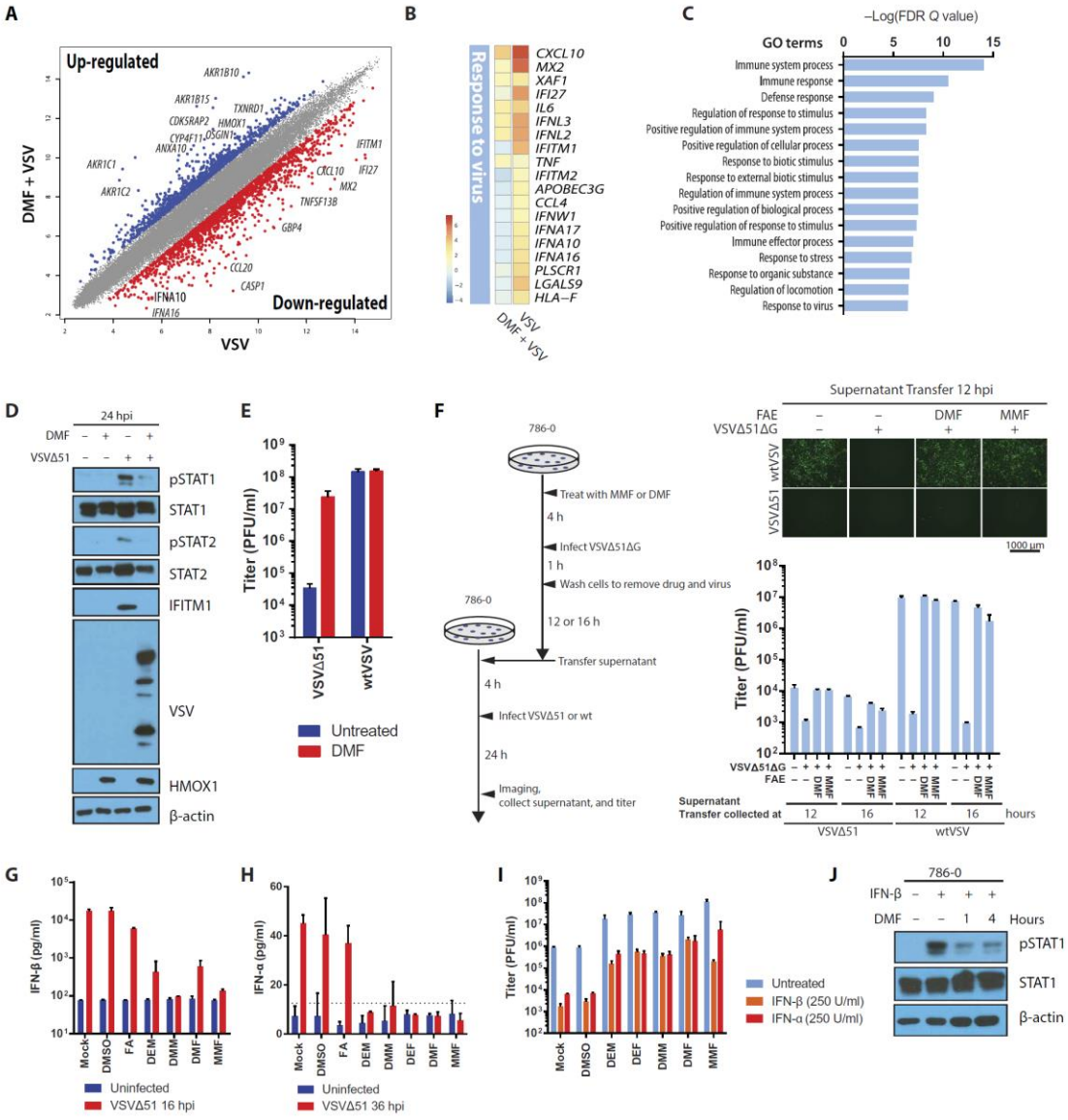
A
Up-regulated
Down-regulated
DMF + VSV
VSV
AKR1B10
AKR1B15
TXNRD1
CDKSRAP2
HMOX1
CYP4F11
OSGIN1
ANXA10
AKR1C1
AKR1C2
IFITM1
CXCL10
IFI27
MX2
TNFSF13B
GBP4
CCL20
CASP1
IFNA10
IFNA16
B
Response to virus
CXCL10
MX2
XAF1
IFI27
IL6
IFNL3
IFNL2
IFITM1
TNF
IFITM2
APOBEC3G
CCL4
IFNW1
IFNA17
IFNA10
IFNA16
PLSCR1
LGALS9
HLA–F
VSV
DMF + VSV
C
–Log(FDR Q value)
GO terms
0
5
10
15
Immune system process
Immune response
Defense response
Regulation of response to stimulus
Positive regulation of immune system process
Positive regulation of cellular process
Response to biotic stimulus
Response to external biotic stimulus
Regulation of immune system process
Positive regulation of biological process
Positive regulation of response to stimulus
Immune effector process
Response to stress
Response to organic substance
Regulation of locomotion
Response to virus
D
24 hpi
DMF
VSVΔ51
pSTAT1
STAT1
pSTAT2
STAT2
IFITM1
VSV
HMOX1
β-actin
E
Titer (PFU/ml)
VSVΔ51
wtVSV
Untreated
DMF
F
786-0
Treat with MMF or DMF
4 h
Infect VSVΔ51ΔG
1 h
Wash cells to remove drug and virus
12 or 16 h
Transfer supernatant
4 h
Infect VSVΔ51 or wt
24 h
Imaging,
collect supernatant, and titer
Supernatant Transfer 12 hpi
FAE
VSVΔ51ΔG
DMF
MMF
wtVSV
VSVΔ51
1000 μm
Titer (PFU/ml)
Supernatant
Transfer collected at
12
16
12
16
hours
VSVΔ51
wtVSV
G
IFN-β (pg/ml)
Mock
DMSO
FA
DEM
DMM
DMF
MMF
Uninfected
VSVΔ51 16 hpi
H
IFN-α (pg/ml)
Mock
DMSO
FA
DEM
DMM
DEF
DMF
MMF
Uninfected
VSVΔ51 36 hpi
I
Titer (PFU/ml)
Mock
DMSO
DEM
DEF
DMM
DMF
MMF
Untreated
IFN-β (250 U/ml)
IFN-α (250 U/ml)
J
786-0
IFN-β
DMF
Hours
pSTAT1
STAT1
β-actin

**Figure 3.5**. **FMAEs inhibit antiviral cytokine production and response to type I interferon.** (**A-C**) Lysates of 786-0 cells treated with FMAEs and infected with VSVΔ51 expressing GFP were collected at 24 hpi, and RNA or protein was extracted. (**A**) Scatter plot showing the expression of all genes in infected 786-0 in the presence (y-axis) or absence (x-axis) of DMF. Blue dots represent genes upregulated by DMF during infection, red dots represent genes downregulated by DMF during infection. (**B**) Heatmap showing the expression of the differentially expressed genes belonging to the "response to virus" GO term. (**C**) List of top GO terms downregulated by FMAEs during viral infection. (**D**) Lysates of 786-0 cells, treated with DMF (150 μM) and infected with VSVΔ51 expressing GFP or left untreated, were collected at 24 hpi and probed for indicated proteins by western blot. (**E**) 786-0 cells were pretreated for 4 hours with DMF (150 μM) or mock treated and infected with VSVΔ51 or wtVSV (MOI: 0.01). Corresponding viral titers were determined from supernatants 48 hours after infection (n=3; mean +/- SD). (**F**) 786-0 cells were treated with DMF (150 μM), MMF (1500 μM), or mock treated for 4 hours and infected with VSVΔ51ΔG at MOI 1. 12 or 16 hpi, supernatants were collected and used to precondition 786-0 cells for 4 hours, and then the cells were infected with VSVΔ51 or wtVSV. Corresponding viral titers were determined 24 hours after infection from supernatants (n=3; mean +/- SD). Representative fluorescent images are shown. (**G-H**) 786-0 cells were treated as in (**A**). (**G**) At 16 hpi, supernatants were collected and assayed by ELISA for IFNβ (n=3; mean +/- SD). (**H**) At 36 hpi, supernatants were collected and assayed by ELISA for IFNα (n=3; mean +/- SD). (**I**) 786-0 cells were treated with FMAEs for 6 hours and with IFNβ or IFNα for 4 hours, and subsequently infected with VSVΔ51 at MOI 0.1. Corresponding viral titers were determined from supernatants 48 hours after infection (n=3; mean +/- SD). (**J**) 786-0 cells were pretreated with 200 μM of DMF for 1 or 4 hours and treated with IFNβ (250 U/ml) for 30 minutes, or left untreated. Cell lysates were extracted and probed for pSTAT1, STAT1, and β-actin by western blot.

To gain mechanistic insight into the effect of FMAEs on the antiviral response, we examined their ability to protect against virus challenge and IFN-mediated antiviral signaling. After treatment with FMAEs (or mock), we infected cells with a spread-deficient version of VSVΔ51 that does not encode the viral G protein (glycoprotein responsible for virus budding, host cell binding, and virus entry; VSVΔ51ΔG) to suppress formation of de novo virions*(223)*. Cell supernatants were collected 12 or 16 hour post infection (hpi), and used to pretreat target cells before infection with VSVΔ51 or wtVSV. Our results show that while the supernatant of cells infected with VSVΔ51ΔG could protect against subsequent viral infection with VSVΔ51 or wtVSV, the addition of DMF or MMF was able to completely overcome this suppressive effect for both VSVΔ51 and wtVSV (Figure 3.5F). Indeed, we observed through ELISA a decrease in the production of IFNβ and IFNα after infection in the presence of FMAEs (Figure 3.5, G and H). Furthermore, treatment of cells with DMF and other FMAEs antagonized the antiviral effects of Type I IFN pretreatment on VSVΔ51 infection (Figure 3.5I). Taken together, these data suggest that FMAEs affect antiviral signaling by repressing production of Type I IFN and downstream signaling through the JAK-STAT pathway. Consistent with this, Western blotting revealed that in cells conditioned with IFNβ at the doses which inhibit VSVΔ51 infection, DMF and DEM inhibited STAT1 phosphorylation, which is involved in transcription and response to type I IFN after viral infection (Figure 3.5J and Supplemental Figure 4C).

*Fumaric and maleic acid esters promote infection through NF-κB inhibition independently of GSH depletion*

Although our data clearly implicated an effect of multiple FMAEs on the antiviral response, the molecular chain of events leading to these effects remained unclear. DMF, DEM, DEF, and MMF share a common α,β-unsaturated carbon, which is attacked by GSH in a Michael addition reaction and which is implicated in the capacity of these compounds to deplete cellular GSH and activate the antioxidant response *(224)*. We therefore tested the impact of dimethyl succinate (DMS) (Figure 3.6A), which lacks this functional moiety. We found that DMS had no impact on viral output (Figure 3.6, B and C), nor did the hydrolysed form of DMS, succinate (S). In contrast with FA, DMS, and S, all other FMAEs were able to deplete GSH (Figure 3.6D). However, the proviral activity of DMF was still evident after pre-depletion of cellular GSH by culturing cells for 10 days in the presence of buthionine sulfoximine (BSO), an inhibitor of glutamate cysteine ligase (GCL) required for the synthesis of GSH (Figure 3.6E).

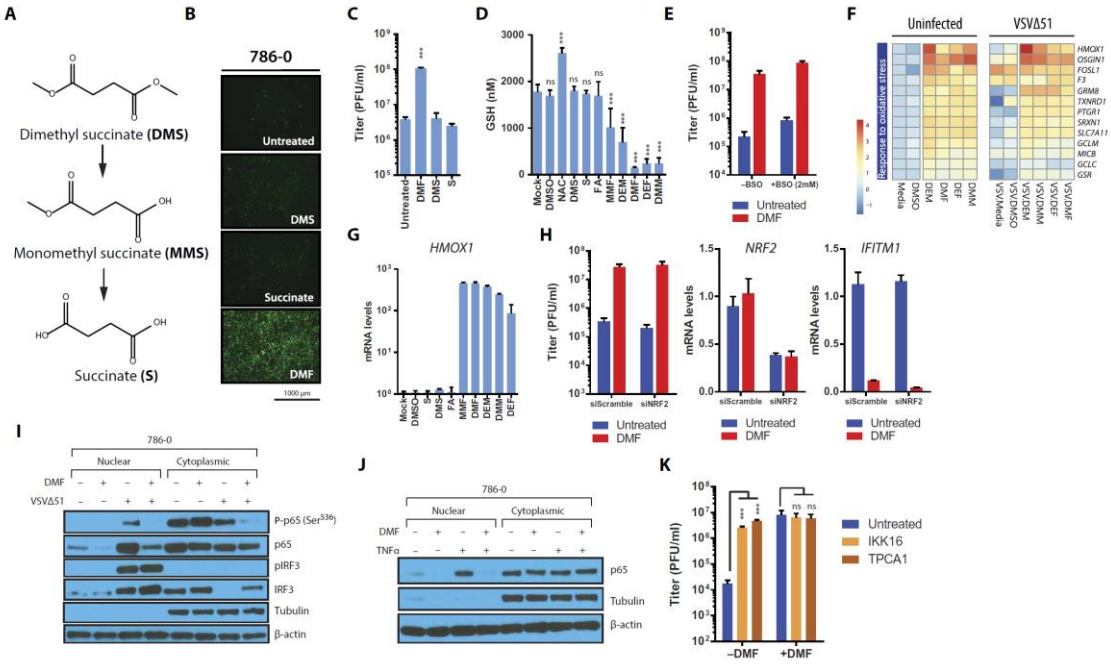
A
Dimethyl succinate (DMS)
Monomethyl succinate (MMS)
Succinate (S)
B
786-0
Untreated
DMS
Succinate
DMF
1000 μm
C
Titer (PFU/ml)
Untreated
DMF
DMS
S
D
GSH (nM)
Mock
DMSO
NAC
DMS
S
FA
MMF
DEM
DMF
DEF
DMM
E
Titer (PFU/ml)
–BSO
+BSO (2mM)
Untreated
DMF
F
Uninfected
VSVΔ51
Response to oxidative stress
HMOX1
OSGIN1
FOSL1
F3
GRM8
TXNRD1
PTGR1
SRXN1
SLC7A11
GCLM
MICB
GCLC
GSR
Mock
DMSO
DMF
DEF
DMM
VSV
G
HMOX1
mRNA levels
H
Titer (PFU/ml)
siScramble
siNRF2
Untreated
DMF
NRF2
IFITM1
mRNA levels
I
786-0
Nuclear
Cytoplasmic
DMF
VSVΔ51
P-p65 (Ser536)
p65
pIRF3
IRF3
Tubulin
β-actin
J
786-0
Nuclear
Cytoplasmic
DMF
TNFα
p65
Tubulin
β-actin
K
Titer (PFU/ml)
Untreated
IKK16
TPCA1
–DMF
+DMF

**Figure 3.6**. **DMF inhibits NF-κB translocation upon infection.** (**A**) Structures of DMS, MMS, S. (**B-C**) 786-0 cells were pretreated with the indicated DMF analogues for 4 hours and subsequently infected with oncolytic VSVΔ51 expressing GFP at an MOI of 0.01. (**B**) 24 hours after infection, fluorescent images were taken of the infected 786-0 cells. (**C**) Corresponding viral titers were determined from supernatants 48 hours after infection (n=3; mean +/- SD; one-way ANOVA; *** $p<0.001$, as compared to the untreated counterpart). (**D**) GSH concentrations were determined in 786-0 cells after a 4-hour treatment with FMAEs (n=4; mean +/- SD; one-way ANOVA; *** $p<0.001$, as compared to the untreated counterpart). (**E**) 786-0 cells were grown in the presence or absence of BSO (2 mM) for 7 days and pretreated with DMF (200 μM) for 4 hours or left untreated, then infected with oncolytic VSVΔ51 expressing GFP at an MOI of 0.01. Corresponding viral titers were determined from supernatants 48 hours after infection (n=3; mean +/- SD).(**F**) Heatmap showing the expression of the differentially expressed oxidative stress genes. Expression of genes was normalized to values obtained for untreated, uninfected control. (**G**) *HMOX1* expression quantified by qPCR from 786-0 cells after a 6-hour treatment with FMAEs (n=3; mean +/- SD). (**H**) siNRF2 knockdown 786-0 cells were treated with DMF or untreated and infected as in (**E**). Corresponding viral titers were determined from supernatants 24 hours after infection. RNA was extracted, and the expression of *NRF2* and *IFITM1* genes was quantified by qPCR (n=3; mean +/- SD). (**I-J**) Cytoplasmic and nuclear protein fractions were extracted from 786-0 cells treated with DMF (200 μM) for 4 hours and (**I)** subsequently infected with oncolytic VSVΔ51 expressing GFP at an MOI of 1 for 8 hours, or (**J**) treated with TNFα (30 ng/ml) for 30 min. Cell lysates were probed for multiple proteins as indicated, by western blot. (**K**) 786-0 cells were pretreated with NF-κB inhibitors targeting IKK [IKK16 (10 μM), TPCA1 (40 μM)] for 4 hours and subsequently co-treated with DMF (150 μM) and oncolytic VSVΔ51 expressing GFP at an MOI of 0.01. Corresponding viral titers were determined from supernatants 24 hours after infection. (n=3; mean +/- SD; one-way ANOVA; *** $p<0.001$, as compared to the untreated counterpart).

In parallel with their impact on antiviral gene expression by microarray, FMAEs also induced robust expression of multiple genes involved in the antioxidant response (Figure 3.6F). In particular, *HMOX1* expression, as determined by real-time PCR, was consistently up-regulated well over 100-fold by FMAEs (Figure 3.6G), but not by treatment with FA, DMS, or S (Figure 3.6G). DMF and other FMAEs induce nuclear translocation of NRF2 via covalent modification of KEAP1, which induces antioxidant genes*(225)*. This is consistent with our observation of the induction of *HMOX1* and other NRF2 target genes by FMAEs but not FA, DMS, or S (Figure 3.6F and G). To determine whether the proviral effect of DMF is dependent on NRF2 activity, siRNA knockout against NRF2 was performed. We found that knockdown of NRF2 did not block the capacity of DMF to enhance VSVΔ51 infection or inhibit antiviral factor *IFITM1* (Figure 3.6H). Furthermore, DMF was able enhance infection in a number of cell lines harboring KEAP1 mutations (A549*(226)*, CT26WT*(227)*) (Figure 3.1D). Altogether these data suggest that the ability of FMAEs to enhance infection requires the α,β-unsaturated carbon involved in GSH depletion, but that neither GSH depletion nor NRF2 activity are likely key mediators of this phenomenon. Given that DMF inhibits LPS-stimulated cytokine production by inhibiting NF-κB nuclear entry*(228, 229)*, we looked at nuclear and cytoplasmic fractionations of infected cells. Probing for NF-κB subunit p65 revealed that upon infection or TFNα stimulation, DMF inhibits phosphorylation and translocation of this transcription factor, involved in the transcription of IFNβ particularly but also in the response to type I IFN (Figure 3.6 I and J). Furthermore, DMF did not improve infection in cells treated with inhibitors of IκB kinase (IKK) degradation using chemical compounds IKK16 and TCPA1*(230, 231)* (Figure 3.6K).

## Discussion

In this study, we demonstrate that fumaric and maleic acid esters like DMF enhance OVs such as VSVΔ51 by increasing viral spread and oncolysis in resistant cancer cells. Furthermore, we show that DMF can overcome the innate immune response of cancer cells in a manner consistent with its modulation of NF-κB activity. This results in a decrease in cytokine production and the inhibition of the type I IFN response at multiple levels, including the NF-κB and JAK-STAT pathways.

FMAEs such as DMF are electrophilic hence they can covalently link to essential thiol groups on various proteins, including KEAP1, which activates NRF2*(189)*. The activation of antioxidative transcription factor NRF2 by DMF has been long thought to be a main mechanism in the treatment of multiple sclerosis (MS), however recent studies suggest that the anti-inflammatory activity of DMF in MS treatment occurs through alternative pathways, independent of NRF2 *(134, 139, 228)*. Consistent with this, we show that enhancement of viral infection by DMF is not mediated by the activation of NRF2. However, NRF2 signaling may nevertheless play a role in some contexts, given a recent study implicating its involvement in sulforaphane-mediated enhancement of infection by VSVΔ51 in prostate cancer cells *(232)*.

DMF blocks the nuclear translocation and DNA binding activity of NF-κB transactivator subunit p65 upon stimulation with TFNα or lipopolysaccharides (LPS) *(139, 212, 228, 229)*. Similarly to KEAP1, DMF also covalently binds p65 cysteines, and in particular cysteine 38 that is essential to block its nuclear translocation and transcriptional activity *(216)*. Consistent with this, here we show that DMF is able to

block the translocation of the NF-κB transcription factor p65 upon viral infection. RNA virus infection triggers the activation of interferon regulatory factor 3 (IRF3) and NF-κB, transcription factors downstream of the viral RNA sensors such as RIG-I-like receptor*(233)*. Both IRF3 and NF-κB are required for the expression of the antiviral cytokine *IFNβ (233)*. However, DMF does not block the translocation of IRF3, but inhibits numerous antiviral and proinflammatory cytokines, promoting the spread of viral infection within the tumor environment. Of note, the wtVSV matrix (M) protein has the ability to inhibit NF-κB activation, while mutation in the M protein found in VSVΔ51 abrogates this function*(234)*. In addition, oncolytic virus infection can be improved in vitro by using compounds that inhibit NF-κB signaling through inhibition of IKK for instance *(79, 235)* as we have confirmed here. However, the capacity of these compounds to enhance oncolytic virus activity in vivo has not been assessed, and they are not approved for human use, in contrast with DMF.

DMF inhibits the cellular response to type I IFN, in part by decreasing IFN production via the modulation of NF-κB, in addition to the inhibition of STAT1 activation upon IFN stimulation. DMF mediates suppression of STAT1 phosphorylation in dendritic cells *(236)*, further supporting our findings. However, the mechanism of suppression of STAT1 by DMF remains unclear. Recent studies found that oxidative stress has a marked impact on signal transduction through the JAK-STAT pathway, impairing STAT1 phosphorylation*(237, 238)*. This could suggest a mechanism whereby ROS induced by DMF indirectly blocks STAT1 phosphorylation and IFN signaling.

Despite an absence of clinical data regarding an increased risk of infections in patients treated with FAEs*(126, 239)*, recent reports of progressive multifocal

leukoencephalopathy (PML), a rare disease of the central nervous system caused by the polyoma JC virus*(240)*, were associated with long term treatment with DMF in several patients*(241–245)*. The susceptibility and occurrence of PML in DMF-treated patients have been widely debated*(246–249)*, however this potential causative mechanism remains to be explored. Given our observation that DMF is able to inhibit type I IFN response upon infection, as well as inhibit DC maturation*(229)*, this suggests that long-term treatment with DMF may increase susceptibility to IFN-sensitive viruses such as polyomaviruses*(250)*. Further investigation to this end is warranted.

Nevertheless, Tecfidera has been safely used by more than 135,000 patients worldwide since its approval. Furthermore, Fumaderm is the most frequently prescribed drug for systemic treatment of psoriasis in Germany. DMF is emerging as a promising anticancer agent that can inhibit melanoma and colon cancer*(129, 149, 150)*. Here we show that DMF can also enhance the therapeutic benefit of oncolytic virotherapy in vivo. The clinical availability of DMF and related FAEs and the recent approval of the first oncolytic virus for the treatment of melanoma *(29, 251)* provide a clear path towards clinical evaluation of this promising combination therapy.

## Materials and Methods

**Study design.** In our hypothesis-driven study, we assessed the therapeutic potential of the clinically approved drug DMF in combination with oncolytic virotherapy in human and murine cancer cell lines (in vitro, ex vivo), in human-derived tumor cell lines, and in

human tumor specimens. The effect of the combination therapy on viral infection was assessed by plaque assay. This study was extended to syngeneic and xenograft tumor models refractory to OV therapy to analyze the effects of combination therapy in vivo. In all experiments, animals were assigned to various experimental groups at random but experimenters were not blinded. For survival studies, sample sizes of 9 to 18 mice per group were used. Mice were euthanized when tumors had reached 1,500 $mm^3$. All outliers were included in the data analysis.

**Drugs, chemicals, and cytokines.** Drugs, chemicals, and cytokines and their respective suppliers and solvents used in this study are listed in table S2.

**Cell lines.** Cells and their respective suppliers and growth media used in this study are listed in table S3. Cells were cultured in HyQ high-glucose Dulbecco's modified Eagle's medium (DMEM) (Hyclone) or Roswell Park Memorial Institute (RPMI)-1640 medium (Corning) supplemented with 10 % fetal calf serum (CanSera) and penicillin/streptomycin (Gibco). All cell lines were incubated at 37 °C in a 5% $CO_2$ humidified incubator. All cells were tested to ensure they are free of mycoplasma contamination.

**Human-derived cell lines.** Ovarian cancer primary cultures were derived from the ascites of individuals with ovarian cancer during routine paracentesis according to Ottawa Health Science Network Research Ethics Board (OHSN-REB) protocol number 20140075-01H. These cells were maintained in complete Dulbecco's Modified Eagle's medium supplemented with 10% fetal bovine serum. These cultures have been characterized and cryopreserved for use as experimental models.

Melanoma primary cultures were derived from excised surgical specimens. The surgeries were performed at the Ottawa Hospital and specimens were taken after the receipt of patient consent according to the OHSN-REB # 20120559-01. Primary cultures were maintained in Roswell Park Memorial Institute (RPMI)-1640 medium supplemented with 10% fetal bovine serum. Primary cultures were established after scalpel-mediated homogenization of tumor specimens and filtration of the homogenate through a 70 μm nylon mesh cell strainer (ThermoFisher Scientific). Homogenate was maintained in culture with periodically refreshed medium until sufficient cellular proliferation occurred for experimental purposes. Both primary melanoma cultures have been characterized and cryopreserved for use as experimental models.

**Viruses and quantification.**

*Rhabodviruses.* The Indiana serotype of VSV (VSVΔ51 or wild type) was used throughout this study and was propagated in Vero cells. VSVΔ51 expressing GFP or firefly luciferase are recombinant derivatives of VSVΔ51 described previously *(48)*. All viruses were propagated on Vero cells and purified on 5–50% Optiprep (Sigma) gradient, and all virus titers were quantified by the standard plaque assay on Vero cells as previously described *(252)*. The number of infectious virus particles was expressed as plaque-forming unit (PFU) per milliliter (ml).

*Adenovirus.* The Ad5-luciferase (adenovirus serotype 5 expressing firefly luciferase) was generously provided by Dr. Jack Gauldie (McMaster University).

*Herpes simplex virus*. The HSV-1 N212 expressing GFP *(253)* was a gift from Dr. Karen Mossman (McMaster University, Canada). HSV virus titers were quantified by the standard plaque assay on Vero cells as previously described *(253)*.

*Sindbis virus.* The Sindbis virus expressing GFP was a gift from Dr. Benjamin tenOever (Icahn School of Medicine at Mount Sinai, NY, USA). The Sindbis virus was quantified by the standard plaque assay in Vero cells. Plaques were counted 3 days after infection.

**Cell viability assay.** The metabolic activity of the cells was assessed using alamarBlue (Bio-Rad) according to the manufacturer's protocol. Fluorescence was measured at 590 nm upon excitation at 530 nm using a Fluoroskan Ascent FL (Thermo Labsystems).

**Microarray and analysis.** 786-0 cells were plated at a density of $1 \times 10^6$ in 6-well dishes and allowed to adhere overnight. The next day, cells were pretreated for 4 hours with DEM (350 μM), DEF (350 μM), DMM (300 μM), DMF (200 μM), or the vehicle. After pre-treatment, the cells were infected with VSVΔ51 at an MOI of 0.01 or mock-infected. 24 hours after infection, RNA was collected using an RNA-easy kit (Qiagen). Biological triplicates were subsequently pooled and RNA quality was measured using Agilent 2100 Bioanalyzer (Agilent Technologies) before hybridization to Affymetrix Human PrimeView Array (The Centre for Applied Genomics, The Hospital for Sick Children, Toronto, Canada). Microarray data were processed using Transcriptome Analysis Console (TAC) 3.0 under default parameters of Gene Level Differential Expression Analysis. Fold change in gene expression was calculated for each gene in relation to uninfected, untreated control. Heatmaps of normalized expression values were generated using R package pheatmap. Volcano plots of gene expression values were generated

using R. Gene ontology enrichment analysis was evaluated using GOrilla *(254)* after correction for multiple hypothesis testing (Benjamini–Hochberg). Raw and processed microarray data have been deposited in NCBI-Gene Expression Omnibus database (GSE97328).

**Mouse tumor models.**

*CT26WT model.* Six-week-old female BALB/c mice obtained from Charles River Laboratories were subcutaneously injected with $5 \times 10^5$ syngeneic CT26WT cells suspended in 100 µl PBS. 11 days after implantation, tumors were treated intratumorally (i.t.) once with 200 mg/kg of DMF (dissolved in DMSO) or the vehicle alone. 4 hours later, tumors were intratumorally injected with $1 \times 10^8$ PFU (in 25 µl PBS) of VSVΔ51 expressing firefly luciferase.

*HT29 model.* Six-week-old female BALB/c nude mice were subcutaneously injected with $5 \times 10^6$ syngeneic HT29 cells suspended in 100 µl serum-free DMEM and 100 µl Geltrex (Thermo Fisher). When tumors grew to approximately 5 mm x 5 mm (11 days after implantation), mice were treated intratumorally once with 200 mg/kg of DMF (dissolved in DMSO) or the vehicle as indicated. Four hours later, tumors were injected intratumorally with $1 \times 10^8$ PFU of VSVΔ51-expressing firefly luciferase.

*B16F10 model.* Six-week-old female C57BL/6 mice obtained from Charles River Laboratories were subcutaneously injected with $5 \times 10^5$ syngeneic B16F10 cells suspended in 100 µl PBS. 11 days after implantation, tumors were treated intratumorally (i.t.) once with 50 mg/kg of DMF (dissolved in DMSO) or the vehicle alone. 4 hours

later, tumors were intratumorally injected with $1 \times 10^8$ PFU (in 25 µl PBS) of VSVΔ51 expressing firefly luciferase.

Tumor sizes were measured every other day using an electronic caliper. Tumor volume was calculated as (length$^2$ × width)/2. For survival studies, mice were euthanized when tumors had reached 1,500 mm$^3$. For in vivo imaging, an IVIS (Perkin Elmer) was used as described previously*(119)*. The bioluminescent signal intensities for each mouse were quantified using Living Image v2.50.1 software. Sample size in all animal experiments was $n \geq 5$. Mice were randomized to the different treatment groups according to tumor size in all experiments. Mice with no palpable tumors on initial treatment day were excluded from the study. The investigators were not blinded to allocation during experiments and outcome assessment. All experiments were performed in accordance with the University of Ottawa Animal Care and Veterinary Services guidelines for animal care under the protocol OHRI-2265 and OHRI-2264.

**Ex vivo mouse model.** BALB/c mice were implanted with subcutaneous CT26WT. Mice were sacrificed after tumors had reached at least 10 mm x 10 mm in size. Tumor, lung, spleen, and brain tissue were extracted from the mice, cut into 2 mm-thick slices and cored into 2 mm x 2 mm pieces using a punch biopsy. Each tissue core was incubated in 1 mL of Dulbecco's Modified Eagle's Medium (DMEM) supplemented with 10% fetal bovine serum and 30 mM HEPES at 37 °C in a 5% $CO_2$ humidified incubator. Cores were treated for 4 hours with the indicated concentrations of chemical compounds. Subsequently, the cores were infected with VSVΔ51-GFP. GFP images were obtained for each core 24 hours after infection.

**Ex vivo human samples.** Tumor samples were acquired from consenting individuals during surgery, and specimens were manipulated as previously described *(255)*. Approval was granted by the Ottawa Health Science Network Research Ethics Board for all studies requiring human tissue samples (OHSN-REB # 2003109-01H and OHSN-REB # 20120559-01). Patient provided their written informed consent in accordance with Declaration of Helsinki guidelines.

**Immunoblotting.** Cells were pelleted and lysed on ice for 30 minutes using 50 mM HEPES, pH 7.4, 150 mM NaCl, 10 mM EDTA, 10 mM $Na_4P_2O_7$, 100 mM NaF, 2 mM $Na_3VO_4$, protease inhibitor cocktail (Roche), and 1% Triton X-100. For nuclear and cytoplasmic extracts, the NE-PER Nuclear and Cytoplasmic Extraction kit (ThermoFisher Scientific) was used according to the provided protocol. After protein determination by Bradford assay (Bio-Rad Protein Assay Solution), 20 μg of clarified cell lysates were electrophoresed on NuPAGE Novex 4-12% Bis-Tris precast gels (ThermoFisher Scientific) using the XCell SureLock mini-cell System (ThermoFisher Scientific) and transferred to nitrocellulose membranes (Hybond-C, Bio-Rad). Blots were blocked with 5% BSA or milk and probed with antibodies specific for phospho-STAT1 (Tyr701, #9171, Cell Signaling Technology, used at 1:1000), STAT1 (#9172, Cell Signaling Technology, used at 1:1000), STAT2 (#72604, Cell Signaling Technology, used at 1:1000), phospho-STAT2 (#88410S, Cell Signaling Technology, used at 1:1000), IFITM1 (#60074-1-Ig, Proteintech Group, used at 1:1000, in 5% milk), VSV (a gift from Dr. Earl Brown, used at 1:2000), HMOX1 (#70081, Cell Signaling Technology, used at 1:2000), or β-actin (#4970, Cell Signaling Technology, used at 1:1000). Blots were then probed with a goat anti-rabbit or mouse peroxidase-conjugated antibodies (Jackson

Immunoresearch Labs). Bands were visualized using the Supersignal West Pico Chemiluminescent substrate (ThermoFisher Scientific).

**ELISA.** 786-0 cells plated in 12-well dishes were pretreated with compound or the vehicle for 4 hours, and subsequently infected with VSVΔ51-GFP at the indicated MOI or left uninfected. Cell supernatants were collected at different times after infection as indicated. IFNα and IFNβ quantifications were performed using the Verikine Human IFNα or IFNβELISA kits (PBL Assay Science) as per the manufacturer's instructions. Absorbance values at 450 nM were measured on a Multiskan Ascent Microplate Reader (MXT Lab Systems).

**Quantitative real-time PCR.** 786-0 cells were treated for 6 hours with the indicated chemical compound or vehicle. Cells were collected and RNA extraction was performed using the Qiagen RNeasy kit (Qiagen). RNA quantity and purity was assessed using a NanoDrop ND-1000 spectrophotometer (Thermo Scientific). RNA was converted to cDNA with RevertAid H Minus First Strand cDNA Synthesis Kit (Thermo Scientific). Real-time PCR reactions were performed according to the manufacturer's protocol with the QuantiTect SYBR Green PCR kit (Qiagen) on a 7500 Fast Real-Time PCR system (Applied Biosystems). Gene expression was calculated relative to GAPDH or β-actin. Fold induction was calculated relative to the untreated/uninfected samples for each gene. List of qPCR primers used:

*GAPDH* (For -ACAGTCAGCCGCATCTTCTT; Rev-GTTAAAAGCAGCCCTGGTGA)

*HMOX1* (For-ACTGCGTTCCTGCTCAACAT; Rev-GGGGCAGAATCTTGCACTTT)

*NRF2* (For-CAACTACTCCCAGGTTGCCC; Rev-AGTGACTGAAACGTAGCCGA)

*IFITM1* (For-CCGTGAAGTCTAGGGACAGG; Rev-GGTAGACTGTCACAGAGCCG)

**Supernatant transfer experiment.** 786-0 cells plated in 12-well dishes were pretreated with FMAEs or the vehicle for 4 hours and subsequently infected with VSVΔ51ΔG-GFP at an MOI of 1. This virus can infect cells and replicate its genome but does not bud or spread further because of the lack of the viral G protein, thus preventing release of viral particles in the supernatant*(256)*. 1 hour after infection, the supernatant was removed to eliminate residual drug and virus and replenished with growth medium supplemented with 10% fetal bovine serum. 12 or 16 hours after infection, supernatants were collected before being transferred to fresh 786-0 cells and processed for further analysis.

**siRNA.** 786-0 cells plated in 12-well dishes were transfected with small interfering RNAs (100 nM) against NRF2 (ON-TARGETplus NFE2L2 siRNA #L-003755-00-0005, GE Dharmacon) or with a non-targeting scrambled siRNA (ON-TARGETplus Non-targeting Control Pool, #D-001810-10-05, GE Dharmacon). Transfections were carried out according to the manufacturer's protocol (Oligofectamine, Life Technologies).

**Glutathione assay.** 786-0 cells plated in a 96-well plate were pretreated with FMAEs or the vehicle for 4 hours, and the glutathione concentrations were determined using the GSH-Glo Glutathione Assay kit (Promega) as per the manufacturer's instructions. The luminescence-based assay is based on the conversion of a luciferin derivative into luciferin in the presence of glutathione, catalyzed by glutathione S-transferase (GST). The signal generated in a coupled reaction with firefly luciferase is proportional to the

amount of glutathione present in the sample. The assay result was normalized using GSH standard solution provided with the kit. Luciferase expression was then measured on a SynergyMx Microplate Reader (BioTek).

**Statistics.** Statistical significance was calculated using Student's *T*-test with Welch's correction, one-way, or two-way ANOVA test, as indicated in the figure legends. For all statistical analyses, differences were considered significant when a *p*-value was below or equal to 0.05. The log-rank (Mantel-Cox) test was used to determine significant differences in plots for survival studies. Statistical analyses were performed using GraphPad Prism 6.0 and Microsoft Excel.

# Chapter 4 - Multi-Modal Potentiation of Oncolytic Virotherapy by Vanadium Compounds

Mohammed Selman[1,2], Christopher Rousso[1,2], Anabel Bergeron[1,3] , Hwan Hee Son[1,2], Ramya Krishnan[1,2], Nader A. El-Sayes[1,2], Oliver Varette[1,2], Andrew Chen[1], Fabrice Le Boeuf[1], Fanny Tzelepis[1], John C. Bell[1,2] , Debbie C. Crans[4,5], Jean-Simon Diallo[1,2]*

[1] Centre for Innovative Cancer Research, Ottawa Hospital Research Institute, Ottawa, Ontario, Canada. [2] Department of Biochemistry, Microbiology and Immunology, University of Ottawa, Ontario, Canada. [3] Faculty of Science, University of Ottawa, Ontario, Canada. [4] Department of Chemistry, Colorado State University, Fort Collins, Colorado, USA. [5] Cell and Molecular Biology Program, Colorado State University, Fort Collins, Colorado, USA

Accepted October 2017; Published in Molecular Therapy.

Contribution: MS, CR, AB, HHS, NAE, OV conducted in vitro experiments. MS, AC, FT, AB, RK performed mouse experiments. FT performed the flow cytometry acquisition and analysis. FLB provided material. JSD, MS participated in the conception and design of the study. MS and JSD drafted the manuscript with editorial contributions from DCC, JCB, FT, RK. JSD, DCC, JCB supervised the study.

**Abstract**

Oncolytic viruses (OV) are an emerging class of anticancer bio-therapeutics that induce antitumor immunity through selective replication in tumor cells. However, the efficacy of OVs as single agents remains limited. We introduce a strategy that boosts the therapeutic efficacy of OVs by combining their activity with immuno-modulating, small molecule protein tyrosine phosphatase inhibitors. We report that vanadium-based phosphatase inhibitors enhance OV infection *in vitro* and *ex vivo*, in resistant tumor cell lines. Furthermore, vanadium compounds increase anti-tumor efficacy in combination with OV in several syngeneic tumor models, leading to systemic and durable responses, even in models otherwise refractory to OV and drug alone. Mechanistically, this involves subverting the antiviral type I IFN response towards a death-inducing and proinflammatory type II IFN response, leading to improved OV spread, increased bystander killing of cancer cells, and enhanced anti-tumor immune-stimulation. Overall, we showcase a new ability of vanadium compounds to simultaneously maximize viral oncolysis and systemic anticancer immunity, offering new avenues for the development of improved immunotherapy strategies.

## Introduction

Oncolytic viruses (OV) are an emerging class of anticancer bio-therapeutics that selectively replicate in and lyse tumor cells, without causing damage to normal cells*(8, 74)*. Multiple OVs have shown efficacy in preclinical models of cancer and in clinical trials*(8)*. Notably, the US Food and Drug Administration (FDA) and European Medicines Agency (EMA) have recently approved T-VEC (Imlygic) for the treatment of melanoma. While OVs can lead to profound anticancer responses as single agents, clinical data show that some patients do not respond to OVs alone and may benefit from combination therapies*(29, 88, 257)*.

Poor infection of tumors is an important factor in the resistance to OV therapy. OV spread, oncolysis, and overall therapeutic efficacy can be improved in resistant tumors among others by using pharmacological compounds that block the cellular innate antiviral immune response mediated by type I interferon (IFN)*(114, 115, 118, 119)*. Beyond direct effects on tumor cells, OVs can remodel the tumor microenvironment and boost anti-tumor immunity by directing immune responses to the tumor niche*(11, 211, 258, 259)*. This immunostimulatory effect can be enhanced by integrating immune stimulatory genes into the viral genome*(221, 260)* or by combination with other forms of immunotherapy such as immune checkpoint inhibitors*(30, 194, 195, 261)*.

Vanadate and other vanadium-based compounds are pan-inhibitors of protein tyrosine phosphatases (PTPs), with a wide range of biological effects*(154, 262)*. Clinically, these compounds have been mostly explored for their antidiabetic potential, demonstrating safety for this indication in phase I/II human trials*(263, 264)*. In more

recent years, a number of vanadium compounds were also found to exhibit anticancer effects in animal models*(162, 164, 166, 265–269)*. Numerous studies suggest that vanadium compounds impact the immune system*(159, 197, 270, 271)*, for example by stimulating and activating T-cells*(270)*. However, the mechanism by which vanadium-based compounds can modulate anticancer immunity has not been investigated.

Given their potential immunostimulatory effects, we assessed the use of selected vanadium compounds as complementary pharmacological agents to OV–mediated immunotherapy. Here we demonstrate an unprecedented ability of these compounds to subvert the type I IFN antiviral response towards a death-inducing and proinflammatory type II IFN response, culminating in the dramatically improved anticancer activity of OVs both *in vitro* and *in vivo*.

## Results

*Vanadate enhances the spread of oncolytic RNA viruses*

Contrasting results have been reported in the few studies that have probed the effect of vanadate (Figure 4.1a) on viral infection*(272, 273)*. To explore this in the context of OVs, we tested the impact of orthovanadate on the growth of a small panel of candidate oncolytic viruses. We included negative single strand RNA viruses Vesicular Stomatitis Virus (VSVΔ51)*(48)* and Measles (Schwarz strain)*(274)*, a positive single strand RNA virus (Sindbis), as well as double-stranded DNA viruses herpes simplex virus-1 (HSV-1 mutant N212)*(275)* and vaccinia virus (deleted for thymidine kinase and expressing GM-CSF)*(276)* (Figure 4.1b). We found that the growth of RNA viruses including Measles, Sindbis, and oncolytic VSVΔ51, but not DNA viruses HSV-1 and vaccinia was enhanced by treatment with vanadate. VSVΔ51 growth was most robustly enhanced and further testing in VSV-resistant 786-0 renal carcinoma cells revealed that vanadate increased viral output, as measured by plaque assay, up to ~400-fold over a 10-1000μM dose range (Figure 4.1c), which was below the median lethal concentration of vanadate (Figure 4.3a). Use of a GFP-expressing VSVΔ51 revealed a corresponding increase in the number of GFP positive, infected cells (Figure 4.1d). A similar impact on viral infection was observed in various human and murine cancer cell lines (Supplemental Figure 1a,b). Single and multi-step growth curves in 786-0 cells revealed that vanadate more robustly enhanced the yield of VSVΔ51 at a low multiplicity of infection (MOI) compared to a high MOI, indicating that vanadate promotes viral spread (compare Figure 4.1e vs. f). Similarly, in the presence of vanadate, VSVΔ51 produced larger plaques, based on both the area of GFP-positive cells as well as the cytopathic

effect observed upon coomassie blue staining (Supplemental Figure 2). The impact of vanadate on viral growth was more pronounced with increasing pre-treatment time (maximum tested 24h), with the effect of vanadate being negligible when provided later than 12h post infection (Supplemental Figure 1c). Similarly, treatment with vanadate after infection reduced its negative effect on vaccinia infection but did not lead to enhancement (Supplemental Figure 1d). Correlating with viral titers and GFP expression data, Figure 4.1g shows that vanadate increased the production of VSVΔ51 genomes in infected 786-0 cells as well as in mouse CT26WT colon cancer cells. In contrast, viral growth was not enhanced in normal adult human GM38 fibroblasts (Figure 4.1h). Using mouse tissue cores obtained from normal lung, muscle, spleen and tumor tissues obtained from mice implanted with CT26WT and DBT (glioma) cells, we further evaluated the impact of vanadate on growth of VSVΔ51-GFP. Fluorescence microscopy images in Figure 4.1i show that vanadate preferentially increased the growth of the virus in tumor cores with no impact on normal tissues.

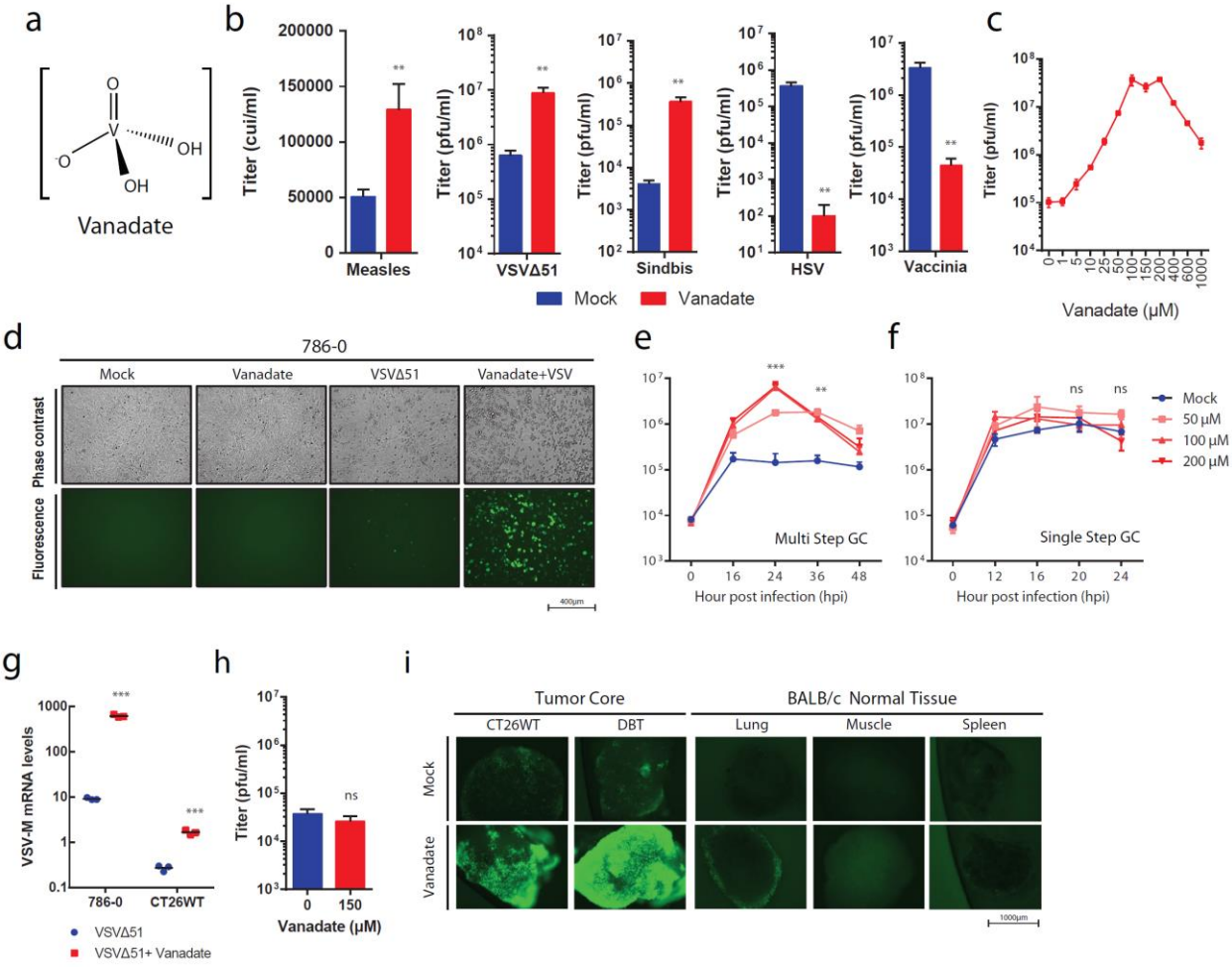
a
Vanadate
b
Titer (cui/ml)
Measles
Titer (pfu/ml)
VSVΔ51
Sindbis
HSV
Vaccinia
Mock
Vanadate
c
Titer (pfu/ml)
Vanadate (μM)
d
786-0
Mock
Vanadate
VSVΔ51
Vanadate+VSV
Phase contrast
Fluorescence
e
Multi Step GC
Hour post infection (hpi)
f
Single Step GC
Hour post infection (hpi)
Mock
50 μM
100 μM
200 μM
g
VSV-M mRNA levels
786-0
CT26WT
VSVΔ51
VSVΔ51+ Vanadate
h
Titer (pfu/ml)
Vanadate (μM)
i
Tumor Core
BALB/c Normal Tissue
CT26WT
DBT
Lung
Muscle
Spleen
Mock
Vanadate

**Figure 4.1. Vanadate enhances VSVΔ51 infection in cancer cells but not normal cells.**

(a) Structure of vanadate ion present at pH 7.4. (b-f,h) Resistant human renal cancer cell lines 786-0, were pretreated with vanadate for 4 hours and subsequently infected with (b-e,h) VSVΔ51 (MOI: 0.01, [150μM]), (b) Measles (MOI: 0.01, [100μM]) , (b)Sindbis (MOI:10, [150μM]), (b) HSV (MOI: 0.01, [150μM]), (b) Vaccinia (MOI: 0.01, [200μM]). (b,c) Corresponding viral titers were determined 24 (VSVΔ51) or 48 (Measles, Sindbis, HSV, Vaccinia) hours post infection (hpi) from supernatants (b,g,h; N=3;Error bars indicate SEM; t-test; NS = no statistical significance, ** $p<0.001$, as compared to the untreated condition counterparts) (c; N=3; Significance enhancement at 100 - 200μm; $p<0.0001$ by 1-way ANOVA; as compared to 0μm condition) (d) 24 hpi fluorescent and phase contrast images were taken of the 786-0 cells treated with mock or 200μM of vanadate . (e) Multi-step, and (f) single-step growth curve of 786-0 pretreated with vanadate and infected with VSVΔ51 (e) MOI: 0.01 or (f) MOI: 3, supernatants were tittered by plaque assay (N=3; Significant enhancement at 50-200μm at indicated time; NS, no statistical significance, ** $p<0.001$, *** $p<0.0001$ by 2-way ANOVA; as compared to Mock condition). (g) 24 hpi, RNA was collected from 786-0 and CT26WT, and expression of VSV-M gene was quantified by qPCR. (h) Normal cell line GM38 were pretreated as in (b) infected with VSVΔ51. Corresponding viral titers were determined 24 hours post infection from supernatants. (i) CT26WT and DBT tumors cores and BALB/c mouse spleen, muscle, lung, and brain tissue cores were pretreated with 300μM of vanadate for 4 hours and subsequently infected with $1x10^4$ PFU of VSVΔ51 expressing GFP. 24 hpi fluorescent images were acquired of the tumor and normal tissue cores. Representative images from each triplicate set are shown.

*Vanadium compounds have unique viral enhancing properties*

Vanadate has been shown to inhibit tyrosine phosphatases, an activity which is linked to its close structural and electronic analogy to phosphate*(262, 277)*. We therefore tested whether phosphate could induce similar effects but found various phosphate salts had no impact on viral growth in contrast to vanadate (Supplemental Figure 3a). Vanadate is a simple oxometalate. We wanted to investigate whether other oxidized transition metals could potentially enhance viral growth. We found that neither aluminum, molybdenum, manganese and tungsten oxides could enhance VSVΔ51 growth (Figure 4.2a). Chromium trioxide modestly enhanced viral growth but only at a single dose (10 μM, Figure 4.2a) and was highly toxic in comparison to vanadate (not shown). The protonation or form of vanadate at different pH had no impact on its activity (Supplemental Figure 3b). Because this suggested the virus-enhancing effect was linked to the vanadium itself, we tested other oxidized vanadium complexes, including metavanadate, vanadium(V) oxytriethoxyde (VOx), vanadium(IV) oxide sulphate (VS) and bismaltolato oxovanadium(IV) (BMOV) (Figure 4.2b). All of these compounds effectively enhanced VSVΔ51 growth (Figure 4.2c,d, Fig S3c). Similar results were obtained using vanadium(IV) tetra-fluoride and vanadium(III) tri-bromide (Figure 4.2e). Interestingly, vanadate's pro-viral activity was abrogated upon inclusion of L-Ascorbic Acid or tiron, both potent metal chelating agents (Figure 4.2f).

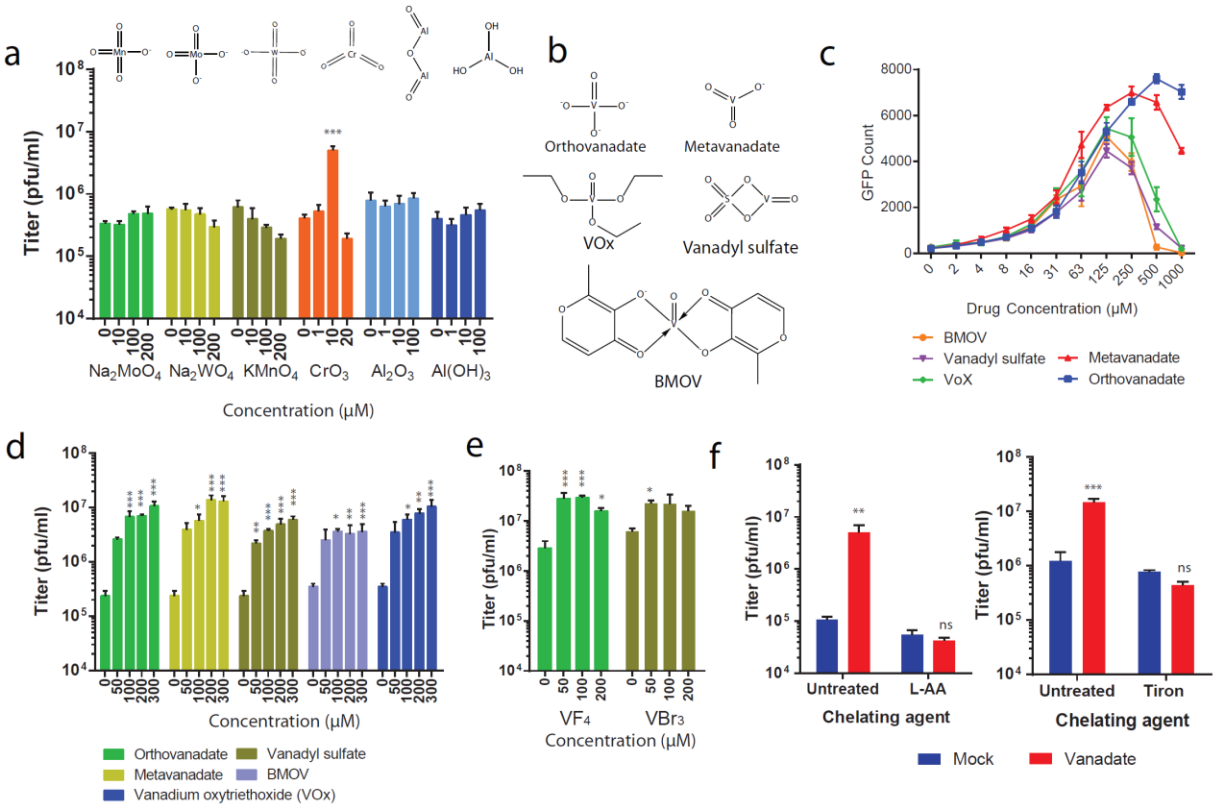
a
Titer (pfu/ml)
Concentration (μM)
Na2MoO4
Na2WO4
KMnO4
CrO3
Al2O3
Al(OH)3
b
Orthovanadate
Metavanadate
VOx
Vanadyl sulfate
BMOV
c
GFP Count
Drug Concentration (μM)
BMOV
Vanadyl sulfate
Metavanadate
VoX
Orthovanadate
d
Titer (pfu/ml)
Concentration (μM)
Orthovanadate
Vanadyl sulfate
Metavanadate
BMOV
Vanadium oxytriethoxide (VOx)
e
Titer (pfu/ml)
VF4
VBr3
Concentration (μM)
f
Titer (pfu/ml)
Untreated
L-AA
Chelating agent
Untreated
Tiron
Chelating agent
ns
Mock
Vanadate

**Figure 4.2 Viral enhancement is dependent on Vanadium.**

786-0 cells were pretreated for 4 hours with indicated concentrations of (a) various oxidized transitional metals, (c-e) vanadates from various sources prepared in a pH 7.4 buffer. In a, c-e, cells were subsequently infected with oncolytic VSVΔ51 expressing GFP at an MOI of 0.01. (a,d,e) Corresponding viral titer were determined 24 hours post infection from supernatants (N=3). (c) Corresponding GFP positive cell counts 24 hours post infection. (b) Structure of vanadium oxometalates are illustrated. (f) 786-0 were pretreated with 200μM of vanadate or mock and treated with chelating agent ascorbic acid (L-AA) or Tiron, then infected with VSVΔ51 (MOI : 0.01). Corresponding viral titers were determined 24 hours post infection from supernatants (N=3). (Error bars indicate SEM. NS, no statistical significance; *$p < 0.05$, **$p < 0.01$, ***$p < 0.001$ by 1 way ANOVA analysis; as compared to 0μm or Mock condition)

*Vanadate enhances virus and cytokine-induced death*

Overall, our data suggested that vanadium compounds enhance the spread of a subset of RNA-based OVs in cancer cells. Next we examined whether this extended to impact oncolytic activity. Figure 3.3a shows indeed that while vanadate had cytotoxic effects on its own at high doses, cancer cell death was vastly enhanced upon co-infection with a low MOI of VSVΔ51, which is otherwise innocuous to 786-0 cells. A similar effect was observed in various human cancer cell lines, and with various vanadium compounds (Supplemental Figure 4). The mode of cell death was found to exhibit characteristics of apoptosis as determined by flow cytometry following staining with Annexin V and 7-AAD (Figure 4.3b). Furthermore, we found that vanadate increased transcription of proapoptotic factors PUMA and Noxa that are normally induced by p53 over the course of viral infection *(278, 279)* (Figure 4.3c). Interestingly, the impact of vanadate on cell death was independent of its promotion of viral spread since increased 786-0 cell death was also observed using UV-inactivated VSV, as well as a G-less (ΔG) version of VSVΔ51 devoid of its capacity to produce glycoprotein (Figure 4.3d). Indeed, G-less VSVΔ51 can infect cells and replicate its genome but does not bud or spread further. Altogether, this suggested the potential involvement of virus-induced bystander killing and so we tested whether antiviral IFN normally secreted following infection of 786-0 cells by VSVΔ51 could produce similar effects in combination with vanadate. Indeed, Figures 3e-f show that Type I IFN (α and β), could lead to cytotoxicity in 786-0 cells in the presence of vanadate. Similar effects were obtained when challenging cells with poly I:C, a toll like receptor 3 (TLR3) agonist.

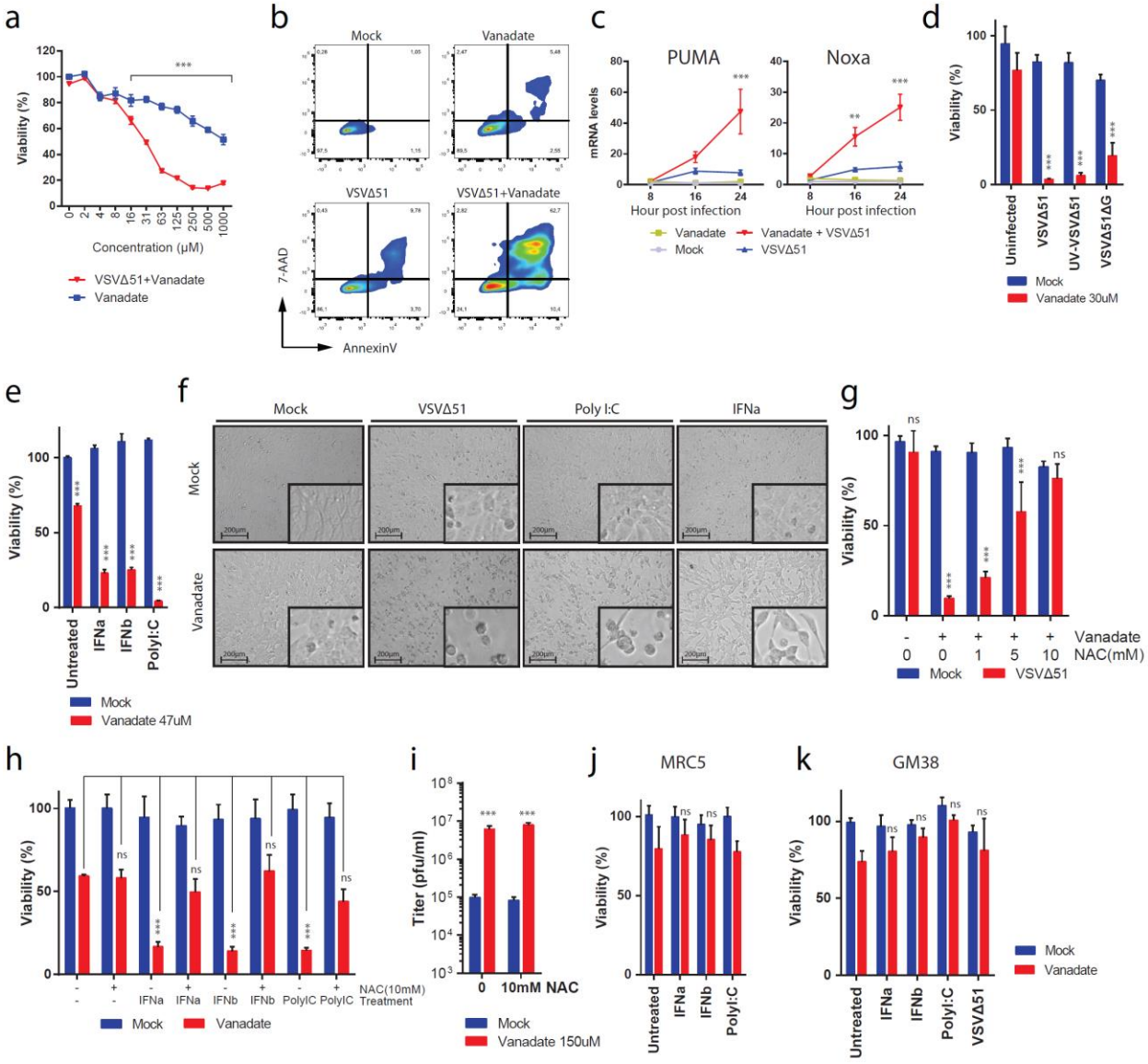
a
Viability (%)
Concentration (μM)
VSVΔ51+Vanadate
Vanadate
b
Mock
Vanadate
VSVΔ51
VSVΔ51+Vanadate
7-AAD
AnnexinV
c
PUMA
Noxa
mRNA levels
Hour post infection
Vanadate
Vanadate + VSVΔ51
Mock
VSVΔ51
d
Viability (%)
Uninfected
VSVΔ51
UV-VSVΔ51
VSVΔ51ΔG
Mock
Vanadate 30uM
e
Viability (%)
Untreated
IFNa
IFNb
Poly I:C
Mock
Vanadate 47uM
f
Mock
VSVΔ51
Poly I:C
IFNa
Mock
Vanadate
g
Viability (%)
Vanadate
NAC(mM)
Mock
VSVΔ51
h
Viability (%)
IFNa
IFNa
IFNb
IFNb
PolyIC
PolyIC
NAC(10mM) Treatment
Mock
Vanadate
i
Titer (pfu/ml)
0
10mM NAC
Mock
Vanadate 150uM
j
MRC5
Viability (%)
Untreated
IFNa
IFNb
Poly I:C
k
GM38
Viability (%)
Untreated
IFNa
IFNb
Poly I:C
VSVΔ51
Mock
Vanadate

**Figure 4.3. Vanadate facilitates virus-induced type I interferon and ROS mediated cell death**.

(a) 786-0 cells were pretreated with a range of concentrations of vanadate for 4 hours and were subsequently infected with VSVΔ51 expressing GFP at an MOI of 0.01. 786-0 cell viability was assayed in cells 24 hours post infection. Results were normalized to the average of the values obtained for the corresponding uninfected, untreated cells (N=4; Error bars indicate SEM; Significance decrease in viability at 16 - 1000µm; ***p<0.0001 by 2 way ANOVA; as compared to uninfected condition). (b) 786-0 were pretreated with vanadate (100µM) for 4 hours and subsequently infected with oncolytic VSVΔ51 expressing GFP at an MOI of 0.01. 24 hours post induction of cell death was determined by annexin V and 7-aminoactinomycin D (7-AAD) staining. Numbers indicate the percentage in each quadrant. (c) Cell lysates of 786-0 treated with vanadate(100µM) and VSVΔ51 expressing GFP were collected at indicated time points, RNA was collected, and expression of PUMA and Noxa genes was quantified by qPCR (N=3; Error bars indicate SEM; **p < 0.01, ***p<0.0001 by 2 way ANOVA; comparing VSVΔ51 condition to vanadate+VSVΔ51 condition). (d-e) 786-0 cells were pretreated with vanadate for 4 hours and subsequently infected with VSVΔ51, UV-inactivated VSVΔ51, VSVΔ51ΔG, or treated with IFNa, IFNb or PolyI:C. Cell viability was assayed 48 hours post infection or treatment. Corresponding cell morphology is presented in panel (f). (g-i) 786-0 cells were co-treated with vanadate and N-acetyl-L-cysteine (NAC) for 4 hours and infected with VSVΔ51 expressing GFP at an MOI of 0.01 (g,i) or with IFNa, IFNb or PolyI:C (h) and cell viability was assayed 48 hours post infection or treatment. In (i), viral titers were determined 24 hours post infection from supernatants (N=3; Error bars indicate SEM; ***p<0.001 by 2way ANOVA; as compared to mock treated condition). (j-k) MRC5 (j) and GM38 (k) normal cells were pre-treated with vanadate for 4 hours and subsequently infected with VSVΔ51 or treated with IFNa, IFNb or PolyI:C. For (d, e, g, h, j, k) cell viability results were normalized to the average of the values obtained for the corresponding uninfected, untreated cells (N=4; Error bars indicate SEM; NS, no statistical significance, ***p<0.0001 by 2-way ANOVA).

The possibility that the effects of vanadate on virus-induced death could be reactive oxygen species (ROS) -mediated was investigated next. To evaluate this, we infected cells treated with vanadate and increasing concentrations of N-Acetyl Cysteine (NAC), which increases cellular glutathione and reduces the levels of cellular ROS. Increasing NAC antagonized vanadate's ability to enhance virus-induced death (Figure 4.3g). Similar results were observed when cells were treated with vanadate and with Type I IFN (α and β) or poly I:C (Figure 4.3h). However, the highest dose of NAC did not abrogate vanadate's ability to increase viral spread (Figure 4.3i), again suggesting that the cytotoxic and virus-enhancing activities of vanadate are distinct. In addition, the observed enhancement of cell death mediated by Type I IFN, poly I:C, and VSVΔ51 by vanadate was not observed in normal adult GM38 or MRC5 human embryonic lung fibroblasts (Figure 4.3j,k).

*Vanadate enhances the oncolytic activity of VSVΔ51 and anti-tumor immunity in vivo*

Given the observation that vanadate enhanced both spread and oncolytic activity of VSVΔ51 *in vitro*, we wondered if the combination of VSVΔ51 and vanadate could have anti-cancer effects in mouse models of cancer. Reports in the literature suggest that vanadate has immunomodulatory properties*(159)*, hence we performed our experiments in a panel of immunocompetent syngeneic mouse tumor models refractory to VSVΔ51 infection. In mice with established CT26WT, 4T1 (breast cancer) and DBT tumors, one single intratumoral injection of vanadate and VSVΔ51 expressing luciferase robustly enhanced virus-associated luciferase gene expression compared to virus alone, as

assessed by an *in vivo* imaging system (IVIS, Figure 4.4a,b). Likewise, vanadyl sulfate (commonly used as a bodybuilding supplement) as well as BMOV evaluated pre-clinically for treatment of diabetes*(264, 280)*, both robustly increased VSVΔ51 viral growth in the DBT model over the course of 3 days post infection (Figure 4.4d,e). Vanadate and VSVΔ51 combination treatment led to significantly improved survival of DBT, CT26WT, and 4T1 tumor-bearing mice compared to the monotherapies (Figure 4.4c). Approximately 80% of DBT tumor-bearing mice and 20% of CT26WT tumor-bearing mice presented complete remission after combination treatment. (Figure 4.4c).

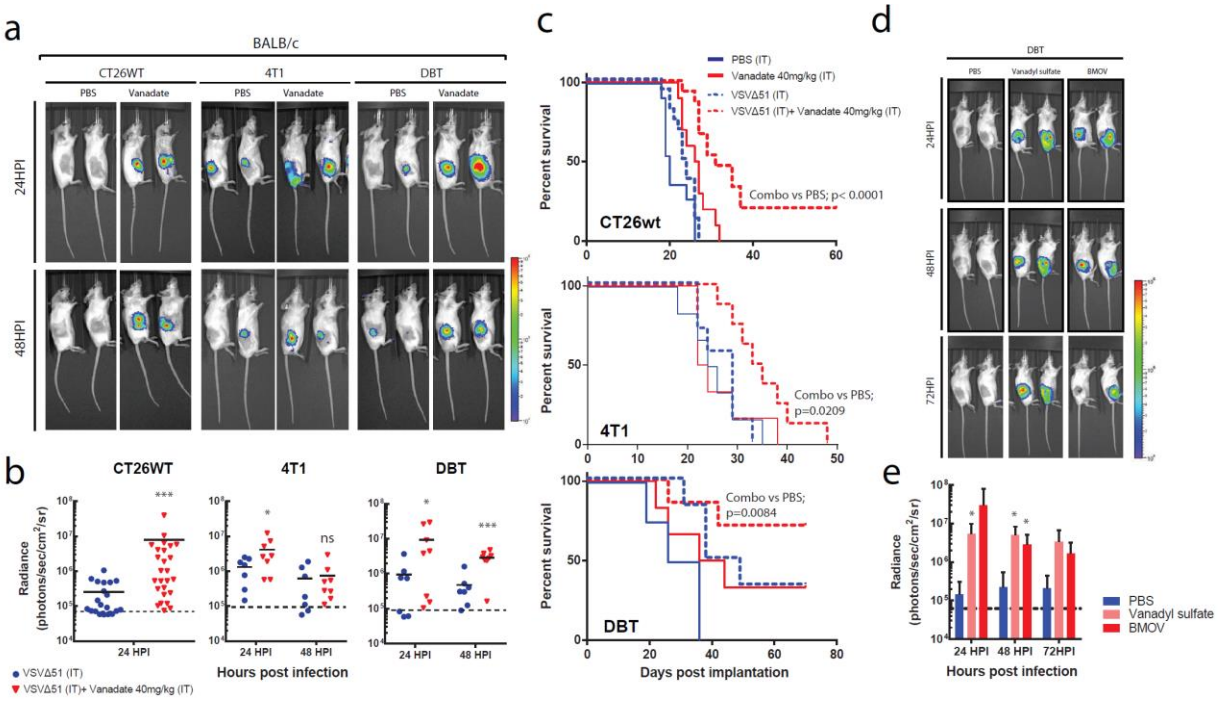
a
BALB/c
CT26WT
4T1
DBT
PBS
Vanadate
24HPI
48HPI
b
CT26WT
4T1
DBT
Radiance (photons/sec/cm²/sr)
24 HPI
48 HPI
Hours post infection
VSVΔ51 (IT)
VSVΔ51 (IT)+ Vanadate 40mg/kg (IT)
c
PBS (IT)
Vanadate 40mg/kg (IT)
VSVΔ51 (IT)
VSVΔ51 (IT)+ Vanadate 40mg/kg (IT)
Percent survival
CT26wt
Combo vs PBS; p< 0.0001
4T1
Combo vs PBS; p=0.0209
DBT
Combo vs PBS; p=0.0084
Days post implantation
d
DBT
PBS
Vanadyl sulfate
BMOV
24HPI
48HPI
72HPI
e
Radiance (photons/sec/cm²/sr)
PBS
Vanadyl sulfate
BMOV
24 HPI
48 HPI
72HPI
Hours post infection

**Figure 4.4. Vanadate increases VSVΔ51 efficacy in resistant syngeneic tumor models.**

(a-c) CT26WT, 4T1, DBT, tumor-bearing mice were treated intratumorally with the vehicle (PBS) or 40mg/kg of vanadate (pH 7.4 prepared from orthovanadate) for 4 hours, and subsequently treated with $1x10^8$ PFU of oncolytic VSVΔ51 expressing firefly-luciferase, intratumorally. (a-b) 24 and 48 hour post infection, viral replication was monitored by IVIS. Representative bioluminescence images of mice are presented in (a), and quantification of luminescence are presented in (b). Scale represented in photons. (N=7-27. Bars indicates mean; NS, no statistical significance; *p < 0.05, ***p<0.001 by 1-tailed t-test; as compared to mock treated condition) (c) Survival was monitored over time. Log-rank (Mantel-Cox) test indicates that the combined treatment is significantly prolonged over PBS alone (CT26WT p< 0.0001, N=10-16; DBT p=0.0084, N=4-7; 4T1p=0.0209, N=6-8). (d,e) DBT tumor-bearing mice were treated intratumorally with the vehicle (PBS), 150mg/kg of Vanadyl sulfate, or 80mg/kg of BMOV and subsequently with $1x10^8$ PFU of oncolytic VSVΔ51 expressing firefly-luciferase, intratumorally. Viral replication was monitored by IVIS, representative bioluminescence images of mice are presented in (d). (e) Quantification of luminescence (N=4-5. Error bars indicate SEM; *p < 0.05 by 1-tailed t-test; as compared to PBS treated condition).

Immune profiling of CT26WT tumors indicated an enhanced leukocyte infiltration with significantly increased T cells (Figure 4.5a), including IFNγ producing CD8+ T cells (Figure 4.5a), in mice treated with the combination of vanadate and VSVΔ51 compared to the monotherapies. This suggested that induction and/or recruitment of T cells to the tumors is improved in the presence of vanadate combined with VSVΔ51, which could contribute to tumor control. Indeed, we observed a correlation between the amount of T cell infiltration and tumor regression (Figure 4.5b) in mice from the combined therapy group with the higher responders (HR) presenting increased infiltration compared to lower responders (LR), even though the enhancement of virus-associated luciferase gene expression was similar between them (Figure 4.5c). This suggests that the amount of tumor infection is not the key determinant for maximum T cell infiltration and indicates an additional need to create a milieu that promotes T cell infiltration following infection. Furthermore, mice that were able to completely eliminate CT26WT tumors (Fig 4.4c) subsequently became immune to rechallenge with the same cancer cells (Fig 4.5d), indicating that combination therapy leads to long term anti-tumor immunity.

Figure 5

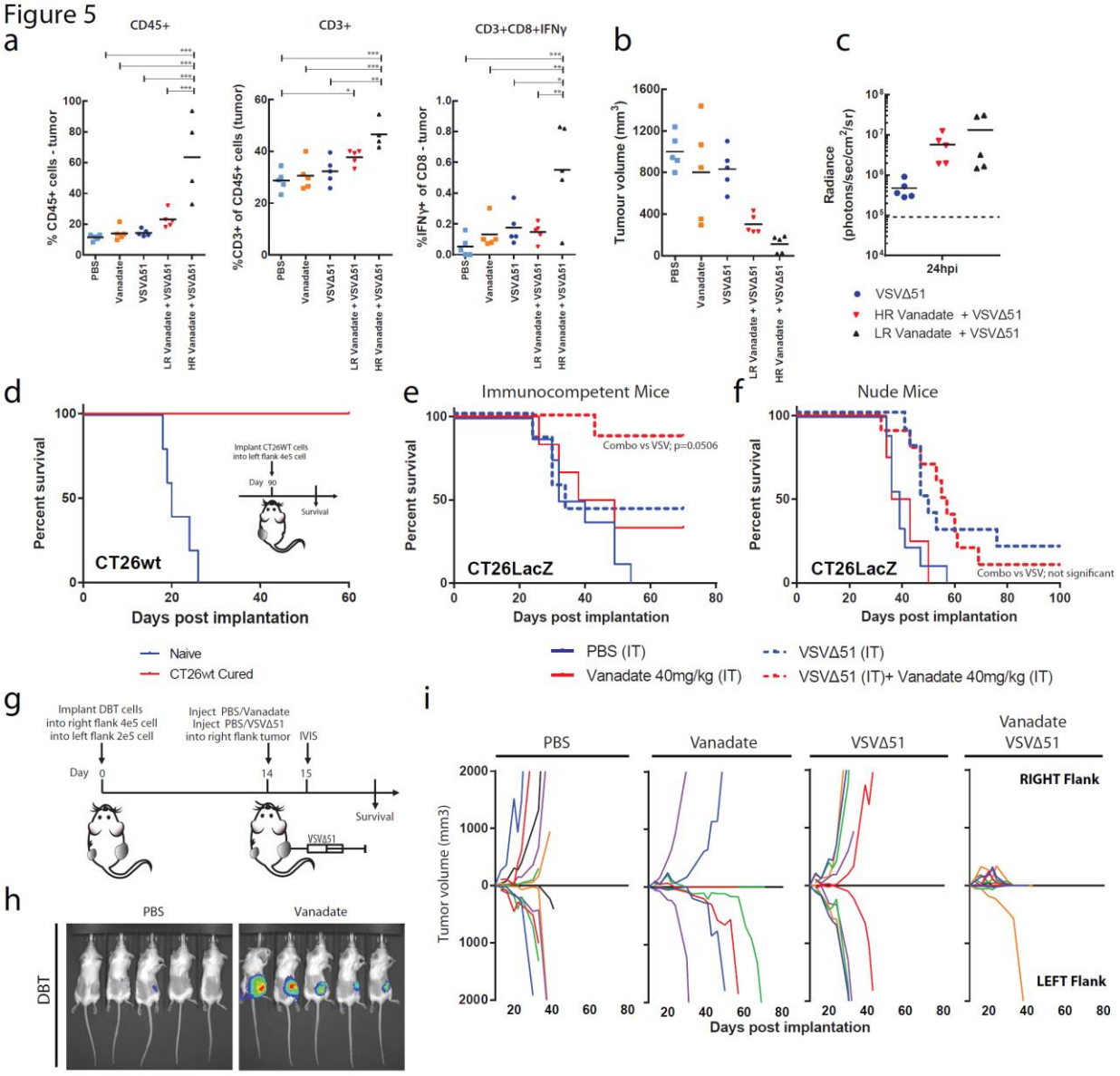
a
CD45+
CD3+
CD3+CD8+IFNγ
% CD45+ cells - tumor
%CD3+ of CD45+ cells (tumor)
%IFNγ+ of CD8 - tumor
PBS
Vanadate
VSVΔ51
LR Vanadate + VSVΔ51
HR Vanadate + VSVΔ51
b
Tumour volume (mm3)
c
Radiance (photons/sec/cm2/sr)
24hpi
VSVΔ51
HR Vanadate + VSVΔ51
LR Vanadate + VSVΔ51
d
Percent survival
Implant CT26WT cells into left flank 4e5 cell
Day 90
Survival
CT26wt
Days post implantation
Naive
CT26wt Cured
e
Immunocompetent Mice
Combo vs VSV; p=0.0506
CT26LacZ
f
Nude Mice
Combo vs VSV; not significant
PBS (IT)
Vanadate 40mg/kg (IT)
VSVΔ51 (IT)
VSVΔ51 (IT)+ Vanadate 40mg/kg (IT)
g
Implant DBT cells into right flank 4e5 cell into left flank 2e5 cell
Inject PBS/Vanadate Inject PBS/VSVΔ51 into right flank tumor
IVIS
Day 0
14
15
Survival
VSVΔ51
h
PBS
Vanadate
DBT
i
PBS
Vanadate
VSVΔ51
Vanadate VSVΔ51
RIGHT Flank
LEFT Flank
Tumor volume (mm3)
Days post implantation

**Figure 4.5. Vanadate /VSVΔ51 co-treatment triggers T-cell infiltration and anti-tumor immunity.**

(a-c) CT26WT tumor-bearing mice were treated intratumorally with the vehicle (PBS) or 40mg/kg of vanadate (pH 7.4 prepared from orthovanadate) for 4 hours, and subsequently treated with $1x10^8$ PFU of oncolytic VSVΔ51 expressing firefly-luciferase, intratumorally. The Vanadate + VSVΔ51 group was divided in 2 groups, High and Low responders (HR and LR), based on median tumor size 10 days post treatment, as shown in (b). Viral replication was monitored 24 hour post infection; quantification of luminescence is presented in (c) (N=5). Tumor volume 10 days post treatment are shown in (b) (N=5). (a) Percentage of CD45+ cells; CD3+ cells of total CD45+ cells; IFNγ expressing CD8+ cells in each tumor was quantified by flow cytometry, 10 days post treatment. (N=4-5; Error bars indicate SEM; * $p<0.05$, ** $p<0.001$, ***$p<0.0001$, by 1-way ANOVA). (d) Survival was monitored after re-implantation of CT26WT in cured and naïve mice from Figure 3.4c (N=3-5). (e) Immunocompetent mice and (f) nude mice bearing the CT26LacZ tumor were treated intratumorally with the vehicle (PBS) or 40mg/kg of vanadate for 4 hours, and subsequently treated with $1x10^8$ PFU of oncolytic VSVΔ51 expressing firefly-luciferase, intratumorally. Log-rank (Mantel-Cox) test indicates that survival in the combined treatment is significantly prolonged over VSVΔ51 alone in the immunocompetent mouse model alone (Immunocompetent mice $p=0.0506$, N=6-8; Nude mice no statistical significance, N=4-10). (g) Schematic representation of treatment schedule for bilateral DBT tumors. (h) Representative bioluminescence images of mice are presented. (i) Growth of treated (right flank) and distant (left flank) DBT tumors (N=4-7).

Next, we investigated the effect of vanadate in the CT26LacZ tumor model, which we have previously shown to be significantly more susceptible to infection with VSVΔ51*(281)*. Here vanadate somewhat decreased virus-associated luminescence (Supplemental Figure 5a), in line with the observation that vanadate did not enhance viral growth in cultured CT26LacZ cells (Supplemental Figure 1a,b). However, the combination of vanadate and VSVΔ51 led to a significant improvement of survival over the monotherapies in this model, reaching nearly 90% complete remissions (Figure 4.5e). While enhanced bystander killing as observed in Fig 3 in part could explain this phenomenon, we wondered whether enhanced adaptive immune responses could play a role in generating such a high cure rate with a single intratumoral dose of vanadate and VSVΔ51. We therefore performed these experiments in athymic nude mice that are devoid of T-cells. Remarkably, while VSVΔ51 alone still delayed tumor progression and led to cures, the combination effect was completely abrogated in this context (Figure 4.5f), albeit virus-associated luminescence was not generally affected (Supplemental Figure 5b). Likewise, the combination therapy did not lead to enhanced efficacy in the HT29 tumors implanted in athymic nude (Supplemental Figure 6c) even though enhancement of VSVΔ51 viral growth was observed (Supplemental Figure 6a,b). These results strongly support an important role of T cell-mediated protection observed in the above-described models and the role of vanadate in eliciting an improved T cell response when combined with VSVΔ51. However, the improved efficacy of vanadate was not observed when the CT26LacZ tumors were infected with non-spreading VSVΔ51 (VSVΔ51ΔG) (Supplemental Figure 5c), indicating that viral growth is essential for the combination therapy effect.

To further evaluate the role of the anti-tumor immune response induced by vanadate / virus treatment in tumor control, we implanted immunocompetent mice with bilateral DBT tumors and injected only the right tumors with the combination of VSVΔ51 and vanadate (or monotherapies / PBS) (Figure 4.5g). Interestingly, we found that while virus-associated luminescence was uniquely enhanced by vanadate in the injected tumors on the right side, the tumors on the left also shrunk following the combination therapy (Fig 4.5h,i). Although some tumors did regress following treatment with vanadate, all of the uninjected (left) tumors did not regress. VSVΔ51 monotherapy did not induce tumor regression in the injected (right) or untreated (left) tumors. Taken together, these results reveal that vanadium compounds have the ability to elicit a robust, systemic protective anti-tumor immune response when combined with VSVΔ51.

*Vanadate inhibits the type I Interferon response and potentiates a proinflammatory response via type II interferon.*

Our *in vitro* results indicated that both OV spread and bystander killing in cancer cells can be enhanced by vanadate. While this likely contributes towards improving OV efficacy *in vivo*, our data suggested that a critical component of the therapeutic efficacy associated to the combination regimen in immunocompetent models involves the generation of anti-tumor T-cell responses. To further understand the cell-autonomous molecular mechanisms involved in stimulating this response while being able to enhance infection, a microarray analysis was performed *in vitro*. We first looked at the gene expression profiles of 786-0 cells 24 h following VSVΔ51 or mock infection in the

presence and absence of vanadate (prepared from solutions of orthovanadate or metavanadate). In line with our demonstration that vanadate stimulates an anti-tumor immune response, gene set-enrichment analyses using GOrilla revealed that vanadate alone induced inflammatory responses, and immune system processes; which were further potentiated in combination with VSVΔ51 (Supplemental Figure 7a). Uniquely, the infection of vanadate treated cells led to the increased expression of a number of proinflammatory cytokines (CCL8, CCL3, IL6, TNF, IFNβ, CCL5) and many genes typically induced by type II IFN (IFNγ), including chemokines such as CXCL9, CXCL10, and CXCL11 (Figure 4.6b,c and Supplemental Figure 7b,c and Table S1). Among others, CXCL9 plays a key role in leukocyte trafficking and its mRNA was up-regulated by more than 100,000 fold during viral infection of vanadate-treated cells compared to mock (Figure 4.6a). We further validated the vanadate-mediated increase in mRNA expression of IFNγ induced chemokines such as CXCL9 in mouse CT26WT cells which were used for our *in vivo* models, as well as its secretion by ELISA in various human cancer cell lines (Supplemental Figure 7c,d). While many genes typically induced by IFNγ were up-regulated upon infection of vanadate-treated cells, IFNγ itself was not up-regulated at any time-point post infection under any condition tested in 786-0 (Figure 4.6a,b). On the other hand, IFNβ mRNA was up-regulated by more than 10-fold 24h following infection (Figure 4.6a) in vanadate treated cells compared to mock. Surprisingly, genes typically induced by Type I IFN were either unaffected or decreased in these conditions (Figure 4.6b,c). Indeed, genes induced by Type I IFN, such as MX2 and IFITM1 with known antiviral function against rhabdoviruses, were robustly downregulated as early as 8h post-infection (Figure 4.6a). Furthermore, protein

expression levels of IFITM1 was potently repressed by vanadate in infected cells 16 and 24h following infection (Supplemental Figure 8).

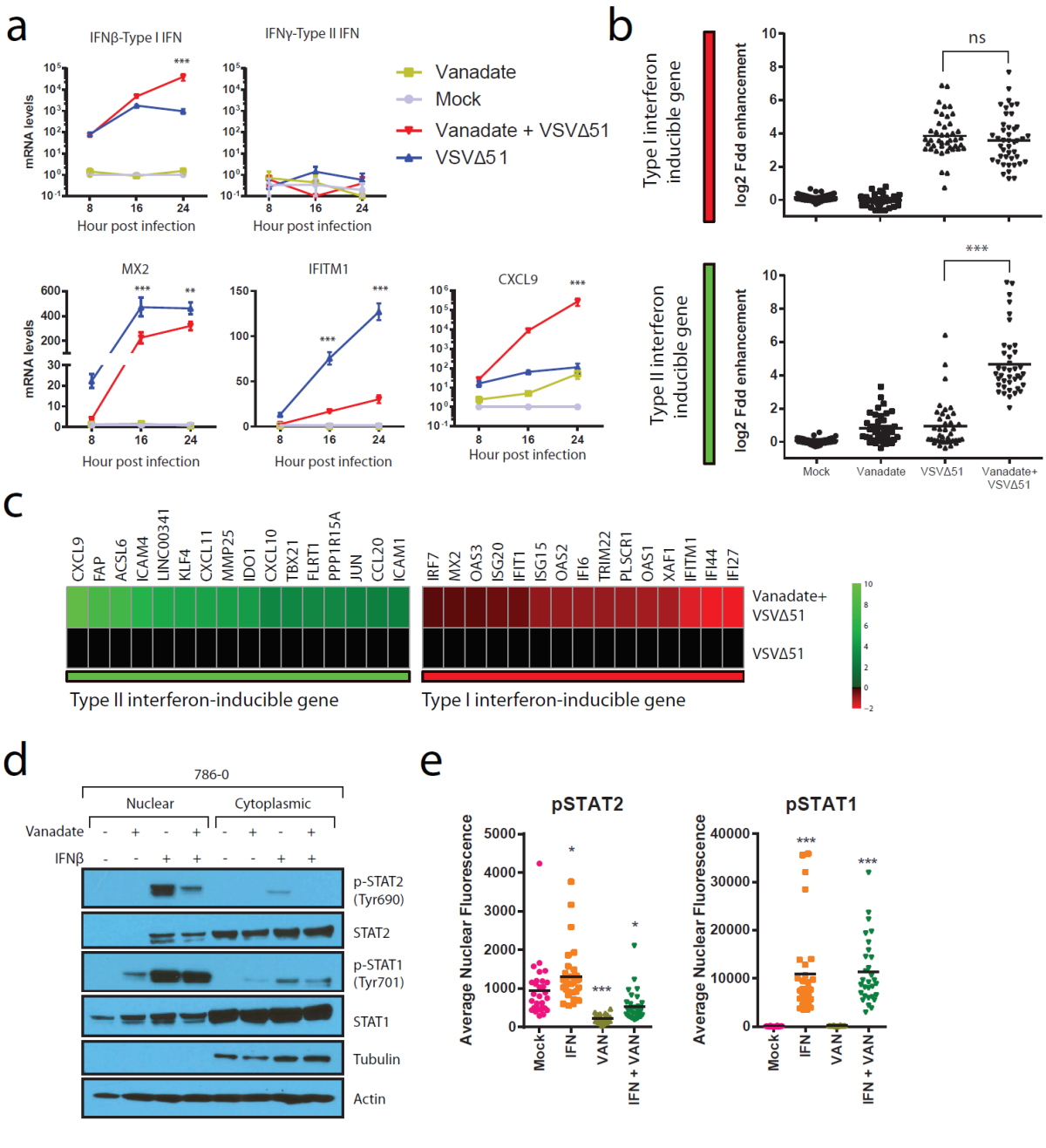
a
IFNβ-Type I IFN
IFNγ-Type II IFN
mRNA levels
Hour post infection
Vanadate
Mock
Vanadate + VSVΔ51
VSVΔ51
MX2
IFITM1
CXCL9
b
Type I interferon inducible gene
Type II interferon inducible gene
log2 Fdd enhancement
ns
***
Mock
Vanadate
VSVΔ51
Vanadate+ VSVΔ51
c
CXCL9
FAP
ACSL6
ICAM4
LINC00341
KLF4
CXCL11
MMP25
IDO1
CXCL10
TBX21
FLRT1
PPP1R15A
JUN
CCL20
ICAM1
IRF7
MX2
OAS3
ISG20
IFIT1
ISG15
OAS2
IFI6
TRIM22
PLSCR1
OAS1
XAF1
IFITM1
IFI44
IFI27
Vanadate+ VSVΔ51
VSVΔ51
Type II interferon-inducible gene
Type I interferon-inducible gene
d
786-0
Nuclear
Cytoplasmic
Vanadate
IFNβ
p-STAT2 (Tyr690)
STAT2
p-STAT1 (Tyr701)
STAT1
Tubulin
Actin
e
pSTAT2
pSTAT1
Average Nuclear Fluorescence
Mock
IFN
VAN
IFN + VAN

**Figure 4.6. Vanadate re-wires antiviral type I IFN signaling towards pro-inflammatory type II IFN response.**

(a-c) Cell lysates of 786-0 treated with vanadate and VSVΔ51 expressing GFP were collected at indicated time points. RNA was extracted and probed for expression of (a) ifnβ, ifnγ, mx2, ifitm1 and cxcl9 genes by qPCR (N=3; Error bars indicate SEM; **p < 0.01, ***p<0.0001 by 2 way ANOVA; comparing the VSVΔ51 condition to the Vanadate+VSVΔ51 condition). (b) RNA was used for gene expression microarray analysis. Data is normalized to untreated control, indicating log2 fold change in gene expression of genes documented to be induced by Type I or Type II IFN. (Bars indicate mean; 1-way ANOVA; NS, no statistical significance, *** p<0.0001, comparing combination treatment to virus alone condition), (c) Heatmap showing the expression levels of the differentially expressed IFN stimulated genes. Expression of genes was normalized to values obtained for mock-treated, infected control. Color scale indicates log2 fold change. (d) 786-0 cells were pretreated with vanadate (1000μM) for 4 hours and challenged with IFNβ (100U/ml). One hour later, fractionated cell lysates were probed for pSTAT1, STAT1, pSTAT2, STAT2 and actin. (e) Immunofluorescence for pSTAT1 and pSTAT2 was performed in 786-0 cells treated with vanadate (1000μM) for 4 hours and with human IFNβ (1000U) for 1 hour. Quantification of the average nuclear fluorescence associated to pSTAT1 or pSTAT2 in each condition (N=30; Bars indicate mean; 1-way ANOVA, * p<0.05, ** p<0.001, *** p<0.0001, as compared to the mock condition counterpart). Microscopy images can be found in Figures S9-11.

Importantly, IFNβ and IFNγ bind to distinct receptors and lead to differential activation of STAT1 and STAT2 (Signal Transducer and Activator of Transcription) transcription factors. Phosphorylation of STATs leads to their dimerization and nuclear translocation to activate transcription of IFN-stimulated genes (ISGs). Some of these genes are regulated by both type I and type II IFNs, whereas others are selectively regulated by one or the other. Type I IFNs induce the phosphorylation of both STAT1 and STAT2, leading to the formation of the ISGF3 complex composed of a STAT1-STAT2 heterodimer and IRF9 that binds specific promoter regions known as IFN-stimulated response elements (ISREs); while type II IFN primarily induce the phosphorylation of STAT1, leading to the formation of STAT1-STAT1 homodimers that bind IFNγ-activated-sequence (GAS) elements*(56)*. Consistent with a shift from a type I towards a type II IFN response, vanadate treatment inhibited the IFNβ-induced phosphorylation of STAT2 and reduced its nuclear accumulation but did not similarly affect STAT1 as observed by Western blot (Figure 4.6d). Supporting this idea, immunofluorescence also revealed that whereas activated STAT1 translocated to the nucleus following infection of vanadate-treated cells (Figure 4.6e, Supplemental Figure 9), STAT2 remained mostly in the cytoplasm (Figure 4.6e, Supplemental Figure 10,11). Remarkably, this suggests that vanadate enhances OV activity through a previously unappreciated mechanism that converts a predominantly antiviral type I IFN response into a type II IFN response, through the preferential repression of STAT2 activation. This signal "rewiring" leads to up-regulation of proinflammatory cytokines and chemokines that favour the generation of a T cell dependent anti-tumor response.

## Discussion

OV therapy as a standalone treatment can be highly effective but treatment resistance remains a frequent occurrence. This is attributed to a number of factors, including a need to robustly infect tumors and ensure the initiation of a robust anti-tumor immune response*(8)*. The latter has prompted many investigators to evaluate OVs in combination with immune checkpoint inhibitors; a strategy has been shown to be effective by several groups in both preclinical models and clinical trials*(30, 193–196)*. However this specific combination strategy is not uniformly effective*(282)*.

We show here that vanadium compounds can provide a significant therapeutic benefit in CT26WT and other various aggressive, treatment-refractory, murine tumor models when combined with OVs, leading to enhanced anti-tumor T-cell responses mediated by the induction of a Type II Interferon-like response in infected cancer cells. The availability of clinically-advanced vanadium candidates such as vanadate, vanadyl sulfate and bis(ethylmaltolato)oxovanadium(IV) (BEOV)*(263, 264, 283)* that have been used in the context of diabetes will greatly facilitate the testing of such combination regimens in human cancer patients. In addition, oncolytic rhabdoviruses derived from VSV and closely related Maraba are currently undergoing clinical evaluation, including in combination with immune checkpoint blockade (NCT02923466, NCT02879760). Altogether, this lays the groundwork for rapid evaluation of our novel approach in humans. However, while many OVs including T-Vec are currently delivered intratumorally in the clinic*(284)*, it will be relevant to further explore alternative regimens and formulations to abrogate the need for intratumoral injection of vanadium

compounds ahead of virus. Oral administration of vanadium compounds is possible and has been extensively tested in the treatment of type II diabetes*(285)*.

In the present work, we tested a range of different vanadium salts and compounds. These compounds are known to undergo different hydrolytic conversions in solution*(154)*. Orthovanadate, metavanadate and vanadium(V) oxytriethoxide all result in a solution of $H_2VO_4^-$ at physiological pH, while the solutions prepared from vanadyl sulfate and vanadium(IV) fluoride will result in a solution of aqueous V(IV) and V(V)*(154)*, and those prepared from bis(maltolato)oxovanadium(IV) will contain both V(IV) and V(V) maltolato complexes*(280)*. Importantly, all of these compounds show a robust capacity to enhance OV activity (Figure 4.2c-e). This suggests significant flexibility in the design of new vanadium-based compounds that may be tailored for use in combination with OVs. Furthermore, these results are consistent with various forms of vanadate binding tightly to several phosphatases with similar Ki values*(262)*.

Protein tyrosine phosphatases are important regulator of cellular processes *(286, 287)* and may have complex functions during the course of viral infection. Here we found that the pan-tyrosine phosphatase inhibitor vanadate, while enhancing all of the RNA viruses in our panel (Rhabdovirus, Alphavirus, Paramyxoviruses), substantially inhibits infection of DNA viruses like vaccinia and HSV. These observations showcase the selective effects of vanadium compounds on RNA viruses, which do not encode viral phosphatases, in contrast with both DNA viruses tested where they serve as important virulence factors*(288, 289)*. Notably, the RNA viruses tested generally lack the ability to counteract Type I IFN signaling. When using wild-type VSV, which more effectively overcomes the type I IFN response compared to VSVΔ51, we found that the positive

impact of vanadate was comparatively reduced *in vitro* (Supplemental Figure 12). Numerous drugs and compounds have been shown to increase the efficacy of OVs by inhibition of Type I IFN production or signalling*(108, 114, 118, 188)*. The ability of vanadium compounds to convert the antiviral Type I IFN to a pro-inflammatory Type II IFN response, leading not only to better OV spread but also to greater anti-tumor immune stimulation during OV treatment is to our knowledge unprecedented.

Previously vanadate has been reported to promote death induced by addition of type I IFN*(290)*, supporting our observations (Figure 4.3). Interestingly, we found that antioxidants could abrogate the priming of apoptosis by vanadate (Figure 4.3g,h), suggesting a potential role of vanadate-induced ROS*(291)* in promoting death initiated by Type I IFN. A role for ROS in modulating IFN activity has also been previously suggested*(292)*, however, this mechanism is unlikely to be at play here given antioxidant treatment did not abrogate enhancement of viral growth (Figure 4.3i). Instead, we found that STAT1 and STAT2 are differently activated by Type I IFN in vanadate-treated cells, ultimately favouring the accumulation of STAT1 in the nucleus (Figure 4.6d-e, Supplemental Figure 9-11). This mechanism is in line with activation of Type II IFN target genes that rely on STAT1-STAT1 homodimers for their transcription, even in absence of IFN-γ. This could also explain the enhanced capacity for Type I IFN to induce cell death (Figure 4.3e-g), given STAT1 has been shown to promote cell death by interacting with TRADD, HDACs, or p53 to increase the expression of target genes such as Noxa and Puma as observed in this study (Figure 4.3c)*(293, 294)*. Notably, type I IFN, such as IFNα (INTRON® A) is widely used for the treatment of renal cancer, although therapeutic results remain limited*(295)*. Further studies investigating the impact of

vanadium compounds on this and other anti-cancer strategies that aim to kill cancer cells through type I IFN or through recruitment of T-cells to the tumor site may be warranted.

## Materials and Methods

**Drugs, chemicals and cytokines.** Drugs, chemicals and cytokines and their respective supplier and solvent used in this study are listed in Table S2. The aqueous chemistry of some of these vanadium compounds lead to conversion of the original compound into vanadate*(296)* under the condition of the studies, and this is also indicated in Table S2.

**Cell lines.** Cells and their respective supplier and growth media used in this study are listed in Table S3. Cells were cultured in HyQ high-glucose Dulbecco's modified Eagle's medium (GE Healthcare Life Sciences Hyclone, Logan, UT) supplemented with 10 % fetal calf serum (CanSera, Etobicoke, Canada), HEPES, penicillin/streptomycin (Gibco Life Technologies, Waltham, MA). All cell lines were incubated at 37 °C in a 5% $CO_2$ humidified incubator. All cells were tested to ensure they are free of mycoplasma contamination.

**Viruses and quantification.**

*Rhabodviruses.*The Indiana serotype of VSV (VSVΔ51 or wild type) was used throughout this study and was propagated in Vero cells. VSVΔ51-expressing GFP or firefly luciferase are recombinant derivatives of VSVΔ51 described previously*(48)*. All viruses were propagated on Vero cells and purified on 5–50% Optiprep (Sigma-Aldrich, St. Louis, MO) gradient and all virus titres were quantified by the standard plaque assay on Vero cells as previously described*(252)*.

*Herpes simplex virus*. The HSV-1 N212 expressing GFP*(253)* was a gift from Dr. Karen Mossman (McMaster University, Canada). HSV virus titres were quantified by the standard plaque assay on Vero cells as previously described*(253)*.

*Measles virus*. The Measles virus (MV) expressing GFP (Schwartz strain) was a gift from Dr. Guy Ungerechts (Ottawa Hospital Research Institute, Canada). MV virus titres were quantified on Vero cells.

*Sindbis virus.* The Sindbis virus expressing GFP was a gift from Dr.Benjamin tenOever (Icahn School of Medicine at Mount Sinai, NY, USA). The Sindbis virus was quantified by the standard plaque assay in Vero cells. Plaques were counted 3 days post-infection.

*Vaccinia virus.* Vaccinia virus (Wyeth strain deleted for thymidine kinase and expressing GM-CSF) was quantified by plaque assay in U20S cells as described previously*(201)*.

**Cell viability assay.** The metabolic activity of the cells was assessed using alamarBlue (Bio-Rad, Mississauga, Canada) according to the manufacturer's protocol. Treated and/or infected cells in a 96-well plate (Corning, Manassas, VA) were treated, at indicated time, with 10µL of alamarBlue in each well and incubated for 2 to 4 hours. Fluorescence was measured at 590nm upon excitation at 530nm using a Fluoroskan Ascent FL (Thermo Labsystems, Beverly, MA).

**Microarray and analysis.** The 786-0 cells were plated at a density of $1 \times 10^6$ in 6-well dishes and allowed to adhere overnight. The next day, cells were pretreated for 4hours with orthovanadate(150µM), metavanadadate (150µM) or the vehicle. Following pre-

treatment, the cells were infected with VSVΔ51 at an MOI of 0.01 or left uninfected. Twenty-four hours post infection, RNA was collected using an RNA-easy kit (Qiagen, Toronto, Canada). Biological triplicates were subsequently pooled and RNA quality was measured using Agilent 2100 Bioanalyzer (Agilent Technologies, Mississauga, Canada) before hybridization. Hybridized to Affymetrix Human PrimeView Array was performed by The Centre for Applied Genomics, The Hospital for Sick Children, Toronto, Canada. Microarray data was processed using Transcriptome Analysis Console (TAC) 3.0 under default parameters of Gene Level Differential Expression Analysis. Fold change in gene expression was calculated for each gene in relation to uninfected, untreated control. Heatmap of normalized expression values were generated using R package pheatmap. Volcano plots of gene expression values were generated using R. Gene ontology enrichments analysis was evaluated using GOrilla*(254)* following correction for multiple hypothesis testing (Benjamini–Hochberg). Raw and processed microarray data have been deposited in the NCBI-Gene Expression Omnibus database (GSE97327).

**Mouse tumor models.** *CT26WT, CT26LacZ, DBT, 4T1 models.* Six-week-old female BALB/c mice obtained from Charles River Laboratories (Senneville, Canada) were given subcutaneous tumors by injecting $3 \times 10^5$ syngeneic CT26WT, CT26-LacZ, or DBT cells, or $2 \times 10^5$ 4T1 cells, suspended in 100μl PBS. 10 days (4T1), 11 days (CT26WT, CT26LacZ) or 13 days (DBT) post implantation, tumors were treated intratumorally once with a chemical compound (dissolved in PBS) or the vehicle as indicated. Four hours later, tumors were injected intratumorally with $1 \times 10^8$ p.f.u. (in 25 μl PBS) of the indicated virus. Tumor sizes were measured every other day using an electronic caliper. Numerical ear tagging system enabled unbiased data collection. Tumor volume was

calculated as =(length$^2$ × width)/2. For survival studies, mice were culled when tumors had reached 1,500 mm$^3$. For *in vivo* imaging, an IVIS (Perkin Elmer) was used as described previously*(119)*. Quantification of the bioluminescent signal intensities in each mouse was measured using Living Image® v2.50.1 software. Mice were randomized to the different treatment groups according to tumor size in all experiments. Mice with no palpable tumors on initial treatment day were excluded from study. The investigators were not blinded to allocation during experiments and outcome assessment.

*HT29 model.* Six-week-old CD1 nude mice were given subcutaneous tumors by injecting $1\times10^6$ syngeneic HT29 cells suspended in 100 µl serum-free DMEM. When tumors grew to approximately 5 mm x 5 mm (between 18 – 25 days post-implantation), mice were treated intratumorally once with a chemical compound (dissolved in PBS) or the vehicle as indicated. Four hours later, tumors were injected intratumorally with $1 \times 10^8$ PFU of the indicated virus. Tumor dimensions were measured every other day with electronic calipers.

All experiments were performed in accordance with the University of Ottawa Animal Care and Veterinary Services guidelines for animal care under the protocol OHRI-2265 and OHRI-2264.

***Ex vivo* tumor model.** BALB/c mice were implanted with subcutaneous CT26WT or DBT cells. Mice were sacrificed after tumors had reached at least 10mm x 10mm in size. Tumor, lung, spleen and brain tissue were extracted from the mice, cut into 2 mm thick slices and cored into 2mm x 2mm pieces using a punch biopsy. Each tissue core was incubated in 1 mL of Dulbecco's Modified Eagle's Medium (DMEM) supplemented with

10% fetal bovine serum, 30 mM HEPES and were incubated at 37 °C in a 5% $CO_2$ humidified incubator. Cores were treated for 4 hours with indicated concentration of chemical compound. Subsequently the cores were then infected VSVΔ51-GFP. GFP pictures were taken for each core 24 hours post infection.

**Flow cytometry.**

*Cell death staining.* The 786-0 cells were plated in 6-well dishes, and treated as indicated. 24hour post infection, cells were collected and stain with Annexin V and 7-AAD according to the manufacturer's protocol, using the APC Annexin V Apoptosis Detection Kit with 7-AAD (BioLegend, San Diego, CA). Collected samples were analysed by flow cytometry on a BD LSRFortessa (data analysed with the FlowJo software).

*Tumor-infiltrating lymphocytes.* 10 days post treatment, BALB/c tumor bearing mice were sacrificed and the tumors were collected and dissociated using the Tumor dissociation Kit-mouse (Miltenyi Biotec, Auburn, CA), according to the manufacturer's instructions. Red blood cells were lysed using ACK lysis buffer. Upon resuspension in R10 buffer (RPMI, 10% FBS), the cells were counted and 1.5e6 cells per condition were stained. Cells were then stained with the FVS780 (BD Biosciences, San Jose, CA) viability, for 15min at room temperature. After washes, cells were incubated with anti-CD16/32 in 0.5% BSA/PBS at 4°C to block nonspecific Ab interaction with Fc receptors. For surface staining, cells were incubated with combinations of anti-CD45-BV786, anti-CD3-AF700 and anti-CD8 PE-CF594 (BD Biosciences) for 30 minutes at 4oC. Cells were then washed twice and resuspended in 1% PFA buffer for analysis. For Intracellular

staining, cells were incubated in the presence of golgiplug for 5h, and stained with anti-IFNγ-PE according to the manufacturer's protocol, using the BD Cytofix/Cytoperm Fixation /Permeabilization Solution Kit (BD Biosciences). Collected samples were analysed by flow cytometry on a BD LSRFortessa and data analysed with the FlowJo software (TreeStar).

**Immunoblotting.** Cells were pelleted and lysed on ice for 30 minutes using 50 mM HEPES, pH 7.4, 150 mM NaCl, 10 mM EDTA, 10 mM $Na_4P_2O_7$, 100 mM NaF, 2 mM $Na_3VO_4$, protease inhibitor cocktail (Roche) and 1% Triton X-100. For nuclear and cytoplasmic extracts the NE-PER™ Nuclear and Cytoplasmic Extraction kit (ThermoFisher Scientific, Rockford IL) was used according to the provided protocol. Following protein determination by Bradford assay (Bio-Rad Protein Assay Solution), 20 μg of clarified cell lysates were electrophoresed on NuPAGE® Novex® 4-12% Bis-Tris precast Gels (ThermoFisher Scientific) using the XCell SureLock® mini-cell System (ThermoFisher Scientific) and transferred on nitrocellulose membranes (Hybond-C, Bio-Rad). Blots were blocked with 5% BSA or milk and probed with antibodies specific for phospho-Stat1 (Tyr701, #9171, Cell Signalling Technology, used at 1:1000) and Stat1 (#9172, Cell Signalling Technology, used at 1:1000), Stat2 (#72604, Cell Signalling Technology, used at 1:1000), phospho-Stat2 (#88410S, Cell Signalling Technology, used at 1:1000), IFITM1 (#60074-1-Ig, Proteintech Group, used at 1:1000), VSV (a gift from Dr Earl Brown, used at 1:2000) or β-Actin (#4970, Cell Signalling Technology, used at 1:1000). Blots were then probed with a goat anti-rabbit or mouse peroxidase-conjugated

antibodies (Jackson Immunoresearch Labs, West Grove, PA). Bands were visualized using the Supersignal West Pico Chemiluminescent substrate (ThermoFisher Scientific). All uncropped western blots are available in Supplemental Figure 13.

**Immunofluorescence.** Cells were cultured on coverslips prior to treatment with vanadate and human IFNβ subsequently. Following 1h incubation with IFNβ , the cells were washed with cold PBS and fixed using ice-cold methanol:acetone (1:1). Blocking buffer (5% FBS, 0.3% triton, PBS) and antibody dilution buffer were used (1% bovine serum albumin, 0.3% triton, PBS). The cells were stained using a rabbit anti-phospho-Stat1 (Tyr701, #9171, Cell Signalling Technology, used at 1:500), Stat2 (#72604, Cell Signalling Technology, used at 1:200), or phospho-Stat2 (#88410S, Cell Signalling Technology, used at 1:200) and subsequently with a goat anti-rabbit-488 secondary antibody (#A-11008, Life Technologies). Prolong gold anti-fade with 4',6-diamidino-2-phenylindole (Molecular Probes) was used to mount the coverslips onto slides. The images were captured using the EVOS microscope (ThermoFisher Scientific). Quantification for nuclear:cytoplasmic ratio or the average nuclear fluorescence was performed on ImageJ.

**Quantitative real-time PCR.** 786-0 or CT26WT cells were pretreated for 4 h with chemical compound or the vehicle , and were infected with VSVΔ51 at MOI 0.01 or left uninfected. 24 hours post infection, cells were collected and RNA extraction was performed using the Qiagen RNeasy kit (Qiagen). RNA quantity and purity was assessed using a NanoDrop ND-1000 spectrophotometer (Thermo Scientific) RNA was converted

to cDNA with RevertAid H Minus First Strand cDNA Synthesis Kit (Thermo Scientific). Real-time PCR reactions were performed according to the manufacturer's protocol with the QuantiTect SYBR Green PCR kit (Qiagen) on a 7500 Fast Real-Time PCR system (Applied Biosystems, Foster City, CA). Gene expression relative to GAPDH or b-actin. Fold induction was calculated relative to the untreated/uninfected samples for each gene. List of qPCR primers used in this study are listed in Table S4.

**ELISA.** 786-0 cells plated in 12-well dishes, were pretreated with drug or the vehicle for 4 h, and subsequently infected with VSVΔ51-GFP at indicated MOI or left uninfected. Cell supernatants were collected at different times post infection as indicated. IFN alpha and IFN beta quantification was performed using the Verikine Human IFN alpha or IFN beta ELISA kit (PBL Assay Science, Piscataway, NJ) by following the manufacturer's instructions. Absorbance values at 450 nM were measured on a Multiskan Ascent Microplate Reader (MXT Lab Systems).

**Cytokine Array**. Supernatants from treated 786-0 cells were assayed screened with the RayBio® Cytokine Antibody Arrays - Human Cytokine Antibody Array System 3 (RayBiotech, Norcross, GA). The assay was performed according to the manufacturer's instructions. Data were analyzed using ImageJ and Analysis Tool for AAH-CYT-3 (RayBiotech).

**Statistics.** Statistical significance was calculated using Student's *T*-test, one-way or two way ANOVA test as indicated in the figure legends. The Log-rank (Mantel-Cox) test was used to determine significant differences in plots for survival studies. Error bars represent

standard error of the mean. Statistical analyses were performed using GraphPad Prism 6.0 and Excel.

# Chapter 5 - General discussion

Cancer is a diverse, heterogeneous disease that requires novel approaches for its effective treatment. Over the past two decades, oncolytic virotherapy has emerged as a promising treatment alternative to the current standard of care for cancer patients. Nevertheless, efficacy in clinical trial remains limited. In Chapter 2 we have emphasized the heterogeneity of cancers, and in particular sarcomas, in their capacity to be infected by oncolytic viruses. Importantly, studies in Chapters 3 and 4 have contributed multiple new ways to improve the efficacy of oncolytic virotherapy in the face of this heterogeneity.

## Crosstalk between type I and II interferon pathways

The balance between the type I and type II interferon pathways plays a critical role in the coordination of the innate and adaptive immune systems *(56, 297, 298)*. Type I IFN leads to the assembly of the ISGF3 complex; composed of STAT1, STAT2, and IRF9. Type II IFN leads the homodimerization of STAT1 to form the GAF complex. ISGF3 and GAF bind respectively to the IRSE and GAS regulatory elements upstream of type I and II IFN inducible genes, and activate the expression of distinct sets of antiviral genes. While stimulation with type I IFN, leads to a type I IFN response inducing an antiviral state*(57)*; we demonstrate in Chapter 4 that vanadate can convert the type I IFN mediated antiviral response to a proinflammatory type II IFN response, resulting in

increased viral infection and in a greater anti-tumor immune stimulation during OV treatment.

Several molecular and pharmacological approaches have been studied for their ability to suppress or activate the interferon signaling pathways *(299)*. However, this pharmacological conversion of a type I IFN response to a type II IFN response is to our knowledge unprecedented. A similar phenotype was observed in a previous study revealing that the antiviral response of IκB kinase epsilon (IKKε)-deficient cells showed a reduced type I IFN response and an enhanced type II IFN response, rendering cells less resistant to viral infection *(300)*. IKKε was shown to reduce STAT1 homodimerization and stabilized the interaction between STAT1 and STAT2, leading to shift the balance of STAT1 from GAF to ISGF3 transcriptional complex.

Type I IFN alone has also been observed to signal through GAS, this crossover in signaling is modulated by the SHP-1 phosphatase that is known to target Tyk2 for dephosphorylation. Overexpression of SHP-1 was shown to suppress type I IFN signaling through GAS, while expression of a mutant SHP-1 reversed that effect, indicating the role of SHP-1 in regulating the crossovers between the type I and type II IFN signaling pathway *(301)*.

Vanadate is not known to inhibit kinases such as IKKε, but its capacity to inhibit phosphatases is well documented. Given this, SHP-1 activity may be an important target of vanadium compounds, and further investigation is warranted to see if it is involved in

the phenomena presented in Chapter 4. Because of its inhibition of cellular phosphatase, vanadate is predicted to increase phosphorylation levels of cellular protein. Surprisingly however, we found that vanadate suppresses STAT2 phosphorylation (Tyr690) upon stimulation with IFNβ, while leaving STAT1 phosphorylation intact. This suppression of STAT2 bolsters the shift of STAT1 from the ISGF3 to GAF transcriptional complex, inducing a potent proinflammatory response. Similar observations were reported in STAT2 deficient cells *(302)*. Furthermore, STAT2 deficient mice also exhibit increased susceptibility to viral infection and enhanced replication of vesicular stomatitis virus *(303)*. The molecular mechanism underlying the suppression of STAT2 activity by vanadate was not determined but could involve the indirect regulation of upstream kinases by phosphatases for example.

Generally, regulatory processes that affect STAT2 also impact STAT1, simultaneously altering both type I and II IFN signaling *(304, 305)*. To our knowledge, a phosphatase dephosphorylating STAT2 directly has yet to be identified *(306)*. Identification of a regulator of STAT2 activity that is decoupled from that of STAT1- may provide clues to the regulation of IFN signaling by vanadate. Recently, threonine 387 was identified as novel phosphorylation site of STAT2 that negatively regulates the formation of the ISGF3 complex. The majority of STAT2 in cells is constitutively phosphorylated on threonine 387, while a cyclin-dependent kinase is hypothesized to mediate its phosphorylation. Mutation of this novel site potentiated the expression of IFN-stimulated genes, and was more effective in protecting cells against viral infection *(307)*. The ability of vanadate to inhibit tyrosine phosphatases is well documented, but

some reports also demonstrate the capacity of vanadium compounds to inhibit serine/threonine phosphatase activity of various proteins *(308–310)*. Whether vanadate affects threonine 387 phosphorylation site is currently unknown, but may give us indication of how vanadate suppresses STAT2 activity.

**The antiapoptotic and proapoptotic effects of vanadate**

Studies on the modulation of apoptosis reveal the intricate effect of vanadate on cell death. Upon induction of cell death using radiation, vanadate was shown to block the induction of apoptosis, by suppressing p53 transactivation and suppressing the conformational change of Bax normally resulting in loss of mitochondrial membrane potential and activation of caspases *(311)*. Furthermore, the suppression of p53-mediated apoptosis by vanadate resulted in the protection of mice from lethal dose of radiation *(312, 313)*. This mechanism by which vanadate can suppress apoptosis is not well understood, but was shown to be independent of its effect on PTPs *(311)*. Vanadate may be useful for inhibiting DNA damage-induced apoptosis, as a radio-protector, but may hinder the efficacy of radiation in cancer treatment.

In contrast to the reported negative effect of vanadate on radiation therapy, various vanadium compounds were described as anti-cancers agents because of their capacity to induce cell death via several mechanisms on their own. The generation of reactive oxygen species by vanadate, was shown to induce cell cycle arrest *(314)* and apoptosis in several cancer models *(315)*. Intriguingly this was found to be dependent on the transactivation of p53 *(316)*. Furthermore, vanadate induced caspase-dependent

apoptosis in thyroid papillary carcinoma cell lines through the PI3K/Akt/mTOR cascade*(317)*. Dioxovanadium complexes were shown to inhibit cancer cell growth by activation of the receptor interacting protein kinase 3 (RIPK3), leading to the induction of necroptosis, an inflammatory programmed cell death *(318)*.

In Chapter 4, we found that vanadate promoted cell death upon exposure to cytokine. Exogenous type I IFN or its induction by poly I:C or viral infection has little to no effect of cell viability in the cancer cell lines used in our study. However in the presence of vanadate, these cytokines and TLR agonists led to a potent proapoptotic response. Vanadate has previously been reported to facilitate IFNα-mediated apoptosis *(319)*, supporting our observations. This effect was found to be specific to type I IFN, as vanadate did not trigger apoptosis upon TFNα stimulation *(319)*. Furthermore vanadate induced caspase 3 activity upon IFN treatment, however it did not require p53 to induced IFN mediated apoptosis *(319)*. Analogously, we found that vanadate potentiated cell death upon infection in several human tumor cell defective in p53 activity (p53 mutant cell lines: JIMT1, OVCA8, MDA-MB-231; HPV positive cell line: Hela). In the study by Gamero et al., cells in which components of the JAK-STAT pathway (STAT1, STAT2, JAK1, and TYK2) were knocked down did not undergo apoptosis in the presence vanadate and IFNα, suggesting STAT dependent pathway leading to apoptosis *(319)*. They found, as we did here, that antioxidants could abrogate the priming of apoptosis by vanadate. This suggests that interferon can mediate apoptosis through the generation of ROS. Several reports have suggested a critical role for ROS in modulating interferon mediated apoptosis *(320–323)*.

**Expanding OV tropism**

Each virus utilizes one or several specific cell surface receptors to gain entry, and the clinical indications will likely depend on the presence of specific viral entry receptors on the cancer cell *(10)*. For example the Coxsackie virus and rhinoviruses are known to rely on cell surface entry receptor ICAM1 *(324, 325)*. Coxsackievirus (CAVATAK™), an RNA virus, was shown to exhibit oncolytic activity both *in vitro* and in preclinical animal models. Its efficacy is limited by low expression of ICAM1 in most tumors. Interestingly, we show that vanadate can potentiate expression of ICAM1 upon infection (Chapter 4, Figure 4.6); similar results were observed with different vanadium compound *(326)*. Chapter 3 and 4 focuses on improving OV therapy in part by boosting viral spread, but a recent report suggests that improving entry or attachment of OV to cancer cells, in addition to viral spread, can drastically improve OV infection *(115)*. It would be of interest to explore and assess the potential of vanadium compounds to further expand tropism and improve efficacy of OVs utilizing ICAM1 as a port of entry into the cancer cell by testing them in combination with Coxsackie virus or rhinoviruses*(327)*.

**Improving Oncolytic rhabdovirus therapy in the treatment of Sarcoma**

Our studies in chapter 2 as well as those of others have suggested that OVs are a promising therapeutic avenue for the treatment of sarcoma *(176, 183, 328–331)*. Our studies particularly bolster the potential for oncolytic rhabdoviruses such as oncolytic VSV and MG1 *(180, 332, 333)*. Single-agents have shown limited promise in clinical

sarcoma models and viral tumor penetration is particularly complex in osteosarcomas because of to the general anatomy of bone tissues *(328)*. Interestingly, in humans, once absorbed, vanadium compounds accumulate preferentially in bone, with a half-life of 5 days, compared to half a day in blood *(334)*. The deposition of vanadium in bone is due to its structural similarity with phosphate *(334)*. Furthermore, numerous novel vanadium compounds were shown to inhibit cell proliferation and differentiation of various human osteosarcoma cell lines *(265, 335–337)*. Hence, to further improve oncolytic virotherapy in sarcoma and osteosarcoma, and given the biological capacity of vanadium compounds, evaluation of the therapeutic potential of using vanadium compounds in combination with oncolytic VSV for the treatment of sarcoma may lead to a more robust treatment.

**Cancer therapy targeting the NF-κB pathway**

The NF-κB pathway in cancer cells promotes tumor initiation and development by maintaining a chronic inflammatory microenvironment, by preventing apoptosis, regulating tumor angiogenesis, promoting tumor metastasis and remodeling of the tumor metabolism *(142)*. Targeting NF-κB as a cancer therapy has been extensively investigated in the past decades *(338)*. Interestingly, constitutive activation of the NF-κB pathway occurs in almost 70% of pancreatic ductal adenocarcinoma (PDA) cases, promoting its tumorigenesis *(339)*. The molecular mechanisms underlying NF-κB activation in PDA has been linked to the G12D mutation in KRAS *(340)*. Most cancer therapies have shown little efficacy in treating PDA, making it one of the most lethal abdominal malignancies *(341)*. Considering that oncolytic VSV has shown some efficacy in pancreatic ductal

adenocarcinoma model *in vitro (22)*, investigating the benefits of the combination therapy with NF-κB inhibitor DMF with oncolytic rhabdoviruses as described in chapter 3, may lead to development of new treatment strategies for PDA.

**Treatment delivery**

In both the case of the treatment of multiple sclerosis with DMF or of type II diabetes with vanadium compounds, the drugs are formulated for oral administration. However, in our studies in Chapter 3 and 4, we opted for intratumoral delivery of vanadium compounds and DMF to ensure co-delivery of virus and drug. We considered that oral gavage may limit the delivery of DMF or vanadate and consequently their ability to enhance viral replication within the tumor, because of to the physical barriers that the drug must face before reaching the tumor (such as digestive system, liver), and poor tumor vascularization. Furthermore, given that currently approved oncolytic viruses (such as T-Vec) are administered intratumorally, we considered it relevant to deliver the drug by the same route. Nevertheless it will be important to explore oral administration routes and other dosing regimens ahead of clinical trials.

Treatment schedules and dosing vary in the different *in vivo* tumor models employed in our studies owing to their baseline characteristics, which are different on several levels (drug class, toxicity of the drug, mouse strain, cancer origin, species, and baseline sensitivity to monotherapies). For example, the estimated lethal dose in 50% of animals (LD50) for vanadate in mice is 60 mg/kg, while the LD50 for DMF in female

mice is 990 mg/kg when administered intraperitoneally. Furthermore, variation in the dosing regimen was based either on toxicity (in the case of vanadate), or because of varying efficacies of the single treatment, which had to be taken into account in order to detect potential synergies (in the case of DMF). In Chapter 2, 3, and 4, the dosing for VSVΔ51 was 1e8 PFU/injection for all tumor models given we know this dose (with anywhere from 1-3 injections within a period of 1 week) to be modestly effective on its own in the all OV-resistant models presented. Overall, we feel this is rather positive given it indicates flexibility in the potential dosing and scheduling regimen used, which would need to be altered when translating from mouse models to human trials.

**Beyond oncolytic immunotherapy**

In chapters 3 and 4, we have identified and characterized the mechanism by which pharmacological drugs based on vanadium or FMAEs are able to break resistance to oncolytic virotherapy. Interestingly, recent studies have described the mechanism of treatment resistance to checkpoint inhibitors, arguably the most impactful cancer immunotherapy in recent history *(342)*.

Similarly to oncolytic viruses, prolonged IFN signaling leads to resistance to immune checkpoint blockade using anti-PD1 *(343)*. Persistent IFN signaling allows tumors to acquire STAT1-related epigenomic changes and increases expression of ISGs and ligands for multiple T-cell inhibitory receptors. Both type I and II IFN signaling results in overactivation of T-cell, and can lead to resistance to anti-PD1 *(343)*. Interestingly, Benci *et al.* demonstrate that resistance to anti-PD1 can be overcome

pharmacologically using JAK inhibitors. We showed in Chapter 3 that fumaric acid esters such as DMF can inhibit IFN production and response in cancer cells. Furthermore, studies have shown the profound effect of DMF on the activity of T-cells*(135)*. Therefore, DMF may prove to be an efficient way to overcome resistance to anti-PD1 treatment. Future assessment of this therapeutic combination may lead to promising treatment alternative for cancer patients.

In contrast to anti-PD1 treatment, non-responders to anti-CTLA-4 treatment in patients with metastatic melanoma were found to have tumors with genomic defects in genes involved in the type II IFN signaling pathway *(344)*. Additionally, mice bearing melanoma tumors with knockdown of IFN-γ receptor 1 (IFNGR1) have diminished response to anti-CTLA-4 therapy *(344)*. Interestingly, we show that vanadate can potentiate type II IFN response, upon viral infection. Similarly, a vanadium compound was found to boost IFN-γ signaling, resulting in increased STAT1 transcriptional activity *(326)*. Hence, the molecular mechanisms underlying resistance to anti-CTLA4, leads to the hypothesis that vanadium compound could break resistance and further potentiate the effect of checkpoint inhibitor anti-CTLA4.

**Concluding thoughts**

The most successful cancer therapies are those that target more than one aspect of tumor biology. A tremendous effort in the field of cancer treatment has been devoted to the development and evaluation of multi-modal therapies, for instance, through

bifunctional antibodies simultaneously targeting PD-L1 and TGF-β, combination of different immune checkpoint inhibitors, or the combination of checkpoint inhibitors with antibody-drug conjugates, oncolytic viruses, or with antiangiogenic therapy *(196, 345–350)*. We show that our newly identified VSes promote viral spread, cytotoxicity and in the case of vanadium compounds, we also demonstrate an enhanced antitumor immunity. Therefore combining viral sensitizers such as vanadium compounds or DMF with OVs are promising multifunctional therapeutic candidates.

Our work also showcases the capacity to chemically re-wire the interferon signaling pathways leading to more effective oncolytic virotherapy. This novel interferon re-wiring may also contribute in the advancement of treatments of bacterial infection, skin lesions or immune disorders such as chronic granulomatous disease *(297, 351)*.

Overall this work has contributed to the cancer therapy field by identifying novel drug treatment strategies to overcome resistance to oncolytic virotherapy, in addition to identifying oncolytic rhabdoviruses as a promising treatment for sarcoma.

## Appendices I – Chapter 2 Supplemental information

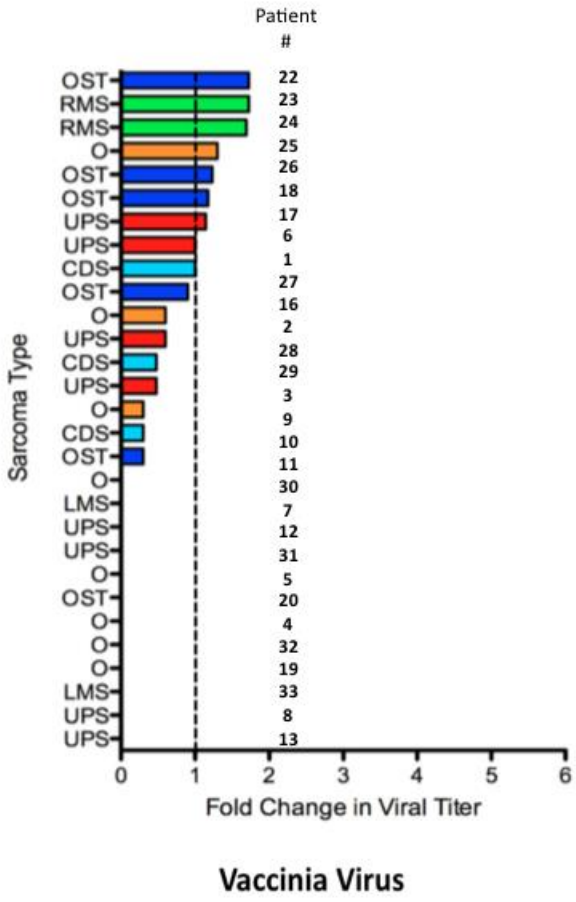


**Supplemental Figure 1:** Various human sarcoma subtypes including Osteosarcoma (OST), Undifferentiated Pleomorphic Sarcoma (UPS), Rhabdomyosarcoma (RMS), Leiomyosarcoma (LMS), Chondrosarcoma (CDS) and other (O) sarcoma explants were process for *ex vivo* infection with VVdd-eGFP. 48 hours after infection with VVdd, explants were homogenized and titered. Fold changes in viral titer compared to input virus have been plotted for each patient with a specific number. Patient number #1 in Maraba plot correspond to patient number #1 in vaccinia plot. Note: Some patients have been processed only for Vaccinia or for Maraba virus.

## Maraba

| Patient# | Age | Sex | Final Pathology | Neoadjuvants | Fold Increase (to T=0) MARABA |
|---|---|---|---|---|---|
| 28 | 56 | M | Well-differentiated liposarcoma | NO | 0 |
| 39 | 46 | F | Undifferentiated Pleomorphic Sarcoma - Grade III | NO | 2 |
| 21 | 80 | M | Chondrosarcoma - Grade II | NO | 4 |
| 38 | 38 | M | Osteosarcoma - Grade II/III | NO | 24 |
| 30 | 70 | M | Dedifferentiated chondrosarcoma - high grade | NO | 28 |
| 27 | 56 | M | Epithelioid Angio Sarcoma | Radiation | 59 |
| 41 | 74 | F | Undifferentiated Pleomorphic Sarcoma - Grade III | Radiation | $1.7x10^2$ |
| 17 | 82 | F | Rhabdomyosarcoma | NO | $2.1x10^2$ |
| 32 | 19 | F | Osteosarcoma | Chemo | $4.9x10^2$ |
| 24 | 54 | M | Chondrosarcoma - Grade II | NO | $8.2x10^2$ |
| 29 | 42 | M | Undifferentiated pleomorphic sarcoma - grade II/III. | NO | $8.8x10^2$ |
| 42 | 12 | F | Osteosarsoma | Chemo | $1.3x10^3$ |
| 35 | 15 | F | Osteosarcoma | NO | $2.2x10^4$ |
| 36 | 45 | M | Recurrent Osteosarcoma - Grade II/III | NO | $2.7x10^4$ |
| 23 | 44 | M | Osteosarcoma - Grade III | NO | $3.5x10^4$ |
| 37 | 79 | M | Undifferentiated Pleomorphic Sarcoma - Grade III | NO | $1.5x10^5$ |
| 26 | 78 | F | Pleomorphic leiomyosarcoma - Grade II/III | NO | $2.9x10^5$ |
| 25 | 61 | F | Fibromyxoid Sarcoma - Grade I | N5O | $3.1x10^4$ |
| 46 | 53 | M | Biphasic Synovial Sarcoma - Grade II | Radiation | $4.5x10^5$ |
| 43 | 60 | M | Undifferentiated Pleomorphic Sarcoma - Grade III | Radiation | $5.8x10^5$ |
| 33 | 22 | M | Leiomyosarcoma Grade I | NO | $6.1x10^5$ |

**Supplemental Figure 2:**

Table summarizing specific number patients, age, gender, pathology, potential use of neoadjuvant, Maraba virus increase compared to virus input (Fold increase).

## Vaccinia

| Patient # | Age | Sex | Final Pathology | Neoadjuvants | Fold Increase (to T=0) VACCINIA |
|---|---|---|---|---|---|
| 22 | 56 | F | Undifferentiated Pleomorphic Sarcoma - Grade III | NO | 0 |
| 23 | 20 | F | Myxoinflammatory Fibroblastic Sarcoma - Grade I | NO | 1 |
| 24 | 53 | M | Undifferentiated Pleomorphic Sarcoma - Grade pending | Radiation | 0 |
| 25 | 12 | M | Malignant Peripheral Nerve Sheath Tumour | Chemo/Rad | 1 |
| 26 | 44 | M | Osteosarcoma - Grade III | NO | 1 |
| 18 | 61 | F | Fibromyxoid Sarcoma - Grade I | NO | 1 |
| 17 | 78 | F | Pleomorphic leiomyosarcoma - Grade II/III | NO | 1 |
| 6 | 56 | M | Epithelioid Angio Sarcoma | Radiation | 1 |
| 1 | 56 | M | Well-differentiated liposarcoma | NO | 1 |
| 27 | 22 | M | Leiomyosarcoma Grade I | NO | 1 |
| 16 | 79 | M | Undifferentiated Pleomorphic Sarcoma - Grade III | NO | 1 |
| 2 | 46 | F | Undifferentiated Pleomorphic Sarcoma - Grade III | NO | 1 |
| 28 | 59 | M | Epithelioid Sarcoma - High Grade | Chemo | 2 |
| 29 | 16 | F | Osteosarcoma - Grade II/III | NO | 2 |
| 3 | 80 | M | Chondrosarcoma - Grade II | NO | 2 |
| 9 | 19 | F | Osteosarcoma | Chemo | 2 |
| 10 | 54 | M | Chondrosarcoma - Grade II | NO | 3 |
| 11 | 42 | M | Undifferentiated pleomorphic sarcoma - grade II/III. | NO | 3 |
| 30 | 18 | n/a | Synovial Sarcoma - Grade II, t(X;18) | NO | 4 |
| 7 | 74 | F | Undifferentiated Pleomorphic Sarcoma - Grade III | Radiation | 4 |
| 12 | 12 | F | Osteosarsoma | Chemo | 8 |
| 31 | 41 | F | Undifferentiated Pleomorphic Sarcoma - Grade III | NO | 10 |
| 5 | 70 | M | Dedifferentiated chondrosarcoma - high grade | NO | 10 |
| 20 | 60 | M | Undifferentiated Pleomorphic Sarcoma - Grade III | Radiation | 14 |
| 4 | 38 | M | Osteosarcoma - Grade II/III | NO | 15 |
| 32 | 44 | M | Osteosarcoma - Grade pending | NO | 17 |
| 19 | 53 | M | Biphasic Synovial Sarcoma - Grade II | Radiation | 20 |
| 33 | 81 | M | Rhabdomyosarcoma - Grade II | NO | 49 |
| 8 | 82 | n/a | Rhabdomyosarcoma | NO | 53 |
| 13 | 15 | F | Osteosarcoma | NO | 53 |

**Supplemental Figure 3:**

Table summarizing specific number patients, age, gender, pathology, potential use of neoadjuvant, Vaccinia virus increase compared to virus input (Fold increase).

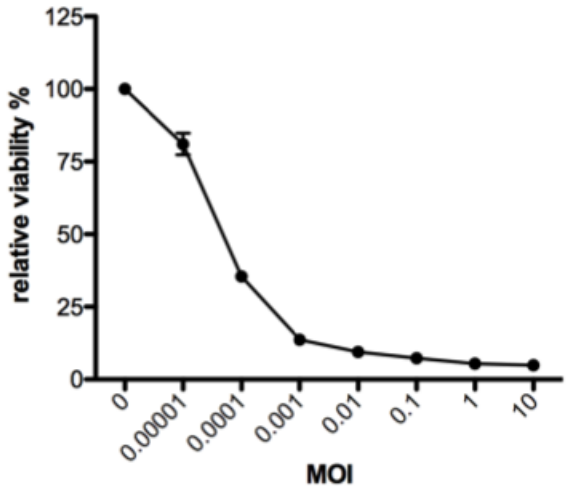


**Supplemental Figure 4:**

S180 sarcoma murine tumor cell line was plated in 96 wells plate and infected with Maraba virus at various MOI. Cell viability have been assessed using Alamar Blue assay 24 hours after infection and plotted.

# Appendices II – Chapter 3 Supplemental information

## Supplementary Materials

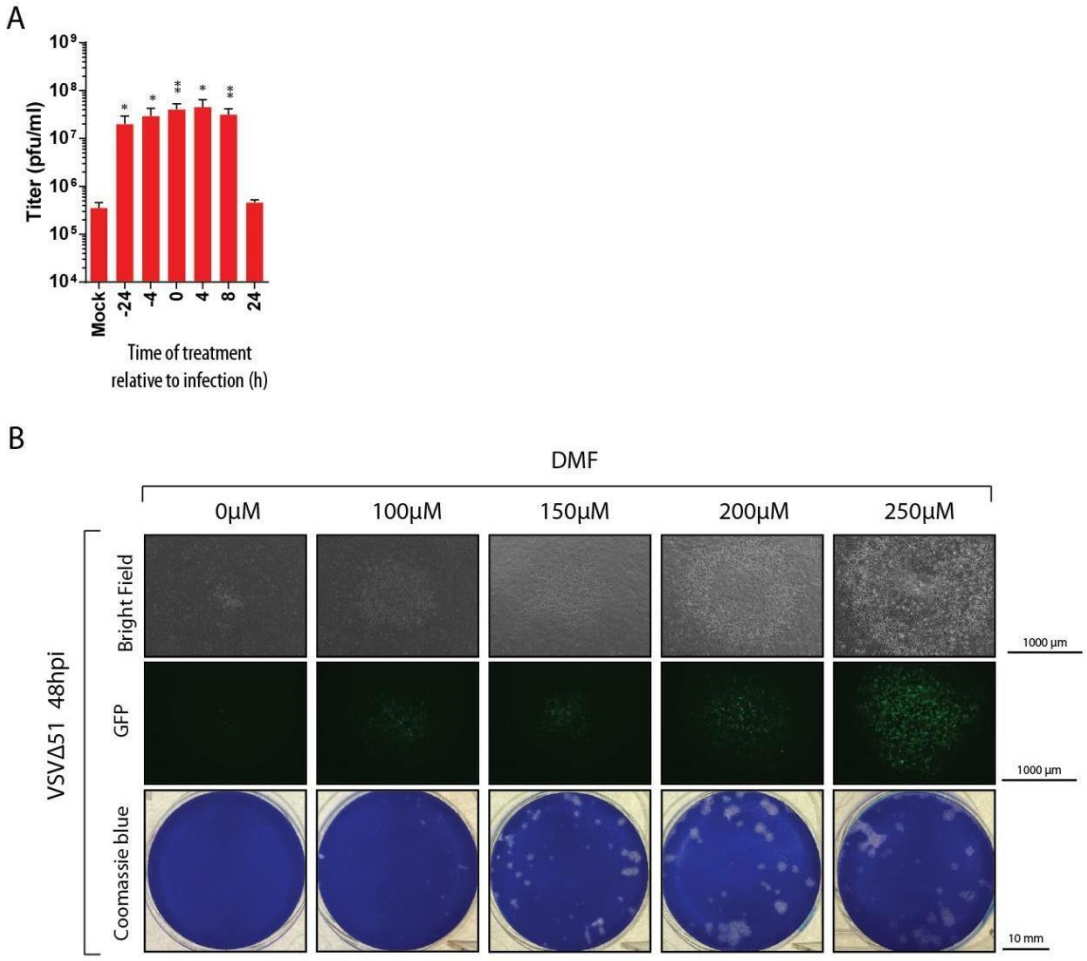


**Supplementary Figure 1 | Dimethyl fumarate promotes viral spread.**

(A) 786-0 cells were treated with 150 µM of DMF at various times before or after infection with VSVΔ51 (MOI: 0.01) or untreated. Supernatants were collected 24 hours after infection and titered by plaque assay (n=3; mean +/- SD; 2-tailed t-test; * $p<0.05$, ** $p<0.01$, as compared to the mock condition counterpart). (B) 786-0 were pretreated with DMF for 4 hours and infected with VSVΔ51 (MOI: 0.0001). An agarose overlay was added after 1 hour of infection. Fluorescence microscopy shows a representative plaque 48 hours after infection. Corresponding images show coomassie blue stain of the full wells.

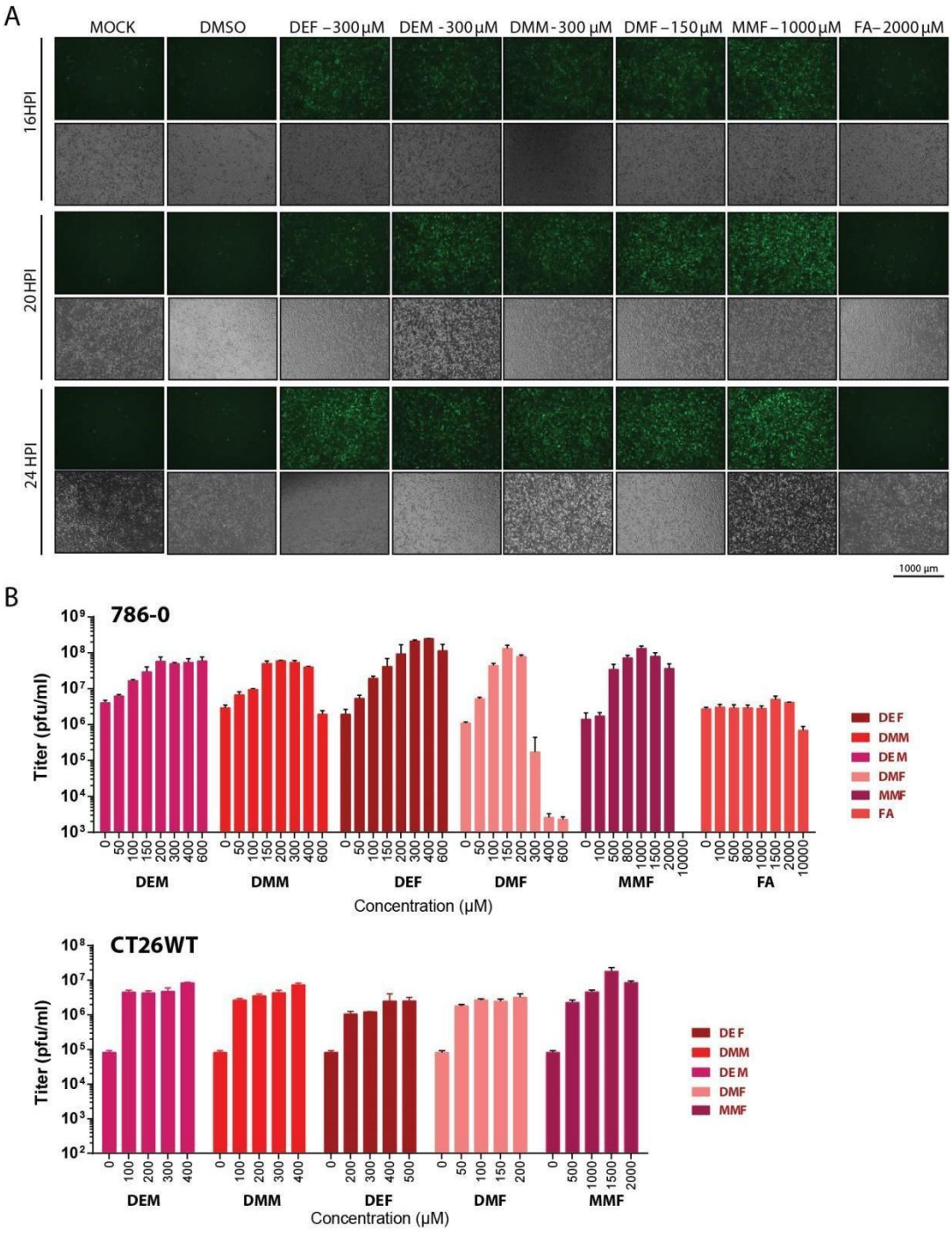


**Supplementary Figure 2 | Fumaric and maleic acid esters enhance VSVΔ51 infection in 786-0 and CT26WT cancer cell lines.**

(A) 786-0 cells were treated with various FMAEs at the indicated concentrations for 4 hours and subsequently infected with VSVΔ51 (MOI: 0.01). 16, 20, and 24 hours after

infection, fluorescent and phase contrast images were taken of the infected 786-0 cells. (B) 786-0 and CT26WT cells were treated as in A, supernatants were collected 48 hours after infection and titered by plaque assay (n=3; mean +/- SD).

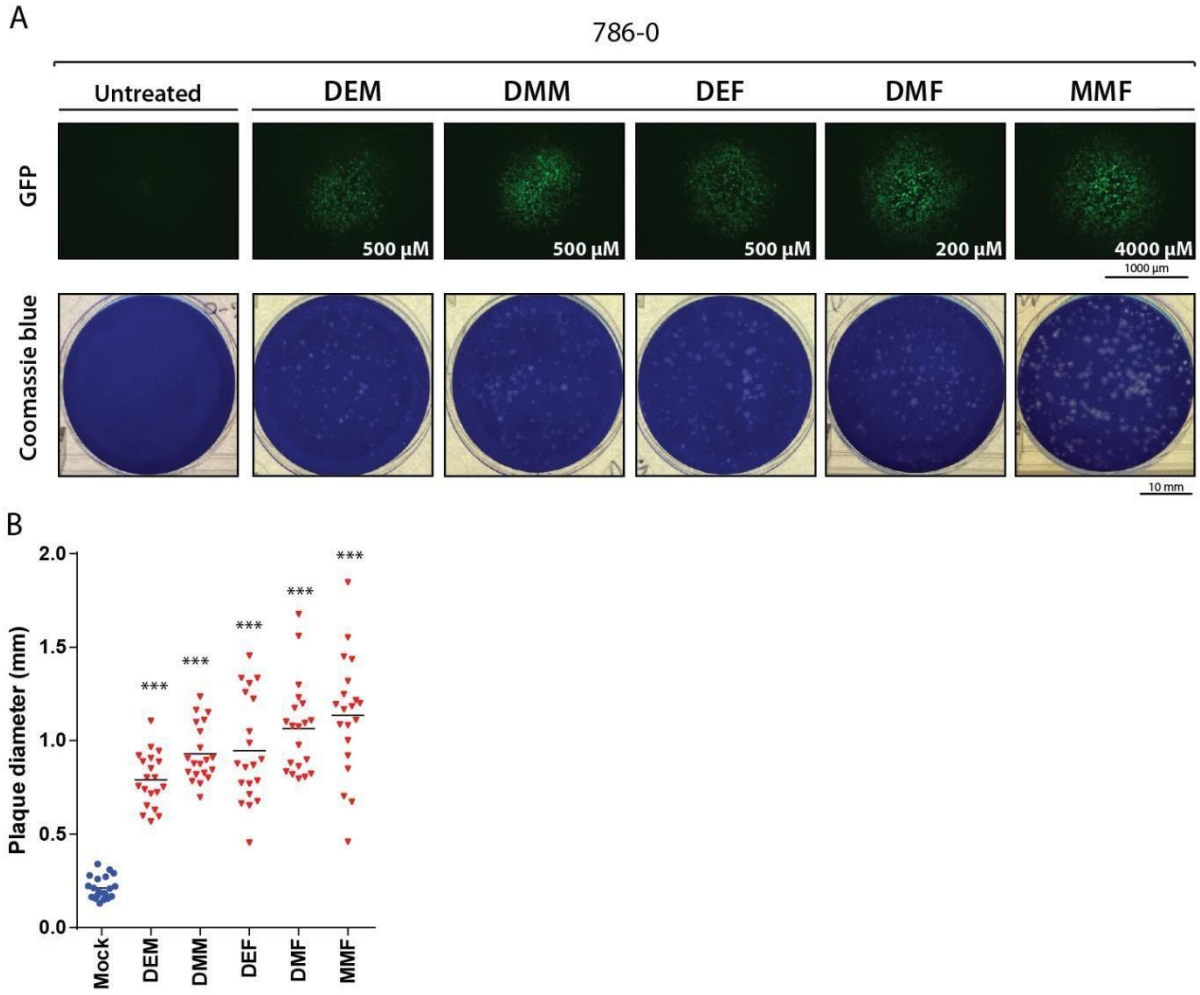


**Supplementary Figure 3 | Fumaric and maleic acid esters enhance VSVΔ51 spread in cancer cells.**

(A-B) 786-0 were pretreated for 4 hours with various FMAEs and subsequently infected with VSVΔ51 expressing GFP. An agarose overlay was added after 1 hour of infection. (A) Fluorescence microscopy of a representative plaque 24 hours after infection. Corresponding images of coomassie blue stain of the full well and (B) a graph showing average plaque diameter illustrate the enhancement of the plaque diameters in presence of DMF (n=20; horizontal lines indicate means; one-way ANOVA; *** $p<0.001$, as compared to the mock condition counterpart).

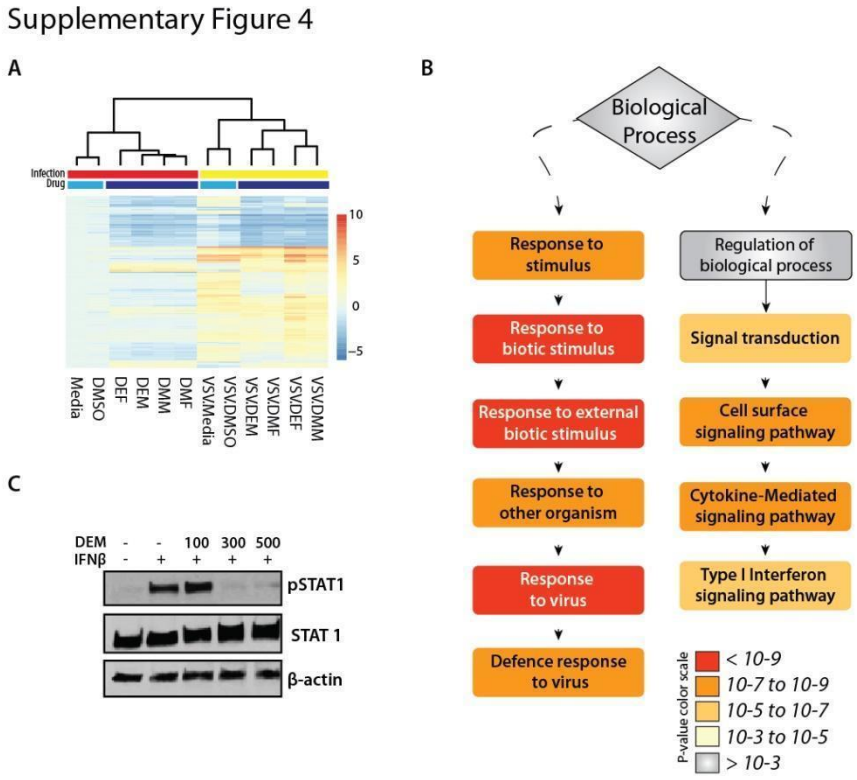


**Supplementary Figure 4 | Fumaric and maleic acid esters inhibit response to type I interferon.**

(A-B) 786-0 cells were treated with FMAEs and infected with VSVΔ51 expressing GFP, and subsequently RNA was extracted at 24 hpi. (A) Heatmap shows the expression of all the differentially expressed genes. (B) Summary of gene ontology relationships, indicating GO terms significantly (p-value scale indicated) downregulated by FMAEs during viral infection. (C) 786-0 cells were pretreated with DEM (100 to 500 μM) for 4 hours and treated with IFNβ (250 U/ml) for 30 minutes. Proteins were extracted and subsequently probed for pSTAT1, STAT1, and β-actin by western blot.

**Supplementary Table 1. Standard deviation values for tumor volumes in Figure 4C.**

| | B16F10 | | | |
|---|---|---|---|---|
| Day | DMSO | DMF | VSV | DMF+VSV |
| 0 | 177.644 | 159.734 | 153.709 | 160.619 |
| 2 | 232.849 | 277.159 | 393.526 | 129.978 |
| 4 | 388.348 | 310.627 | 386.855 | 72.5561 |
| 6 | 658.211 | 751.935 | 492.506 | 128.841 |
| 8 | 1166.15 | 718.937 | 743.246 | 312.845 |
| 11 | 192.018 | 1273.24 | 866.483 | 366.908 |

| | CT26WT | | | |
|---|---|---|---|---|
| Day | DMSO | DMF | VSV | DMF+VSV |
| 0 | 50.7341 | 23.2868 | 59.3684 | 71.1136 |
| 2 | 48.1156 | 103.949 | 51.9085 | 27.6197 |
| 4 | 191.351 | 116.149 | 124.168 | 67.2113 |
| 6 | 201.58 | 232.034 | 263.93 | 61.5816 |
| 8 | 283.47 | 350.74 | 313.59 | 156.107 |

| | | | | |
|---|---|---|---|---|
| | 7 | 9 | 5 | |
| 12 | 686.484 | 523.454 | 751.551 | 373.339 |

| | **HT29** | | | |
|---|---|---|---|---|
| Day | DMSO | DMF | VSV | DMF+VSV |
| 0 | 45.4185 | 30.366 | 43.1642 | 46.0185 |
| 2 | 65.0771 | 23.311 | 34.218 | 29.6766 |
| 4 | 57.3734 | 23.1099 | 117.193 | 118.603 |
| 6 | 93.8009 | 42.5675 | 117.252 | 119.602 |
| 8 | 95.1697 | 37.3649 | 160.159 | 82.4382 |
| 12 | 149.759 | 70.5263 | 261.305 | 55.8793 |
| 14 | 186.6 | 78.8529 | 318.846 | 135.389 |
| 19 | 254.345 | 129.089 | 421.99 | 189.064 |
| 22 | 338.377 | 201.387 | 443.702 | 152.971 |
| 27 | 374.755 | 229.596 | 379.341 | 194.364 |
| 33 | 629.57 | 524.04 | 494.45 | 246.646 |

| | | | | |
|---|---|---|---|---|
| | 7 | 5 | 3 | |
| 38 | 435.187 | 673.153 | 684.567 | 260.016 |

**Supplementary Table 2. List of drugs, chemicals, and cytokines used in this study.**

| Name | Abbreviation | Solvent | Supplier |
|---|---|---|---|
| **Diethyl maleate** | DEM | DMSO | Sigma-Aldrich |
| **Diethyl fumarate** | DEF | DMSO | Sigma-Aldrich |
| **Dimethyl maleate** | DMM | DMSO | Sigma-Aldrich |
| **Diethyl fumarate** | DMF | DMSO | Sigma-Aldrich |
| **Monomethyl fumarate** | MMF | Water | Sigma-Aldrich |
| **Fumaric acid** | FA | DMSO | Sigma-Aldrich |
| **Dimethyl succinate** | DMS | DMSO | Sigma-Aldrich |
| **Sodium succinate dibasic hexahydrate** | S | Water | Sigma-Aldrich |
| **IKK16** | IKK16 | DMSO | Cayman Chemical |
| **TPCA1** | TPCA1 | DMSO | Abcam |
| **L-Glutathione, reduced** | GSH | Water | Cayman Chemical |
| **N-acetyl-L-cysteine** | NAC | Water | Sigma-Aldrich |
| **L-Buthionine-sulfoximine** | BSO | Water | Sigma-Aldrich |
| **D-Luciferin, potassium salt** | Luciferin | PBS | Biotium |
| **Human IFN 2a alpha** | IFNα | PBS | Sigma-Aldrich |
| **Human IFN beta** | IFNβ | PBS | PBL |
| **Human TNF alpha** | TNFα | PBS | R&D Systems |

**Supplementary Table 3. List of cell lines used in this study.**

| Cell Line | Organism | Tissue | Cell type | Growth media | Vendor | Catalog number |
|---|---|---|---|---|---|---|
| Vero | African green monkey | Kidney | | DMEM | ATCC | CCL-81 |
| 786-0 | human | Kidney | Renal cell adenocarcinoma | DMEM | ATCC | CRL-1932 |
| A549 | human | Lung | Carcinoma | RPMI | ATCC | CCL-185 |
| HT29 | human | Colon | Colorectal Adenocarcinoma | DMEM | ATCC | HTB-38 |
| M14 | human | Skin | Melanoma | DMEM | * | |
| OVCA433 | human | Ovary | Adenocarcinoma | RPMI | * | |
| SKOV3 | human | Ovary | Adenocarcinoma | RPMI | ATCC | HTB-77 |
| CT26WT | mouse | Colon | Carcinoma | DMEM | ATCC | CRL-2638 |
| EKVX | human | Lung | Non-small cell lung carcinoma | RPMI | * | |
| 76-9 | Mouse | | Rhabdomyosarcoma | RPMI | ** | |
| HT1080 | human | | Fibrosarcoma | DMEM | * | |
| H226 | human | Lung | Squamous cell lung carcinoma | RPMI | ATCC | CRL-5826 |
| B16F10 | mouse | Skin | Melanoma | DMEM | ATCC | CRL-6475 |
| EMT6 | mouse | Breast | Carcinoma | DMEM | ATCC | CRL-2755 |
| K7M2 | Mouse | Bone *derived from metastatic site (lung) | Osteosarcoma | DMEM | ATCC | CRL-2836 |

ATCC - American Type Culture Collection; None of the cell lines listed are present in the commonly misidentified cell lines database maintained by ICLAC. * The M14, OVCA433, HT1080 and EKVX cell lines were provided by Dr. John Bell (Ottawa Hospital Research Institute, Ottawa, Ontario, Canada). ** The rhabdomyosarcoma cell

lines were generously provided by Dr. Martin Holcik (Children's Hospital of Eastern Ontario Research Institute (CHEO), Ottawa, ON, Canada).

## Appendices III – Chapter 3 Supplemental information

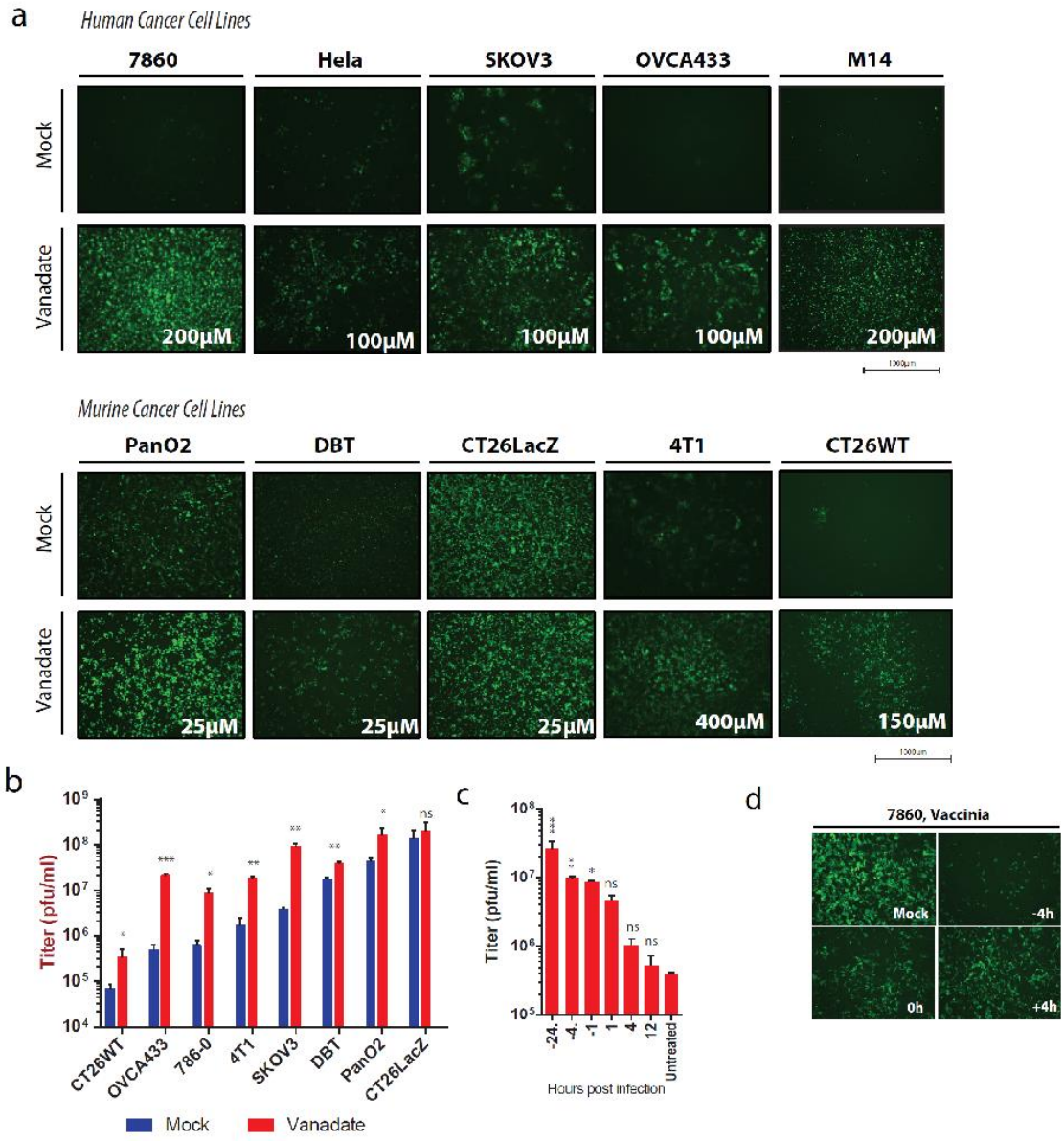


Figure S1 | Vanadate enhances VSVΔ51 infection in resistant cancer cells.

Various human and murine cancer cell lines were pretreated for 4 hours with the indicated concentration of vanadate and were subsequently infected with oncolytic VSVΔ51 expressing GFP at an MOI of 0.01. (a) Corresponding fluorescent images are presented and (b) viral titer were determined 24 hours post infection from supernatants (N=3; Error bars indicate SEM; 2-tail t-test; NS, no statistical significance; * $p<0.05$, ** $p<0.001$, *** $p<0.0001$, as compared to the mock condition counterpart). (c) 786-0 cells treated with 200µM of vanadate at various time pre or post infection with VSVΔ51 (MOI: 0.01) or left untreated, supernatants were collected 24 hours post infection, and tittered by plaque assay (N=3; Error bars indicate SEM; 1 way ANOVA; * $p<0.05$, **

$p<0.001$, *** $p<0.0001$, as compared to the untreated condition counterpart). (d) 786-0 cells treated with 100μM of vanadate at various time pre or post infection with the vaccinia virus expressing GFP (MOI: 0.01) or left untreated. Corresponding fluorescent images are presented.

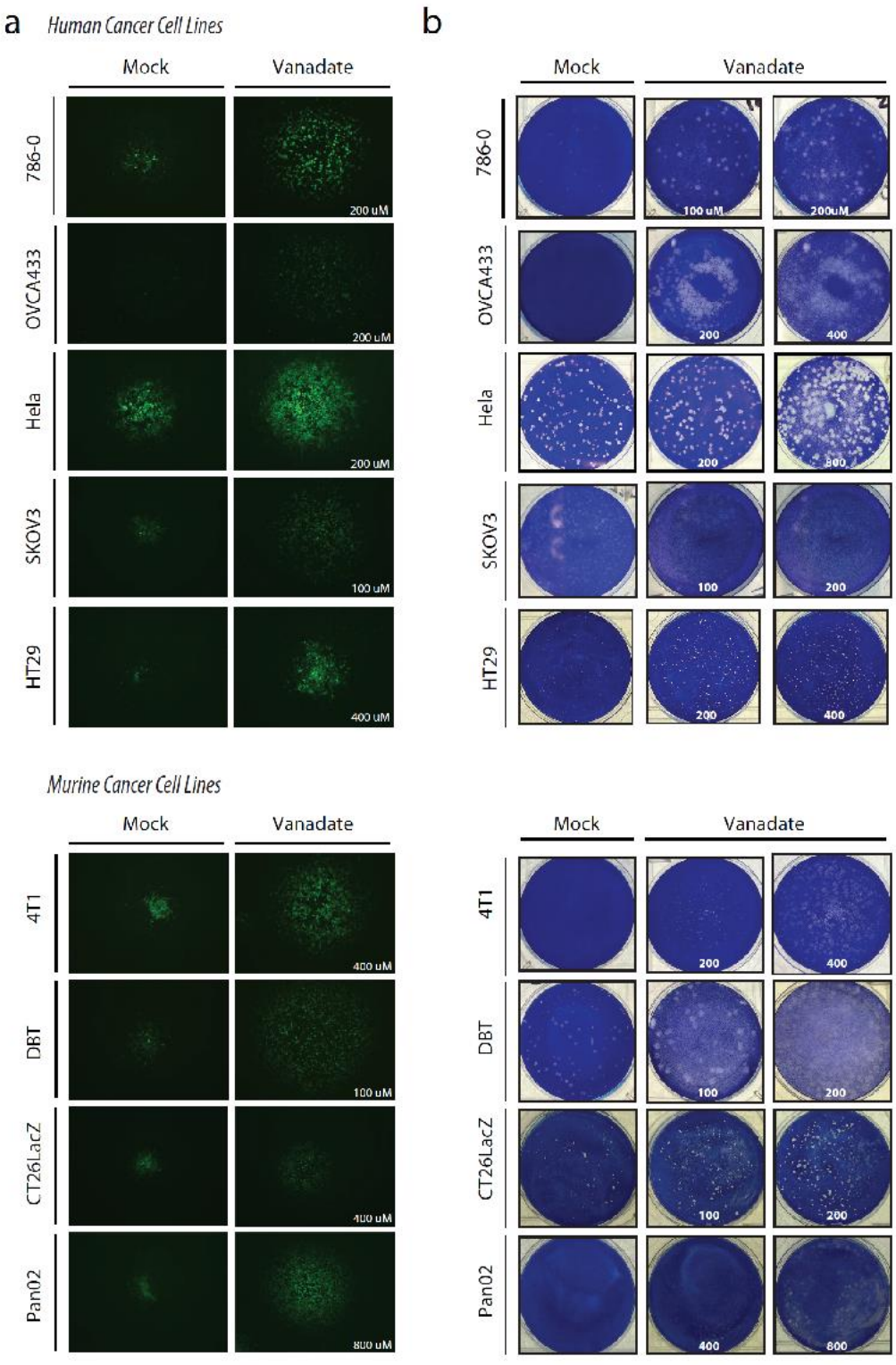
a
Human Cancer Cell Lines
Mock
Vanadate
786-0
200 uM
OVCA433
200 uM
Hela
200 uM
SKOV3
100 uM
HT29
400 uM
b
Mock
Vanadate
786-0
100 uM
200uM
OVCA433
200
400
Hela
200
800
SKOV3
100
200
HT29
200
400
Murine Cancer Cell Lines
Mock
Vanadate
4T1
400 uM
DBT
100 uM
CT26LacZ
400 uM
Pan02
800 uM
Mock
Vanadate
4T1
200
400
DBT
100
200
CT26LacZ
100
200
Pan02
400
800

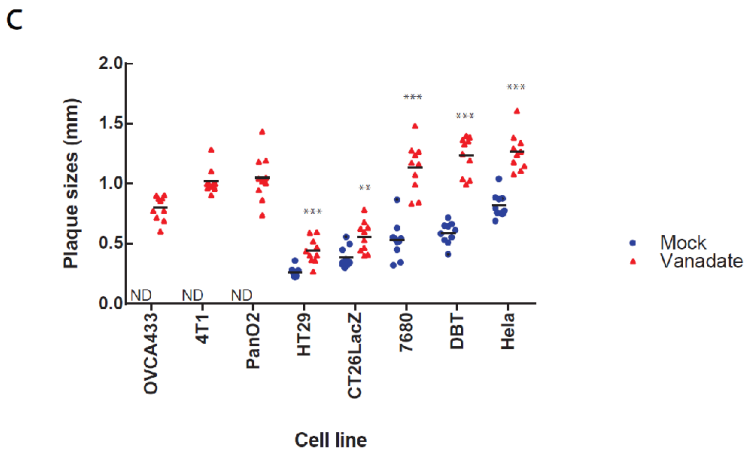


Figure S2 | Vanadate enhances VSVΔ51 spread in cancer cells.

Various human and murine cancer cell lines were pretreated for 4 hours with the indicated concentration of vanadate and were subsequently infected with oncolytic VSVΔ51 expressing GFP, an agarose overlay was added after 1 hour of infection. (a) Fluorescence microscopy of a representative plaque 24 hour after infection. (b) Corresponding image of coomassie blue stain of the full well in (a), and (c) average plaque diameter of (b) illustrating the enhancement of the plaque diameters in presence of vanadate. (N=10; Bars indicate mean; ND, not detected; 2-tail t-test; ** $p<0.001$, *** $p<0.0001$, as compared to the mock condition counterpart)

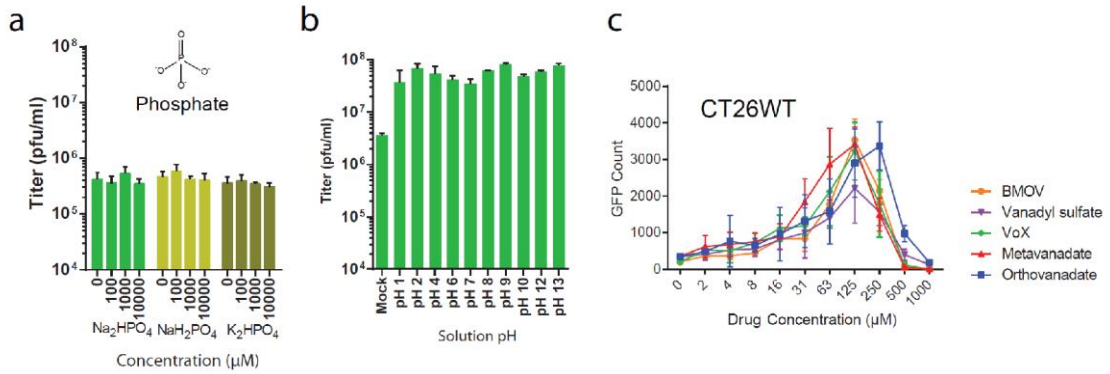


Figure S3 | Viral enhancement is dependent on Vanadium.

(a,b) 786-0 or (c) CT2WT were pretreated for 4 hours with various concentration (a) of phosphate salts or pyrophosphate, (b) vanadate solutions at various pH values, (c) solution of various vanadium compounds and were subsequently infected with oncolytic VSVΔ51 expressing GFP at an MOI of 0.01. (a,b) Corresponding viral titer were determined 24 hours post infection from supernatants (N=3). (c) Corresponding GFP positive cell counts 24 hours post infection. Error bars indicate SEM.

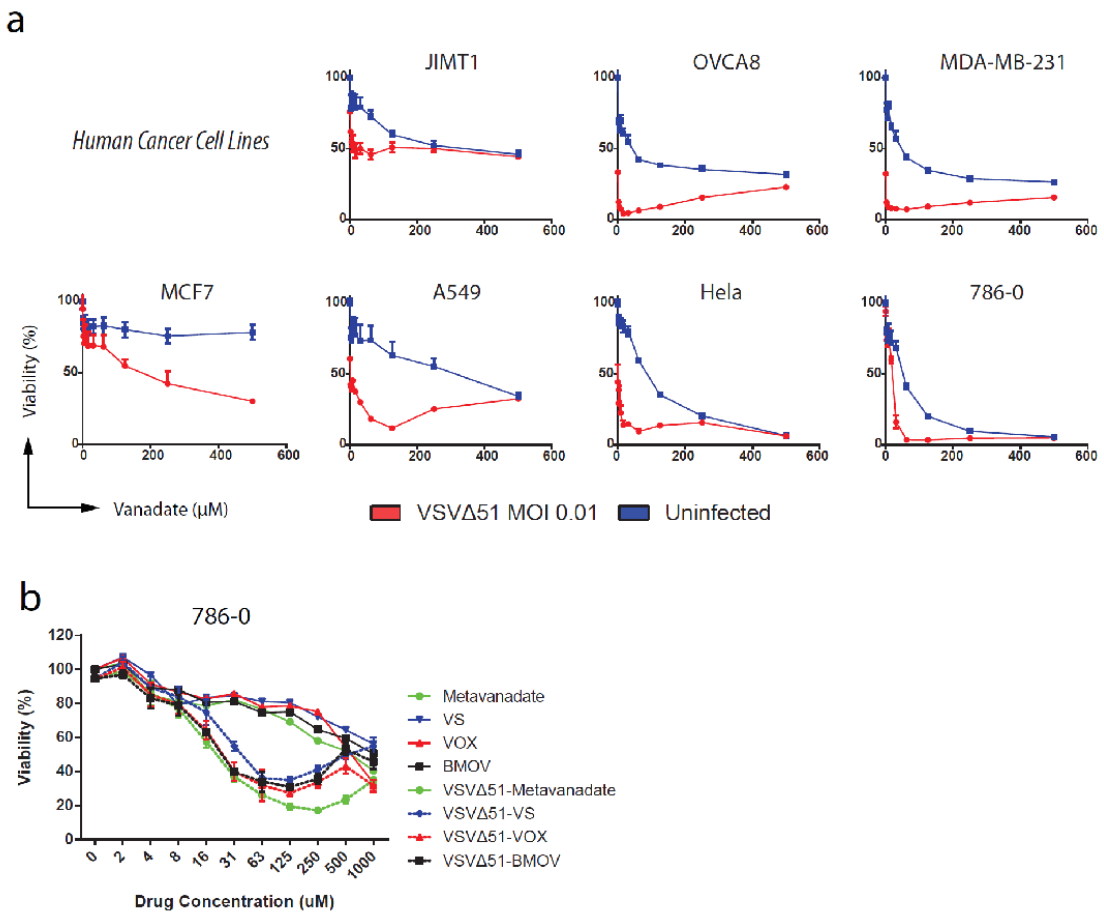


Figure S4 | Vanadate enhances viral oncolysis in various human cancer cell lines.

(a) Various human cancer cell lines were pretreated for 4 hours with a range of concentration of vanadate and were subsequently infected with oncolytic VSVΔ51 expressing GFP at an MOI of 0.01. Cell viability was assayed in 786-0 cells 48 hours post infection. Results were normalized to the average of the values obtained for the corresponding uninfected, untreated cells (N=4). Error bars indicate SEM .(b) 786-0 were pretreated for 4 hours with a range of concentration of various vanadate based compounds and were subsequently infected with oncolytic VSVΔ51 expressing GFP at an MOI of 0.01. Cell viability was assayed in 786-0 cells 24 hours post infection. Results were normalized to the average of the values obtained for the corresponding uninfected, untreated cells (N=4), error bars indicate SEM.

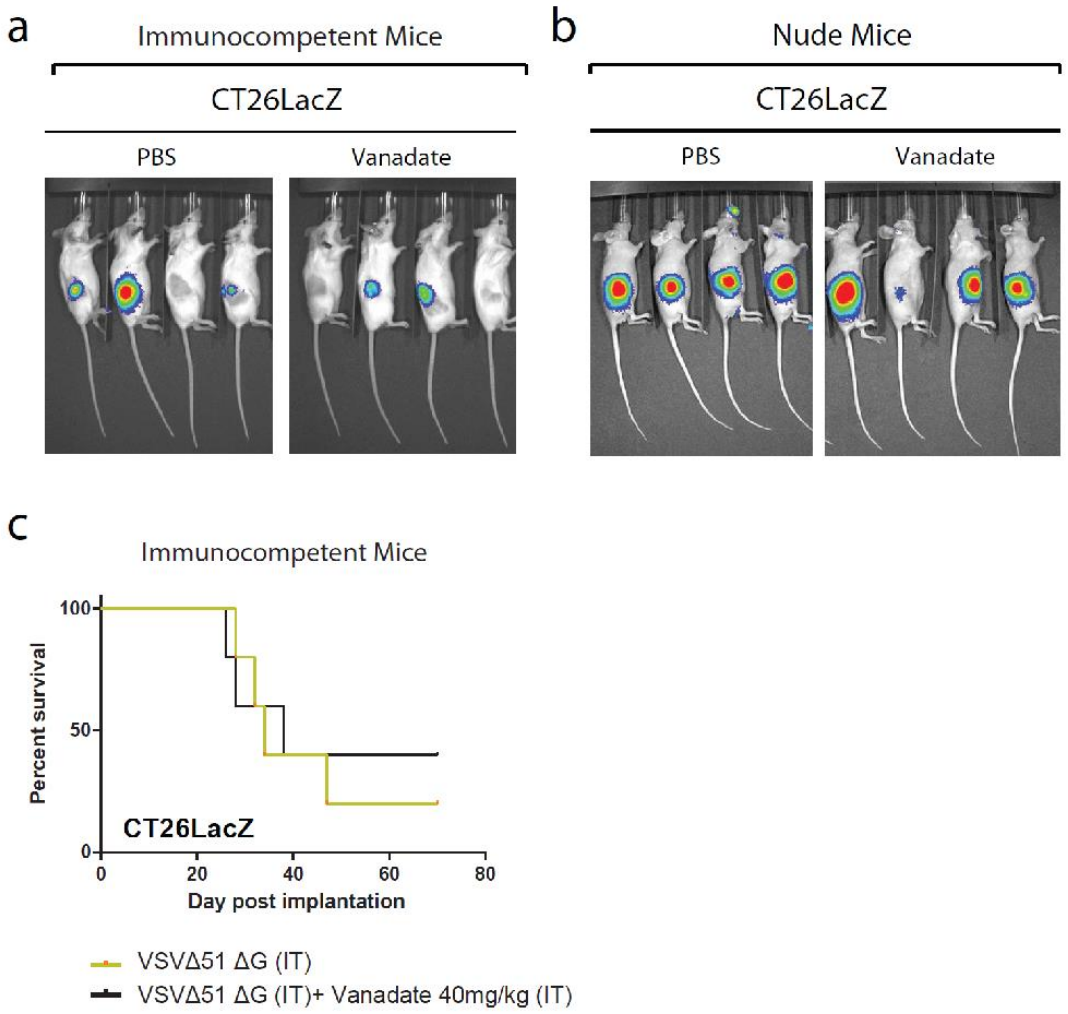


Figure S5 | Effect of vanadate and VSVΔ51 treatment in the CT26LacZ murine tumor model

CT26-LacZ tumor-bearing (a,c) immunocompetent mice and (b) nude mice were treated intratumorally with the vehicle (PBS) or 40mg/kg of vanadate for 4 hours, and (a,b) subsequently treated with $1x10^8$PFU of oncolytic VSVΔ51 expressing firefly-luciferase or (c) VSVΔ51ΔG, intratumorally. (a,b) Representative bioluminescence images of mice presented, 24 hours following infection. (c) Survival was monitored over time. Log-rank (Mantel-Cox) test indicates that the combined treatment is not significantly prolonged over VSVΔ51ΔG alone in the immunocompetent mice model (N=5).

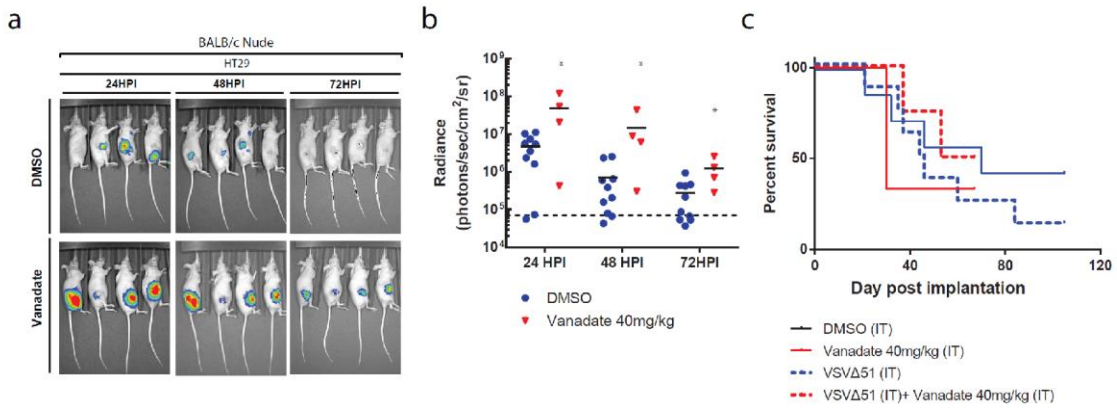


Figure S6 | Effect of vanadate and VSVΔ51 treatment in the HT29 human tumor xenograft model

(a-c) HT29 tumor-bearing mice were treated intratumorally with the vehicle (DMSO) or 40mg/kg of vanadate for 4 hours, and subsequently treated with $1x10^8$PFU of oncolytic VSVΔ51 expressing firefly-luciferase, intratumorally. 24, 48 and 72 hours post infection, viral replication was monitored. Representative bioluminescence images of mice are presented. (b) Quantification of luminescence. Scale represented in photons. (N=4-10. Bars indicates mean; *$p < 0.05$, by 1-tailed t-test; as compared to DMSO treated condition). (c) Survival was monitored over time. Log-rank (Mantel-Cox) test indicates that the combined treatment does not significantly prolong survival over DMSO treatment or virus alone (N=4-10).

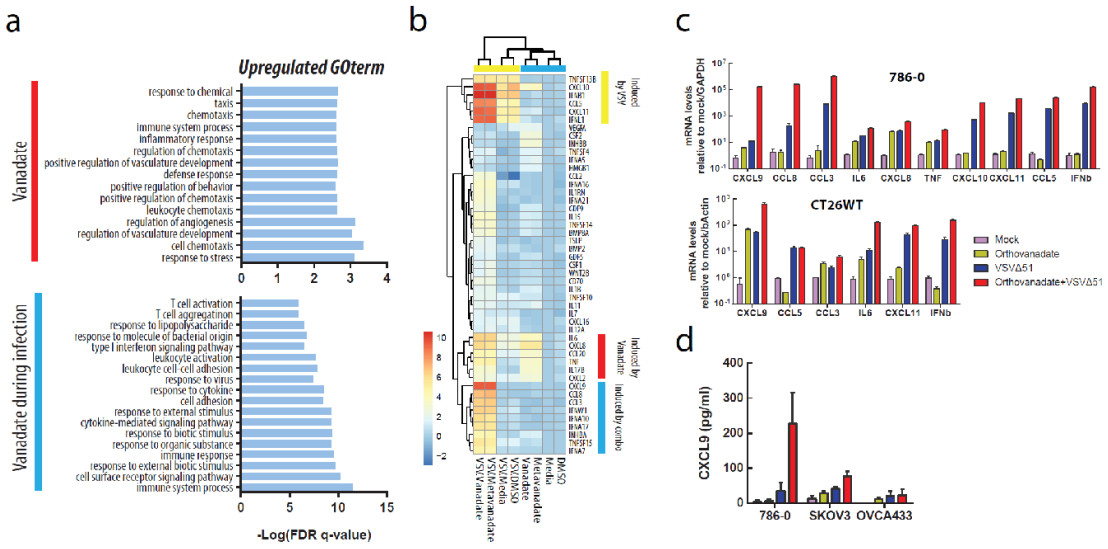


Figure S7 | Vanadate potentiates immune system processes and increases cytokine expression following VSVΔ51 infection of cancer cells.

(a-d) The 786-0 and (c) CT26WT cells were pretreated for 4 hours with vehicle (buffer pH 7.4), or with vanadate (from a solutions prepared from orthovanadate or metavanadate) and infected with VSVΔ51 (MOI: 0.01), or left uninfected. 24 hours post infection RNA was extracted and supernatants were collected. (a,b) RNA was subsequently processed for hybridization on an Affymetrix Human PrimeView Array (N=1, pooled biological triplicate for each experimental condition), or (c) processed for qPCR quantification. (a) Upregulated GOterm graphed in presence of vanadate with or without infection. (b) Heatmap showing the expression levels of the differentially expressed cytokines and chemokines. Expression of genes was normalized to values obtained for untreated, uninfected control. Hierarchical clustering of genes from all samples was also performed. In the heatmap, red indicates relatively higher expression and blue indicates relatively lower expression relative to untreated, uninfected control (Log2 fold change). (b) Gene expression of various cytokines and chemokines in 786-0 and CT26wt, quantified by qPCR. (d) Quantified CXCL9 from supernatant of 786-0, SKOV3 and OVCA433, 24hour following infection as in (a).

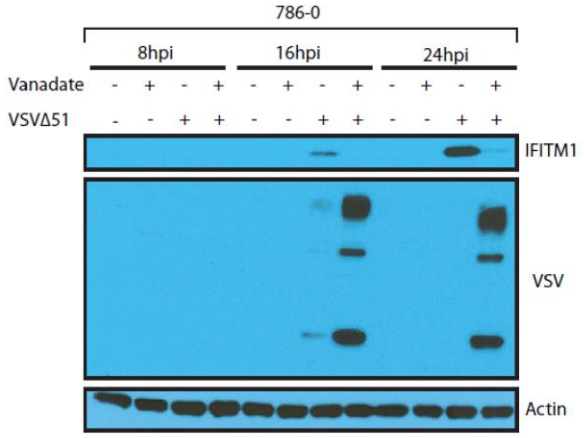


Figure S8 | Effect of vanadate on expression of antiviral proteins IFITM1 during infection.

Cell lysates of 786-0 treated with vanadate and VSVΔ51 expressing GFP was collected at indicated time points. Protein was extracted and probed for IFITM1, VSV and actin by western blot.

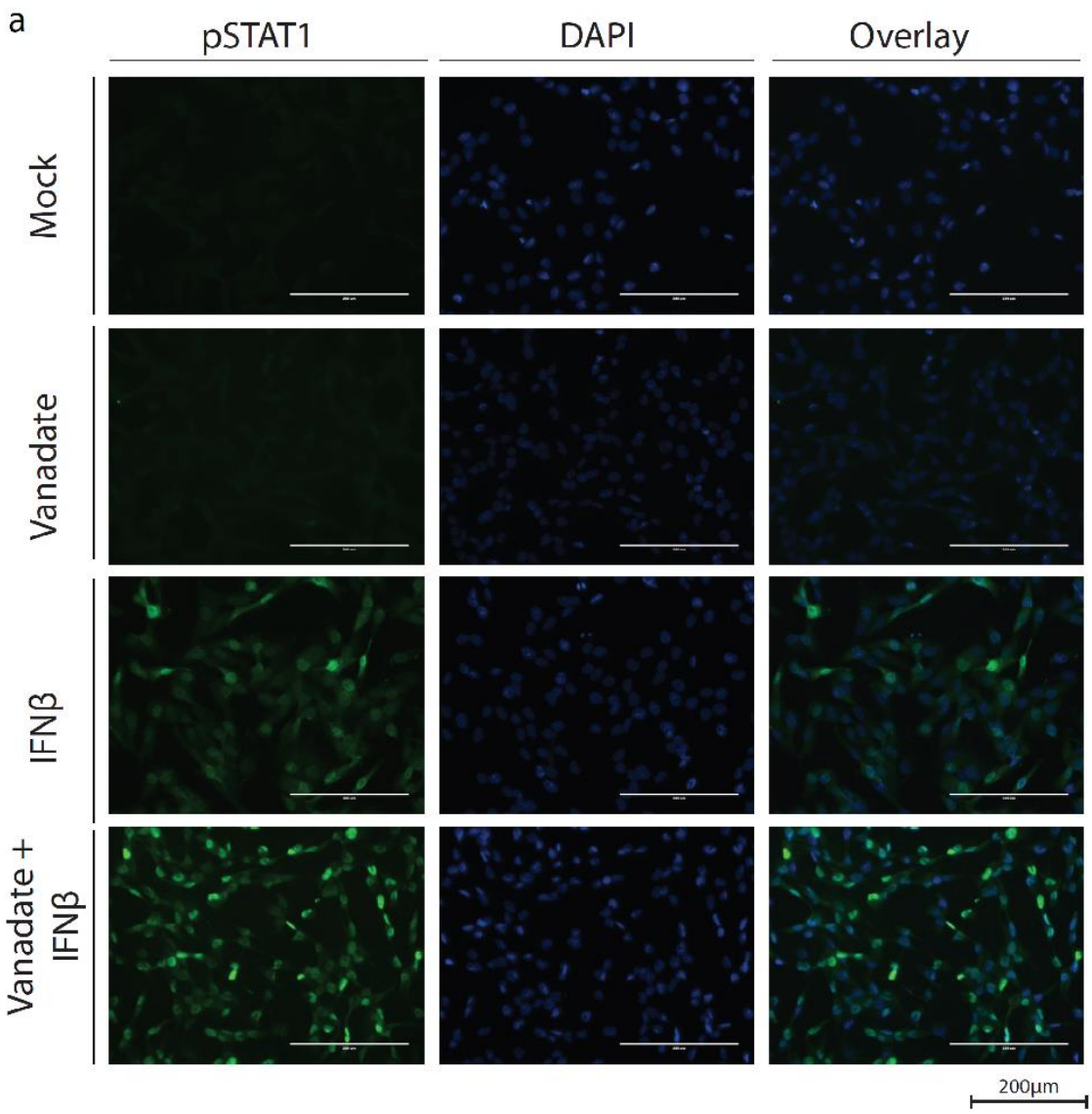


Figure S9 | pSTAT1 Immunofluorescence.

Immunofluorescence of 786-0 cells treated with vanadate (1000µM) for 4 hours and with human IFNβ (1000U) for 1 hour. Cells were fixed and stained with DAPI (blue) and STAT1 (green) antibody. (a) Objective (× 20), scale bar, 200 µm.

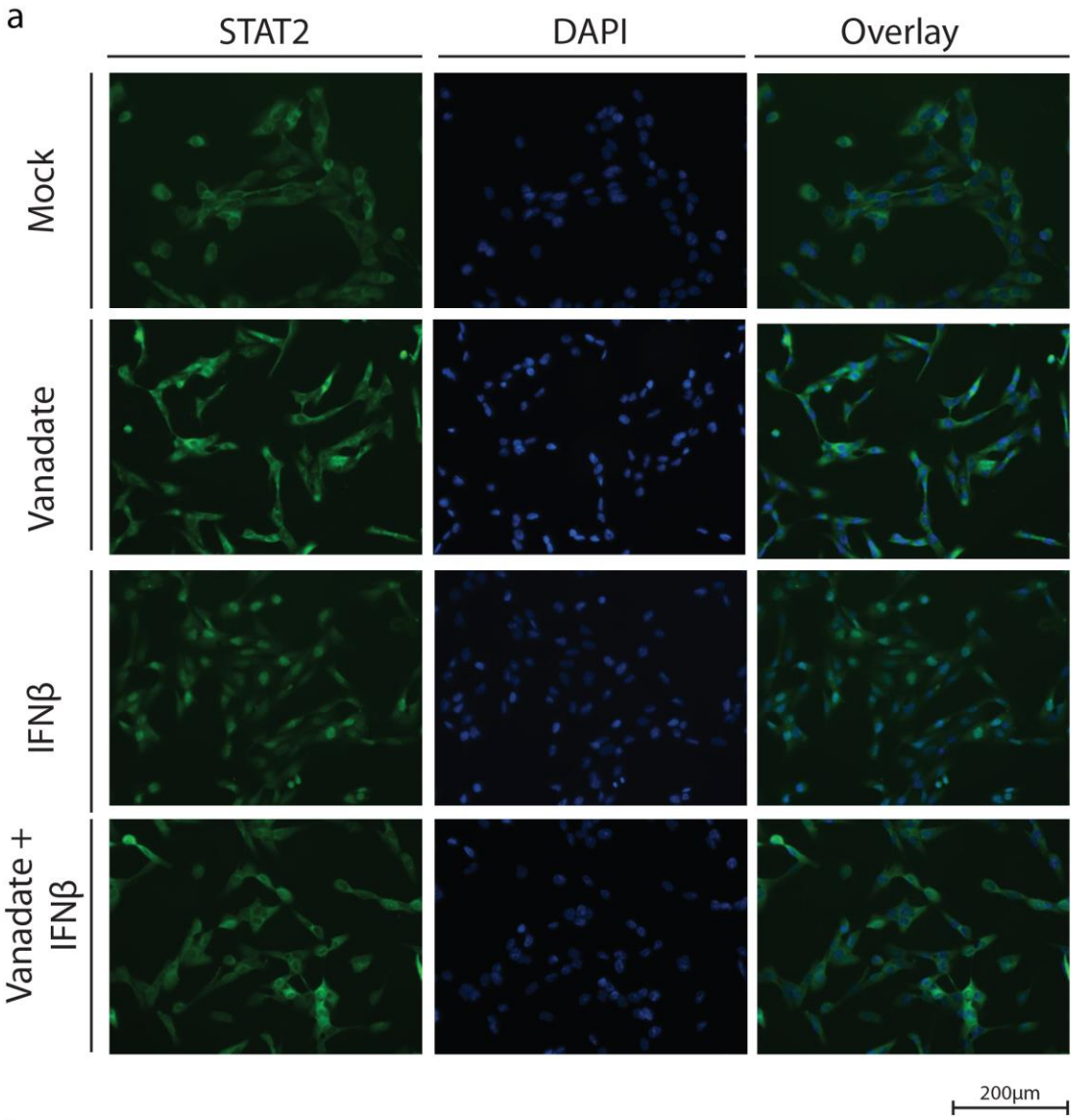
a
STAT2
DAPI
Overlay
Mock
Vanadate
IFNβ
Vanadate + IFNβ
200µm
b
STAT2
Nuclear : Cytoplasmic Ratio
***
0
1
2
3
4
Mock
IFN
VAN
IFN + VAN

Figure S10 | STAT2 Immunofluorescence.

Immunofluorescence of 786-0 cells treated with vanadate (1000μM) for 4 hours and with human IFNβ (1000U) for 1 hour. Cells were fixed and stained with DAPI (blue) and STAT2 (green) antibody. (a) Objective (× 20), scale bar, 200 μm. (b) Quantification of nuclear:cytoplasmic ratio and the average nuclear fluorescence in each condition (N=30; Bars indicate mean; 1-way ANOVA, * $p<0.05$, ** $p<0.001$, *** $p<0.0001$, as compared to the mock condition counterpart.)

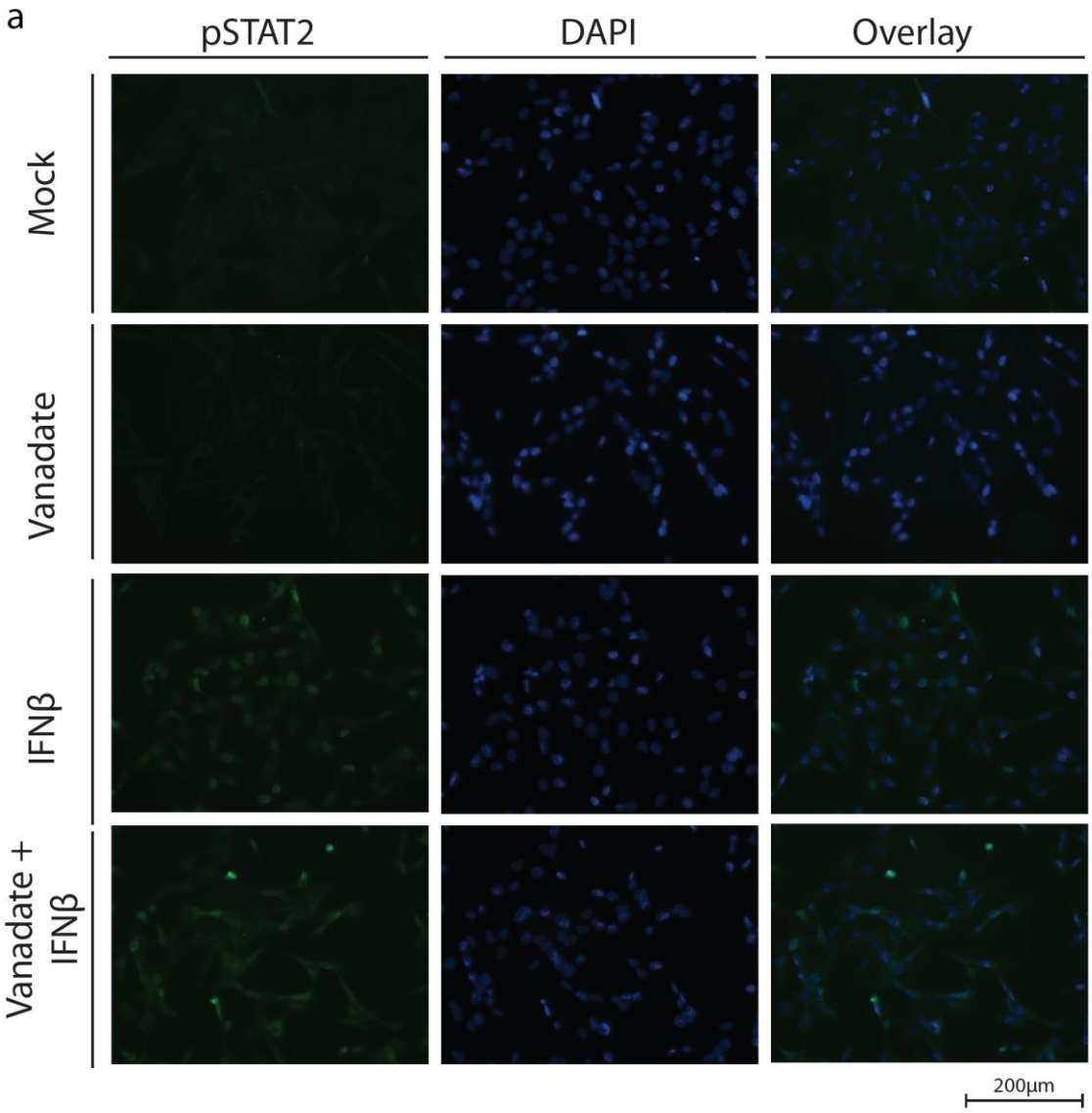
a
pSTAT2
DAPI
Overlay
Mock
Vanadate
IFNβ
Vanadate + IFNβ
200μm
b
pSTAT2
Nuclear : Cytoplasmic Ratio
6
4
2
0
***
Mock
IFN
VAN
IFN + VAN

Figure S11 | pSTAT2 Immunofluorescence.

Immunofluorescence of 786-0 cells treated with vanadate (1000μM) for 4 hours and with human IFNβ (1000U) for 1 hour. Cells were fixed and stained with DAPI (blue) and pSTAT2 (green) antibody. (a) Objective (× 20), scale bar, 200 μm. (b) Quantification of nuclear:cytoplasmic ratio in each condition (N=30; Bars indicate mean; 1-way ANOVA, * $p<0.05$, ** $p<0.001$, *** $p<0.0001$, as compared to the mock condition counterpart.)

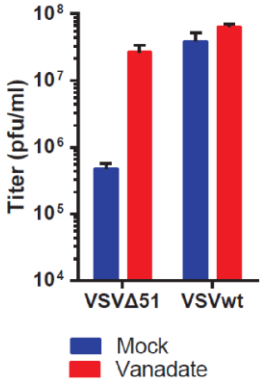


Figure S12 | Effect of Vanadate on wtVSV infection .

The 786-0 cells were pretreated for 4 hours with vanadate or mock treated and infected with VSVΔ51 or wtVSV (MOI: 0.01). Corresponding viral titer were determined 24 hours post infection from supernatants (N=3).

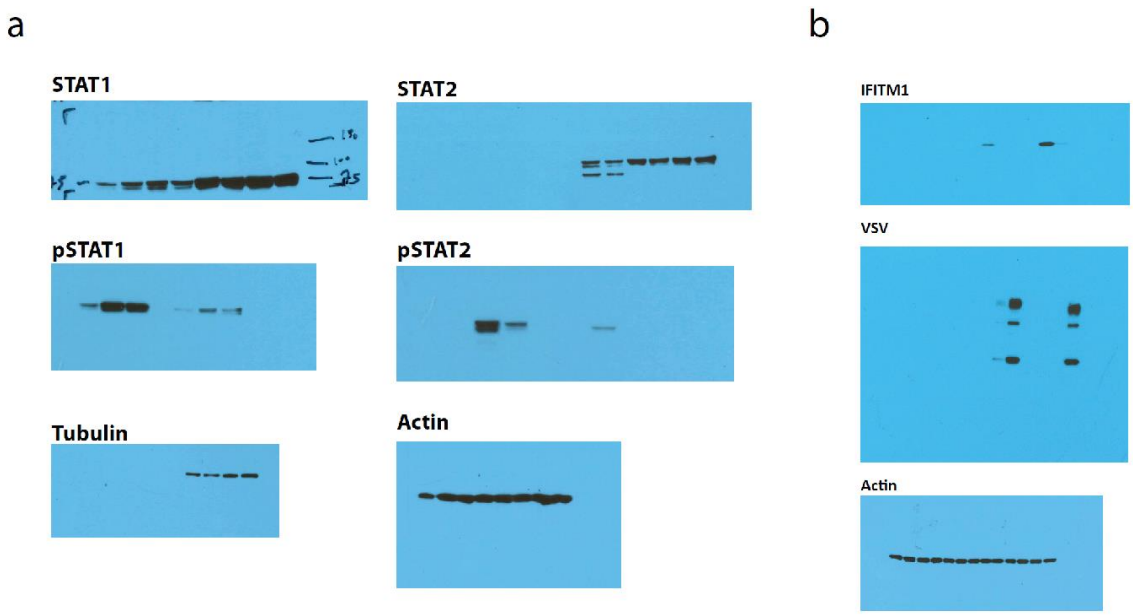


Figure S13 | Uncropped western blots.

Uncropped western blots for (a) Figure 4.6d and (b) Supplemental Figure 8.

Table S1 | Human Cytokine Array.

The 786-0 cells were pretreated for 4 hours with vanadate and were subsequently infected with oncolytic VSVΔ51 expressing GFP at an MOI of 0.01. 24 hours following infection, cytokine array was performed. Normalized (with Background Subtraction) values to positive and negative control sample are indicated in table below.

| | Condition | | | |
|---|---|---|---|---|
| **Cytokine** | **Mock** | **Van** | **VSV** | **VAN+VSV** |
| **ENA-78** | 149.75 | 246.14 | 77.64 | 274.71 |
| **G-CSF** | 0.00 | 22.47 | 0.00 | 0.00 |
| **GM-CSF** | 147.25 | 765.83 | 0.00 | 148.63 |
| **GRO** | 974.25 | 1,551.16 | 830.82 | 1,447.05 |
| **GRO-alpha** | 100.25 | 66.08 | 197.37 | 1.34 |
| **I-309** | 206.75 | 110.35 | 73.00 | 0.00 |
| **IL-1alpha** | 118.25 | 93.17 | 82.27 | 0.00 |
| **IL-1beta** | 254.25 | 228.96 | 257.24 | 165.36 |
| **IL-2** | 190.75 | 58.81 | 0.00 | 246.93 |
| **IL-3** | 184.25 | 426.20 | 332.17 | 689.09 |
| **IL-4** | 65.75 | 129.18 | 0.00 | 133.40 |
| **IL-5** | 0.00 | 13.22 | 0.00 | 97.84 |
| **IL-6** | 4,663.75 | 11,150.84 | 13,903.79 | 13,375.43 |
| **IL-7** | 25.75 | 159.91 | 89.22 | 78.43 |
| **IL-8** | 16,791.25 | 15,279.01 | 16,587.83 | 14,039.57 |
| **IL-10** | 172.75 | 152.31 | 18.54 | 99.34 |
| **IL12-p40** | 206.75 | 92.18 | 91.15 | 156.70 |
| **IL-13** | 1.75 | 0.00 | 201.62 | 0.00 |
| **IL-15** | 0.00 | 37.33 | 176.13 | 30.32 |
| **IFN-gamma** | 63.75 | 42.62 | 265.35 | 4.63 |
| **MCP-1** | 6,617.75 | 8,770.74 | 8,352.24 | 9,187.08 |
| **MCP-2** | 0.00 | 232.92 | 0.00 | 468.61 |
| **MCP-3** | 0.00 | 91.52 | 66.05 | 309.07 |
| **M-CSF** | 299.75 | 665.40 | 932.40 | 979.19 |
| **MDC** | 180.25 | 250.76 | 259.95 | 523.58 |
| **MIG** | 0.00 | 0.00 | 0.00 | 53.03 |
| **MIP-1-delta** | 41.75 | 103.08 | 111.24 | 299.51 |
| **RANTES** | 738.25 | 519.04 | 10,671.28 | 9,910.98 |
| **SCF** | 278.75 | 129.84 | 225.96 | 264.85 |
| **SDF-1** | 334.25 | 270.26 | 234.84 | 383.46 |
| **TARC** | 185.75 | 382.92 | 396.68 | 390.33 |
| **TGF-beta 1** | 64.75 | 163.21 | 295.87 | 15.98 |
| **TNF-alpha** | 239.75 | 116.96 | 0.00 | 511.03 |
| **TNF-beta** | 0.00 | 156.60 | 0.00 | 178.21 |
| **EGF** | 0.00 | 476.75 | 307.45 | 502.37 |
| **IGF-1** | 0.00 | 364.42 | 412.90 | 424.39 |
| **Angiogenin** | 1,108.75 | 1,259.10 | 2,373.11 | 1,651.11 |
| **Oncostatin M** | 155.75 | 680.59 | 656.24 | 1,008.47 |
| **TPO** | 125.75 | 128.52 | 242.95 | 338.95 |
| **VEGF** | 232.75 | 594.03 | 357.67 | 509.54 |
| **PDGF-BB** | 313.25 | 293.05 | 179.61 | 177.02 |
| **Leptin** | 62.25 | 185.35 | 130.94 | 142.06 |

**Table S2 | List of Drugs, chemicals and cytokines used in this study.**

| Name | Formula | Abbreviation | Solvent | Form in media (pH 7.4) | Supplier |
|---|---|---|---|---|---|
| Sodium orthovanadate | $Na_3VO_4$ | vanadate | Water | $H_2VO_4^-$ | Sigma-Aldrich |
| Ammonium metavanadate | $NH_4VO_3$ | metavanadate | Water | $H_2VO_4^-$ | Sigma-Aldrich |
| Vanadium(IV) oxide sulfate hydrate (Vanadyl sulfate) | $VOSO_4 \cdot xH_2O$ | VS | Water | $VO^{2+}$ and $H_2VO_4^-$ | Sigma-Aldrich |
| Vanadium(V) oxytriethoxide | $OV(OC_2H_5)_3$ | VOx | DMSO | $H_2VO_4^-$ | Sigma-Aldrich |
| Bis(maltolato)oxovanadium(IV) | $C_{12}H_{10}O_7V$ | BMOV | DMSO | V(IV) and V(V) maltolato Complexes, and $H_2VO_4^-$ | Sigma-Aldrich |
| Vanadium(III) bromide | $VBr_3$ | $VBr_3$ | Water | Hydrated V(III), $VO^{2+}$ and $H_2VO_4^-$ | Sigma-Aldrich |
| Vanadium(IV) fluoride | $VF_4$ | $VF_4$ | Water | $VO^{2+}$ and $H_2VO_4^-$ | Santa Cruz |
| potassium permanganate | $KMnO_4$ | $KMnO_4$ | Water | | Sigma-Aldrich |
| Chromium(VI) oxide | $CrO_3$ | $CrO_3$ | Water | | Sigma-Aldrich |
| L-Ascorbic acid | $C_6H_8O_6$ | L-AA | Water | | Sigma-Aldrich |
| Tiron | $(OH)_2C_6H_2(SO_3Na)_2 \cdot H_2O$ | Tiron | Water | | Sigma-Aldrich |
| Potassium Phosphate | $K_2HPO_4$ | $K_2HPO_4$ | Water | $H_2PO_4^-$ | Fisher Scientific |
| Sodium phosphate monobasic monohydrate | $NaH_2PO_4\ H_2O$ | $NaH_2PO_4\ H_2O$ | Water | $H_2PO_4^-$ | Fisher Scientific |
| Sodium phosphate dibasic anhydrous | $NaHPO_4$ | $NaHPO_4$ | Water | $H_2PO_4^-$ | Fisher Scientific |
| Sodium phosphate monobasic anhydrous | $NaH_2PO_4$ | $NaH_2PO_4$ | Water | $H_2PO_4^-$ | Fisher Scientific |
| Tetrasodium pyrophosphate | $Na_4P_2O_7$ | $Na_4P_2O_7$ | Water | | Sigma-Aldrich |
| D-Luciferin, potassium salt | $C_{11}H_7KN_2O_3S_2$ | Luciferin | PBS | | Biotium |
| Human IFN 2a alpha | | IFNa | PBS | | Sigma-Aldrich |
| Human IFN beta | | IFNb | PBS | | PBL |

**Table S3 | List of cell lines used in this study.**

| Cell Line | Organism | Tissue | Cell type | Growth media | Vendor | Catalog number |
|---|---|---|---|---|---|---|
| Vero | African green monkey | Kidney | | DMEM | ATCC | CCL-81 |
| 786-O | Human | Kidney | Renal cell adenocarcinoma | DMEM | ATCC | CRL-1932 |
| A549 | Human | Lung | Carcinoma | RPMI | ATCC | CCL-185 |
| GM38 | Human | | Normal Fibroblast | DMEM | Coriell Institute for Medical research | GM00038 |
| HeLa | Human | Cervix | Adenocarcinoma | DMEM | ATCC | CCL2 |
| HT29 | Human | Colon | Colorectal Adenocarcinoma | DMEM | ATCC | HTB-38 |
| JIMT-1 | Human | Breast | Carcinoma | DMEM | DSMZ | ACC-589 |
| M14 | Human | Skin | Melanoma | DMEM | * | |
| MCF7 | Human | Breast | Adenocarcinoma | DMEM | ATCC | HTB-22 |
| MDA-MB-231 | Human | Breast | Adenocarcinoma | DMEM | ATCC | HTB-26 |
| OVCA433 | Human | Ovary | Adenocarcinoma | RPMI | * | |
| OVCAR8 | Human | Ovary | Adenocarcinoma | RPMI | * | |
| SKOV3 | Human | Ovary | Adenocarcinoma | RPMI | ATCC | HTB-77 |
| 4T1 | Mouse | Breast | Carcinoma | DMEM | ATCC | CRL-2539 |
| CT26LacZ (CT26.CL25) | Mouse | Colon | Carcinoma | DMEM | ATCC | CRL-2639 |
| CT26WT | Mouse | Colon | Carcinoma | DMEM | ATCC | CRL-2638 |
| PanO2 | Mouse | Pancreas | Carcinoma | DMEM | * | |
| DBT | Mouse | Brain | Glioma | DMEM | ** | |

ATCC - American Type Culture Collection (Manassas, VA); DSMZ- Deutsche Sammlung von Mikroorganismen und Zellkulturen (Braunschweig, Germany). None of the cell lines listed was present in the commonly misidentified cell lines database maintained by ICLAC. * The M14, OVCA433, OVCAR8, PanO2 cell lines were a generous gift from Dr. John Bell (Ottawa Hospital Research Institute, Ottawa, Ontario, Canada). ** The DBT cell line was a generous gift from Robert C. Rostomily, (University of Washington, School of Medicine, Seattle, WA, USA).

**Table S4 | List of primers used in this study.**

| Model | Gene | Forward Primer (5'->3') | Reverse Primer (5'->3') |
|---|---|---|---|
| **VSV** | M | ATACTCAGATGTGGCAGCCG | GATCTGCCAATACCGCTGGA |
| **Human** | CXCL9 | AGTGCAAGGAACCCCAGTAG | AGGGCTTGGGGCAAATTGTT |
| | CCL8 | TGCTGAAGCTCACACCCTTG | GGAAACTGAATCTGGCTGAGCA |
| | CCL3 | TTCCGTCACCTGCTCAGAAT | CAGCAGCAAGTGATGCAGAGA |
| | IL6 | ACCCCCAATAAATATAGGACTGGA | GAAGGCGCTTGTGGAGAAGG |
| | CXCL8 | ACCGGAAGGAACCATCTCAC | GGCAAAACTGCACCTTCACAC |
| | TNF | GCTGCACTTTGGAGTGATCG | GAGGGTTTGCTACAACATGGG |
| | CXCL10 | CTGAGCCTACAGCAGAGGAAC | AGGTACTCCTTGAATGCCACTT |
| | CXCL11 | CAGCATTTCTACTCCTTCCAAGA | TGGGGAAGCCTTGAACAACT |
| | CCL5 | GCAGTCGTCCACAGGTCAAG | TCTTCTCTGGGTTGGCACAC |
| | IFNβ | CATTACCTGAAGGCCAAGGA | CAGCATCTGCTGGTTGAAGA |
| | IFNγ | TCTTTTGGATGCTCTGGTCA | TTCAGCTCTGCATCGTTTTG |
| | GAPDH | ACAGTCAGCCGCATCTTCTT | GTTAAAAGCAGCCCTGGTGA |
| | MX2 | GAACGTGCAGCGAGCTTGTC | AAGGCTTGTGGGCCTTAGAC |
| | IFITM1 | CCGTGAAGTCTAGGGACAGG | GGTAGACTGTCACAGAGCCG |
| **Mouse** | CXCL9 | CAGTGTGGAGTTCGAGGAACC | TTTGTTGCAATTGGGGCTTGG |
| | CCL3 | CCATATGGAGCTGACACCCC | TCAGGAAAATGACACCTGGCT |
| | IL6 | TCCTCTCTGCAAGAGACTTCC | GGTCTGTTGGGAGTGGTATCC |
| | CXCL11 | CAGCTGCTCAAGGCTTCCTTA | CAACTTTGTCGCAGCCGTTA |
| | CCL5 | CTGCTGCTTTGCCTACCTCT | CGAGTGACAAACACGACTGC |
| | IFNβ | CAGTGTGGAGTTCGAGGAACC | TTTGTTGCAATTGGGGCTTGG |
| | beta Actin | AGGTCTCAAACATGATCTG | AGGTATCCTGACCCTGAAG |

## References


1. D. Hanahan, R. A. Weinberg, Hallmarks of cancer: the next generation, *Cell* **144**, 646–674 (2011).

2. D. M. Pardoll, The blockade of immune checkpoints in cancer immunotherapy, *Nat. Rev. Cancer* **12**, 252–264 (2012).

3. Canadian Cancer Statistics 2012: (611042012-001) (2012), doi:10.1037/e611042012-001.

4. C. C. Statistics, Canadian Cancer Society's Advisory Committee On Cancer Statistics. in, *Canadian Cancer Society, Canadian Cancer Society* (2015).

5. C. Dalba, D. Klatzmann, C. R. Logg, N. Kasahara, Beyond oncolytic virotherapy: replication-competent retrovirus vectors for selective and stable transduction of tumors, *Curr. Gene Ther.* **5**, 655–667 (2005).

6. J. K.-K. Li, Oncolytic bluetongue viruses: promise, progress, and perspectives, *Front. Microbiol.* **2**, 46 (2011).

7. C. Levaditi, S. Nicolau, Affinite du virus herpetique pour les neoplasmes epitheliaux, *CR Soc. Biol* **87**, 498–500 (1922).

8. S. J. Russell, K.-W. Peng, J. C. Bell, Oncolytic virotherapy, *Nat. Biotechnol.* **30**, 658–670 (2012).

9. M. Liang, Clinical Development of Oncolytic Viruses in China, *Curr. Pharm. Biotechnol.* **13**, 1852–1857 (2012).

10. F. J. Kohlhapp, H. L. Kaufman, Molecular Pathways: Mechanism of Action for Talimogene Laherparepvec, a New Oncolytic Virus Immunotherapy, *Clin. Cancer Res.* **22**, 1048–1054 (2016).

11. B. D. Lichty, C. J. Breitbach, D. F. Stojdl, J. C. Bell, Going viral with cancer immunotherapy, *Nat. Rev. Cancer* **14**, 559–567 (2014).

12. H. H. Wong, N. R. Lemoine, Y. Wang, Oncolytic Viruses for Cancer Therapy: Overcoming the Obstacles, *Viruses* **2**, 78–106 (2010).

13. J. Hughes, P. Wang, G. Alusi, H. Shi, Y. Chu, J. Wang, V. Bhakta, I. McNeish, A. McCart, N. R. Lemoine, Y. Wang, Lister strain vaccinia virus with thymidine kinase gene deletion is a tractable platform for development of a new generation of oncolytic virus, *Gene Ther.* **22**, 476–484 (2015).

14. J. K. Kaufmann, S. Bossow, C. Grossardt, S. Sawall, J. Kupsch, P. Erbs, J. C. Hassel, C. von Kalle, A. H. Enk, D. M. Nettelbeck, G. Ungerechts, Chemovirotherapy of malignant melanoma with a targeted and armed oncolytic measles virus, *J. Invest. Dermatol.* **133**, 1034–1042 (2013).

15. T. Nakamura, S. J. Russell, Engineering oncolytic measles viruses for targeted cancer therapy, *Molecular Targeting in Oncology* (2008) (available at http://link.springer.com/content/pdf/10.1007/978-1-59745-337-0.pdf#page=434).

16. J. K. Fan, N. Wei, M. Ding, J. F. Gu, X. R. Liu, B. H. Li, R. Qi, W. D. Huang, Y. H. Li, X. Q. Xiong, J. Wang, R. S. Li, X. Y. Liu, Targeting Gene-ViroTherapy for prostate cancer by DD3-driven oncolytic virus-harboring interleukin-24 gene, *Int. J. Cancer* **127**, 707–717 (2010).

17. W. Zhang, K. Ge, Q. Zhao, X. Zhuang, Z. Deng, L. Liu, J. Li, Y. Zhang, Y. Dong, Y. Zhang, S. Zhang, B. Liu, A novel oHSV-1 targeting telomerase reverse transcriptase-positive cancer cells via tumor-specific promoters regulating the expression of ICP4, *Oncotarget* **6**, 20345–20355 (2015).

18. F. Garrido, N. Aptsiauri, E. M. Doorduijn, A. M. Garcia Lora, T. van Hall, The urgent need to recover MHC class I in cancers for effective immunotherapy, *Curr. Opin. Immunol.* **39**, 44–51 (2016).

19. E. A. Chiocca, S. D. Rabkin, Oncolytic viruses and their application to cancer immunotherapy, *Cancer Immunol Res* **2**, 295–300 (2014).

20. R. J. Prestwich, K. J. Harrington, H. S. Pandha, R. G. Vile, A. A. Melcher, F. Errington, Oncolytic viruses: a novel form of immunotherapy, *Expert Rev. Anticancer Ther.* **8**, 1581–1588 (2008).

21. Z. S. Guo, Z. Liu, S. Kowalsky, M. Feist, P. Kalinski, B. Lu, W. J. Storkus, D. L. Bartlett, Oncolytic Immunotherapy: Conceptual Evolution, Current Strategies, and Future Perspectives, *Front. Immunol.* **8**, 555 (2017).

22. A. M. Murphy, D. M. Besmer, M. Moerdyk-Schauwecker, N. Moestl, D. A. Ornelles, P. Mukherjee, V. Z. Grdzelishvili, Vesicular stomatitis virus as an oncolytic agent against pancreatic ductal adenocarcinoma, *J. Virol.* **86**, 3073–3087 (2012).

23. A. Arvin, G. Campadelli-Fiume, E. Mocarski, P. S. Moore, B. Roizman, R. Whitley, K. Yamanishi, *Human Herpesviruses: Biology, Therapy, and Immunoprophylaxis* (Cambridge University Press, 2007).

24. D. K. B. Rao, Herpes Viruses – An Overview, *iosrphr* **4**, 39–41 (2014).

25. M. Aghi, R. L. Martuza, Oncolytic viral therapies - the clinical experience, *Oncogene* **24**, 7802–7816 (2005).

26. K. J. Looker, A. S. Magaret, M. T. May, K. M. E. Turner, P. Vickerman, S. L. Gottlieb, L. M. Newman, Global and Regional Estimates of Prevalent and Incident Herpes Simplex Virus Type 1 Infections in 2012, *PLoS One* **10**, e0140765 (2015).

27. S. Varghese, S. D. Rabkin, Oncolytic herpes simplex virus vectors for cancer virotherapy, *Cancer Gene Ther.* **9**, 967–978 (2002).

28. J. C. C. Hu, R. S. Coffin, C. J. Davis, N. J. Graham, N. Groves, P. J. Guest, K. J. Harrington,

N. D. James, C. A. Love, I. McNeish, L. C. Medley, A. Michael, C. M. Nutting, H. S. Pandha, C. A. Shorrock, J. Simpson, J. Steiner, N. M. Steven, D. Wright, R. C. Coombes, A phase I study of OncoVEXGM-CSF, a second-generation oncolytic herpes simplex virus expressing granulocyte macrophage colony-stimulating factor, *Clin. Cancer Res.* **12**, 6737–6747 (2006).

29. R. H. I. Andtbacka, H. L. Kaufman, F. Collichio, T. Amatruda, N. Senzer, J. Chesney, K. A. Delman, L. E. Spitler, I. Puzanov, S. S. Agarwala, M. Milhem, L. Cranmer, B. Curti, K. Lewis, M. Ross, T. Guthrie, G. P. Linette, G. A. Daniels, K. Harrington, M. R. Middleton, W. H. Miller Jr, J. S. Zager, Y. Ye, B. Yao, A. Li, S. Doleman, A. VanderWalde, J. Gansert, R. S. Coffin, Talimogene Laherparepvec Improves Durable Response Rate in Patients With Advanced Melanoma, *J. Clin. Oncol.* **33**, 2780–2788 (2015).

30. A. Ribas, R. Dummer, I. Puzanov, A. VanderWalde, R. H. I. Andtbacka, O. Michielin, A. J. Olszanski, J. Malvehy, J. Cebon, E. Fernandez, J. M. Kirkwood, T. F. Gajewski, L. Chen, K. S. Gorski, A. A. Anderson, S. J. Diede, M. E. Lassman, J. Gansert, F. S. Hodi, G. V. Long, Oncolytic Virotherapy Promotes Intratumoral T Cell Infiltration and Improves Anti-PD-1 Immunotherapy, *Cell* **170**, 1109–1119.e10 (2017).

31. D. M. Knipe, P. M. Howley, *Fields' Virology* (Lippincott Williams & Wilkins, 2007).

32. G. McFadden, Poxvirus tropism, *Nat. Rev. Microbiol.* **3**, 201–213 (2005).

33. W. M. Chan, G. McFadden, Oncolytic Poxviruses, *Annu Rev Virol* **1**, 119–141 (2014).

34. T.-C. Liu, E. Galanis, D. Kirn, Clinical trial results with oncolytic virotherapy: a century of promise, a decade of progress, *Nat. Clin. Pract. Oncol.* **4**, 101–117 (2007).

35. A. E. Merrick, E. J. Ilett, A. A. Melcher, JX-594, a targeted oncolytic poxvirus for the treatment of cancer, *Curr. Opin. Investig. Drugs* **10**, 1372–1382 (2009).

36. B.-H. Park, T. Hwang, T.-C. Liu, D. Y. Sze, J.-S. Kim, H.-C. Kwon, S. Y. Oh, S.-Y. Han, J.-H. Yoon, S.-H. Hong, A. Moon, K. Speth, C. Park, Y.-J. Ahn, M. Daneshmand, B. G. Rhee, H. M. Pinedo, J. C. Bell, D. H. Kirn, Use of a targeted oncolytic poxvirus, JX-594, in patients with refractory primary or metastatic liver cancer: a phase I trial, *Lancet Oncol.* **9**, 533–542 (2008).

37. H. Fukuhara, Y. Ino, T. Todo, Oncolytic virus therapy: A new era of cancer treatment at dawn, *Cancer Sci.* **107**, 1373–1379 (2016).

38. J. Heo, T. Reid, L. Ruo, C. J. Breitbach, S. Rose, M. Bloomston, M. Cho, H. Y. Lim, H. C. Chung, C. W. Kim, J. Burke, R. Lencioni, T. Hickman, A. Moon, Y. S. Lee, M. K. Kim, M. Daneshmand, K. Dubois, L. Longpre, M. Ngo, C. Rooney, J. C. Bell, B.-G. Rhee, R. Patt, T.-H. Hwang, D. H. Kirn, Randomized dose-finding clinical trial of oncolytic immunotherapeutic vaccinia JX-594 in liver cancer, *Nat. Med.* **19**, 329–336 (2013).

39. K. L. Norman, K. Hirasawa, A.-D. Yang, M. A. Shields, P. W. K. Lee, Reovirus oncolysis: the Ras/RalGEF/p38 pathway dictates host cell permissiveness to reovirus infection, *Proc. Natl. Acad. Sci. U. S. A.* **101**, 11099–11104 (2004).

40. J. Downward, Targeting RAS signalling pathways in cancer therapy, *Nat. Rev. Cancer* **3**, 11–22 (2003).

41. J. E. Strong, M. C. Coffey, D. Tang, P. Sabinin, P. W. Lee, The molecular basis of viral

oncolysis: usurpation of the Ras signaling pathway by reovirus, *EMBO J.* **17**, 3351–3362 (1998).

42. D. G. Morris, X. Feng, L. M. DiFrancesco, K. Fonseca, P. A. Forsyth, A. H. Paterson, M. C. Coffey, B. Thompson, REO-001: A phase I trial of percutaneous intralesional administration of reovirus type 3 dearing (Reolysin®) in patients with advanced solid tumors, *Invest. New Drugs* **31**, 696–706 (2013).

43. J. Gong, E. Sachdev, A. C. Mita, M. M. Mita, Clinical development of reovirus for cancer therapy: An oncolytic virus with immune-mediated antitumor activity, *World J Methodol* **6**, 25–42 (2016).

44. A. A. V. Albertini, E. Baquero, A. Ferlin, Y. Gaudin, Molecular and cellular aspects of rhabdovirus entry, *Viruses* **4**, 117–139 (2012).

45. D. Finkelshtein, A. Werman, D. Novick, S. Barak, M. Rubinstein, LDL receptor and its family members serve as the cellular receptors for vesicular stomatitis virus, *Proc. Natl. Acad. Sci. U. S. A.* **110**, 7306–7311 (2013).

46. D. Blondel, G. Maarifi, S. Nisole, M. K. Chelbi-Alix, Resistance to Rhabdoviridae Infection and Subversion of Antiviral Responses, *Viruses* **7**, 3675–3702 (2015).

47. M. Ahmed, M. O. McKenzie, S. Puckett, M. Hojnacki, L. Poliquin, D. S. Lyles, Ability of the matrix protein of vesicular stomatitis virus to suppress beta interferon gene expression is genetically correlated with the inhibition of host RNA and protein synthesis, *J. Virol.* **77**, 4646–4657 (2003).

48. D. F. Stojdl, B. D. Lichty, B. R. tenOever, J. M. Paterson, A. T. Power, S. Knowles, R. Marius, J. Reynard, L. Poliquin, H. Atkins, E. G. Brown, R. K. Durbin, J. E. Durbin, J. Hiscott, J. C. Bell, VSV strains with defects in their ability to shutdown innate immunity are potent systemic anti-cancer agents, *Cancer Cell* **4**, 263–275 (2003).

49. D. F. Stojdl, B. Lichty, S. Knowles, R. Marius, H. Atkins, N. Sonenberg, J. C. Bell, Exploiting tumor-specific defects in the interferon pathway with a previously unknown oncolytic virus, *Nat. Med.* **6**, 821–825 (2000).

50. J. Brun, D. McManus, C. Lefebvre, K. Hu, T. Falls, H. Atkins, J. C. Bell, J. A. McCart, D. Mahoney, D. F. Stojdl, Identification of genetically modified Maraba virus as an oncolytic rhabdovirus, *Mol. Ther.* **18**, 1440–1449 (2010).

51. J. Zhang, L.-H. Tai, C. S. Ilkow, A. A. Alkayyal, A. A. Ananth, C. T. de Souza, J. Wang, S. Sahi, L. Ly, C. Lefebvre, T. J. Falls, K. B. Stephenson, A. B. Mahmoud, A. P. Makrigiannis, B. D. Lichty, J. C. Bell, D. F. Stojdl, R. C. Auer, Maraba MG1 virus enhances natural killer cell function via conventional dendritic cells to reduce postoperative metastatic disease, *Mol. Ther.* **22**, 1320–1332 (2014).

52. J. G. Pol, L. Zhang, B. W. Bridle, K. B. Stephenson, J. Rességuier, S. Hanson, L. Chen, N. Kazdhan, J. L. Bramson, D. F. Stojdl, Y. Wan, B. D. Lichty, Maraba virus as a potent oncolytic vaccine vector, *Mol. Ther.* **22**, 420–429 (2014).

53. D. J. Jonker, S. J. Hotte, A. R. Abdul Razak, D. J. Renouf, B. Lichty, J. C. Bell, J. Powers, C. J. Breitbach, D. F. Stojdl, K. B. Stephenson, J. L. Bramson, J. Hummel, C. G. Lemay, J.-C. Cutz, J. Wells, R. Eady, X. Sun, D. Tu, J. Dancey, Phase I study of oncolytic virus (OV) MG1

maraba/MAGE-A3 (MG1MA3), with and without transgenic MAGE-A3 adenovirus vaccine (AdMA3) in incurable advanced/metastatic MAGE-A3-expressing solid tumours: CCTG IND.214, *J. Clin. Orthod.* **35**, e14637–e14637 (2017).

54. A. S. Aitken, D. G. Roy, M.-C. Bourgeois-Daigneault, Taking a Stab at Cancer; Oncolytic Virus-Mediated Anti-Cancer Vaccination Strategies, *Biomedicines* **5** (2017), doi:10.3390/biomedicines5010003.

55. A. S. Aitken, D. G. Roy, N. T. Martin, S. Sad, J. C. Bell, M.-C. Bourgeois-Daigneault, Brief Communication; A Heterologous Oncolytic Bacteria-Virus Prime-Boost Approach for Anticancer Vaccination in Mice, *J. Immunother.* (2017), doi:10.1097/CJI.0000000000000208.

56. L. C. Platanias, Mechanisms of type-I- and type-II-interferon-mediated signalling, *Nat. Rev. Immunol.* **5**, 375–386 (2005).

57. L. B. Ivashkiv, L. T. Donlin, Regulation of type I interferon responses, *Nat. Rev. Immunol.* **14**, 36–49 (2014).

58. J. R. Schoenborn, C. B. Wilson, in *Advances in Immunology*, (Academic Press, 2007), vol. 96, pp. 41–101.

59. J. W. Schoggins, C. M. Rice, Interferon-stimulated genes and their antiviral effector functions, *Curr. Opin. Virol.* **1**, 519–525 (2011).

60. M. Rieder, K.-K. Conzelmann, in *Advances in Virus Research*, A. C. Jackson, Ed. (Academic Press, 2011), vol. 79, pp. 91–114.

61. S. Balachandran, P. C. Roberts, L. E. Brown, H. Truong, A. K. Pattnaik, D. R. Archer, G. N. Barber, Essential role for the dsRNA-dependent protein kinase PKR in innate immunity to viral infection, *Immunity* **13**, 129–141 (2000).

62. J. Verhelst, P. Hulpiau, X. Saelens, Mx proteins: antiviral gatekeepers that restrain the uninvited, *Microbiol. Mol. Biol. Rev.* **77**, 551–566 (2013).

63. F. McNab, K. Mayer-Barber, A. Sher, A. Wack, A. O'Garra, Type I interferons in infectious disease, *Nat. Rev. Immunol.* **15**, 87–103 (2015).

64. M. J. Lenardo, C. M. Fan, T. Maniatis, D. Baltimore, The involvement of NF-kappa B in beta-interferon gene regulation reveals its role as widely inducible mediator of signal transduction, *Cell* **57**, 287–294 (1989).

65. K. Honda, T. Taniguchi, IRFs: master regulators of signalling by Toll-like receptors and cytosolic pattern-recognition receptors, *Nat. Rev. Immunol.* **6**, 644–658 (2006).

66. J. Wang, S. H. Basagoudanavar, X. Wang, E. Hopewell, R. Albrecht, A. García-Sastre, S. Balachandran, A. A. Beg, NF-κB RelA Subunit Is Crucial for Early IFN-β Expression and Resistance to RNA Virus Replication, *The Journal of Immunology* **185**, 1720–1729 (2010).

67. M. G. Santoro, A. Rossi, C. Amici, NF-kappaB and virus infection: who controls whom, *EMBO J.* **22**, 2552–2560 (2003).

68. S. Ghosh, M. J. May, E. B. Kopp, NF-kappa B and Rel proteins: evolutionarily conserved mediators of immune responses, *Annu. Rev. Immunol.* **16**, 225–260 (1998).

69. A. Oeckinghaus, M. S. Hayden, S. Ghosh, Crosstalk in NF-κB signaling pathways, *Nat. Immunol.* **12**, 695–708 (2011).

70. C. E. Stewart, R. E. Randall, C. S. Adamson, Inhibitors of the interferon response enhance virus replication in vitro, *PLoS One* **9**, e112014 (2014).

71. B. S. Parker, J. Rautela, P. J. Hertzog, Antitumour actions of interferons: implications for cancer therapy, *Nat. Rev. Cancer* **16**, 131–144 (2016).

72. R. J. Critchley-Thorne, D. L. Simons, N. Yan, A. K. Miyahira, F. M. Dirbas, D. L. Johnson, S. M. Swetter, R. W. Carlson, G. A. Fisher, A. Koong, S. Holmes, P. P. Lee, Impaired interferon signaling is a common immune defect in human cancer, *Proc. Natl. Acad. Sci. U. S. A.* **106**, 9010–9015 (2009).

73. B. N. Bidwell, C. Y. Slaney, N. P. Withana, S. Forster, Y. Cao, S. Loi, D. Andrews, T. Mikeska, N. E. Mangan, S. A. Samarajiwa, N. A. de Weerd, J. Gould, P. Argani, A. Möller, M. J. Smyth, R. L. Anderson, P. J. Hertzog, B. S. Parker, Silencing of Irf7 pathways in breast cancer cells promotes bone metastasis through immune escape, *Nat. Med.* **18**, 1224–1231 (2012).

74. C. S. Ilkow, S. L. Swift, J. C. Bell, J.-S. Diallo, From scourge to cure: tumour-selective viral pathogenesis as a new strategy against cancer, *PLoS Pathog.* **10**, e1003836 (2014).

75. B. D. Lichty, A. T. Power, D. F. Stojdl, J. C. Bell, Vesicular stomatitis virus: re-inventing the bullet, *Trends Mol. Med.* **10**, 210–216 (2004).

76. K.-X. Zhang, Y. Matsui, B. A. Hadaschik, C. Lee, W. Jia, J. C. Bell, L. Fazli, A. I. So, P. S. Rennie, Down-regulation of type I interferon receptor sensitizes bladder cancer cells to vesicular stomatitis virus-induced cell death, *Int. J. Cancer* **127**, 830–838 (2010).

77. K. P. Kotredes, A. M. Gamero, Interferons as inducers of apoptosis in malignant cells, *J. Interferon Cytokine Res.* **33**, 162–170 (2013).

78. S. Indraccolo, Interferon-alpha as angiogenesis inhibitor: learning from tumor models, *Autoimmunity* **43**, 244–247 (2010).

79. M. Cataldi, N. R. Shah, S. A. Felt, V. Z. Grdzelishvili, Breaking resistance of pancreatic cancer cells to an attenuated vesicular stomatitis virus through a novel activity of IKK inhibitor TPCA-1, *Virology* **485**, 340–354 (2015).

80. V. Saloura, L.-C. S. Wang, Z. G. Fridlender, J. Sun, G. Cheng, V. Kapoor, D. H. Sterman, R. N. Harty, A. Okumura, G. N. Barber, R. G. Vile, M. J. Federspiel, S. J. Russell, L. Litzky, S. M. Albelda, Evaluation of an attenuated vesicular stomatitis virus vector expressing interferon-beta for use in malignant pleural mesothelioma: heterogeneity in interferon responsiveness defines potential efficacy, *Hum. Gene Ther.* **21**, 51–64 (2010).

81. Y.-P. Liu, L. Suksanpaisan, M. B. Steele, S. J. Russell, K.-W. Peng, Induction of antiviral genes by the tumor microenvironment confers resistance to virotherapy, *Sci. Rep.* **3**, 2375 (2013).

82. S. Berchtold, J. Lampe, T. Weiland, I. Smirnow, S. Schleicher, R. Handgretinger, H.-G. Kopp, J. Reiser, F. Stubenrauch, N. Mayer, N. P. Malek, M. Bitzer, U. M. Lauer, Innate immune defense defines susceptibility of sarcoma cells to measles vaccine virus-based oncolysis, *J. Virol.* **87**, 3484–3501 (2013).

83. V. Monsurrò, S. Beghelli, R. Wang, S. Barbi, S. Coin, G. Di Pasquale, S. Bersani, M. Castellucci, C. Sorio, S. Eleuteri, A. Worschech, J. A. Chiorini, P. Pederzoli, H. Alter, F. M. Marincola, A. Scarpa, Anti-viral state segregates two molecular phenotypes of pancreatic adenocarcinoma: potential relevance for adenoviral gene therapy, *J. Transl. Med.* **8**, 10 (2010).

84. I. Liikanen, V. Monsurrò, L. Ahtiainen, M. Raki, T. Hakkarainen, I. Diaconu, S. Escutenaire, O. Hemminki, J. D. Dias, V. Cerullo, A. Kanerva, S. Pesonen, D. Marzioni, M. Colombatti, A. Hemminki, Induction of interferon pathways mediates in vivo resistance to oncolytic adenovirus, *Mol. Ther.* **19**, 1858–1866 (2011).

85. Y. Sun, Tumor microenvironment and cancer therapy resistance, *Cancer Lett.* **380**, 205–215 (2016).

86. M. J. V. Vähä-Koskela, F. Le Boeuf, C. Lemay, N. De Silva, J.-S. Diallo, J. Cox, M. Becker, Y. Choi, A. Ananth, C. Sellers, S. Breton, D. Roy, T. Falls, J. Brun, A. Hemminki, A. Hinkkanen, J. C. Bell, Resistance to two heterologous neurotropic oncolytic viruses, Semliki Forest virus and vaccinia virus, in experimental glioma, *J. Virol.* **87**, 2363–2366 (2013).

87. F. J. Zemp, B. A. McKenzie, X. Lun, L. Maxwell, K. M. Reilly, G. McFadden, V. Wee Yong, P. A. Forsyth, Resistance to Oncolytic Myxoma Virus Therapy in Nf1−/−/Trp53−/− Syngeneic Mouse Glioma Models Is Independent of Anti-Viral Type-I Interferon, *PLoS One* **8**, e65801 (2013).

88. F. Le Boeuf, M. Selman, H. Hee Son, A. Bergeron, A. Chen, J. Tsang, D. Butterwick, R. Arulanandam, N. E. Forbes, F. Tzelepis, J. C. Bell, J. Werier, H. Abdelbary, J.-S. Diallo, Oncolytic Maraba virus MG1 as a treatment for Sarcoma, *Int. J. Cancer* (2017), doi:10.1002/ijc.30813.

89. M. Vähä-Koskela, A. Hinkkanen, Tumor Restrictions to Oncolytic Virus, *Biomedicines* **2**, 163–194 (2014).

90. R. Bilbao, M. Bustos, P. Alzuguren, M. J. Pajares, M. Drozdzik, C. Qian, J. Prieto, A blood--tumor barrier limits gene transfer to experimental liver cancer: the effect of vasoactive compounds, *Gene Ther.* **7** (2000) (available at https://www.researchgate.net/profile/Pilar_Alzuguren/publication/12218545_Bilbao_R_Bustos_M_Alzuguren_P_Pajares_MJ_Drozdzik_M_Qian_C_Prieto_JA_blood-tumor_barrier_limits_gene_transfer_to_experimental_liver_cancer_the_effect_of_vasoactive_compounds_Gene_Ther_7_1824-1832/links/57a3642c08ae3f4529220a02/Bilbao-R-Bustos-M-Alzuguren-P-Pajares-MJ-Drozdzik-M-Qian-C-Prieto-JA-blood-tumor-barrier-limits-gene-transfer-to-experimental-liver-cancer-the-effect-of-vasoactive-compounds-Gene-Ther-7-1824-18.pdf).

91. T. D. McKee, P. Grandi, W. Mok, G. Alexandrakis, N. Insin, J. P. Zimmer, M. G. Bawendi, Y. Boucher, X. O. Breakefield, R. K. Jain, Degradation of fibrillar collagen in a human melanoma xenograft improves the efficacy of an oncolytic herpes simplex virus vector, *Cancer Res.* **66**, 2509–2513 (2006).

92. N. Kuriyama, H. Kuriyama, C. M. Julin, K. Lamborn, M. A. Israel, Pretreatment with protease is a useful experimental strategy for enhancing adenovirus-mediated cancer gene therapy, *Hum. Gene Ther.* **11**, 2219–2230 (2000).

93. S. Schäfer, S. Weibel, U. Donat, Q. Zhang, R. J. Aguilar, N. G. Chen, A. A. Szalay, Vaccinia

virus-mediated intra-tumoral expression of matrix metalloproteinase 9 enhances oncolysis of PC-3 xenograft tumors, *BMC Cancer* **12**, 366 (2012).

94. C.-S. Hong, W. Fellows, A. Niranjan, S. Alber, S. Watkins, J. B. Cohen, J. C. Glorioso, P. Grandi, Ectopic matrix metalloproteinase-9 expression in human brain tumor cells enhances oncolytic HSV vector infection, *Gene Ther.* **17**, 1200–1205 (2010).

95. W. Hou, P. Sampath, J. J. Rojas, S. H. Thorne, Oncolytic Virus-Mediated Targeting of PGE 2 in the Tumor Alters the Immune Status and Sensitizes Established and Resistant Tumors to Immunotherapy, *Cancer Cell* **30**, 108–119 (2016).

96. G. Fulci, N. Dmitrieva, D. Gianni, E. J. Fontana, X. Pan, Y. Lu, C. S. Kaufman, B. Kaur, S. E. Lawler, R. J. Lee, C. B. Marsh, D. J. Brat, N. van Rooijen, A. O. Stemmer-Rachamimov, A. S. Rachamimov, F. H. Hochberg, R. Weissleder, R. L. Martuza, E. A. Chiocca, Depletion of peripheral macrophages and brain microglia increases brain tumor titers of oncolytic viruses, *Cancer Res.* **67**, 9398–9406 (2007).

97. N. E. Forbes, R. Krishnan, J.-S. Diallo, Pharmacological modulation of anti-tumor immunity induced by oncolytic viruses, *Front. Oncol.* **4**, 191 (2014).

98. J.-S. Diallo, F. Le Boeuf, F. Lai, J. Cox, M. Vaha-Koskela, H. Abdelbary, H. MacTavish, K. Waite, T. Falls, J. Wang, R. Brown, J. E. Blanchard, E. D. Brown, D. H. Kirn, J. Hiscott, H. Atkins, B. D. Lichty, J. C. Bell, A high-throughput pharmacoviral approach identifies novel oncolytic virus sensitizers, *Mol. Ther.* **18**, 1123–1129 (2010).

99. M. Kim, M. Nitschké, B. Sennino, P. Murer, B. J. Schriver, A. M. Bell, A. Subramanian, C. E. McDonald, J. Wang, H. Cha, M.-C. Bourgeois-Daigneault, D. H. Kirn, J. C. Bell, N. De Silva, C. J. Breitbach, D. M. McDonald, Amplification of oncolytic vaccinia virus widespread tumor cell killing by sunitinib through multiple mechanisms, *Cancer Res.* (2017), doi:10.1158/0008-5472.CAN-15-3308.

100. R. Garza-Morales, K. Yaddanapudi, R. Perez-Hernandez, E. Riedinger, K. M. McMasters, H. Shirwan, E. Yolcu, J. G. Gomez-Gutierrez, Temozolomide renders murine cancer cells susceptible to oncolytic adenovirus replication and oncolysis, *Cancer Biol. Ther.* , 0 (2017).

101. G. Herbein, D. Wendling, Histone deacetylases in viral infections, *Clin. Epigenetics* **1**, 13–24 (2010).

102. H.-M. Chang, M. Paulson, M. Holko, C. M. Rice, B. R. G. Williams, I. Marié, D. E. Levy, Induction of interferon-stimulated gene expression and antiviral responses require protein deacetylase activity, *Proc. Natl. Acad. Sci. U. S. A.* **101**, 9578–9583 (2004).

103. T. Katsura, S. Iwai, Y. Ota, H. Shimizu, K. Ikuta, Y. Yura, The effects of trichostatin A on the oncolytic ability of herpes simplex virus for oral squamous cell carcinoma cells, *Cancer Gene Ther.* **16**, 237–245 (2009).

104. T.-C. Liu, P. Castelo-Branco, S. D. Rabkin, R. L. Martuza, Trichostatin A and oncolytic HSV combination therapy shows enhanced antitumoral and antiangiogenic effects, *Mol. Ther.* **16**, 1041–1047 (2008).

105. H. MacTavish, J.-S. Diallo, B. Huang, M. Stanford, F. Le Boeuf, N. De Silva, J. Cox, J. G. Simmons, T. Guimond, T. Falls, J. A. McCart, H. Atkins, C. Breitbach, D. Kirn, S. Thorne, J. C.

Bell, Enhancement of vaccinia virus based oncolysis with histone deacetylase inhibitors, *PLoS One* **5**, e14462 (2010).

106. T. L.-A. Nguyên, H. Abdelbary, M. Arguello, C. Breitbach, S. Leveille, J.-S. Diallo, A. Yasmeen, T. A. Bismar, D. Kirn, T. Falls, Others, Chemical targeting of the innate antiviral response by histone deacetylase inhibitors renders refractory cancers sensitive to viral oncolysis, *Proceedings of the National Academy of Sciences* **105**, 14981–14986 (2008).

107. S. Kaur, L. Lal, A. Sassano, B. Majchrzak-Kita, M. Srikanth, D. P. Baker, E. Petroulakis, N. Hay, N. Sonenberg, E. N. Fish, L. C. Platanias, Regulatory effects of mammalian target of rapamycin-activated pathways in type I and II interferon signaling, *J. Biol. Chem.* **282**, 1757–1768 (2007).

108. T. Alain, X. Lun, Y. Martineau, P. Sean, B. Pulendran, E. Petroulakis, F. J. Zemp, C. G. Lemay, D. Roy, J. C. Bell, G. Thomas, S. C. Kozma, P. A. Forsyth, M. Costa-Mattioli, N. Sonenberg, Vesicular stomatitis virus oncolysis is potentiated by impairing mTORC1-dependent type I IFN production, *Proc. Natl. Acad. Sci. U. S. A.* **107**, 1576–1581 (2010).

109. X. Fu, L. Tao, A. Rivera, X. Zhang, Rapamycin enhances the activity of oncolytic herpes simplex virus against tumor cells that are resistant to virus replication, *Int. J. Cancer* **129**, 1503–1510 (2011).

110. Z. K. Jiang, M. Johnson, D. L. Moughon, J. Kuo, M. Sato, L. Wu, Rapamycin enhances adenovirus-mediated cancer imaging and therapy in pre-immunized murine hosts, *PLoS One* **8**, e73650 (2013).

111. B. K. Jha, I. Polyakova, P. Kessler, B. Dong, B. Dickerman, G. C. Sen, R. H. Silverman, Inhibition of RNase L and RNA-dependent protein kinase (PKR) by sunitinib impairs antiviral innate immunity, *J. Biol. Chem.* **286**, 26319–26326 (2011).

112. B. K. Jha, B. Dong, C. T. Nguyen, I. Polyakova, R. H. Silverman, Suppression of antiviral innate immunity by sunitinib enhances oncolytic virotherapy, *Mol. Ther.* **21**, 1749–1757 (2013).

113. S. Verstovsek, H. Kantarjian, R. A. Mesa, A. D. Pardanani, J. Cortes-Franco, D. A. Thomas, Z. Estrov, J. S. Fridman, E. C. Bradley, S. Erickson-Viitanen, K. Vaddi, R. Levy, A. Tefferi, Safety and efficacy of INCB018424, a JAK1 and JAK2 inhibitor, in myelofibrosis, *N. Engl. J. Med.* **363**, 1117–1127 (2010).

114. D. Escobar-Zarate, Y.-P. Liu, L. Suksanpaisan, S. J. Russell, K.-W. Peng, Overcoming cancer cell resistance to VSV oncolysis with JAK1/2 inhibitors, *Cancer Gene Ther.* **20**, 582–589 (2013).

115. S. A. Felt, G. N. Droby, V. Z. Grdzelishvili, Ruxolitinib and Polycation Combination Treatment Overcomes Multiple Mechanisms of Resistance of Pancreatic Cancer Cells to Oncolytic Vesicular Stomatitis Virus, *J. Virol.* **91** (2017), doi:10.1128/JVI.00461-17.

116. F. B. Yebdri, J. Van Grevenynghe, V. A. Tang, M.-L. Goulet, J. H. Wu, D. F. Stojdl, J. Hiscott, R. Lin, Triptolide-mediated inhibition of interferon signaling enhances vesicular stomatitis virus-based oncolysis, *Mol. Ther.* **21**, 2043–2053 (2013).

117. D. V. Titov, B. Gilman, Q.-L. He, S. Bhat, W.-K. Low, Y. Dang, M. Smeaton, A. L. Demain, P. S. Miller, J. F. Kugel, J. A. Goodrich, J. O. Liu, XPB, a subunit of TFIIH, is a target

of the natural product triptolide, *Nat. Chem. Biol.* **7**, 182–188 (2011).

118. R. Arulanandam, C. Batenchuk, O. Varette, C. Zakaria, V. Garcia, N. E. Forbes, C. Davis, R. Krishnan, R. Karmacharya, J. Cox, A. Sinha, A. Babawy, K. Waite, E. Weinstein, T. Falls, A. Chen, J. Hamill, N. De Silva, D. P. Conrad, H. Atkins, K. Garson, C. Ilkow, M. Kærn, B. Vanderhyden, N. Sonenberg, T. Alain, F. Le Boeuf, J. C. Bell, J.-S. Diallo, Microtubule disruption synergizes with oncolytic virotherapy by inhibiting interferon translation and potentiating bystander killing, *Nat. Commun.* **6**, 6410 (2015).

119. M. H. Dornan, R. Krishnan, A. M. Macklin, M. Selman, N. El Sayes, H. H. Son, C. Davis, A. Chen, K. Keillor, P. J. Le, C. Moi, P. Ou, C. Pardin, C. R. Canez, F. Le Boeuf, J. C. Bell, J. C. Smith, J.-S. Diallo, C. N. Boddy, First-in-class small molecule potentiators of cancer virotherapy, *Sci. Rep.* **6**, 26786 (2016).

120. D. J. Mahoney, C. Lefebvre, K. Allan, J. Brun, C. A. Sanaei, S. Baird, N. Pearce, S. Grönberg, B. Wilson, M. Prakesh, A. Aman, M. Isaac, A. Mamai, D. Uehling, R. Al-Awar, T. Falls, T. Alain, D. F. Stojdl, Virus-tumor interactome screen reveals ER stress response can reprogram resistant cancers for oncolytic virus-triggered caspase-2 cell death, *Cancer Cell* **20**, 443–456 (2011).

121. S. T. Beug, V. A. Tang, E. C. LaCasse, H. H. Cheung, C. E. Beauregard, J. Brun, J. P. Nuyens, N. Earl, M. St-Jean, J. Holbrook, H. Dastidar, D. J. Mahoney, C. Ilkow, F. Le Boeuf, J. C. Bell, R. G. Korneluk, Smac mimetics and innate immune stimuli synergize to promote tumor death, *Nat. Biotechnol.* **32**, 182–190 (2014).

122. D.-S. Kim, H. Dastidar, C. Zhang, F. J. Zemp, K. Lau, M. Ernst, A. Rakic, S. Sikdar, J. Rajwani, V. Naumenko, D. R. Balce, B. W. Ewanchuk, P. Taylor, R. M. Yates, C. Jenne, C. Gafuik, D. J. Mahoney, Smac mimetics and oncolytic viruses synergize in driving anticancer T-cell responses through complementary mechanisms, *Nat. Commun.* **8**, 344 (2017).

123. A. Atwan, J. R. Ingram, R. Abbott, M. J. Kelson, T. Pickles, A. Bauer, V. Piguet, in *Cochrane Database of Systematic Reviews*, (2015).

124. D. Smith, Fumaric acid esters for psoriasis: a systematic review, *Ir. J. Med. Sci.* **186**, 161–177 (2017).

125. E. D. Deeks, Dimethyl Fumarate: A Review in Relapsing-Remitting MS, *Drugs* **76**, 243–254 (2016).

126. L. Kappos, R. Gold, D. H. Miller, D. G. Macmanus, E. Havrdova, V. Limmroth, C. H. Polman, K. Schmierer, T. A. Yousry, M. Yang, M. Eraksoy, E. Meluzinova, I. Rektor, K. T. Dawson, A. W. Sandrock, G. N. O'Neill, BG-12 Phase IIb Study Investigators, Efficacy and safety of oral fumarate in patients with relapsing-remitting multiple sclerosis: a multicentre, randomised, double-blind, placebo-controlled phase IIb study, *Lancet* **372**, 1463–1472 (2008).

127. N. H. R. Litjens, E. van Strijen, C. van Gulpen, H. Mattie, J. T. van Dissel, H. B. Thio, P. H. Nibbering, In vitro pharmacokinetics of anti-psoriatic fumaric acid esters, *BMC Pharmacol.* **4**, 22 (2004).

128. U. Mrowietz, K. Asadullah, Dimethylfumarate for psoriasis: more than a dietary curiosity, *Trends Mol. Med.* **11**, 43–48 (2005).

129. Z. Al-Jaderi, A. A. Maghazachi, Utilization of Dimethyl Fumarate and Related Molecules for Treatment of Multiple Sclerosis, Cancer, and Other Diseases, *Front. Immunol.* **7**, 278 (2016).

130. S. Menegon, A. Columbano, S. Giordano, The Dual Roles of NRF2 in Cancer, *Trends Mol. Med.* **22**, 578–593 (2016).

131. Q. Ma, Role of nrf2 in oxidative stress and toxicity, *Annu. Rev. Pharmacol. Toxicol.* **53**, 401–426 (2013).

132. K. Itoh, N. Wakabayashi, Y. Katoh, T. Ishii - Genes to …, 2003, Keap1 regulates both cytoplasmic- nuclear shuttling and degradation of Nrf2 in response to electrophiles, *Wiley Online Library* (2003) (available at http://onlinelibrary.wiley.com/doi/10.1046/j.1365-2443.2003.00640.x/full).

133. T. Suzuki, H. Motohashi, M. Yamamoto, Toward clinical application of the Keap1-Nrf2 pathway, *Trends Pharmacol. Sci.* **34**, 340–346 (2013).

134. U. Schulze-Topphoff, M. Varrin-Doyer, K. Pekarek, C. M. Spencer, A. Shetty, S. A. Sagan, B. A. C. Cree, R. A. Sobel, B. T. Wipke, L. Steinman, R. H. Scannevin, S. S. Zamvil, Dimethyl fumarate treatment induces adaptive and innate immune modulation independent of Nrf2, *Proceedings of the National Academy of Sciences* **113**, 4777–4782 (2016).

135. M. M. Blewett, J. Xie, B. W. Zaro, K. M. Backus, A. Altman, J. R. Teijaro, B. F. Cravatt, Chemical proteomic map of dimethyl fumarate-sensitive cysteines in primary human T cells, *Sci. Signal.* **9**, rs10 (2016).

136. N. Traverso, R. Ricciarelli, M. Nitti, B. Marengo, A. L. Furfaro, M. A. Pronzato, U. M. Marinari, C. Domenicotti, Role of glutathione in cancer progression and chemoresistance, *Oxid. Med. Cell. Longev.* **2013**, 972913 (2013).

137. T. J. Schmidt, M. Ak, U. Mrowietz, Reactivity of dimethyl fumarate and methylhydrogen fumarate towards glutathione and N-acetyl-L-cysteine--preparation of S-substituted thiosuccinic acid esters, *Bioorg. Med. Chem.* **15**, 333–342 (2007).

138. I. Kastrati, M. I. Siklos, E. L. Calderon-Gierszal, L. El-Shennawy, G. Georgieva, E. N. Thayer, G. R. J. Thatcher, J. Frasor, Dimethyl Fumarate Inhibits the Nuclear Factor κB Pathway in Breast Cancer Cells by Covalent Modification of p65 Protein, *J. Biol. Chem.* **291**, 3639–3647 (2016).

139. G. O. Gillard, B. Collette, J. Anderson, J. Chao, R. H. Scannevin, D. J. Huss, J. D. Fontenot, DMF, but not other fumarates, inhibits NF-κB activity in vitro in an Nrf2-independent manner, *J. Neuroimmunol.* **283**, 74–85 (2015).

140. I. Lastres-Becker, A. J. García-Yagüe, R. H. Scannevin, M. J. Casarejos, S. Kügler, A. Rábano, A. Cuadrado, Repurposing the NRF2 Activator Dimethyl Fumarate as Therapy Against Synucleinopathy in Parkinson's Disease, *Antioxid. Redox Signal.* **25**, 61–77 (2016).

141. X. Xie, Y. Zhao, C.-Y. Ma, X.-M. Xu, Y.-Q. Zhang, C.-G. Wang, J. Jin, X. Shen, J.-L. Gao, N. Li, Z.-J. Sun, D.-L. Dong, Dimethyl fumarate induces necroptosis in colon cancer cells through GSH depletion/ROS increase/MAPKs activation pathway, *Br. J. Pharmacol.* **172**, 3929–3943 (2015).

142. Y. Xia, S. Shen, I. M. Verma, NF-κB, an active player in human cancers, *Cancer Immunol Res* **2**, 823–830 (2014).

143. J. P. Nicolay, K. Müller-Decker, A. Schroeder, M. Brechmann, M. Möbs, C. Géraud, C. Assaf, S. Goerdt, P. H. Krammer, K. Gülow, Dimethyl fumarate restores apoptosis sensitivity and inhibits tumor growth and metastasis in CTCL by targeting NF-κB, *Blood* **128**, 805–815 (2016).

144. T. Valero, S. Steele, K. Neumüller, A. Bracher, H. Niederleithner, H. Pehamberger, P. Petzelbauer, R. Loewe, Combination of dacarbazine and dimethylfumarate efficiently reduces melanoma lymph node metastasis, *J. Invest. Dermatol.* **130**, 1087–1094 (2010).

145. B. Gu, L. M. DeAngelis, Enhanced cytotoxicity of bioreductive antitumor agents with dimethyl fumarate in human glioblastoma cells, *Anticancer Drugs* **16**, 167–174 (2005).

146. F. Li, G. Sethi, Targeting transcription factor NF-kappaB to overcome chemoresistance and radioresistance in cancer therapy, *Biochim. Biophys. Acta* **1805**, 167–180 (2010).

147. K. D. Held, E. R. Epp, E. P. Clark, J. E. Biaglow, Effect of dimethyl fumarate on the radiation sensitivity of mammalian cells in vitro, *Radiat. Res.* **115**, 495–502 (1988).

148. W. G. Kirlin, J. Cai, M. J. DeLong, E. J. Patten, D. P. Jones, Dietary compounds that induce cancer preventive phase 2 enzymes activate apoptosis at comparable doses in HT29 colon carcinoma cells, *J. Nutr.* **129**, 1827–1835 (1999).

149. N. E. B. Saidu, G. Noé, O. Cerles, L. Cabel, N. Kavian-Tessler, S. Chouzenoux, M. Bahuaud, C. Chéreau, C. Nicco, K. Leroy, B. Borghese, F. Goldwasser, F. Batteux, J. Alexandre, Dimethyl Fumarate Controls the NRF2/DJ-1 Axis in Cancer Cells: Therapeutic Applications, *Mol. Cancer Ther.* **16**, 529–539 (2017).

150. R. Loewe, T. Valero, S. Kremling, B. Pratscher, R. Kunstfeld, H. Pehamberger, P. Petzelbauer, Dimethylfumarate impairs melanoma growth and metastasis, *Cancer Res.* **66**, 11888–11896 (2006).

151. I. Kaluzki, I. Hrgovic, T. Hailemariam-Jahn, M. Doll, J. Kleemann, E. M. Valesky, S. Kippenberger, R. Kaufmann, N. Zoeller, M. Meissner, Dimethylfumarate inhibits melanoma cell proliferation via p21 and p53 induction and bcl-2 and cyclin B1 downregulation, *Tumour Biol.* **37**, 13627–13635 (2016).

152. Y. Yamazoe, M. Tsubaki, H. Matsuoka, T. Satou, T. Itoh, T. Kusunoki, Y. Kidera, Y. Tanimori, K. Shoji, H. Nakamura, M. Ogaki, S. Nishiura, S. Nishida, Dimethylfumarate inhibits tumor cell invasion and metastasis by suppressing the expression and activities of matrix metalloproteinases in melanoma cells, *Cell Biol. Int.* **33**, 1087–1094 (2009).

153. W. H. Schlesinger, E. M. Klein, A. Vengosh, Global biogeochemical cycle of vanadium, *Proc. Natl. Acad. Sci. U. S. A.* **114**, E11092–E11100 (2017).

154. D. C. Crans, J. J. Smee, E. Gaidamauskas, L. Yang, The chemistry and biochemistry of vanadium and the biological activities exerted by vanadium compounds, *Chem. Rev.* **104**, 849–902 (2004).

155. D. Rehder, in *Interrelations between Essential Metal Ions and Human Diseases*, Metal Ions in Life Sciences. (Springer, Dordrecht, 2013), pp. 139–169.

156. E. Irving, A. W. Stoker, Vanadium Compounds as PTP Inhibitors, *Molecules* **22** (2017), doi:10.3390/molecules22122269.

157. J. C. Pessoa, S. Etcheverry, D. Gambino, Vanadium compounds in medicine, *Coord. Chem. Rev.* **301**, 24–48 (2015).

158. T. Scior, J. Antonio Guevara-Garcia, Q.-T. Do, P. Bernard, S. Laufer, Why Antidiabetic Vanadium Complexes are Not in the Pipeline of "Big Pharma" Drug Research? A Critical Review, *Curr. Med. Chem.* **23**, 2874–2891 (2016).

159. O. Tsave, S. Petanidis, E. Kioseoglou, M. P. Yavropoulou, J. G. Yovos, D. Anestakis, A. Tsepa, A. Salifoglou, Role of Vanadium in Cellular and Molecular Immunology: Association with Immune-Related Inflammation and Pharmacotoxicology Mechanisms, *Oxid. Med. Cell. Longev.* **2016**, 4013639 (2016).

160. V. Imbert, J. F. Peyron, D. Farahi Far, B. Mari, P. Auberger, B. Rossi, Induction of tyrosine phosphorylation and T-cell activation by vanadate peroxide, an inhibitor of protein tyrosine phosphatases, *Biochem. J* **297 ( Pt 1)**, 163–173 (1994).

161. C. Huang, M. Ding, J. Li, S. S. Leonard, Y. Rojanasakul, V. Castranova, V. Vallyathan, G. Ju, X. Shi, Vanadium-induced Nuclear Factor of Activated T Cells Activation through Hydrogen Peroxide, *J. Biol. Chem.* **276**, 22397–22403 (2001).

162. A. M. Evangelou, Vanadium in cancer treatment, *Crit. Rev. Oncol. Hematol.* **42**, 249–265 (2002).

163. K. Takenaga, Suppression of metastatic potential of high-metastatic Lewis lung carcinoma cells by vanadate, an inhibitor of tyrosine phosphatase, through inhibiting cell-substrate adhesion, *Invasion Metastasis* **16**, 97–106 (1996).

164. L. G. Naso, I. Badiola, J. Marquez Clavijo, M. Valcarcel, C. Salado, E. G. Ferrer, P. A. M. Williams, Inhibition of the metastatic progression of breast and colorectal cancer in vitro and in vivo in murine model by the oxidovanadium(IV) complex with luteolin, *Bioorg. Med. Chem.* **24**, 6004–6011 (2016).

165. S. Lamouille, J. Xu, R. Derynck, Molecular mechanisms of epithelial–mesenchymal transition, *Nat. Rev. Mol. Cell Biol.* **15**, nrm3758 (2014).

166. S. Petanidis, E. Kioseoglou, K. Domvri, P. Zarogoulidis, J. M. Carthy, D. Anestakis, A. Moustakas, A. Salifoglou, In vitro and ex vivo vanadium antitumor activity in (TGF-β)-induced EMT. Synergistic activity with carboplatin and correlation with tumor metastasis in cancer patients, *Int. J. Biochem. Cell Biol.* **74**, 121–134 (2016).

167. L. Novotny, S. B. Kombian, Vanadium: Possible Use in Cancer Chemoprevention and Therapy, *J. Can. Res. Updates* **3**, 97–102 (2014).

168. H. J. Thompson, N. D. Chasteen, L. D. Meeker, Dietary vanadyl (IV) sulfate inhibits chemically-induced mammary carcinogenesis, *Carcinogenesis* **5**, 849–851 (1984).

169. A. Bishayee, S. Oinam, M. Basu, M. Chatterjee, Vanadium chemoprevention of 7,12-dimethylbenz(a)anthracene-induced rat mammary carcinogenesis: probable involvement of representative hepatic phase I and II xenobiotic metabolizing enzymes, *Breast Cancer Res. Treat.*

**63**, 133–145 (2000).

170. S. Manna, S. Das, M. Chatterjee, M. Janarthan, M. Chatterjee, Combined supplementation of vanadium and fish oil suppresses tumor growth, cell proliferation and induces apoptosis in DMBA-induced rat mammary carcinogenesis, *J. Cell. Biochem.* **112**, 2327–2339 (2011).

171. R. S. Ray, M. Basu, B. Ghosh, K. Samanta, M. Chatterjee, Vanadium, a versatile biochemical effector in chemical rat mammary carcinogenesis, *Nutr. Cancer* **51**, 184–196 (2005).

172. T. J. Bocklage, R. Quinn, B. Schmit, C. Verschraegen, *Bone and Soft Tissue Tumors: A Multidisciplinary Review with Case Presentations* (JP Medical Ltd, 2014).

173. L. Mirabello, R. J. Troisi, S. A. Savage, Osteosarcoma incidence and survival rates from 1973 to 2004: data from the Surveillance, Epidemiology, and End Results Program, *Cancer* **115**, 1531–1543 (2009).

174. R. Gorlick, in *Pediatric and Adolescent Osteosarcoma*, Cancer Treatment and Research. (Springer, Boston, MA, 2009), pp. 467–478.

175. J. Y. Ou, H. Spraker-Perlman, A. C. Dietz, R. R. Smits-Seemann, S. Kaul, A. C. Kirchhoff, Conditional survival of pediatric, adolescent, and young adult soft tissue sarcoma and bone tumor patients, *Cancer Epidemiol.* **50**, 150–157 (2017).

176. M. Garcia-Moure, N. Martinez-Vélez, A. Patiño-García, M. M. Alonso, Oncolytic adenoviruses as a therapeutic approach for osteosarcoma: A new hope, *Journal of Bone Oncology* (2016), doi:10.1016/j.jbo.2016.12.001.

177. T. Sasaki, H. Tazawa, J. Hasei, T. Kunisada, A. Yoshida, Y. Hashimoto, S. Yano, R. Yoshida, F. Uno, S. Kagawa, Y. Morimoto, Y. Urata, T. Ozaki, T. Fujiwara, Preclinical evaluation of telomerase-specific oncolytic virotherapy for human bone and soft tissue sarcomas, *Clin. Cancer Res.* **17**, 1828–1838 (2011).

178. J. C. Paglino, A. N. van den Pol, Vesicular stomatitis virus has extensive oncolytic activity against human sarcomas: rare resistance is overcome by blocking interferon pathways, *J. Virol.* **85**, 9346–9358 (2011).

179. S. Atsumi, A. Matsumine, H. Toyoda, R. Niimi, T. Iino, T. Nakamura, T. Matsubara, K. Asanuma, Y. Komada, A. Uchida, A. Sudo, Oncolytic virotherapy for human bone and soft tissue sarcomas using live attenuated poliovirus, *Int. J. Oncol.* **41**, 893–902 (2012).

180. T. Kubo, S. Shimose, T. Matsuo, J. Fujimori, T. Sakaguchi, M. Yamaki, K. Shinozaki, S. L. C. Woo, M. Ochi, Oncolytic vesicular stomatitis virus administered by isolated limb perfusion suppresses osteosarcoma growth, *J. Orthop. Res.* **29**, 795–800 (2011).

181. S. Kubo, K. Haga, A. Tamamoto, D. J. Palmer, P. Ng, Adenovirus–retrovirus hybrid vectors achieve highly enhanced tumor transduction and antitumor efficacy in vivo, *Molecular* (2011) (available at https://www.nature.com/mt/journal/v19/n1/full/mt2010182a.html).

182. S. Sugiura, F. Goshima, H. Takakuwa, T. Sata, T. Nakashima, Y. Nishiyama, Treatment of solid sarcomas in immunocompetent mice with novel, oncolytic herpes simplex viruses, *Otolaryngol. Head Neck Surg.* **130**, 470–478 (2004).

183. C. K. Lettieri, P. Hingorani, E. A. Kolb, Progress of oncolytic viruses in sarcomas, *Expert*

*Rev. Anticancer Ther.* **12**, 229–242 (2012).

184. R. Vile, D. Ando, D. Kirn, The oncolytic virotherapy treatment platform for cancer: unique biological and biosafety points to consider, *Cancer Gene Ther.* **9**, 1062–1067 (2002).

185. T. Delaunay, M. Violland, N. Boisgerault, S. Dutoit, V. Vignard, C. Münz, M. Gannage, B. Dréno, K. Vaivode, D. Pjanova, N. Labarrière, Y. Wang, E. A. Chiocca, F. L. Boeuf, J. C. Bell, P. Erbs, F. Tangy, M. Grégoire, J.-F. Fonteneau, Oncolytic viruses sensitize human tumor cells for NY-ESO-1 tumor antigen recognition by CD4+ effector T cells, *Oncoimmunology* , 00–00 (2017).

186. G. Fulci, L. Breymann, D. Gianni, K. Kurozomi, S. S. Rhee, J. Yu, B. Kaur, D. N. Louis, R. Weissleder, M. A. Caligiuri, E. A. Chiocca, Cyclophosphamide enhances glioma virotherapy by inhibiting innate immune responses, *Proc. Natl. Acad. Sci. U. S. A.* **103**, 12873–12878 (2006).

187. N. Hasegawa, M. Abei, K. K. Yokoyama, K. Fukuda, E. Seo, R. Kawashima, Y. Nakano, T. Yamada, K. Nakade, H. Hamada, Y. Obata, I. Hyodo, Cyclophosphamide enhances antitumor efficacy of oncolytic adenovirus expressing uracil phosphoribosyltransferase (UPRT) in immunocompetent Syrian hamsters, *Int. J. Cancer* **133**, 1479–1488 (2013).

188. T. L.-A. Nguyên, H. Abdelbary, M. Arguello, C. Breitbach, S. Leveille, J.-S. Diallo, A. Yasmeen, T. A. Bismar, D. Kirn, T. Falls, V. E. Snoulten, B. C. Vanderhyden, J. Werier, H. Atkins, M. J. V. Vähä-Koskela, D. F. Stojdl, J. C. Bell, J. Hiscott, Chemical targeting of the innate antiviral response by histone deacetylase inhibitors renders refractory cancers sensitive to viral oncolysis, *Proc. Natl. Acad. Sci. U. S. A.* **105**, 14981–14986 (2008).

189. R. A. Linker, D.-H. Lee, S. Ryan, A. M. van Dam, R. Conrad, P. Bista, W. Zeng, X. Hronowsky, A. Buko, S. Chollate, G. Ellrichmann, W. Brück, K. Dawson, S. Goelz, S. Wiese, R. H. Scannevin, M. Lukashev, R. Gold, Fumaric acid esters exert neuroprotective effects in neuroinflammation via activation of the Nrf2 antioxidant pathway, *Brain* **134**, 678–692 (2011).

190. P. Albrecht, I. Bouchachia, N. Goebels, N. Henke, H. H. Hofstetter, A. Issberner, Z. Kovacs, J. Lewerenz, D. Lisak, P. Maher, A.-K. Mausberg, K. Quasthoff, C. Zimmermann, H.-P. Hartung, A. Methner, Effects of dimethyl fumarate on neuroprotection and immunomodulation, *J. Neuroinflammation* **9**, 163 (2012).

191. C. B. Burness, E. D. Deeks, Dimethyl fumarate: a review of its use in patients with relapsing-remitting multiple sclerosis, *CNS Drugs* **28**, 373–387 (2014).

192. J. J. Hoefnagel, H. B. Thio, R. Willemze, Long- term safety aspects of systemic therapy with fumaric acid esters in severe psoriasis, *British Journal of* (2003) (available at http://onlinelibrary.wiley.com/doi/10.1046/j.1365-2133.2003.05433.x/full).

193. I. Puzanov, M. M. Milhem, D. Minor, O. Hamid, A. Li, L. Chen, M. Chastain, K. S. Gorski, A. Anderson, J. Chou, H. L. Kaufman, R. H. I. Andtbacka, Talimogene Laherparepvec in Combination With Ipilimumab in Previously Untreated, Unresectable Stage IIIB-IV Melanoma, *J. Clin. Oncol.* **34**, 2619–2626 (2016).

194. W. Shen, M. M. Patnaik, A. Ruiz, S. J. Russell, K.-W. Peng, Immunovirotherapy with vesicular stomatitis virus and PD-L1 blockade enhances therapeutic outcome in murine acute myeloid leukemia, *Blood* **127**, 1449–1458 (2016).

195. Z. Liu, R. Ravindranathan, P. Kalinski, Z. S. Guo, D. L. Bartlett, Rational combination of oncolytic vaccinia virus and PD-L1 blockade works synergistically to enhance therapeutic efficacy, *Nat. Commun.* **8**, 14754 (2017).

196. A. Samson, K. J. Scott, D. Taggart, E. J. West, E. Wilson, G. J. Nuovo, S. Thomson, R. Corns, R. K. Mathew, M. J. Fuller, T. J. Kottke, J. M. Thompson, E. J. Ilett, J. V. Cockle, P. van Hille, G. Sivakumar, E. S. Polson, S. J. Turnbull, E. S. Appleton, G. Migneco, A. S. Rose, M. C. Coffey, D. A. Beirne, F. J. Collinson, C. Ralph, D. Alan Anthoney, C. J. Twelves, A. J. Furness, S. A. Quezada, H. Wurdak, F. Errington-Mais, H. Pandha, K. J. Harrington, P. J. Selby, R. G. Vile, S. D. Griffin, L. F. Stead, S. C. Short, A. A. Melcher, Intravenous delivery of oncolytic reovirus to brain tumor patients immunologically primes for subsequent checkpoint blockade, *Sci. Transl. Med.* **10** (2018), doi:10.1126/scitranslmed.aam7577.

197. T. Mustelin, T. Vang, N. Bottini, Protein tyrosine phosphatases and the immune response, *Nat. Rev. Immunol.* **5**, 43–57 (2005).

198. W. J. A. J. Hendriks, A. Elson, S. Harroch, A. W. Stoker, Protein tyrosine phosphatases: functional inferences from mouse models and human diseases, *FEBS J.* **275**, 816–830 (2008).

199. K. M. Doody, A. Bourdeau, M. L. Tremblay, T-cell protein tyrosine phosphatase is a key regulator in immune cell signaling: lessons from the knockout mouse model and implications in human disease, *Immunol. Rev.* **228**, 325–341 (2009).

200. R. G. Maki, A. A. Jungbluth, S. Gnjatic, G. K. Schwartz, D. R. D'Adamo, M. L. Keohan, M. J. Wagner, K. Scheu, R. Chiu, E. Ritter, J. Kachel, I. Lowy, L. J. Old, G. Ritter, A Pilot Study of Anti-CTLA4 Antibody Ipilimumab in Patients with Synovial Sarcoma, *Sarcoma* **2013**, 168145 (2013).

201. C. J. Breitbach, J. Burke, D. Jonker, J. Stephenson, A. R. Haas, L. Q. M. Chow, J. Nieva, T.-H. Hwang, A. Moon, R. Patt, A. Pelusio, F. Le Boeuf, J. Burns, L. Evgin, N. De Silva, S. Cvancic, T. Robertson, J.-E. Je, Y.-S. Lee, K. Parato, J.-S. Diallo, A. Fenster, M. Daneshmand, J. C. Bell, D. H. Kirn, Intravenous delivery of a multi-mechanistic cancer-targeted oncolytic poxvirus in humans, *Nature* **477**, 99–102 (2011).

202. S. Kubo, K. Haga, A. Tamamoto, D. J. Palmer, P. Ng, H. Okamura, N. Kasahara, Adenovirus-retrovirus hybrid vectors achieve highly enhanced tumor transduction and antitumor efficacy in vivo, *Mol. Ther.* **19**, 76–82 (2011).

203. J. H. Kim, J. Y. Oh, B. H. Park, D. E. Lee, J. S. Kim, H. E. Park, M. S. Roh, J. E. Je, J. H. Yoon, S. H. Thorne, D. Kirn, T. H. Hwang, Systemic armed oncolytic and immunologic therapy for cancer with JX-594, a targeted poxvirus expressing GM-CSF, *Mol. Ther.* **14**, 361–370 (2006).

204. C. M. Sanfilippo, J. A. Blaho, ICP0 gene expression is a herpes simplex virus type 1 apoptotic trigger, *J. Virol.* **80**, 6810–6821 (2006).

205. J.-S. Diallo, D. Roy, H. Abdelbary, N. De Silva, J. C. Bell, Ex vivo infection of live tissue with oncolytic viruses, *J. Vis. Exp.* (2011), doi:10.3791/2854.

206. F. Le Boeuf, J.-S. Diallo, J. A. McCart, S. Thorne, T. Falls, M. Stanford, F. Kanji, R. Auer, C. W. Brown, B. D. Lichty, K. Parato, H. Atkins, D. Kirn, J. C. Bell, Synergistic interaction between oncolytic viruses augments tumor killing, *Mol. Ther.* **18**, 888–895 (2010).

207. F. Le Bœuf, C. Batenchuk, M. Vähä-Koskela, S. Breton, D. Roy, C. Lemay, J. Cox, H. Abdelbary, T. Falls, G. Waghray, H. Atkins, D. Stojdl, J.-S. Diallo, M. Kærn, J. C. Bell, Model-based rational design of an oncolytic virus with improved therapeutic potential, *Nat. Commun.* **4**, 1974 (2013).

208. E. G. Demicco, R. G. Maki, D. C. Lev, A. J. Lazar, New therapeutic targets in soft tissue sarcoma, *Adv. Anat. Pathol.* **19**, 170–180 (2012).

209. J. L. Rowell, D. O. McCarthy, C. E. Alvarez, Dog models of naturally occurring cancer, *Trends Mol. Med.* **17**, 380–388 (2011).

210. N. M. Durham, K. Mulgrew, K. McGlinchey, N. R. Monks, H. Ji, R. Herbst, J. Suzich, S. A. Hammond, E. J. Kelly, Oncolytic VSV Primes Differential Responses to Immuno-oncology Therapy, *Mol. Ther.* **25**, 1917–1932 (2017).

211. D. Zamarin, R. B. Holmgaard, S. K. Subudhi, J. S. Park, M. Mansour, P. Palese, T. Merghoub, J. D. Wolchok, J. P. Allison, Localized oncolytic virotherapy overcomes systemic tumor resistance to immune checkpoint blockade immunotherapy, *Sci. Transl. Med.* **6**, 226ra32 (2014).

212. R. Loewe, W. Holnthoner, M. Gröger, M. Pillinger, F. Gruber, D. Mechtcheriakova, E. Hofer, K. Wolff, P. Petzelbauer, Dimethylfumarate Inhibits TNF-Induced Nuclear Entry of NF-κB/p65 in Human Endothelial Cells, *The Journal of Immunology* **168**, 4781–4787 (2002).

213. J. C. U. Lehmann, J. J. Listopad, C. U. Rentzsch, F. H. Igney, A. von Bonin, H. H. Hennekes, K. Asadullah, W.-D. F. Docke, Dimethylfumarate induces immunosuppression via glutathione depletion and subsequent induction of heme oxygenase 1, *J. Invest. Dermatol.* **127**, 835–845 (2007).

214. S. X. Lin, L. Lisi, C. Dello Russo, P. E. Polak, A. Sharp, G. Weinberg, S. Kalinin, D. L. Feinstein, The anti-inflammatory effects of dimethyl fumarate in astrocytes involve glutathione and haem oxygenase-1, *ASN Neuro* **3** (2011), doi:10.1042/AN20100033.

215. A. Atwan, J. R. Ingram, R. Abbott, M. J. Kelson, T. Pickles, A. Bauer, V. Piguet, Oral fumaric acid esters for psoriasis, *Cochrane Database Syst. Rev.* , CD010497 (2015).

216. I. Kastrati, M. I. Siklos, E. L. Calderon-Gierszal, L. El-Shennawy, G. Georgieva, E. N. Thayer, G. R. J. Thatcher, J. Frasor, Dimethyl Fumarate Inhibits the Nuclear Factor κB Pathway in Breast Cancer Cells by Covalent Modification of p65 Protein, *J. Biol. Chem.* **291**, 3639–3647 (2016).

217. C. Sheridan, Gene therapy finds its niche, *Nat. Biotechnol.* **29**, 121–128 (2011).

218. D. Moharregh-Khiabani, R. A. Linker, R. Gold, M. Stangel, Fumaric Acid and its esters: an emerging treatment for multiple sclerosis, *Curr. Neuropharmacol.* **7**, 60–64 (2009).

219. R. Bomprezzi, Dimethyl fumarate in the treatment of relapsing–remitting multiple sclerosis: an overview, *Ther. Adv. Neurol. Disord.* (2015), doi:10.1177/1756285614564152.

220. C. G. Lemay, J. L. Rintoul, A. Kus, J. M. Paterson, V. Garcia, T. J. Falls, L. Ferreira, B. W. Bridle, D. P. Conrad, V. A. Tang, J.-S. Diallo, R. Arulanandam, F. Le Boeuf, K. Garson, B. C. Vanderhyden, D. F. Stojdl, B. D. Lichty, H. L. Atkins, K. A. Parato, J. C. Bell, R. C. Auer,

Harnessing oncolytic virus-mediated antitumor immunity in an infected cell vaccine, *Mol. Ther.* **20**, 1791–1799 (2012).

221. M.-C. Bourgeois-Daigneault, D. G. Roy, T. Falls, K. Twumasi-Boateng, L. E. St-Germain, M. Marguerie, V. Garcia, M. Selman, V. A. Jennings, J. Pettigrew, S. Amos, J.-S. Diallo, B. Nelson, J. C. Bell, Oncolytic vesicular stomatitis virus expressing interferon-σ has enhanced therapeutic activity, *Molecular Therapy - Oncolytics* **3**, 16001 (2016).

222. M. Selman, C. Rousso, A. Bergeron, H. H. Son, R. Krishnan, N. A. El-Sayes, O. Varette, A. Chen, F. Le Boeuf, F. Tzelepis, J. C. Bell, D. Crans, J.-S. Diallo, Multi-Modal Potentiation of Oncolytic Virotherapy by Vanadium Compounds, *Mol. Ther.* **0** (2017), doi:10.1016/j.ymthe.2017.10.014.

223. C. S. Robison, M. A. Whitt, The membrane-proximal stem region of vesicular stomatitis virus G protein confers efficient virus assembly, *J. Virol.* **74**, 2239–2246 (2000).

224. L. B. Sullivan, E. Martinez-Garcia, H. Nguyen, A. R. Mullen, E. Dufour, S. Sudarshan, J. D. Licht, R. J. Deberardinis, N. S. Chandel, The proto-oncometabolite fumarate binds glutathione to amplify ROS-dependent signaling, *Mol. Cell* **51**, 236–248 (2013).

225. M. S. Brennan, M. F. Matos, B. Li, X. Hronowski, B. Gao, P. Juhasz, K. J. Rhodes, R. H. Scannevin, Dimethyl Fumarate and Monoethyl Fumarate Exhibit Differential Effects on KEAP1, NRF2 Activation, and Glutathione Depletion In Vitro, *PLoS One* **10**, e0120254 (2015).

226. B. E. Hast, E. W. Cloer, D. Goldfarb, H. Li, P. F. Siesser, F. Yan, V. Walter, N. Zheng, D. N. Hayes, M. B. Major, Cancer-derived mutations in KEAP1 impair NRF2 degradation but not ubiquitination, *Cancer Res.* **74**, 808–817 (2014).

227. J. C. Castle, M. Loewer, S. Boegel, J. de Graaf, C. Bender, A. D. Tadmor, V. Boisguerin, T. Bukur, P. Sorn, C. Paret, M. Diken, S. Kreiter, Ö. Türeci, U. Sahin, Immunomic, genomic and transcriptomic characterization of CT26 colorectal carcinoma, *BMC Genomics* **15**, 190 (2014).

228. V. A. McGuire, T. Ruiz-Zorrilla Diez, C. H. Emmerich, S. Strickson, M. S. Ritorto, R. V. Sutavani, A. Weiβ, K. F. Houslay, A. Knebel, P. J. Meakin, I. R. Phair, M. L. J. Ashford, M. Trost, J. S. C. Arthur, Dimethyl fumarate blocks pro-inflammatory cytokine production via inhibition of TLR induced M1 and K63 ubiquitin chain formation, *Sci. Rep.* **6**, 31159 (2016).

229. H. Peng, M. Guerau-de-Arellano, V. B. Mehta, Y. Yang, D. J. Huss, T. L. Papenfuss, A. E. Lovett-Racke, M. K. Racke, Dimethyl fumarate inhibits dendritic cell maturation via nuclear factor κB (NF-κB) and extracellular signal-regulated kinase 1 and 2 (ERK1/2) and mitogen stress-activated kinase 1 (MSK1) signaling, *J. Biol. Chem.* **287**, 28017–28026 (2012).

230. P. L. Podolin, J. F. Callahan, B. J. Bolognese, Y. H. Li, K. Carlson, T. G. Davis, G. W. Mellor, C. Evans, A. K. Roshak, Attenuation of murine collagen-induced arthritis by a novel, potent, selective small molecule inhibitor of IkappaB Kinase 2, TPCA-1 (2-[(aminocarbonyl)amino]-5-(4-fluorophenyl)-3-thiophenecarboxamide), occurs via reduction of proinflammatory cytokines and antigen-induced T cell Proliferation, *J. Pharmacol. Exp. Ther.* **312**, 373–381 (2005).

231. R. Waelchli, B. Bollbuck, C. Bruns, T. Buhl, J. Eder, R. Feifel, R. Hersperger, P. Janser, L. Revesz, H.-G. Zerwes, A. Schlapbach, Design and preparation of 2-benzamido-pyrimidines as inhibitors of IKK, *Bioorg. Med. Chem. Lett.* **16**, 108–112 (2006).

232. D. Olagnier, R. R. Lababidi, S. B. Hadj, A. Sze, Y. Liu, S. D. Naidu, M. Ferrari, Y. Jiang, C. Chiang, V. Beljanski, M.-L. Goulet, E. V. Knatko, A. T. Dinkova-Kostova, J. Hiscott, R. Lin, Activation of Nrf2 Signaling Augments Vesicular Stomatitis Virus Oncolysis via Autophagy-Driven Suppression of Antiviral Immunity, *Mol. Ther.* (2017), doi:10.1016/j.ymthe.2017.04.022.

233. J. Hiscott, Convergence of the NF-κB and IRF pathways in the regulation of the innate antiviral response, *Cytokine Growth Factor Rev.* **18**, 483–490 (2007).

234. A. J. Varble, C. D. Ried, W. J. Hammond, K. A. Marquis, M. C. Woodruff, M. C. Ferran, The vesicular stomatitis virus matrix protein inhibits NF-κB activation in mouse L929 cells, *Virology* **499**, 99–104 (2016).

235. Z. Du, M. A. Whitt, J. Baumann, J. M. Garner, C. L. Morton, A. M. Davidoff, L. M. Pfeffer, Inhibition of type I interferon-mediated antiviral action in human glioma cells by the IKK inhibitors BMS-345541 and TPCA-1, *J. Interferon Cytokine Res.* **32**, 368–377 (2012).

236. K. Ghoreschi, J. Brück, C. Kellerer, C. Deng, H. Peng, O. Rothfuss, R. Z. Hussain, A. R. Gocke, A. Respa, I. Glocova, N. Valtcheva, E. Alexander, S. Feil, R. Feil, K. Schulze-Osthoff, R. A. Rupec, A. E. Lovett-Racke, R. Dringen, M. K. Racke, M. Röcken, Fumarates improve psoriasis and multiple sclerosis by inducing type II dendritic cells, *J. Exp. Med.* **208**, 2291–2303 (2011).

237. D. Di Bona, M. Cippitelli, C. Fionda, C. Cammà, A. Licata, A. Santoni, A. Craxì, Oxidative stress inhibits IFN-α-induced antiviral gene expression by blocking the JAK–STAT pathway, *J. Hepatol.* **45**, 271–279 (2006/8).

238. N. Kaur, B. Lu, R. K. Monroe, S. M. Ward, S. W. Halvorsen, Inducers of oxidative stress block ciliary neurotrophic factor activation of Jak/STAT signaling in neurons, *J. Neurochem.* **92**, 1521–1530 (2005).

239. R. Gold, L. Kappos, D. L. Arnold, A. Bar-Or, G. Giovannoni, K. Selmaj, C. Tornatore, M. T. Sweetser, M. Yang, S. I. Sheikh, K. T. Dawson, DEFINE Study Investigators, Placebo-controlled phase 3 study of oral BG-12 for relapsing multiple sclerosis, *N. Engl. J. Med.* **367**, 1098–1107 (2012).

240. B. J. Brew, N. W. S. Davies, P. Cinque, D. B. Clifford, A. Nath, Progressive multifocal leukoencephalopathy and other forms of JC virus disease, *Nat. Rev. Neurol.* **6**, 667–679 (2010).

241. D. J. Nieuwkamp, J.-L. Murk, B. W. van Oosten, C. H. P. Cremers, J. Killestein, M. C. Viveen, W. Van Hecke, D. W. Frijlink, M. P. Wattjes, PML in Dutch MS Patients Consortium, PML in a patient without severe lymphocytopenia receiving dimethyl fumarate, *N. Engl. J. Med.* **372**, 1474–1476 (2015).

242. U. Ermis, J. Weis, J. B. Schulz, PML in a patient treated with fumaric acid, *N. Engl. J. Med.* **368**, 1657–1658 (2013).

243. B. W. van Oosten, J. Killestein, F. Barkhof, C. H. Polman, M. P. Wattjes, PML in a patient treated with dimethyl fumarate from a compounding pharmacy, *N. Engl. J. Med.* **368**, 1658–1659 (2013).

244. N. Dammeier, V. Schubert, T.-K. Hauser, A. Bornemann, F. Bischof, Case report of a patient with progressive multifocal leukoencephalopathy under treatment with dimethyl fumarate,

*BMC Neurol.* **15**, 108 (2015).

245. T. Rosenkranz, M. Novas, C. Terborg, PML in a patient with lymphocytopenia treated with dimethyl fumarate, *N. Engl. J. Med.* **372**, 1476–1478 (2015).

246. E. E. Longbrake, R. T. Naismith, B. J. Parks, G. F. Wu, A. H. Cross, Dimethyl fumarate-associated lymphopenia: Risk factors and clinical significance, *Mult Scler J Exp Transl Clin* **1** (2015), doi:10.1177/2055217315596994.

247. K. Lehmann-Horn, H. Penkert, P. Grein, U. Leppmeier, S. Teuber-Hanselmann, B. Hemmer, A. Berthele, PML during dimethyl fumarate treatment of multiple sclerosis: How does lymphopenia matter?, *Neurology* **87**, 440–441 (2016).

248. M. T. Sweetser, K. T. Dawson, C. Bozic, Manufacturer's response to case reports of PML, *N. Engl. J. Med.* **368**, 1659–1661 (2013).

249. D. Dubey, B. C. Kieseier, H. P. Hartung, B. Hemmer, C. Warnke, T. Menge, W. A. Miller-Little, O. Stuve, Dimethyl fumarate in relapsing–remitting multiple sclerosis: rationale, mechanisms of action, pharmacokinetics, efficacy and safety, *Expert Rev. Neurother.* **15**, 339–346 (2015).

250. J. K. G. Co, S. Verma, U. Gurjav, L. Sumibcay, V. R. Nerurkar, Interferon- alpha and - beta restrict polyomavirus JC replication in primary human fetal glial cells: implications for progressive multifocal leukoencephalopathy therapy, *J. Infect. Dis.* **196**, 712–718 (2007).

251. P. A. Ott, F. S. Hodi, Talimogene Laherparepvec for the Treatment of Advanced Melanoma, *Clin. Cancer Res.* **22**, 3127–3131 (2016).

252. J.-S. Diallo, M. Vähä-Koskela, F. Le Boeuf, J. Bell, Propagation, purification, and in vivo testing of oncolytic vesicular stomatitis virus strains, *Methods Mol. Biol.* **797**, 127–140 (2012).

253. P. T. Sobol, J. E. Boudreau, K. Stephenson, Y. Wan, B. D. Lichty, K. L. Mossman, Adaptive antiviral immunity is a determinant of the therapeutic success of oncolytic virotherapy, *Mol. Ther.* **19**, 335–344 (2011).

254. E. Eden, R. Navon, I. Steinfeld, D. Lipson, Z. Yakhini, GOrilla: a tool for discovery and visualization of enriched GO terms in ranked gene lists, *BMC Bioinformatics* **10**, 48 (2009).

255. J.-S. Diallo, D. Roy, H. Abdelbary, N. De Silva, J. C. Bell, Ex vivo infection of live tissue with oncolytic viruses, *J. Vis. Exp.* (2011), doi:10.3791/2854.

256. A. Roberts, L. Buonocore, R. Price, J. Forman, J. K. Rose, Attenuated vesicular stomatitis viruses as vaccine vectors, *J. Virol.* **73**, 3723–3732 (1999).

257. S. E. Lawler, E. A. Chiocca, Oncolytic Virus-Mediated Immunotherapy: A Combinatorial Approach for Cancer Treatment, *J. Clin. Oncol.* **33**, 2812–2814 (2015).

258. C. S. Ilkow, M. Marguerie, C. Batenchuk, J. Mayer, D. Ben Neriah, S. Cousineau, T. Falls, V. A. Jennings, M. Boileau, D. Bellamy, D. Bastin, C. T. de Souza, A. Alkayyal, J. Zhang, F. Le Boeuf, R. Arulanandam, L. Stubbert, P. Sampath, S. H. Thorne, P. Paramanthan, A. Chatterjee, R. M. Strieter, M. Burdick, C. L. Addison, D. F. Stojdl, H. L. Atkins, R. C. Auer, J.-S. Diallo, B. D. Lichty, J. C. Bell, Reciprocal cellular cross-talk within the tumor microenvironment promotes oncolytic virus activity, *Nat. Med.* **21**, 530–536 (2015).

259. H. Kalkavan, P. Sharma, S. Kasper, I. Helfrich, A. A. Pandyra, A. Gassa, I. Virchow, L. Flatz, T. Brandenburg, S. Namineni, M. Heikenwalder, B. Höchst, P. A. Knolle, G. Wollmann, D. von Laer, I. Drexler, J. Rathbun, P. M. Cannon, S. Scheu, J. Bauer, J. Chauhan, D. Häussinger, G. Willimsky, M. Löhning, D. Schadendorf, S. Brandau, M. Schuler, P. A. Lang, K. S. Lang, Spatiotemporally restricted arenavirus replication induces immune surveillance and type I interferon-dependent tumour regression, *Nat. Commun.* **8**, 14447 (2017).

260. D. Zamarin, R. B. Holmgaard, J. Ricca, T. Plitt, P. Palese, P. Sharma, T. Merghoub, J. D. Wolchok, J. P. Allison, Intratumoral modulation of the inducible co-stimulator ICOS by recombinant oncolytic virus promotes systemic anti-tumour immunity, *Nat. Commun.* **8**, 14340 (2017).

261. D. Saha, R. L. Martuza, S. D. Rabkin, Macrophage Polarization Contributes to Glioblastoma Eradication by Combination Immunovirotherapy and Immune Checkpoint Blockade, *Cancer Cell* **32**, 253–267.e5 (2017).

262. C. C. McLauchlan, B. J. Peters, G. R. Willsky, Vanadium–phosphatase complexes: Phosphatase inhibitors favor the trigonal bipyramidal transition state geometries, *Coord. Chem. Rev.* (2015) (available at http://www.sciencedirect.com/science/article/pii/S0010854514003555).

263. K. H. Thompson, J. Lichter, C. LeBel, M. C. Scaife, J. H. McNeill, C. Orvig, Vanadium treatment of type 2 diabetes: a view to the future, *J. Inorg. Biochem.* **103**, 554–558 (2009).

264. K. H. Thompson, C. Orvig, Vanadium in diabetes: 100 years from Phase 0 to Phase I, *J. Inorg. Biochem.* **100**, 1925–1935 (2006).

265. A. Bishayee, A. Waghray, M. A. Patel, M. Chatterjee, Vanadium in the detection, prevention and treatment of cancer: the in vivo evidence, *Cancer Lett.* **294**, 1–12 (2010).

266. J. Costa Pessoa, Thirty years through vanadium chemistry, *J. Inorg. Biochem.* **147**, 4–24 (2015).

267. C. Rozzo, D. Sanna, E. Garribba, M. Serra, A. Cantara, G. Palmieri, M. Pisano, Antitumoral effect of vanadium compounds in malignant melanoma cell lines, *J. Inorg. Biochem.* **174**, 14–24 (2017).

268. J.-X. Wu, Y.-H. Hong, X.-G. Yang, Bis(acetylacetonato)-oxidovanadium(IV) and sodium metavanadate inhibit cell proliferation via ROS-induced sustained MAPK/ERK activation but with elevated AKT activity in human pancreatic cancer AsPC-1 cells, *J. Biol. Inorg. Chem.* **21**, 919–929 (2016).

269. O. Clark, I. Park, A. Di Florio, A.-C. Cichon, S. Rustin, R. Jugov, R. Maeshima, A. W. Stoker, Oxovanadium-based inhibitors can drive redox-sensitive cytotoxicity in neuroblastoma cells and synergise strongly with buthionine sulfoximine, *Cancer Lett.* **357**, 316–327 (2015).

270. J. J. O'Shea, D. W. McVicar, T. L. Bailey, C. Burns, M. J. Smyth, Activation of human peripheral blood T lymphocytes by pharmacological induction of protein-tyrosine phosphorylation, *Proc. Natl. Acad. Sci. U. S. A.* **89**, 10306–10310 (1992).

271. M. Ustarroz-Cano, I. Garcia-Pelaez, S. Cervantes-Yepez, N. Lopez-Valdez, T. I. Fortoul, Thymic cytoarchitecture changes in mice exposed to vanadium, *J. Immunotoxicol.* **14**, 9–14 (2017).

272. Y. J. Gordon, E. Romanowski, J. Berman, P. Vikoren, L. S. Lin, D. Schlessinger, T. Araullo-Cruz, Vanadate promotes reactivation and iontophoresis-induced ocular shedding of latent HSV-1 W in different host animals, *Curr. Eye Res.* **9**, 1015–1021 (1990).

273. F. Yamamoto, H. Fujioka, M. Iinuma, M. Takano, K. Maeno, Y. Nagai, Y. Ito, Enhancement of Newcastle Disease Virus-Induced Fusion of Mouse L Cells by Sodium Vanadate, *Microbiol. Immunol.* **28**, 75–83 (1984).

274. R. Veinalde, C. Grossardt, L. Hartmann, M.-C. Bourgeois-Daigneault, J. C. Bell, D. Jäger, C. von Kalle, G. Ungerechts, C. E. Engeland, Oncolytic measles virus encoding interleukin-12 mediates potent anti-tumor effects through T cell activation, *Oncoimmunology* **0**, 00–00.

275. K. L. Mossman, P. F. Macgregor, J. J. Rozmus, A. B. Goryachev, A. M. Edwards, J. R. Smiley, Herpes simplex virus triggers and then disarms a host antiviral response, *J. Virol.* **75**, 750–758 (2001).

276. K. A. Parato, C. J. Breitbach, F. Le Boeuf, J. Wang, C. Storbeck, C. Ilkow, J.-S. Diallo, T. Falls, J. Burns, V. Garcia, F. Kanji, L. Evgin, K. Hu, F. Paradis, S. Knowles, T.-H. Hwang, B. C. Vanderhyden, R. Auer, D. H. Kirn, J. C. Bell, The oncolytic poxvirus JX-594 selectively replicates in and destroys cancer cells driven by genetic pathways commonly activated in cancers, *Mol. Ther.* **20**, 749–758 (2012).

277. M. J. Gresser, A. S. Tracey, P. J. Stankiewicz, The interaction of vanadate with tyrosine kinases and phosphatases, *Adv Prot Phosphatases* **4**, 35–57 (1987).

278. C. Lallemand, B. Blanchard, M. Palmieri, P. Lebon, E. May, M. G. Tovey, Single-stranded RNA viruses inactivate the transcriptional activity of p53 but induce NOXA-dependent apoptosis via post-translational modifications of IRF-1, IRF-3 and CREB, *Oncogene* **26**, 328–338 (2007).

279. A. Takaoka, S. Hayakawa, H. Yanai, D. Stoiber, H. Negishi, H. Kikuchi, S. Sasaki, K. Imai, T. Shibue, K. Honda, T. Taniguchi, Integration of interferon-alpha/beta signalling to p53 responses in tumour suppression and antiviral defence, *Nature* **424**, 516–523 (2003).

280. C. Orvig, P. Caravan, L. Gelmini, N. Glover, F. G. Herring, H. Li, J. H. McNeill, S. J. Rettig, I. A. Setyawati, Reaction chemistry of BMOV, bis(maltolato)oxovanadium(IV), a potent insulin mimetic agent, *J. Am. Chem. Soc.* **117**, 12759–12770 (1995).

281. J. J. Ruotsalainen, M. U. Kaikkonen, M. Niittykoski, M. W. Martikainen, C. G. Lemay, J. Cox, N. S. De Silva, A. Kus, T. J. Falls, J.-S. Diallo, F. Le Boeuf, J. C. Bell, S. Ylä-Herttuala, A. E. Hinkkanen, M. J. Vähä-Koskela, Clonal variation in interferon response determines the outcome of oncolytic virotherapy in mouse CT26 colon carcinoma model, *Gene Ther.* **22**, 65–75 (2015).

282. K. G. Shim, S. Zaidi, J. Thompson, T. Kottke, L. Evgin, K. R. Rajani, M. Schuelke, C. B. Driscoll, A. Huff, J. S. Pulido, R. G. Vile, Inhibitory Receptors Induced by VSV Viroimmunotherapy Are Not Necessarily Targets for Improving Treatment Efficacy, *Mol. Ther.* **25**, 962–975 (2017).

283. D. C. Crans, Antidiabetic, Chemical, and Physical Properties of Organic Vanadates as Presumed Transition-State Inhibitors for Phosphatases, *J. Org. Chem.* **80**, 11899–11915 (2015).

284. P. K. Bommareddy, A. Patel, S. Hossain, H. L. Kaufman, Talimogene Laherparepvec (T-

VEC) and Other Oncolytic Viruses for the Treatment of Melanoma, *Am. J. Clin. Dermatol.* **18**, 1–15 (2017).

285. D. M. Smith, R. M. Pickering, G. T. Lewith, A systematic review of vanadium oral supplements for glycaemic control in type 2 diabetes mellitus, *QJM* **101**, 351–358 (2008).

286. S. Li, M. Zhu, R. Pan, T. Fang, Y.-Y. Cao, S. Chen, X. Zhao, C.-Q. Lei, L. Guo, Y. Chen, C.-M. Li, E. Jokitalo, Y. Yin, H.-B. Shu, D. Guo, The tumor suppressor PTEN has a critical role in antiviral innate immunity, *Nat. Immunol.* **17**, 241–249 (2016).

287. N. K. Tonks, Protein tyrosine phosphatases: from genes, to function, to disease, *Nat. Rev. Mol. Cell Biol.* **7**, 833–846 (2006).

288. J.-Y. Wang, C.-L. Yeh, H.-C. Chou, C.-H. Yang, Y.-N. Fu, Y.-T. Chen, H.-W. Cheng, C.-Y. F. Huang, H.-P. Liu, S.-F. Huang, Y.-R. Chen, Vaccinia H1-related phosphatase is a phosphatase of ErbB receptors and is down-regulated in non-small cell lung cancer, *J. Biol. Chem.* **286**, 10177–10184 (2011).

289. B. He, M. Gross, B. Roizman, The gamma(1)34.5 protein of herpes simplex virus 1 complexes with protein phosphatase 1alpha to dephosphorylate the alpha subunit of the eukaryotic translation initiation factor 2 and preclude the shutoff of protein synthesis by double-stranded RNA-activated protein kinase, *Proc. Natl. Acad. Sci. U. S. A.* **94**, 843–848 (1997).

290. A. M. Gamero, A. C. Larner, Vanadate facilitates interferon alpha-mediated apoptosis that is dependent on the Jak/Stat pathway, *J. Biol. Chem.* **276**, 13547–13553 (2001).

291. C. Huang, Z. Zhang, M. Ding, J. Li, J. Ye, S. S. Leonard, H. M. Shen, L. Butterworth, Y. Lu, M. Costa, Y. Rojanasakul, V. Castranova, V. Vallyathan, X. Shi, Vanadate induces p53 transactivation through hydrogen peroxide and causes apoptosis, *J. Biol. Chem.* **275**, 32516–32522 (2000).

292. A. R. Simon, U. Rai, B. L. Fanburg, B. H. Cochran, Activation of the JAK-STAT pathway by reactive oxygen species, *Am. J. Physiol.* **275**, C1640–52 (1998).

293. H. S. Kim, M.-S. Lee, STAT1 as a key modulator of cell death, *Cell. Signal.* **19**, 454–465 (2007).

294. P. A. Townsend, T. M. Scarabelli, S. M. Davidson, R. A. Knight, D. S. Latchman, A. Stephanou, STAT-1 interacts with p53 to enhance DNA damage-induced apoptosis, *J. Biol. Chem.* **279**, 5811–5820 (2004).

295. R. M. Bukowski, Immunotherapy in renal cell carcinoma, *Oncology* **13**, 801–10; discussion 810, 813 (1999).

296. A. Levina, D. C. Crans, P. A. Lay, Speciation of metal drugs, supplements and toxins in media and bodily fluids controls in vitro activities, *Coord. Chem. Rev.* (2017), doi:10.1016/j.ccr.2017.01.002.

297. R. M. B. Teles, T. G. Graeber, S. R. Krutzik, D. Montoya, M. Schenk, D. J. Lee, E. Komisopoulou, K. Kelly-Scumpia, R. Chun, S. S. Iyer, E. N. Sarno, T. H. Rea, M. Hewison, J. S. Adams, S. J. Popper, D. A. Relman, S. Stenger, B. R. Bloom, G. Cheng, R. L. Modlin, Type I Interferon Suppresses Type II Interferon–Triggered Human Anti-Mycobacterial Responses,

*Science* **339**, 1448–1453 (2013).

298. A. Deczkowska, K. Baruch, M. Schwartz, Type I/II Interferon Balance in the Regulation of Brain Physiology and Pathology, *Trends Immunol.* **37**, 181–192 (2016).

299. G. Miklossy, T. S. Hilliard, J. Turkson, Therapeutic modulators of STAT signalling for human diseases, *Nat. Rev. Drug Discov.* **12**, 611–629 (2013).

300. S.-L. Ng, B. A. Friedman, S. Schmid, J. Gertz, R. M. Myers, B. R. Tenoever, T. Maniatis, IκB kinase epsilon (IKK(epsilon)) regulates the balance between type I and type II interferon responses, *Proc. Natl. Acad. Sci. U. S. A.* **108**, 21170–21175 (2011).

301. W. Min, J. S. Pober, D. R. Johnson, Original Contributions-Vascular Biology-Interferon Induction of TAP1: The Phosphatase SHP-1 Regulates Crossover Between the IFN-a/b and the IFN-g Signal-Transduction Pathways, *Circ. Res.* **83**, 815–823 (1998).

302. J. Ho, C. Pelzel, A. Begitt, M. Mee, H. M. Elsheikha, D. J. Scott, U. Vinkemeier, STAT2 Is a Pervasive Cytokine Regulator due to Its Inhibition of STAT1 in Multiple Signaling Pathways, *PLoS Biol.* **14**, e2000117 (2016).

303. C. Park, S. Li, E. Cha, C. Schindler, Immune response in Stat2 knockout mice, *Immunity* **13**, 795–804 (2000).

304. H. C. Steen, A. M. Gamero, STAT2 phosphorylation and signaling, *JAKSTAT* **2**, e25790 (2013).

305. K. Blaszczyk, H. Nowicka, K. Kostyrko, A. Antonczyk, J. Wesoly, H. A. R. Bluyssen, The unique role of STAT2 in constitutive and IFN-induced transcription and antiviral responses, *Cytokine Growth Factor Rev.* **29**, 71–81 (2016).

306. F.-D. Böhmer, K. Friedrich, Protein tyrosine phosphatases as wardens of STAT signaling, *JAKSTAT* **3**, e28087 (2014).

307. Y. Wang, J. Nan, B. Willard, X. Wang, J. Yang, G. R. Stark, Negative regulation of type I IFN signaling by phosphorylation of STAT2 on T387, *EMBO J.* , e201694834 (2016).

308. M. Morioka, K. Fukunaga, T. Kawano, S. Hasegawa, K. Korematsu, Y. Kai, J. Hamada, E. Miyamoto, Y. Ushio, Serine/threonine phosphatase activity of calcineurin is inhibited by sodium orthovanadate and dithiothreitol reverses the inhibitory effect, *Biochem. Biophys. Res. Commun.* **253**, 342–345 (1998).

309. R. G. Uhrig, A.-M. Labandera, J. Muhammad, M. Samuel, G. B. Moorhead, Rhizobiales-like Phosphatase 2 from Arabidopsis thaliana Is a Novel Phospho-tyrosine-specific Phospho-protein Phosphatase (PPP) Family Protein Phosphatase, *J. Biol. Chem.* **291**, 5926–5934 (2016).

310. D. Parra-Diaz, Q. Wei, E. Y. Lee, L. Echegoyen, D. Puett, Binding of vanadium (IV) to the phosphatase calcineurin, *FEBS Lett.* **376**, 58–60 (1995).

311. A. Morita, J. Zhu, N. Suzuki, A. Enomoto, Y. Matsumoto, M. Tomita, T. Suzuki, K. Ohtomo, Y. Hosoi, Sodium orthovanadate suppresses DNA damage-induced caspase activation and apoptosis by inactivating p53, *Cell Death Differ.* **13**, 499–511 (2006).

312. A. Morita, S. Yamamoto, B. Wang, K. Tanaka, N. Suzuki, S. Aoki, A. Ito, T. Nanao, S.

Ohya, M. Yoshino, J. Zhu, A. Enomoto, Y. Matsumoto, O. Funatsu, Y. Hosoi, M. Ikekita, Sodium orthovanadate inhibits p53-mediated apoptosis, *Cancer Res.* **70**, 257–265 (2010).

313. B. Wang, K. Tanaka, A. Morita, Y. Ninomiya, K. Maruyama, K. Fujita, Y. Hosoi, M. Nenoi, Sodium orthovanadate (vanadate), a potent mitigator of radiation-induced damage to the hematopoietic system in mice, *J. Radiat. Res.* **54**, 620–629 (2013).

314. Z. Zhang, C. Huang, J. Li, S. S. Leonard, R. Lanciotti, L. Butterworth, X. Shi, Vanadate-induced cell growth regulation and the role of reactive oxygen species, *Arch. Biochem. Biophys.* **392**, 311–320 (2001).

315. T. M. F. Günther, M. R. Kviecinski, C. C. Baron, K. B. Felipe, M. S. Farias, F. O. da Silva, N. C. F. Bücker, C. T. Pich, E. A. Ferreira, D. W. Filho, J. Verrax, P. B. Calderon, R. C. Pedrosa, Sodium orthovanadate associated with pharmacological doses of ascorbate causes an increased generation of ROS in tumor cells that inhibits proliferation and triggers apoptosis, *Biochem. Biophys. Res. Commun.* **430**, 883–888 (2013).

316. C. Huang, Z. Zhang, M. Ding, J. Li, J. Ye, S. S. Leonard, H. M. Shen, L. Butterworth, Y. Lu, M. Costa, Y. Rojanasakul, V. Castranova, V. Vallyathan, X. Shi, Vanadate induces p53 transactivation through hydrogen peroxide and causes apoptosis, *J. Biol. Chem.* **275**, 32516–32522 (2000).

317. A. P. Gonçalves, A. Videira, P. Soares, V. Máximo, Orthovanadate-induced cell death in RET/PTC1-harboring cancer cells involves the activation of caspases and altered signaling through PI3K/Akt/mTOR, *Life Sci.* **89**, 371–377 (2011).

318. S. R. Rana, V. McCaffrey, B. J. Rabquer, Vanadium Complex Induced Cancer Cell Death via RIPK3 Activated Necroptosis, *The FASEB Journal* **31**, 876.6–876.6 (2017).

319. A. M. Gamero, A. C. Larner, Vanadate Facilitates Interferon α-mediated Apoptosis That Is Dependent on the Jak/Stat Pathway, *J. Biol. Chem.* **276**, 13547–13553 (2001).

320. Y. Watanabe, O. Suzuki, T. Haruyama, T. Akaike, Interferon-gamma induces reactive oxygen species and endoplasmic reticulum stress at the hepatic apoptosis, *J. Cell. Biochem.* **89**, 244–253 (2003).

321. S. Rakshit, B. S. Chandrasekar, B. Saha, E. S. Victor, S. Majumdar, D. Nandi, Interferon-gamma induced cell death: Regulation and contributions of nitric oxide, cJun N-terminal kinase, reactive oxygen species and peroxynitrite, *Biochim. Biophys. Acta* **1843**, 2645–2661 (2014).

322. H. Y. Yim, Y. Yang, J.-S. Lim, M. S. Lee, D.-E. Zhang, K. I. Kim, The mitochondrial pathway and reactive oxygen species are critical contributors to interferon-α/β-mediated apoptosis in Ubp43-deficient hematopoietic cells, *Biochem. Biophys. Res. Commun.* **423**, 436–440 (2012).

323. J. P. Parody, M. P. Ceballos, A. D. Quiroga, D. E. Frances, C. E. Carnovale, G. B. Pisani, M. L. Alvarez, M. C. Carrillo, FoxO3a modulation and promotion of apoptosis by interferon-α2b in rat preneoplastic liver, *Liver Int.* **34**, 1566–1577 (2014).

324. C. Xiao, C. M. Bator, V. D. Bowman, E. Rieder, Y. He, B. Hébert, J. Bella, T. S. Baker, E. Wimmer, R. J. Kuhn, M. G. Rossmann, Interaction of coxsackievirus A21 with its cellular receptor, ICAM-1, *J. Virol.* **75**, 2444–2451 (2001).

325. J. Ylä-Pelto, L. Tripathi, P. Susi, Therapeutic Use of Native and Recombinant Enteroviruses, *Viruses* **8**, 57 (2016).

326. M. Audette, L. Larouche, I. Lussier, N. Fugère, Stimulation of the ICAM-1 gene transcription by the peroxovanadium compound [bpV(Pic)] involves STAT-1 but not NF-κB activation in 293 cells : Regulation of ICAM-1 transcription by bpV(Pic), *Eur. J. Biochem.* **268**, 1828–1836 (2001).

327. H. Ganjian, C. Zietz, D. Mechtcheriakova, D. Blaas, R. Fuchs, ICAM-1 Binding Rhinoviruses Enter HeLa Cells via Multiple Pathways and Travel to Distinct Intracellular Compartments for Uncoating, *Viruses* **9** (2017), doi:10.3390/v9040068.

328. P. Hingorani, V. Sampson, C. Lettieri, E. A. Kolb, Oncolytic viruses for potential osteosarcoma therapy, *Adv. Exp. Med. Biol.* **804**, 259–283 (2014).

329. A. Ketola, A. Hinkkanen, F. Yongabi, P. Furu, A.-M. Määttä, T. Liimatainen, R. Pirinen, M. Björn, T. Hakkarainen, K. Mäkinen, J. Wahlfors, R. Pellinen, Oncolytic Semliki forest virus vector as a novel candidate against unresectable osteosarcoma, *Cancer Res.* **68**, 8342–8350 (2008).

330. P. Hingorani, W. Zhang, J. Lin, L. Liu, C. Guha, E. A. Kolb, Systemic administration of reovirus (Reolysin) inhibits growth of human sarcoma xenografts, *Cancer* **117**, 1764–1774 (2011).

331. T. D. Pencavel, M. J. Wilkinson, D. C. Mansfield, A. A. Khan, R. Seth, E. M. Karapanagiotou, V. Roulstone, R. J. Aguilar, N. G. Chen, A. A. Szalay, A. J. Hayes, K. J. Harrington, Isolated limb perfusion with melphalan, tumour necrosis factor-alpha and oncolytic vaccinia virus improves tumour targeting and prolongs survival in a rat model of advanced extremity sarcoma, *Int. J. Cancer* **136**, 965–976 (2015).

332. F. Le Boeuf, M. Selman, H. Hee Son, A. Bergeron, A. Chen, J. Tsang, D. Butterwick, R. Arulanandam, N. E. Forbes, F. Tzelepis, J. C. Bell, J. Werier, H. Abdelbary, J.-S. Diallo, Oncolytic Maraba virus MG1 as a treatment for Sarcoma, *Int. J. Cancer* (2017), doi:10.1002/ijc.30813.

333. J. C. Paglino, A. N. van den Pol, Vesicular stomatitis virus has extensive oncolytic activity against human sarcomas: rare resistance is overcome by blocking interferon pathways, *J. Virol.* **85**, 9346–9358 (2011).

334. D. A. Barrio, S. B. Etcheverry, Vanadium and bone development: putative signaling pathways, *Can. J. Physiol. Pharmacol.* **84**, 677–686 (2006).

335. M. S. Molinuevo, A. M. Cortizo, S. B. Etcheverry, Vanadium(IV) complexes inhibit adhesion, migration and colony formation of UMR106 osteosarcoma cells, *Cancer Chemother. Pharmacol.* **61**, 767–773 (2008).

336. I. E. León, N. Butenko, A. L. Di Virgilio, C. I. Muglia, E. J. Baran, I. Cavaco, S. B. Etcheverry, Vanadium and cancer treatment: Antitumoral mechanisms of three oxidovanadium(IV) complexes on a human osteosarcoma cell line, *J. Inorg. Biochem.* **134**, 106–117 (2014).

337. I. E. León, J. F. Cadavid-Vargas, A. Resasco, F. Maschi, M. A. Ayala, C. Carbone, S. B.

Etcheverry, In vitro and in vivo antitumor effects of the VO-chrysin complex on a new three-dimensional osteosarcoma spheroids model and a xenograft tumor in mice, *J. Biol. Inorg. Chem.* **21**, 1009–1020 (2016).

338. V. Baud, M. Karin, Is NF-kappaB a good target for cancer therapy? Hopes and pitfalls, *Nat. Rev. Drug Discov.* **8**, 33–40 (2009).

339. L. Prabhu, R. Mundade, M. Korc, P. J. Loehrer, T. Lu, Critical role of NF-κB in pancreatic cancer, *Oncotarget* **5**, 10969–10975 (2014).

340. J. Ling, Y. 'an Kang, R. Zhao, Q. Xia, D.-F. Lee, Z. Chang, J. Li, B. Peng, J. B. Fleming, H. Wang, J. Liu, I. R. Lemischka, M.-C. Hung, P. J. Chiao, KrasG12D-induced IKK2/β/NF-κB activation by IL-1α and p62 feedforward loops is required for development of pancreatic ductal adenocarcinoma, *Cancer Cell* **21**, 105–120 (2012).

341. A. Stathis, M. J. Moore, Advanced pancreatic carcinoma: current treatment and future challenges, *Nat. Rev. Clin. Oncol.* **7**, 163–172 (2010).

342. P. Sharma, S. Hu-Lieskovan, J. A. Wargo, A. Ribas, Primary, Adaptive, and Acquired Resistance to Cancer Immunotherapy, *Cell* **168**, 707–723 (2017).

343. J. L. Benci, B. Xu, Y. Qiu, T. J. Wu, H. Dada, C. Twyman-Saint Victor, L. Cucolo, D. S. M. Lee, K. E. Pauken, A. C. Huang, T. C. Gangadhar, R. K. Amaravadi, L. M. Schuchter, M. D. Feldman, H. Ishwaran, R. H. Vonderheide, A. Maity, E. J. Wherry, A. J. Minn, Tumor Interferon Signaling Regulates a Multigenic Resistance Program to Immune Checkpoint Blockade, *Cell* **167**, 1540–1554.e12 (2016).

344. J. Gao, L. Z. Shi, H. Zhao, J. Chen, L. Xiong, Q. He, T. Chen, J. Roszik, C. Bernatchez, S. E. Woodman, P.-L. Chen, P. Hwu, J. P. Allison, A. Futreal, J. A. Wargo, P. Sharma, Loss of IFN-γ Pathway Genes in Tumor Cells as a Mechanism of Resistance to Anti-CTLA-4 Therapy, *Cell* **167**, 397–404.e9 (2016).

345. Y. Lan, D. Zhang, C. Xu, K. W. Hance, B. Marelli, J. Qi, H. Yu, G. Qin, A. Sircar, V. M. Hernández, M. H. Jenkins, R. E. Fontana, A. Deshpande, G. Locke, H. Sabzevari, L. Radvanyi, K.-M. Lo, Enhanced preclinical antitumor activity of M7824, a bifunctional fusion protein simultaneously targeting PD-L1 and TGF-β, *Sci. Transl. Med.* **10** (2018), doi:10.1126/scitranslmed.aan5488.

346. P. Müller, M. Kreuzaler, T. Khan, D. S. Thommen, K. Martin, K. Glatz, S. Savic, N. Harbeck, U. Nitz, O. Gluz, M. von Bergwelt-Baildon, H. Kreipe, S. Reddy, M. Christgen, A. Zippelius, Trastuzumab emtansine (T-DM1) renders HER2+ breast cancer highly susceptible to CTLA-4/PD-1 blockade, *Sci. Transl. Med.* **7**, 315ra188 (2015).

347. E. Allen, A. Jabouille, L. B. Rivera, I. Lodewijckx, R. Missiaen, V. Steri, K. Feyen, J. Tawney, D. Hanahan, I. P. Michael, G. Bergers, Combined antiangiogenic and anti-PD-L1 therapy stimulates tumor immunity through HEV formation, *Sci. Transl. Med.* **9** (2017), doi:10.1126/scitranslmed.aak9679.

348. M. Schmittnaegel, N. Rigamonti, E. Kadioglu, A. Cassará, C. Wyser Rmili, A. Kiialainen, Y. Kienast, H.-J. Mueller, C.-H. Ooi, D. Laoui, M. De Palma, Dual angiopoietin-2 and VEGFA inhibition elicits antitumor immunity that is enhanced by PD-1 checkpoint blockade, *Sci. Transl. Med.* **9** (2017), doi:10.1126/scitranslmed.aak9670.

349. E. Nolan, P. Savas, A. N. Policheni, P. K. Darcy, F. Vaillant, C. P. Mintoff, S. Dushyanthen, M. Mansour, J.-M. B. Pang, S. B. Fox, Kathleen Cuningham Foundation Consortium for Research into Familial Breast Cancer (kConFab), C. M. Perou, J. E. Visvader, D. H. D. Gray, S. Loi, G. J. Lindeman, Combined immune checkpoint blockade as a therapeutic strategy for BRCA1-mutated breast cancer, *Sci. Transl. Med.* **9** (2017), doi:10.1126/scitranslmed.aal4922.

350. M. Selman, P. Ou, C. Rousso, A. Bergeron, R. Krishnan, L. Pikor, A. Chen, B. A. Keller, C. Ilkow, J. C. Bell, J.-S. Diallo, Dimethyl fumarate potentiates oncolytic virotherapy through NF-κB inhibition, *Sci. Transl. Med.* **10**, eaao1613 (2018).

351. P. R. Errante, J. B. Frazão, A. Condino-Neto, The use of interferon-gamma therapy in chronic granulomatous disease, *Recent Pat. Antiinfect. Drug Discov.* **3**, 225–230 (2008).